

Bayesian Characterizations of Properties of Stochastic Processes with Applications

Sucharita Roy and Sourabh Bhattacharya¹

¹Sucharita Roy is an Assistant Professor and HOD of Department of Mathematics, St. Xavier's College, Kolkata, pursuing PhD in Interdisciplinary Statistical Research Unit, Indian Statistical Institute, 203, B. T. Road, Kolkata 700108. Sourabh Bhattacharya is an Associate Professor in Interdisciplinary Statistical Research Unit, Indian Statistical Institute, 203, B. T. Road, Kolkata 700108. Corresponding e-mail: sourabh@isical.ac.in.

Abstract

In this article, we primarily propose a novel Bayesian characterization of stationary and nonstationary stochastic processes. In practice, this theory aims to distinguish between global stationarity and nonstationarity for both parametric and nonparametric stochastic processes. Interestingly, our theory builds on our previous work on Bayesian characterization of infinite series, which was applied to verification of the (in)famous Riemann Hypothesis. Thus, there seems to be interesting and important connections between pure mathematics and Bayesian statistics, with respect to our proposed ideas. We validate our proposed method with simulation and real data experiments associated with different setups. In particular, applications of our method include stationarity and nonstationarity determination in various time series models, spatial and spatio-temporal setups, and convergence diagnostics of Markov Chain Monte Carlo. Our results demonstrate very encouraging performance, even in very subtle situations.

Using similar principles, we also provide a novel Bayesian characterization of mutual independence among any number of random variables, using which we characterize the properties of point processes, including characterizations of Poisson point processes, complete spatial randomness, stationarity and nonstationarity. Applications to simulation experiments with ample Poisson and non-Poisson point process models again indicate quite encouraging performance of our proposed ideas.

We further propose a novel recursive Bayesian method for determination of frequencies of oscillatory stochastic processes, based on our general principle. Simulation studies and real data experiments with varieties of time series models consisting of single and multiple frequencies bring out the worth of our method.

Keywords: *Bayesian theory; Markov Chain Monte Carlo; Spatial and spatio-temporal processes; Stationary and nonstationary stochastic processes; Tests for stationarity; Time series*

Contents

1	Introduction	4
2	Requisite definitions and associated results – prelude to the key concept	6
3	The key concept	9
4	A recursive Bayesian procedure for studying stationarity	10
4.1	Development of the stage-wise likelihoods	11
4.2	Development of recursive Bayesian posteriors	12
5	Characterization of stationarity properties of the underlying process	13
6	Computation of the sup norm between empirical distribution functions associated with \hat{P}_j and \tilde{P}_K	15
7	Choice of the cardinality of \mathcal{N}_i	16
8	Stationarity of covariance structure	17
9	Characterization of stationarity and nonstationarity using non-recursive Bayesian posteriors	19
10	First illustration: AR(1) model	19
10.1	Case 1: Large sample size, form of the model known	20
10.1.1	Sample size	20
10.1.2	Construction of bound	20
10.1.3	Implementation	20
10.1.4	Results	21
10.2	Case 2: Relatively small sample size, form of the model known	21
10.2.1	Sample size	21
10.2.2	Construction of bound	21
10.2.3	Implementation	23
10.2.4	Results	23
10.3	Case 3: Relatively small sample size, form of the model unknown	23
10.3.1	Sample size	23
10.3.2	Construction of bound	23
10.3.3	Implementation	25
10.3.4	Results	25
10.3.5	Comparison with classical tests of nonstationarity	25
11	Second illustration: AR(2), ARCH(1) and GARCH(1,1) models	27
11.1	Application to AR(2)	27
11.2	Application to ARCH(1)	27
11.3	Application to GARCH(1,1)	30

12 Third illustration: MCMC convergence diagnostics	33
12.1 A brief overview of TMCMC	33
12.2 Optimal scaling of TMCMC	35
12.3 TMCMC example 1: product of 100 standard normal densities	35
12.4 TMCMC example 2: mixture normal densities	36
13 Fourth illustration: detection of stationarity and nonstationarity in spatial data	39
13.1 Data generation	40
13.2 Implementation of our method to detect strict stationarity	40
13.2.1 Choice of \hat{C}_1	40
13.3 Results	41
13.4 Implementation of our method to detect covariance stationarity	41
13.4.1 Choice of \hat{C}_1	42
13.5 Detection of strict nonstationarity in mixtures of stationary and nonstationary co- variances	42
13.6 Detection of covariance nonstationarity in mixtures of stationary and nonstationary covariances	44
13.7 Spatial experiments with smaller data sets	44
13.8 Comparison with existing methods	48
14 Fifth illustration: detection of stationarity and nonstationarity in spatio-temporal data	48
14.1 Choice of the bound c_j in the spatio-temporal case	49
14.2 Spatial and temporal stationarity	50
14.3 Spatio-temporal nonstationarity	50
14.4 Results	50
14.5 Investigation of spatio-temporal stationarity with smaller sample size	54
14.6 Comparison with existing methods	54
14.6.1 Simulations under stationarity with exponential spatial covariance function	54
14.6.2 Simulations under stationarity with Whittle spatial covariance function . .	56
14.6.3 Simulations under nonstationarity	56
14.6.4 Overall comparison of our results with those of Bandopadhyay <i>et al.</i> (2017)	62
15 Real data analyses for spatial and spatio-temporal data	64
15.1 Spatial ozone data	64
15.2 Spatio-temporal PM 10 data	64
15.3 Spatio-temporal PM 2.5 data	67
16 Bayesian characterization of point processes	67
16.1 Discussion on edge correction	74
16.2 Characterization of stationarity and nonstationarity of point processes	74
16.3 Characterization of mutual independence among random variables	75
16.4 Mutual independence in the point process setup	79
16.5 Computational strategy for mutual independence assessment	80
16.6 Example 1: Detection of HPP and IHPP and their properties	80

16.6.1	Homogeneity detection	81
16.6.2	Stationarity detection	82
16.6.3	Validation of Poisson assumption	83
16.7	Example 2: Homogeneous log-Gaussian Cox process	84
16.8	Example 3: Inhomogeneous log-Gaussian Cox process	85
16.9	Example 4: Inhomogeneous log-Gaussian Cox process	87
16.10	Example 5: Homogeneous Matérn cluster process	87
16.11	Example 6: Inhomogeneous Matérn cluster process with μ inhomogeneous	92
16.12	Example 7: Matérn cluster process with κ Inhomogeneous	93
16.13	Example 8: Homogeneous Thomas process	95
16.14	Example 9: Inhomogeneous Thomas process with μ inhomogeneous	95
16.15	Example 10: Inhomogeneous Thomas process with κ inhomogeneous	98
16.16	Example 11: Inhomogeneous Thomas process with κ and μ the same inhomogeneous function	100
16.17	Example 12: Inhomogeneous Thomas process with κ and μ different inhomogeneous functions	100
16.18	Example 13: Inhomogeneous Thomas Process with interchanged inhomogeneous κ and μ	100
16.19	Example 14: Homogeneous Neyman-Scott process	103
16.20	Example 15: Inhomogeneous Neyman-Scott process	105
16.21	Example 16: Strauss process	108
16.22	Example 17: Another Strauss process	109
17	Bayesian determination of frequencies of oscillatory stochastic processes	109
17.1	The key idea for Bayesian frequency determination	109
17.2	Bayesian theory for finite M	112
17.3	Choice of r , M and $\{q_1, \dots, q_M\}$	113
17.4	Infinite number of frequencies	114
17.5	Simulation study with a single frequency	115
17.6	Simulation study with multiple frequencies	120
17.7	Real data example: El Niño and fish population	124
17.7.1	SOI series	124
17.7.2	Harmonics	132

1 Introduction

In various areas of statistics dealing with stochastic processes, ascertainment of stationarity or non-stationarity of the process behind the observed data, is the primary requirement before postulating a stochastic model. In statistics, empirical plots of the data for visualizing stationarity is quite popular, particularly in the time series context. However, rigorous ascertainment of stationarity is likely to be carried out via appropriate hypotheses testing procedures. In the parametric time series context, stationarity is usually characterized by specific parameters, and by devising suitable testing methods, inference regarding stationarity can be obtained. Using the result of such a test, appropriate stationarity or nonstationary models can then be built for statistical analysis of the given data. Although many tests exist in the time series literature, both parametric and non-parametric, they are meant for specific types of time series. Some related works in this regard are Dickey and Fuller (1979), Kwiatkowski *et al.* (1992), Philips and Perron (1988), Breitung (2002), Basu *et al.* (2009), Cardinali and Nason (2018), van Delft *et al.* (2018). In the real data scenario, where the parametric form may itself be called in question, reliability of the tests for stationarity need not be taken for granted.

A very important time series example where studying stationarity property is of utmost importance, is the Markov time series generated by Markov Chain Monte Carlo (MCMC) methods, particularly in the Bayesian posterior context. Although in principle there exist many formal theories for addressing MCMC convergence, they are usually difficult to establish for realistic problems. As a result, plenty of empirical (mostly ad-hoc) methods emerged for diagnosis of convergence of the MCMC sample to the target posterior distribution, and many such methods are based on visualizing the graphical plots of the MCMC sample. The available empirical diagnostic tools have the ill reputation of give false impressions about convergence or non-convergence in realistic situations. Moreover, in reality, the target posteriors can often be multimodal, and in such cases, the performances of such diagnostic tools can be even poorer. For more about MCMC convergence diagnostics, see, for example, Gelman and Rubin (1992), Geweke (1992), Raftery and Lewis (1992), Robert (1995), Gilks and Roberts (1996), Cowles and Carlin (1996), Brooks and Gelman (1998), Brooks and Roberts (1998), Brooks *et al.* (2011), Robert and Casella (2004), Roy (2019).

Compared to the time series literature, tests for stationarity in the spatial and spatio-temporal statistics domains are much less developed, and confined to checking covariance stationarity only, under assumptions that are often difficult to check in practice. Some relevant works in this regard are Ephraty *et al.* (2001), Fuentes (2002), Guan *et al.* (2004), Fuentes (2005), Li *et al.* (2008), Jun and Genton (2012), Bandopadhyay and Rao (2017), Bandopadhyay *et al.* (2017).

In the point process literature, except some simple tests for complete spatial randomness (see, for example, O’Sullivan and Unwin (2003), Waller and Gotway (2004) and Schabenberger and Gotway (2005)), there does not seem to exist any formal method to test for Poisson versus non-Poisson point process, or stationarity versus nonstationarity.

Motivated by the aforementioned problems, we seek a general principle that can attempt to effectively address all such issues. Interestingly, the recursive Bayesian idea proposed in Roy and Bhattacharya (2020) to characterize infinite series, turned out to have fruitful extension to our current situations. Indeed, the recursive Bayesian concept of Roy and Bhattacharya (2020) enabled them to study convergence of infinite series whose convergence properties are hitherto unknown. One such infinite series is also a characterization of the most difficult unsolved problem of mathematics, namely, the Riemann hypothesis. The most surprising result obtained by Roy

and Bhattacharya (2020) is failure to accept Riemann hypothesis, based on their theory, method and implementation. Since the idea of Roy and Bhattacharya (2020) is primarily about studying deterministic infinite series, one may be left wondering how this can be useful from the statistical perspective. However, the key concept there is to view the deterministic terms of the series as realizations from some general stochastic process, then to relate convergence of the series to a quantity that can be interpreted as probability of convergence of the series under the stochastic process, and finally to build a recursive Bayesian procedure such that the posterior distribution of the probability of convergence tends to one if and only if the series converges and to zero if and only if it diverges.

From the above summary of the idea of Roy and Bhattacharya (2020) it can be perceived that the deterministic terms of the infinite series can be easily replaced with random elements if necessary. For study of stationarity and nonstationarity, we again relate stationarity to a quantity that admits interpretation as probability that the process is stationary, and apply the same concept of recursive Bayesian method for characterizations of stationarity and nonstationarity.

In the point process setup, we apply similar principles to characterize complete spatial randomness, using properties of Poisson point process. To characterize Poisson point process, we first need to characterize mutual independence among a set of random variables. Once we characterize such mutual independence, again using similar principles and recursive Bayesian concept as before, as we show, characterization of Poisson point process is not difficult to achieve. For mutual independence we make use of simple break-ups of joint distribution of random variables into products of conditional distributions and Bayesian nonparametrics based on Dirichlet process (Ferguson (1974)). The latter particularly improves computational efficiency.

Our Bayesian idea can be used in another seemingly unrelated setup, namely, determination of frequencies of oscillations of oscillating stochastic processes. The basic idea here is to first provide an appropriate bijective transformation to the data such that the transformed process takes values on $[0, 1]$. The transformed process can then be raised to some appropriate power such that the oscillations become as explicit as possible. Dividing up the interval $[0, 1]$ into appropriate sub-intervals, we consider the proportions of oscillations contained in the sub-intervals. These can then be related to the frequencies of oscillation of the underlying stochastic process, and again facilitates characterization with our recursive Bayesian principle. We characterize single and multiple frequencies, as well as infinite number of frequencies of oscillation.

The basic aim of this paper is to render our characterization theories amenable to practical applications. To this end, we provide ample illustrations of our methods and implementations with simulated and real data sets, in each of the aforementioned areas of statistics. Most of our codes are written in C, parallelised using MPI (Message Passing Interface), and implemented in parallel architectures. Some parallelized R codes are also used in conjunction with our parallel C codes. Very fast computation is the result of our efforts.

The rest of our article is structured as follows. We begin our treatise in Section 2 with some necessary definitions and prove results associated with them. With these, we elucidate the key concept behind our proposed ideas in Section 3, and then introduce our recursive Bayesian procedure for studying stationarity in Section 4. In Section 5, we characterize stationarity and nonstationarity using the recursive Bayesian procedure. Some relevant computational techniques and their theoretical validation are provided in Section 6, and issues related to discretization associated with our method are discussed in Section 7. Characterization of second order stationarity, that is stationarity of covariance structure, is considered in Section 8. Discussion of the role of non-recursive

Bayesian procedures for characterizations is provided in Section 9.

In Section 10, we provide detailed illustration of our theory on characterization of stationarity and nonstationarity with AR(1) models, along with comparisons with classical tests for stationarity. In Section 11, we illustrate our theory and methods on more complicated time series models, such as AR(2), ARCH(1) and GARCH(1,1). MCMC convergence diagnostics with our Bayesian method is considered in Section 12.

In Section 13 we illustrate detection of strict and covariance stationarity and nonstationarity in spatial setups, along with comparisons with existing tests for covariance stationarity. Section 14 is about application of our ideas in spatio-temporal contexts, with comparisons with existing tests for covariance stationarity. Applications to real spatial and spatio-temporal data sets are considered in Section 15.

In Section 16, using our main principles, we provide Bayesian characterizations of properties of point processes, such as complete spatial randomness, Poisson point processes along with stationarity and nonstationarity. As a necessary part of such characterizations, we also characterize mutual independence among a set of random variables, in the same section. In different subsections of the same section we illustrate our theories and methods with various instances of point processes.

Our Bayesian characterization associated with (multiple) frequency determination of oscillating stochastic processes is detailed in Section 17, and illustrated with many examples.

2 Requisite definitions and associated results – prelude to the key concept

Consider a stochastic process $\mathbf{X} = \{X_s : s \in \mathcal{S}\}$, where \mathcal{S} is some arbitrary index set. We assume that $\mathcal{S} = \cup_{i=1}^{\infty} \mathcal{M}_i$ such that \mathcal{M}_i are disjoint, and $\{X_s : s \in \mathcal{M}_i\}$ is stationary. In other words, we assume that \mathbf{X} is locally stationary. We show below that most stochastic processes are approximately locally stationary. For simplicity of exposition, we consider the case where s is one-dimensional; the higher-dimensional case is a simple generalization.

Theorem 1 *For any (s_1, \dots, s_m) , for $m \geq 1$, let F_{s_1, \dots, s_m} denote the joint distribution function of $(X_{s_1}, \dots, X_{s_m})$. Assume that for any (x_1, \dots, x_m) , F_{s_1, \dots, s_m} is differentiable in sufficiently small neighborhoods of (x_1, \dots, x_m) , and that for $i = 1, \dots, m$, $X_{s_i+h} = X_{s_i} + O_P(h)$, as $h \rightarrow 0$. Then for any (x_1, \dots, x_m) , $F_{s_1+h, \dots, s_m+h}(x_1, \dots, x_m) = F_{s_1, \dots, s_m}(x_1, \dots, x_m) + O_P(h)$, as $h \rightarrow 0$.*

Proof. Let us first assume that X_s are deterministic variables satisfying $X_{s_i+h} = X_{s_i} + O(h)$, as $h \rightarrow 0$, $i = 1, \dots, m$. Then by Taylor's series expansion up to the first order, using the above condition, reveals that $F_{s_1+h, \dots, s_m+h}(x_1, \dots, x_m) = F_{s_1, \dots, s_m}(x_1, \dots, x_m) + O(h)$. Hence, the result follows by an application of Theorem 7.15 of Schervish (1995). ■

Remark 2 *The condition $X_{s+h} = X_s + O_P(h)$, as $h \rightarrow 0$ is satisfied by stochastic processes X_s with almost surely differentiable paths, for example, Gaussian processes, with sufficiently smooth covariance structure (see, for example, Adler (1981), Adler and Taylor (2007)). Also, non-smooth processes that are mean square continuous, in the sense that $E(X_{s+h} - X_s)^2 \rightarrow 0$, as $h \rightarrow 0$, for any s , also satisfy the property. Furthermore, discrete processes such as Poisson processes satisfy*

the above property. Also note that the differentiability condition of F_{s_1, \dots, s_m} is satisfied by most distribution functions, including the step functions corresponding to discrete distributions.

Note that local stationarity does not imply that the entire process is even asymptotically stationary. However, as we show below, global stationarity is also possible under our setup. Our goal is to distinguish between global (asymptotic) stationarity and nonstationarity.

For all practical purposes, we shall consider realizations of \mathbf{X} at discrete index points, that is, points on the set $\tilde{\mathcal{S}} = \cup_{i=1}^{\infty} \mathcal{N}_i$, where \mathcal{N}_i is a discretization of \mathcal{M}_i and $\{X_s : s \in \mathcal{N}_i, |\mathcal{N}_i| = n_i\}$, where $|\mathcal{N}_i|$ is the cardinality of \mathcal{N}_i , is stationary. We assume that $|\mathcal{N}_i| \rightarrow \infty$, for each i . In particular, if s is one-dimensional, then $\mathcal{N}_i = \left\{s_r : \sum_{k=1}^{i-1} n_k \leq r \leq \sum_{k=1}^i n_k\right\}$, and $|\mathcal{N}_i| = n_i \rightarrow \infty$ for each i ; we set $n_0 = 0$.

In practice, one can not observe the entire stochastic process \mathbf{X} , even on the discrete set $\tilde{\mathcal{S}}$. Hence, let us assume that only $\mathbf{X}_K = \{X_s : s \in \cup_{i=1}^K \mathcal{N}_i\}$ has been observed, for sufficiently large K .

For any Borel set C , consider

$$\hat{P}_i(C) = n_i^{-1} \sum_{s \in \mathcal{N}_i} I(X_s \in C). \quad (2.1)$$

Now let

$$\begin{aligned} \tilde{P}_K(C) &= \frac{\sum_{s \in \cup_{i=1}^K \mathcal{N}_i} I(X_s \in C)}{\sum_{i=1}^K n_i} \\ &= \frac{\sum_{i=1}^K n_i \hat{P}_i(C)}{\sum_{i=1}^K n_i} = \sum_{i=1}^K \hat{p}_{iK} \hat{P}_i(C), \end{aligned} \quad (2.2)$$

where $\hat{p}_{ik} = n_i / \sum_{j=1}^K n_j$. By the Glivenko-Cantelli theorem for stationary random variables (see Stute and Schumann (1980))

$$\sup_C \left| \hat{P}_i(C) - P_i(C) \right| \xrightarrow{a.s.} 0, \text{ as } n_i \rightarrow \infty, \quad (2.3)$$

where $P_i(C)$ is the probability that any random variable in \mathcal{N}_i belongs to C . Note that $P_i(C)$ may itself be a random variable unless $\{X_s : s \in \mathcal{N}_i, |\mathcal{N}_i| = n_i\}$ is also ergodic. Randomness of $P_i(C)$ is not a cause for concern, however, for the methodology that we propose.

Let us now assume that

$$\hat{p}_{iK} = \frac{n_i}{\sum_{j=1}^K n_j} \rightarrow p_{iK} = \frac{p_i}{\sum_{j=1}^K p_j}, \quad (2.4)$$

as $n_j \rightarrow \infty$, for $j = 1, \dots, K$. Here $0 \leq p_i \leq 1$, such that $\sum_{i=1}^{\infty} p_i = 1$.

Let $P_{\infty}(C) = \sum_{i=1}^{\infty} p_i P_i(C)$. Then we have the following theorem.

Theorem 3

$$\lim_{K \rightarrow \infty} \lim_{n_i \rightarrow \infty, i=1, \dots, K} \sup_C \left| \tilde{P}_K(C) - P_{\infty}(C) \right| = 0, \text{ almost surely.} \quad (2.5)$$

Proof.

$$\begin{aligned}
& \sup_C \left| \tilde{P}_K(C) - P_\infty(C) \right| \\
&= \sup_C \left| \sum_{i=1}^K \hat{p}_{iK} \hat{P}_i(C) - \sum_{i=1}^K p_i P_i(C) - \sum_{i=K+1}^{\infty} p_i P_i(C) \right| \\
&\leq \sup_C \left| \sum_{i=1}^K \hat{p}_{iK} \hat{P}_i(C) - \sum_{i=1}^K p_i P_i(C) \right| + \sup_C \left| \sum_{i=K+1}^{\infty} p_i P_i(C) \right| \\
&\leq \sum_{i=1}^K p_i \left[\sup_C \left| \hat{P}_i(C) - P_i(C) \right| \right] + \sum_{i=1}^K \left[\sup_C \hat{P}_i(C) \right] |\hat{p}_{iK} - p_i| + \sum_{i=K+1}^{\infty} p_i \left[\sup_C P_i(C) \right].
\end{aligned} \tag{2.6}$$

Now, due to (2.3), given K ,

$$\sum_{i=1}^K p_i \left[\sup_C \left| \hat{P}_i(C) - P_i(C) \right| \right] \rightarrow 0, \text{ almost surely as } n_i \rightarrow \infty, i = 1, \dots, K.$$

Hence,

$$\lim_{K \rightarrow \infty} \lim_{n_i \rightarrow \infty, i=1, \dots, K} \sum_{i=1}^K p_i \left[\sup_C \left| \hat{P}_i(C) - P_i(C) \right| \right] = 0, \text{ almost surely.} \tag{2.7}$$

As $n_i \rightarrow \infty$ for $j = 1, \dots, K$ and $K \rightarrow \infty$, the second term of (2.6) can be shown to converge to zero in the following way:

$$\begin{aligned}
& \lim_{n_i \rightarrow \infty, i=1, \dots, K} \sum_{i=1}^K \left[\sup_C \hat{P}_i(C) \right] |\hat{p}_{iK} - p_i| \\
&\leq \lim_{n_i \rightarrow \infty, i=1, \dots, K} \sum_{i=1}^K |\hat{p}_{iK} - p_i| = \sum_{i=1}^K |p_{iK} - p_i| = \sum_{i=K+1}^{\infty} p_i \rightarrow 0, \text{ as } K \rightarrow \infty.
\end{aligned} \tag{2.8}$$

For the third term of (2.6), note that

$$\sum_{i=K+1}^{\infty} p_i \left[\sup_C P_i(C) \right] \leq \sum_{i=K+1}^{\infty} p_i \rightarrow 0, \text{ as } K \rightarrow \infty. \tag{2.9}$$

The result follows by combining (2.6), (2.7), (2.8) and (2.9). ■

Note that stationarity of the process \mathbf{X} is characterized by $P_i = P$ for $i = 1, 2, \dots$, in which case $P_\infty = P$. Observe that if $P_i = P_\infty$ for $i = 1, \dots, \infty$, it then follows that $P_\infty = P$. Asymptotic stationarity is characterized by $P_i = P$ for $i \geq i_0$, for some $i_0 > 1$. In this case, if $P_j = P_{i_0, \infty} = \frac{\sum_{i=i_0+1}^{\infty} p_i P_i}{\sum_{i=i_0+1}^{\infty} p_i}$, for $j > i_0$, then $P_i = P$ for $i > i_0$. On the other hand, if \mathbf{X} is nonstationary and not even asymptotically stationary, then $P_i \neq P_j$ for infinitely many $j \neq i$. The latter condition also implies that there does not exist $i_0 > 1$ such that $P_j = P_{i_0, \infty}$ for $j > i_0$. Hence, there exists no

$i_0 > 1$ such that $P_i = P$ for $i > i_0$.

Theorem 4 \mathbf{X} is stationary if and only if for $i \geq 1$, $\sup_C \left| \hat{P}_i(C) - \tilde{P}_K(C) \right| \rightarrow 0$ almost surely, as $n_i \rightarrow \infty$ satisfying (2.4), $i = 1, \dots, K$, $K \rightarrow \infty$.

Proof. Note that $\sup_C \left| \hat{P}_i(C) - \tilde{P}_K(C) \right| \leq \sup_C \left| \hat{P}_i(C) - P_\infty(C) \right| + \sup_C \left| \tilde{P}_K(C) - P_\infty(C) \right|$. The first part of the right hand side tends to zero almost surely as $n_i \rightarrow \infty$ satisfying (2.4), $i = 1, \dots, K$, $K \rightarrow \infty$, if and only if \mathbf{X} is stationary, and the second part tends to zero almost surely by Theorem 3. ■

Theorem 5 \mathbf{X} is nonstationary if and only if $\sup_C \left| \hat{P}_i(C) - \tilde{P}_K(C) \right| > 0$ almost surely, as $n_i \rightarrow \infty$ satisfying (2.4), $i = 1, \dots, K$, $K \rightarrow \infty$.

Proof. Note that

$$\left| \hat{P}_i(C) - \tilde{P}_K(C) \right| \geq \left| \left| \hat{P}_i(C) - P_\infty(C) \right| - \left| \tilde{P}_K(C) - P_\infty(C) \right| \right|. \quad (2.10)$$

By Theorem 3, for any $\epsilon_1 > 0$,

$$\left| \tilde{P}_K(C) - P_\infty(C) \right| < \epsilon_1, \quad (2.11)$$

for all C , for sufficiently large n_i satisfying (2.4) and sufficiently large K . Also,

$$\left| \hat{P}_i(C) - P_\infty(C) \right| \geq \left| |P_i(C) - P_\infty(C)| - \left| \hat{P}_i(C) - P_i(C) \right| \right|. \quad (2.12)$$

By (2.3), for any $\epsilon_2 > 0$, $\left| \hat{P}_i(C) - P_i(C) \right| < \epsilon_2$, for all C , as $n_i \rightarrow \infty$. But $|P_i(C) - P_\infty(C)| > 0$, at least for some C , since $P_i \neq P_j$ for infinitely many $j \neq i$. Since $\epsilon_2 (> 0)$ is arbitrary, it follows from these arguments and (2.12), that

$$\left| \hat{P}_i(C) - P_\infty(C) \right| > 0, \text{ for some } C, \text{ for sufficiently large } n_i. \quad (2.13)$$

Since $\epsilon_1 (> 0)$ in (2.11) is also arbitrary, combining (2.13), (2.11) and (2.10) it is evident that the right hand side of (2.10) is positive for some C for sufficiently large n_i satisfying (2.4) and sufficiently large K . Hence,

$$\sup_C \left| \hat{P}_i(C) - \tilde{P}_K(C) \right| > 0$$

almost surely, as $n_i \rightarrow \infty$ satisfying (2.4), $i = 1, \dots, K$, $K \rightarrow \infty$. ■

3 The key concept

Let $p_{j,n_j} = P \left(\sup_C \left| \hat{P}_j(C) - \tilde{P}_K(C) \right| \leq c_j \right)$. As will be seen later, this can be interpreted as the

probability that the underlying process is stationary when the observed data is $\mathbb{I} \left\{ \sup_C \left| \hat{P}_j(C) - \tilde{P}_K(C) \right| \leq c_j \right\}$.

Note that, for stationarity, due to Theorem 4, for $j = 1, \dots, K$, as $n_j \rightarrow \infty$, $K \rightarrow \infty$, the latter converges to one almost surely. Since $p_{j,n_j} = E \left[\mathbb{I} \left\{ \sup_C \left| \hat{P}_j(C) - \tilde{P}_K(C) \right| \leq c_j \right\} \right]$, uniform integrability leads one to expect that for $j \geq 1$, for any choice of the non-negative monotonically decreasing sequence $\{c_j\}_{j=1}^\infty$,

$$\begin{aligned} & \lim_{K \rightarrow \infty} \lim_{n_j \rightarrow \infty, j=1, \dots, K} p_{j,n_j} \\ &= \lim_{K \rightarrow \infty} \lim_{n_j \rightarrow \infty, j=1, \dots, K} P \left(\sup_C \left| \hat{P}_i(C) - \tilde{P}_K(C) \right| \leq c_j \right) \\ &= \lim_{K \rightarrow \infty} \lim_{n_j \rightarrow \infty, j=1, \dots, K} E \left[\mathbb{I} \left\{ \sup_C \left| \hat{P}_i(C) - \tilde{P}_K(C) \right| \leq c_j \right\} \right] \\ &= 1. \end{aligned}$$

Similarly, for nonstationarity, we expect, using Theorem 5 that for $j \geq j_0 \geq 1$,

$$\lim_{K \rightarrow \infty} \lim_{n_j \rightarrow \infty, j=1, \dots, K} p_{j,n_j} = 0$$

almost surely, for any choice of the non-negative monotonically decreasing sequence $\{c_j\}_{j=1}^\infty$.

In reality it is not known if p_{j,n_j} converges to zero or one, since it is not known if \mathbf{X} is stationary or nonstationary. Thus, we consider learning about p_{j,n_j} from the data \mathbf{X}_K and some appropriate prior on p_{j,n_j} in the form of the posterior $\pi(p_{j,n_j} | \mathbf{X}_K)$. As we will show,

$$\lim_{K \rightarrow \infty} \lim_{n_j \rightarrow \infty, j=1, \dots, K} \pi(p_{j,n_j} | \mathbf{X}_K) = 1, \text{ almost surely}$$

for $j \geq 1$ and any choice of the non-negative monotonically decreasing sequence $\{c_j\}_{j=1}^\infty$, characterizes stationarity of \mathbf{X} and

$$\lim_{K \rightarrow \infty} \lim_{n_j \rightarrow \infty, j=1, \dots, K} \pi(p_{j,n_j} | \mathbf{X}_K) = 0, \text{ almost surely}$$

for $j \geq j_0 \geq 1$, for any choice of the non-negative monotonically decreasing sequence $\{c_j\}_{j=1}^\infty$, characterizes nonstationarity of \mathbf{X} .

In Section 4 we devise a recursive Bayesian methodology that achieves the goal discussed above.

4 A recursive Bayesian procedure for studying stationarity

Since we view X_i as realizations from some random process, we first formalize the notion in terms of the relevant probability space. Let $(\Omega, \mathcal{A}, \mu)$ be a probability space, where Ω is the sample space, \mathcal{A} is the Borel σ -field on Ω , and μ is some probability measure. Let, for $i = 1, 2, 3, \dots$, $X_i : \Omega \mapsto \mathbb{R}$ be real valued random variables measurable with respect to the Borel σ -field \mathcal{B} on \mathbb{R} . As in Schervish (1995), we can then define a σ -field of subsets of \mathbb{R}^∞ with respect to which $X = (X_1, X_2, \dots)$ is measurable. Indeed, let us define \mathbb{B}^∞ to be the smallest σ -field containing

sets of the form

$$B = \left\{ X : X_{i_1} \leq r_1, X_{i_2} \leq r_2, \dots, X_{i_p} \leq r_p, \text{ for some } p \geq 1, \right. \\ \left. \text{some integers } i_1, i_2, \dots, i_p, \text{ and some real numbers } r_1, r_2, \dots, r_p \right\}.$$

Since B is an intersection of finite number of sets of the form $\{X : X_{i_j} \leq r_j\}; j = 1, \dots, p$, all of which belong to \mathcal{A} (since X_{i_j} are measurable) it follows that $X^{-1}(B) \in \mathcal{A}$, so that X is measurable with respect to $(\mathbb{R}^\infty, \mathbb{B}^\infty, P)$, where P is the probability measure induced by μ .

Alternatively, note that it is possible to represent any stochastic process $\{X_i : i \in \mathcal{I}\}$, for fixed i as a random variable $\omega \mapsto X_i(\omega)$, where $\omega \in \mathfrak{S}$; \mathfrak{S} being the set of all functions from \mathcal{I} into \mathbb{R} . Also, fixing $\omega \in \mathfrak{S}$, the function $i \mapsto X_i(\omega); i \in \mathcal{I}$, represents a path of $X_i; i \in \mathcal{I}$. Indeed, we can identify ω with the function $i \mapsto X_i(\omega)$ from \mathcal{I} to \mathbb{R} ; see, for example, Øksendal (2000), for a lucid discussion.

This latter identification will be convenient for our purpose, and we adopt this in this article. Note that the σ -algebra \mathcal{F} induced by X is generated by sets of the form

$$\{\omega : \omega(i_1) \in B_1, \omega(i_2) \in B_2, \dots, \omega(i_k) \in B_k\},$$

where $B_j \subset \mathbb{R}; j = 1, \dots, k$, are Borel sets in \mathbb{R} .

4.1 Development of the stage-wise likelihoods

Let $\{c_j\}_{j=1}^\infty$ be a non-negative decreasing sequence and

$$Y_{j,n_j} = \mathbb{I} \left\{ \sup_C \left| \hat{P}_j(C) - \tilde{P}_K(C) \right| \leq c_j \right\}. \quad (4.1)$$

Let, for $j \geq 1$,

$$P(Y_{j,n_j} = 1) = p_{j,n_j}. \quad (4.2)$$

Hence, the likelihood of p_{j,n_j} , given y_{j,n_j} , is given by

$$L(p_{j,n_j}) = p_{j,n_j}^{y_{j,n_j}} (1 - p_{j,n_j})^{1-y_{j,n_j}} \quad (4.3)$$

It is important to relate p_{j,n_j} to stationarity of the underlying series. Note that p_{j,n_j} is the probability that $\sup_C \left| \hat{P}_j(C) - \tilde{P}_K(C) \right|$ falls below c_j . Thus, p_{j,n_j} can be interpreted as the probability that the process \mathbf{X} is stationary when the data observed is Y_{j,n_j} . If \mathbf{X} is stationary, then due to Theorem 4 it is to be expected *a posteriori*, that for $j \geq 1$, for any non-negative decreasing sequence $\{c_j\}_{j=1}^\infty$,

$$p_{j,n_j} \rightarrow 1 \quad \text{as } n_j \rightarrow \infty, \text{ satisfying (2.4).} \quad (4.4)$$

Indeed, as we will formally show, condition (4.4) is both necessary and sufficient for stationarity of \mathbf{X} .

On the other hand, if \mathbf{X} is nonstationary, then there exists $j_0 \geq 1$ such that for every $j > j_0$, as $n_j \rightarrow \infty$ satisfying (2.4), $\sup_C \left| \hat{P}_j(C) - \tilde{P}_K(C) \right| > c_j$, for any non-negative decreasing sequence

$\{c_j\}_{j=1}^\infty$, due to Theorem 5. Here we expect, *a posteriori*, that

$$p_{j,n_j} \rightarrow 0 \quad \text{as } n_j \rightarrow \infty, \text{ satisfying (2.4),} \quad (4.5)$$

for $j \geq j_0 \geq 1$. Again, we will prove formally that the above condition is both necessary and sufficient for divergence.

In what follows we shall first construct a recursive Bayesian methodology that formally characterizes convergence and divergence in terms of formal posterior convergence related to (4.4) and (4.5).

4.2 Development of recursive Bayesian posteriors

We assume that $\{y_{j,n_j}; j = 1, 2, \dots\}$ is observed successively at stages indexed by j . That is, we first observe y_{1,n_1} , and based on our prior belief regarding the first stage probability, p_{1,n_1} , compute the posterior distribution of p_{1,n_1} given y_{1,n_1} , which we denote by $\pi(p_{1,n_1}|y_{1,n_1})$. Based on this posterior we construct a prior for the second stage, and compute the posterior $\pi(p_{2,n_2}|y_{2,n_2})$. We continue this procedure for as many stages as we desire. Details follow.

Consider the sequences $\{\alpha_j\}_{j=1}^\infty$ and $\{\beta_j\}_{j=1}^\infty$, where $\alpha_j = \beta_j = 1/j^2$ for $j = 1, 2, \dots$. At the first stage of our recursive Bayesian algorithm, that is, when $j = 1$, let us assume that the prior is given by

$$\pi(p_{1,n_1}) \equiv \text{Beta}(\alpha_1, \beta_1), \quad (4.6)$$

where, for $a > 0$ and $b > 0$, $\text{Beta}(a, b)$ denotes the Beta distribution with mean $a/(a+b)$ and variance $(ab)/\{(a+b)^2(a+b+1)\}$. Combining this prior with the likelihood (4.3) (with $j = 1$), we obtain the following posterior of p_{1,n_1} given y_{1,n_1} :

$$\pi(p_{1,n_1}|y_{1,n_1}) \equiv \text{Beta}(\alpha_1 + y_{1,n_1}, \beta_1 + 1 - y_{1,n_1}). \quad (4.7)$$

At the second stage (that is, for $j = 2$), for the prior of p_{2,n_2} we consider the posterior of p_{1,n_1} given y_{1,n_1} associated with the $\text{Beta}(\alpha_1 + \alpha_2, \beta_1 + \beta_2)$ prior. That is, our prior on p_{2,n_2} is given by:

$$\pi(p_{2,n_2}) \equiv \text{Beta}(\alpha_1 + \alpha_2 + y_{1,n_1}, \beta_1 + \beta_2 + 1 - y_{1,n_1}). \quad (4.8)$$

The reason for such a prior choice is that the uncertainty regarding convergence of the series is reduced once we obtain the posterior at the first stage, so that at the second stage the uncertainty regarding the prior is expected to be lesser compared to the first stage posterior. With our choice, it is easy to see that the prior variance at the second stage, given by

$$\{(\alpha_1 + \alpha_2 + y_{1,n_1})(\beta_1 + \beta_2 + 1 - y_{1,n_1})\} / \{(\alpha_1 + \alpha_2 + \beta_1 + \beta_2 + 1)^2(\alpha_1 + \alpha_2 + \beta_1 + \beta_2 + 2)\},$$

is smaller than the first stage posterior variance, given by

$$\{(\alpha_1 + y_{1,n_1})(\beta_1 + 1 - y_{1,n_1})\} / \{(\alpha_1 + \beta_1 + 1)^2(\alpha_1 + \beta_1 + 2)\}.$$

The posterior of p_{2,n_2} given y_{2,n_2} is then obtained by combining the second stage prior (4.8)

with (4.3) (with $j = 2$). The form of the posterior at the second stage is thus given by

$$\pi(p_{2,n_2}|y_{2,n_2}) \equiv \text{Beta}(\alpha_1 + \alpha_2 + y_{1,n_1} + y_{2,n_2}, \beta_1 + \beta_2 + 2 - y_{1,n_1} - y_{2,n_2}). \quad (4.9)$$

Continuing this way, at the k -th stage, where $k > 1$, we obtain the following posterior of p_{k,n_k} :

$$\pi(p_{k,n_k}|y_{k,n_k}) \equiv \text{Beta}\left(\sum_{j=1}^k \alpha_j + \sum_{j=1}^k y_{j,n_j}, k + \sum_{j=1}^k \beta_j - \sum_{j=1}^k y_{j,n_j}\right). \quad (4.10)$$

It follows from (4.10) that

$$E(p_{k,n_k}|y_{k,n_k}) = \frac{\sum_{j=1}^k \alpha_j + \sum_{j=1}^k y_{j,n_j}}{k + \sum_{j=1}^k \alpha_j + \sum_{j=1}^k \beta_j}; \quad (4.11)$$

$$\text{Var}(p_{k,n_k}|y_{k,n_k}) = \frac{(\sum_{j=1}^k \alpha_j + \sum_{j=1}^k y_{j,n_j})(k + \sum_{j=1}^k \beta_j - \sum_{j=1}^k y_{j,n_j})}{(k + \sum_{j=1}^k \alpha_j + \sum_{j=1}^k \beta_j)^2(1 + k + \sum_{j=1}^k \alpha_j + \sum_{j=1}^k \beta_j)}. \quad (4.12)$$

Since $\sum_{j=1}^k \alpha_j = \sum_{j=1}^k \beta_j = \sum_{j=1}^k \frac{1}{j^2}$, (4.11) and (4.12) admit the following simplifications:

$$E(p_{k,n_k}|y_{k,n_k}) = \frac{\sum_{j=1}^k \frac{1}{j^2} + \sum_{j=1}^k y_{j,n_j}}{k + 2 \sum_{j=1}^k \frac{1}{j^2}}; \quad (4.13)$$

$$\text{Var}(p_{k,n_k}|y_{k,n_k}) = \frac{(\sum_{j=1}^k \frac{1}{j^2} + \sum_{j=1}^k y_{j,n_j})(k + \sum_{j=1}^k \frac{1}{j^2} - \sum_{j=1}^k y_{j,n_j})}{(k + 2 \sum_{j=1}^k \frac{1}{j^2})^2(1 + k + 2 \sum_{j=1}^k \frac{1}{j^2})}. \quad (4.14)$$

5 Characterization of stationarity properties of the underlying process

Based on our recursive Bayesian theory we have the following theorem that characterizes stationarity of \mathbf{X} in terms of the limit of the posterior probability of p_{k,n_k} , as $n_k \rightarrow \infty$ satisfying (2.4) and $K \rightarrow \infty$. We also assume, for the sake of generality, that for any $\omega \in \mathfrak{S} \cap \mathfrak{N}^c$, where $\mathfrak{N} (\subset \mathfrak{S})$ has zero probability measure, the non-negative monotonically decreasing sequence $\{c_j\}_{j=1}^\infty$ depends upon ω , so that we shall denote the sequence by $\{c_j(\omega)\}_{j=1}^\infty$. In other words, we allow $\{c_j(\omega)\}_{j=1}^\infty$ to depend upon the corresponding data $X(\omega)$. Since $\sup_C \left| \hat{P}_j(C) - \tilde{P}_K(C) \right| \leq 1$ and tends to zero in the case of stationarity, there exists a monotonically decreasing sequence $\{c_j(\omega)\}_{j=1}^\infty$ such that for n_j ; $j = 1, \dots, K$ sufficiently large satisfying (2.4),

$$\sup_C \left| \hat{P}_j(C)(\omega) - \tilde{P}_K(C)(\omega) \right| \leq c_j(\omega), \text{ for } j \geq 1. \quad (5.1)$$

Theorem 6 For all $\omega \in \mathfrak{S} \cap \mathfrak{N}^c$, where \mathfrak{N} is some null set having probability measure zero, \mathbf{X} is stationary if and only if for any monotonically decreasing sequence $\{c_j(\omega)\}_{j=1}^\infty$,

$$\pi(\mathcal{N}_1|y_{k,n_k}(\omega)) \rightarrow 1, \quad (5.2)$$

as $k \rightarrow \infty$ and $n_j \rightarrow \infty$ for $j = 1, \dots, K$ satisfying (2.4) and $K \rightarrow \infty$, where \mathcal{N}_1 is any neighborhood of 1 (one).

Proof. Let, for $\omega \in \mathfrak{S} \cap \mathfrak{N}^c$, where \mathfrak{N} is some null set having probability measure zero, \mathbf{X} be stationary. Then, by (5.1), $\sup_C \left| \hat{P}_j(C)(\omega) - \tilde{P}_K(C)(\omega) \right| \leq c_j(\omega)$ for n_j sufficiently large satisfying (2.4), given any choice of the monotonically decreasing sequence $\{c_j(\omega)\}_{j=1}^\infty$. Hence, $y_{j,n_j}(\omega) = 1$ for sufficiently large n_j , satisfying (2.4), for $j \geq 1$. Hence, in this case, $\sum_{j=1}^k y_{j,n_j}(\omega) = k$. Also, $\sum_{j=1}^k \frac{1}{j^2} \rightarrow \frac{\pi^2}{6}$, as $k \rightarrow \infty$. Consequently, it is easy to see that

$$\mu_k = E(p_{k,n_k} | y_{k,n_k}(\omega)) \sim \frac{\frac{\pi^2}{6} + k}{k + \frac{\pi^2}{3}} \rightarrow 1, \text{ as } k \rightarrow \infty, \text{ and,} \quad (5.3)$$

$$\sigma_k^2 = Var(p_{k,n_k} | y_{k,n_k}(\omega)) \sim \frac{(\frac{\pi^2}{6} + k)(\frac{\pi^2}{6})}{(k + \frac{\pi^2}{3})^2(1 + k + \frac{\pi^2}{3})} \rightarrow 0 \text{ as } k \rightarrow \infty. \quad (5.4)$$

In the above, for any two sequences $\{a_k\}_{k=1}^\infty$ and $\{b_k\}_{k=1}^\infty$, $a_k \sim b_k$ indicates $\frac{a_k}{b_k} \rightarrow 1$, as $k \rightarrow \infty$. Now let \mathcal{N}_1 denote any neighborhood of 1, and let $\epsilon > 0$ be sufficiently small such that $\mathcal{N}_1 \supseteq \{1 - p_{k,n_k} < \epsilon\}$. Combining (5.3) and (5.4) with Chebychev's inequality ensures that (5.2) holds.

Now assume that (5.2) holds. Then for any given $\epsilon > 0$,

$$\pi(p_{k,n_k} > 1 - \epsilon | y_{k,n_k}(\omega)) \rightarrow 1, \text{ as } k \rightarrow \infty. \quad (5.5)$$

Hence,

$$E(p_{k,n_k} | y_{k,n_k}(\omega)) \rightarrow 1; \quad (5.6)$$

$$Var(p_{k,n_k} | y_{k,n_k}(\omega)) \rightarrow 0, \quad (5.7)$$

as $k \rightarrow \infty$. If \mathbf{X} is nonstationary, then there exists $j_0(\omega)$ such that for each $j \geq j_0(\omega)$, for sufficiently large n_j satisfying $\sup_C \left| \hat{P}_j(C)(\omega) - \tilde{P}_K(C)(\omega) \right| > c_j(\omega)$, for $j \geq j_0(\omega)$, for any choice of non-negative sequence $\{c_j(\omega)\}_{j=1}^\infty$ monotonically converging to zero. Hence, in this situation, $0 \leq \sum_{j=1}^k y_{j,n_j}(\omega) \leq j_0(\omega)$. Substituting this in (4.13) and (4.14), it is easy to see that, as $k \rightarrow \infty$,

$$E(p_{k,n_k} | y_{k,n_k}(\omega)) \rightarrow 0; \quad (5.8)$$

$$Var(p_{k,n_k} | y_{k,n_k}(\omega)) \rightarrow 0, \quad (5.9)$$

so that (5.6) is contradicted. \blacksquare

We now prove the following theorem that provides necessary and sufficient conditions for nonstationarity of \mathbf{X} in terms of the limit of the posterior probability of $p_{k,n_k}(\omega)$, as $n_k \rightarrow \infty$ satisfying (2.4).

Theorem 7 \mathbf{X} is nonstationary if and only if for any $\omega \in \mathfrak{S} \cap \mathfrak{N}^c$ where \mathfrak{N} is some null set having probability measure zero, for any choice of the non-negative, monotonically decreasing sequence

$$\{c_j(\omega)\}_{j=1}^\infty, \quad \pi(\mathcal{N}_0|y_{k,n_k}(\omega)) \rightarrow 1, \quad (5.10)$$

as $k \rightarrow \infty$ and $n_j \rightarrow \infty$, $j = 1, \dots, K$ satisfying (2.4), and $K \rightarrow \infty$, where \mathcal{N}_0 is any neighborhood of 0 (zero).

Proof. Assume that \mathbf{X} is nonstationary. Then there exists $j_0(\omega) \geq 1$ such that for every $j \geq j_0(\omega)$, $\sup_C |\hat{P}_j(C)(\omega) - \tilde{P}_K(C)(\omega)| > c_j(\omega)$, for sufficiently large n_j , for any choice of non-negative sequence $\{c_j(\omega)\}_{j=1}^\infty$ monotonically converging to zero. From the proof of the sufficient condition of Theorem 6 it follows that (5.8) and (5.9) hold. Let $\epsilon > 0$ be small enough so that $\mathcal{N}_0 \supseteq \{p_{k,n_k} < \epsilon\}$. Then combining Chebychev's inequality with (5.8) and (5.9) it is easy to see that (5.10) holds.

Now assume that (5.10) holds. Then for any given $\epsilon > 0$,

$$\pi(p_{k,n_k} < \epsilon | y_{k,n_k}(\omega)) \rightarrow 1, \text{ as } k \rightarrow \infty. \quad (5.11)$$

It follows that

$$E(p_{k,n_k} | y_{k,n_k}(\omega)) \rightarrow 0; \quad (5.12)$$

$$Var(p_{k,n_k} | y_{k,n_k}(\omega)) \rightarrow 0, \quad (5.13)$$

as $k \rightarrow \infty$.

If \mathbf{X} is stationary, then by Theorem 6, $\pi(\mathcal{N}_1 | y_{k,n_k}(\omega)) \rightarrow 1$ as $k \rightarrow \infty$, for all sequences $\{n_j\}_{j=1}^\infty$, so that $E(p_{k,n_k} | y_{k,n_k}(\omega)) \rightarrow 1$, which is a contradiction to (5.12). \blacksquare

6 Computation of the sup norm between empirical distribution functions associated with \hat{P}_j and \tilde{P}_K

In all practical applications that involves identifying stationarity or nonstationarity by our method, it is needed to compute the sup norms $\sup_C |\hat{P}_j(C) - \tilde{P}_K(C)|$; $j \geq 1$. For this purpose, it is sufficient to compute $\sup_{-\infty < x < \infty} |\hat{F}_j(x) - \tilde{F}_K(x)|$, where $\hat{F}_j(x)$ and $\tilde{F}_K(x)$ stand for the empirical distribution functions corresponding to \hat{P}_j and \tilde{P}_K . Lemma 8 provides the formula for the desired sup norm.

Lemma 8 *Let $\hat{F}_j(x)$ and $\tilde{F}_K(x)$ denote the empirical distribution functions corresponding to empirical probability distributions \hat{P}_j and \tilde{P}_K , respectively. Then it holds that*

$$\sup_{-\infty < x < \infty} |\hat{F}_j(x) - \tilde{F}_K(x)| = 1 - \tilde{F}_K(\hat{x}_j), \quad (6.1)$$

where $\hat{x}_j = \max \mathcal{N}_j$, provided that $\hat{x}_j \neq \max \{\cup_{k=1}^K \mathcal{N}_k\}$.

Proof. Since both $\hat{F}_j(x)$ and $\tilde{F}_K(x)$ are empirical distribution functions, their jumps occur at the order statistics associated with the sample data. Now, by inspection it can be seen that, if

$\hat{x}_j \neq \max \left\{ \bigcup_{k=1}^K \mathcal{N}_k \right\}$, then

$$|\hat{F}_j(\hat{x}_j) - \tilde{F}_K(\hat{x}_j)| = 1 - \tilde{F}_K(\hat{x}_j). \quad (6.2)$$

For the r -th order statistic value $x_{(t)}$, $t \geq 1$ such that $x_{(t)} \neq \hat{x}_j$, $|\hat{F}_j(\hat{x}_j) - \tilde{F}_K(\hat{x}_j)|$ is of the form $\left| \frac{\ell}{n_j} - \frac{r}{\sum_{k=1}^K n_k} \right|$, where $1 < \ell < n_j$, $1 < r < \sum_{k=1}^K n_k$. But, for $1 \leq m \leq \sum_{k=1}^K n_k$,

$$1 - \frac{m}{\sum_{k=1}^K n_k} \geq \left| \frac{\ell}{n_j} - \frac{r}{\sum_{k=1}^K n_k} \right|. \quad (6.3)$$

Since $1 - \tilde{F}_K(\hat{x}_j)$ in (6.2) is of the form $1 - \frac{m}{\sum_{k=1}^K n_k}$, it follows from (6.3) that (6.1) holds. ■

Remark 9 Lemma 8 gives the formula for the sup norm when $\hat{x}_j \neq \max \left\{ \bigcup_{k=1}^K \mathcal{N}_k \right\}$. In fact, (6.1) is no longer valid when $\hat{x}_j = \max \left\{ \bigcup_{k=1}^K \mathcal{N}_k \right\}$. Note that there exists exactly one $k \geq 1$ such that $\hat{x}_{j^*} = \max \left\{ \bigcup_{k=1}^K \mathcal{N}_k \right\}$. For that j^* , there is no direct formula for the sup norm, and it is desirable to compute the sup norm by evaluating the differences between the empirical distribution functions at all the sample order statistics. However, just for a single k , such elaborate computation is not worthwhile. Instead it makes sense to construct \hat{F}_{j^*} based on all the observations in \mathcal{N}_{j^*} except \hat{x}_{j^*} . Hence, if \tilde{x}_{j^*} is the maximum of $\mathcal{N}_{j^*} \setminus \{\hat{x}_{j^*}\}$, then in that case, $\sup_{-\infty < x < \infty} |\hat{F}_{j^*}(x) - \tilde{F}_K(x)| = 1 - \tilde{F}_K(\tilde{x}_{j^*})$, which is what we shall use in our practical applications.

7 Choice of the cardinality of \mathcal{N}_i

An important ingredient of our method, particularly tied to practical implementation, is the choice of the number of random variables in the sets \mathcal{N}_i . Recall that \mathcal{N}_i is discretization of an index set \mathcal{M}_i , on which s varies continuously, such that $\{X_s : s \in \mathcal{M}_i\}$ is stationary. Let the closure of \mathcal{M}_i , denoted by $\overline{\mathcal{M}_i}$, be compact.

Let the index $s \in \mathbb{R}^p$, for $p \geq 1$. For $j = 1, 2, \dots$, consider p -dimensional balls $B_p(c_j, r)$ with centers c_j and radius $r > 0$ such that for any $s \in \overline{\mathcal{M}_i}$, there exists $j \geq 1$ such that $s \in B_p(c_j, r)$. Then the set $\{B_p(c_j, \epsilon) : j \geq 1\}$ constitutes an open cover for $\overline{\mathcal{M}_i}$. By compactness, there exists a set $\{B_p(c_{j_k}, \epsilon) : k = 1, \dots, n_i\}$, for finite $n_i \geq 1$ such that $\overline{\mathcal{M}_i} \subseteq \bigcup_{k=1}^{n_i} B_p(c_{j_k}, \epsilon)$. It follows that

$$\text{Vol}(\overline{\mathcal{M}_i}) \leq \sum_{k=1}^{n_i} \text{Vol}(B_p(c_{j_k}, \epsilon)), \quad (7.1)$$

where for any set S , $\text{Vol}(S)$ denotes the volume of S . Since $\text{Vol}(B_p(c_{j_k}, \epsilon)) = \text{Vol}(B_p(\mathbf{0}, \epsilon))$, the p -dimensional ball with center $\mathbf{0}$, and since $\text{Vol}(B_p(\mathbf{0}, \epsilon)) = \frac{\pi^{p/2}}{\Gamma(p/2+1)} \epsilon^p$, it follows from (7.1) that

$$n_i \geq \left(\frac{\text{Vol}(\overline{\mathcal{M}_i})}{\epsilon^p} \right) \left(\frac{\Gamma(p/2+1)}{\pi^{p/2}} \right). \quad (7.2)$$

For example, if \mathcal{M}_i is a p -dimensional hypercube with $c_i (> 0)$ being the length of each edge, then

it follows from (7.2) that $n_i \geq \left(\frac{c_i}{\epsilon}\right)^p \left(\frac{\Gamma(p/2+1)}{\pi^{p/2}}\right)$. For example, if $p = 1$ and $c = 3\epsilon$, then $n \geq 1.5$; if $p = 2$ and $c = 3\epsilon$, then $n \geq 2.865$; $p = 3$ and $c = 3\epsilon$, implies $n \geq 6.446$, etc. Similar idea has been considered in Section 1.2.1 of Giraud (2015), in the context of large p . In our illustrations, the total number of observations are allocated to a substantially large number of cubes of dimensions one, two and three. Consequently, c/ϵ is not expected to be significantly larger than one. As such, we take care such that the cube containing the minimum number of observations has at least three observations.

8 Stationarity of covariance structure

Let $Y_{(s_1, s_2)} = X_{s_1} X_{s_2}$, $\mathcal{N}_{ih} = \{(s_1, s_2) \in \mathcal{N}_i : \|s_1 - s_2\| = h\}$, and $n_{ih} = |\mathcal{N}_{ih}|$.

$$\widehat{Cov}_{ih} = \frac{\sum_{(s_1, s_2) \in \mathcal{N}_{ih}} Y_{(s_1, s_2)}}{2n_{ih}} - \left(\frac{\sum_{s_1 \in \mathcal{N}_{ih}} X_{s_1}}{n_{ih}}\right) \left(\frac{\sum_{s_2 \in \mathcal{N}_{ih}} X_{s_2}}{n_{ih}}\right). \quad (8.1)$$

Noting that $Y_{(s_1, s_2)}$, where $(s_1, s_2) \in \mathcal{N}_i$, is stationary, it follows by the ergodic theorem that

$$\widehat{Cov}_{ih} \xrightarrow{a.s.} Cov_{ih} = Cov(X_{s_1}, X_{s_2}) \text{ where } \|s_1 - s_2\| = h. \quad (8.2)$$

Let

$$\widetilde{Cov}_{Kh} = \sum_{i=1}^K \tilde{p}_{iKh} \widehat{Cov}_{ih}, \quad (8.3)$$

where $\tilde{p}_{iKh} = n_{ih} / \sum_{j=1}^K n_{jh}$, with $\sum_{i=1}^\infty p_{ih} = 1$, and

$$Cov_{\infty, h} = \sum_{i=1}^\infty \tilde{p}_{ih} Cov_{ih}, \quad (8.4)$$

We assume that

$$\tilde{p}_{iKh} \rightarrow p_{iKh} = \frac{p_{ih}}{\sum_{j=1}^K p_{jh}}, \text{ as } n_{ih} \rightarrow \infty; i = 1, \dots, K. \quad (8.5)$$

Theorem 10 *Let*

$$\sum_{i=1}^\infty p_{ih} |Cov_{ih}| < \infty. \quad (8.6)$$

Then

$$\lim_{K \rightarrow \infty} \lim_{n_{ih} \rightarrow \infty; i=1, \dots, K} \left| \widetilde{Cov}_{Kh} - Cov_{\infty, h} \right| = 0. \quad (8.7)$$

Proof.

$$\left| \widetilde{Cov}_{Kh} - Cov_{\infty, h} \right| \leq \sum_{i=1}^K \left| \widehat{Cov}_{ih} \right| |\tilde{p}_{iKh} - p_{ih}| + \sum_{i=1}^K p_{ih} \left| \widehat{Cov}_{ih} - Cov_{ih} \right| + \sum_{K+1}^\infty p_i |Cov_{ih}|. \quad (8.8)$$

Due to (8.5), $\sum_{i=1}^K \left| \widehat{Cov}_{ih} \right| |\tilde{p}_{iKh} - p_{ih}| \rightarrow \sum_{i=1}^K |Cov_{ih}| |p_{iKh} - p_{ih}|$ as $n_{ih} \rightarrow \infty$; $i = 1, \dots, K$. Due to (8.6), $|Cov_{ih}| < L$, for some $L > 0$, for all $i \geq 1$. Hence, the first term on the right hand side of (8.8) is bounded above by $L \sum_{j=K+1}^{\infty} p_i$, which tends to zero, as $K \rightarrow \infty$, since $\sum_{i=1}^{\infty} p_i = 1$.

Using (8.2), it is seen that the second term of the right hand side of (8.8) also tends to zero as $n_{ih} \rightarrow \infty$; $i = 1, \dots, K$, satisfying (8.5) and as $K \rightarrow \infty$.

The last term on the right hand side of (8.8) tends to zero as $K \rightarrow \infty$ due to (8.6). ■

Note that the covariance structure of \mathbf{X} is stationary if and only if $Cov_{ih} = Cov_{\infty,h}$ for all $i \geq 1$ and all $h > 0$, and is nonstationary if and only if $Cov_{ih} \neq Cov_{\infty,h}$ for all $i \geq 1$ for some $h > 0$.

Theorem 11 *The covariance structure of \mathbf{X} is stationary if and only if for $i \geq 1$, for all $h > 0$,*

$$\lim_{K \rightarrow \infty} \lim_{n_{jh} \rightarrow \infty; j=1, \dots, K} \left| \widehat{Cov}_{ih} - \widetilde{Cov}_{Kh} \right| = 0.$$

Proof. Using Theorem 10, the proof follows in the same way as the proof of Theorem 4, with the probabilities replaced with the respective covariances. ■

Theorem 12 *The covariance structure of \mathbf{X} is nonstationary if and only if for $i \geq 1$, for some $h > 0$,*

$$\lim_{K \rightarrow \infty} \lim_{n_{jh} \rightarrow \infty; j=1, \dots, K} \left| \widehat{Cov}_{ih} - \widetilde{Cov}_{Kh} \right| > 0.$$

Proof. Using Theorem 10, the proof follows in the same way as the proof of Theorem 5, with the probabilities replaced with the respective covariances. ■

Now define $Y_{j,n_{jh}} = \mathbb{I} \left\{ \left| \widehat{Cov}_{ih} - \widetilde{Cov}_{Kh} \right| < c_{jh} \right\}$. Then the following characterization theorems hold, the proofs of which are the similar to those of Theorems 6 and 7.

Theorem 13 *For all $\omega \in \mathfrak{S} \cap \mathfrak{N}^c$, where \mathfrak{N} is some null set having probability measure zero, \mathbf{X} is stationary if and only if for any $h > 0$, there exists a monotonically decreasing sequence $\{c_{jh}(\omega)\}_{j=1}^{\infty}$ such that*

$$\pi(\mathcal{N}_1 | y_{k,n_{kh}}(\omega)) \rightarrow 1, \quad (8.9)$$

as $k \rightarrow \infty$ and $n_{jh} \rightarrow \infty$ for $j = 1, \dots, K$ satisfying (2.4) and $K \rightarrow \infty$, where \mathcal{N}_1 is any neighborhood of 1 (one).

Theorem 14 *\mathbf{X} is nonstationary if and only if for some $h > 0$, and for any $\omega \in \mathfrak{S} \cap \mathfrak{N}^c$ where \mathfrak{N} is some null set having probability measure zero, for any choice of the non-negative, monotonically decreasing sequence $\{c_{jh}(\omega)\}_{j=1}^{\infty}$,*

$$\pi(\mathcal{N}_0 | y_{k,n_{kh}}(\omega)) \rightarrow 1, \quad (8.10)$$

as $k \rightarrow \infty$ and $n_{jh} \rightarrow \infty$, $j = 1, \dots, K$ satisfying (2.4), and $K \rightarrow \infty$, where \mathcal{N}_0 is any neighborhood of 0 (zero).

9 Characterization of stationarity and nonstationarity using non-recursive Bayesian posteriors

Observe that it is not strictly necessary for the prior at any stage to depend upon the previous stage. Indeed, we may simply assume that $\pi(p_{j,n_j}) \equiv \text{Beta}(\alpha_j, \beta_j)$, for $j = 1, 2, \dots$. In this case, the posterior of p_{k,n_k} given y_{k,n_k} is simply $\text{Beta}(\alpha_k + y_{k,n_k}, 1 + \beta_k - y_{k,n_k})$. The posterior mean and variance are then given by

$$E(p_{k,n_k}|y_{k,n_k}(\omega)) = \frac{\alpha_k + y_{k,n_k}(\omega)}{1 + \alpha_k + \beta_k}; \quad (9.1)$$

$$\text{Var}(p_{k,n_k}|y_{k,n_k}(\omega)) = \frac{(\alpha_k + y_{k,n_k}(\omega))(1 + \beta_k - y_{k,n_k}(\omega))}{(1 + \alpha_k + \beta_k)^2(2 + \alpha_k + \beta_k)}. \quad (9.2)$$

Since $y_{k,n_k}(\omega)$ (or $y_{k,n_{k_h}}(\omega)$) converges to 1 or 0 as $n_k \rightarrow \infty$, accordingly as \mathbf{X} is stationary or nonstationary (or the covariance structure of \mathbf{X} is stationary or nonstationary), it is easily seen, provided that $\alpha_k \rightarrow 0$ and $\beta_k \rightarrow 0$ as $k \rightarrow \infty$, that (9.1) converges to 1 (respectively, 0) if and only if \mathbf{X} is (covariance) stationary (respectively, (covariance) nonstationary). Importantly, if we choose $\alpha_k = \beta_k = 0$ for all $k \geq 1$, then $k \rightarrow \infty$ is no longer needed, and the results continue to hold if $n_k \rightarrow \infty$.

Thus, characterization of stationarity or nonstationarity of \mathbf{X} is possible even with the non-recursive approach. Indeed, note that the prior parameters α_k and β_k are more flexible compared to those associated with the recursive approach. This is because, in the non-recursive approach we only require $\alpha_k \rightarrow 0$ and $\beta_k \rightarrow 0$ as $k \rightarrow \infty$, so that convergence of the series $\sum_{j=1}^{\infty} \alpha_j$ and $\sum_{j=1}^{\infty} \beta_j$ are not necessary, unlike the recursive approach. However, choosing α_k and β_k to be of sufficiently small order ensures much faster convergence of the posterior mean and variance as compared to the recursive approach.

Unfortunately, an important drawback of the non-recursive approach is that it does not admit extension to the case of general oscillatory stochastic processes. On the other hand, as we show subsequently, the principles of our recursive theory can be easily adopted to develop a Bayesian theory for determining (multiple) frequencies of oscillating stochastic processes. In other words, the recursive approach seems to be more powerful from the perspective of development of a general Bayesian principle for learning about the basic characteristics of the underlying stochastic process. Moreover, as our examples demonstrate, the recursive posteriors converge sufficiently fast to the correct degenerate distributions, obviating the need to consider the non-recursive approach. Consequently, we do not further pursue the non-recursive approach in this article but reserve the topic for further investigation in the future.

10 First illustration: AR(1) model

Let us consider the following AR(1) model: $X_t = \rho X_{t-1} + \epsilon_t$; $t \geq 1$, where $\epsilon_t \stackrel{iid}{\sim} N(0, 1)$, and $X_0 \sim U(-1, 1)$, the uniform distribution on $(-1, 1)$. It is well-known that $\{X_t : t \geq 1\}$ is (asymptotically) stationary if and only if $|\rho| < 1$. We illustrate the performance of our methodology after generating the data from the above AR(1) model for various values of ρ , which we pretend to be unknown for illustration. In particular, we consider three different setups in this regard. In the first

setup, we consider samples of sizes 2×10^8 from the AR(1) model, and assume that the form of the true model is known, and that only ρ is unknown. In the second setup, we generate samples of sizes 2500 from the AR(1) model, and assume as before that only ρ is unknown. In the last setup, we draw samples of sizes 2500 from the AR(1) model, and assume that the entire data-generating model is unknown.

10.1 Case 1: Large sample size, form of the model known

10.1.1 Sample size

We draw samples of sizes 2×10^8 from the AR(1) model for various values of ρ and evaluate the performance of our Bayesian methodology, setting $n = 10^4$ and $K = 2 \times 10^4$.

10.1.2 Construction of bound

An important ingredient of our proposed method is the construction of the bounds $c_j(\omega)$. In this case, we construct the bounds as follows. We first draw a sample of size 2×10^8 from the AR(1) model with $\rho = 0.99999$. With this sample, for $j = 1, \dots, K$, we form the sup norms $\tilde{c}_j = \sup_{-\infty < x < \infty} |\hat{F}_j(x) - \tilde{F}_K(x)|$ according to Lemma 8 and Remark 9. We then set c_j as

$$c_j = \tilde{c}_j + 10^6 \times (0.99999 - |\hat{\rho}|) / \log(\log(j+1)), \quad (10.1)$$

where $\hat{\rho}$ is the maximum likelihood estimator (MLE) of ρ based on the observed sample. If the MLE of ρ does not exist, we set $\hat{\rho} \equiv 1$.

To explain the strategy behind (10.1), note that for $\rho = 0.99999$, the AR(1) process, although stationary, is very close to nonstationarity. So, for any value of ρ such that $|\rho| < 0.99999$, \tilde{c}_j is expected to be larger than c_j . Hence, in such cases, stationarity is to be expected. On the other hand, if $|\rho| \geq 1$, \tilde{c}_j is expected to be smaller than c_j , so that nonstationarity is implied. For simplicity we assume that values of ρ such that $0.99999 < |\rho| < 1$ are not of interest.

To further improve the bound, we add the quantity $10^6 \times (0.99999 - |\hat{\rho}|) / \log(\log(j+1))$ to \tilde{c}_j . The significance of this addition is as follows. If $|\hat{\rho}| < 0.99999$, this quantity is positive but tends to zero at a slow rate. This enhances the conclusion of stationarity. Similarly, if $|\hat{\rho}| > 0.99999$, the quantity is negative and tends to zero slowly, favouring nonstationarity. Multiplication with 10^6 inflates the quantity for more prominence.

10.1.3 Implementation

Note that at each stage j , we need to compute the sup norm given by Lemma 8 (also, Remark 9). This requires evaluation of \tilde{F}_K at \hat{x}_j (or \tilde{x}_{j*}). We carry out this evaluations by splitting the summations of the indicator functions associated with \tilde{F}_K on 104 parallel cores on a VMWare, and obtaining the final result on a single node, which also carries out the iterative procedure. The entire exercise takes about 6 minutes in the case of stationarity and about 3 minutes in the case of nonstationarity.

10.1.4 Results

We implement our method when the data is generated from the AR(1) model with ρ randomly selected from $U(-1, 1)$, and with ρ taking the values 0.99, 0.995, 0.999, 0.9999, 1, 1.00005, 1.05 and 2. Figure 10.1 shows that in all the cases, our method correctly detects stationarity and nonstationarity. That even with such subtle differences among the true values of ρ our method performs so well, is quite encouraging.

10.2 Case 2: Relatively small sample size, form of the model known

10.2.1 Sample size

We draw samples of sizes 2500 from the AR(1) model for those values of ρ as in Section 10.1 and evaluate the performance of our Bayesian methodology, setting $n = 50$ and $K = 50$.

10.2.2 Construction of bound

In this case, we choose the basic form of the bounds in a similar manner as in Section 10.1, but make it adaptive with the iterations to suit the small sample situation.

As before, we first draw a sample of size 2×10^8 from the AR(1) model with $\rho = 0.99999$. With this sample, for $j = 1, \dots, K$, we form the sup norms $\tilde{c}_j = \sup_{-\infty < x < \infty} |\hat{F}_j(x) - \tilde{F}_K(x)|$ according to Lemma 8 and Remark 9. We then set c_j as

$$c_j = \tilde{c}_j + \hat{C}_j \times (0.99999 - |\hat{\rho}| + \hat{\epsilon}_j) / \log(\log(j + 1)), \quad (10.2)$$

where $\hat{C}_1 = 1$, $\hat{\epsilon}_1 = 0$, and for $j > 1$, we adaptively modify these values as follows:

- If $|\hat{\rho}| > 0.9985$,
 1. If $y_j = 1$, then $\hat{\epsilon}_{j+1} = \hat{\epsilon}_j + 0.001$ and $\hat{C}_{j+1} = \hat{C}_j + 1$.
 2. If $y_j = 0$, then $\hat{\epsilon}_{j+1} = \hat{\epsilon}_j - 0.001$ and $\hat{C}_{j+1} = \hat{C}_j + 1$.
- If $0.9955 < |\hat{\rho}| \leq 0.9985$,
 1. $y_j = 1$, then $\hat{\epsilon}_{j+1} = \hat{\epsilon}_j + 0.01$ and $\hat{C}_{j+1} = \hat{C}_j + 1$.
 2. $y_j = 0$, then $\hat{\epsilon}_{j+1} = \hat{\epsilon}_j - 0.01$ and $\hat{C}_{j+1} = \hat{C}_j + 1$.
- If $0 < |\hat{\rho}| \leq 0.9955$,
 1. If $y_j = 1$, then $\hat{\epsilon}_{j+1} = \hat{\epsilon}_j + 0.05$ and $\hat{C}_{j+1} = \hat{C}_j + 1$.
 2. If $y_j = 0$, then $\hat{\epsilon}_{j+1} = \hat{\epsilon}_j - 0.05$ and $\hat{C}_{j+1} = \hat{C}_j + 1$.

To appreciate the above strategy, first note that for small samples, the MLE of ρ need not be adequately close to the true value of ρ , and hence we need to add a quantity $\hat{\epsilon}_j$ to make up for the inadequacy. We select $\hat{\epsilon}_j$ adaptively, increasing its value for the next iteration if $y_j = 1$, so that in the next iteration stationarity is preferred, given the current value of y_j . If $y_j = 0$ in the current iteration, we decrease the current value of $\hat{\epsilon}_j$, so that nonstationarity is favoured in the next

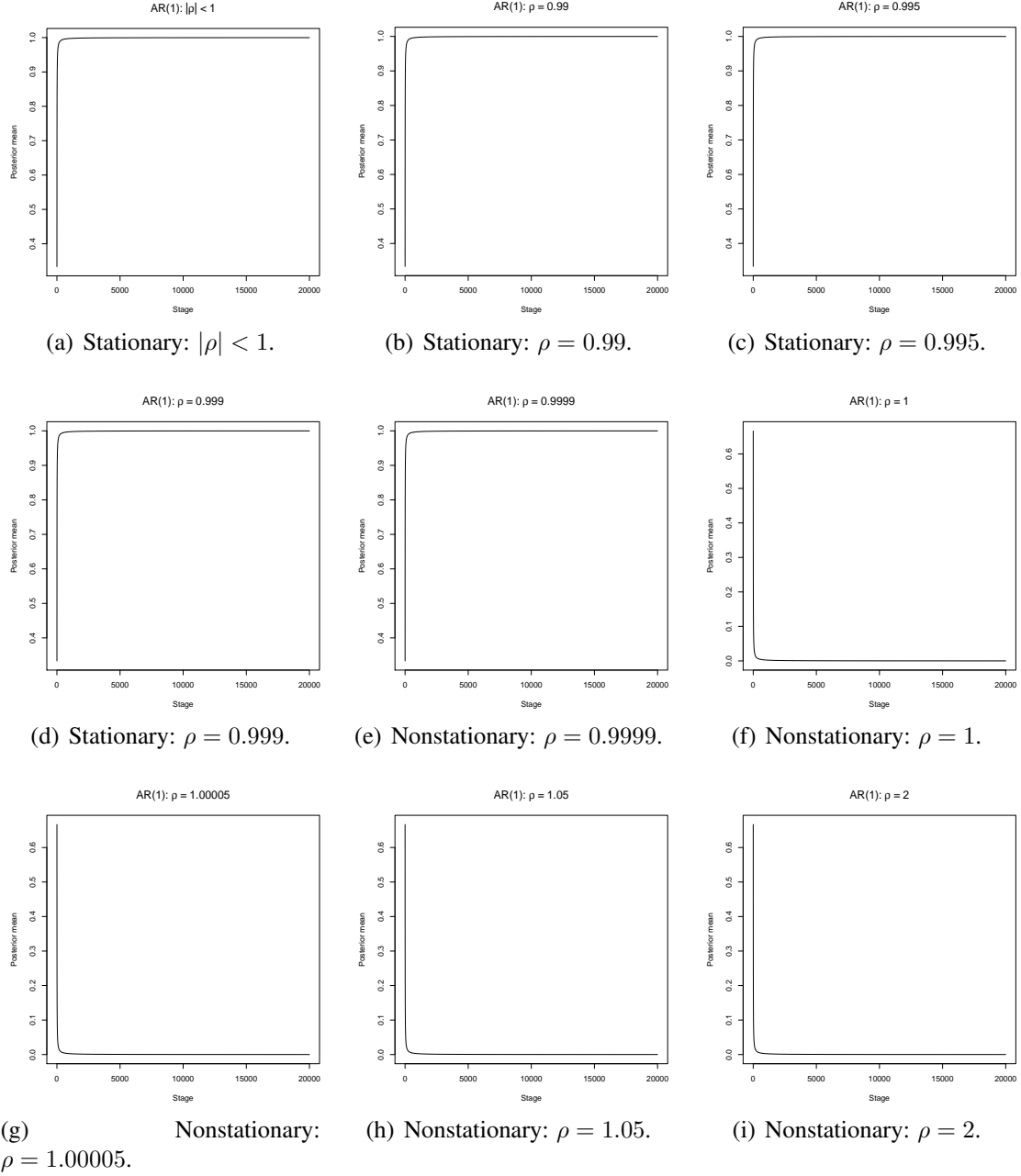


Figure 10.1: Parametric AR(1) example with $K = 20000$ and $n = 10000$.

iteration. We also increase the value of \hat{C}_j by one, at every iteration, rather than keeping it constant over the iterations. Thus, the prominence of the quantity $\hat{C}_j \times (0.99999 - |\hat{\rho}| + \hat{\epsilon}_j) / \log(\log(j+1))$ increases with the iterations.

The increment and decrement of $\hat{\epsilon}_j$ depends upon the magnitude of $\hat{\rho}$. If $|\hat{\rho}| > 0.9985$, that is, when the model is close to nonstationarity, we increase/decrease $\hat{\epsilon}_j$ by 0.001 only, since larger quantities, if added, can wrongly indicate stationarity.

When $0.9955 < |\hat{\rho}| \leq 0.9985$, we consider adding/subtracting 0.01 to $\hat{\epsilon}_j$; this larger quantity is expected to make up for the uncertainty associated with stationarity and nonstationarity when $0.9955 < |\hat{\rho}| \leq 0.9985$.

On the other hand, when $0 < |\hat{\rho}| \leq 0.9955$, we add/subtract 0.05 to $\hat{\epsilon}_j$, since we expect our algorithm to favour stationarity in this situation. The choice 0.05, which is larger than the quantities in the previous cases, is expected to facilitate diagnosis of stationarity.

10.2.3 Implementation

The implementation remains the same as before. For this small sample, even with 2 cores, the results are delivered almost instantly.

10.2.4 Results

As before, we implement our method when the data is generated from the AR(1) model with ρ randomly selected from $U(-1, 1)$, and with ρ taking the values 0.99, 0.995, 0.999, 0.9999, 1, 1.00005, 1.05 and 2. Figure 10.2 shows that, except in the case where the true value of ρ is 0.9999, our method correctly detects stationarity and nonstationarity. That even with such small sample, and with such subtle differences among the true values of ρ , our method performs well, is quite encouraging, despite its fallibility at $\rho = 0.9999$. Indeed, with such small sample, correct detection of stationarity in the case of so subtle difference with nonstationarity is perhaps not to be expected.

10.3 Case 3: Relatively small sample size, form of the model unknown

10.3.1 Sample size

We draw samples of sizes 2500 from the AR(1) model for those values of ρ as in Sections 10.1 and 10.2 and evaluate the performance of our Bayesian methodology, setting $n = 50$ and $K = 50$, assuming that the model itself is unknown.

10.3.2 Construction of bound

Since we assume now that the model itself is unknown, there is no provision of obtaining the MLE of ρ and constructing bounds on its basis. We also can not compute \tilde{c}_j , since it requires knowledge of the underlying model. Hence, in the absence of such information, we set

$$c_j = \hat{C}_j / \log(j+1), \quad (10.3)$$

where $\hat{C}_1 = 1$, and for $j > 1$, $\hat{C}_j = \hat{C}_{j-1} + 0.05$ if $y_{j-1} = 1$ and $\hat{C}_j = \hat{C}_{j-1} - 0.05$ if $y_{j-1} = 0$.

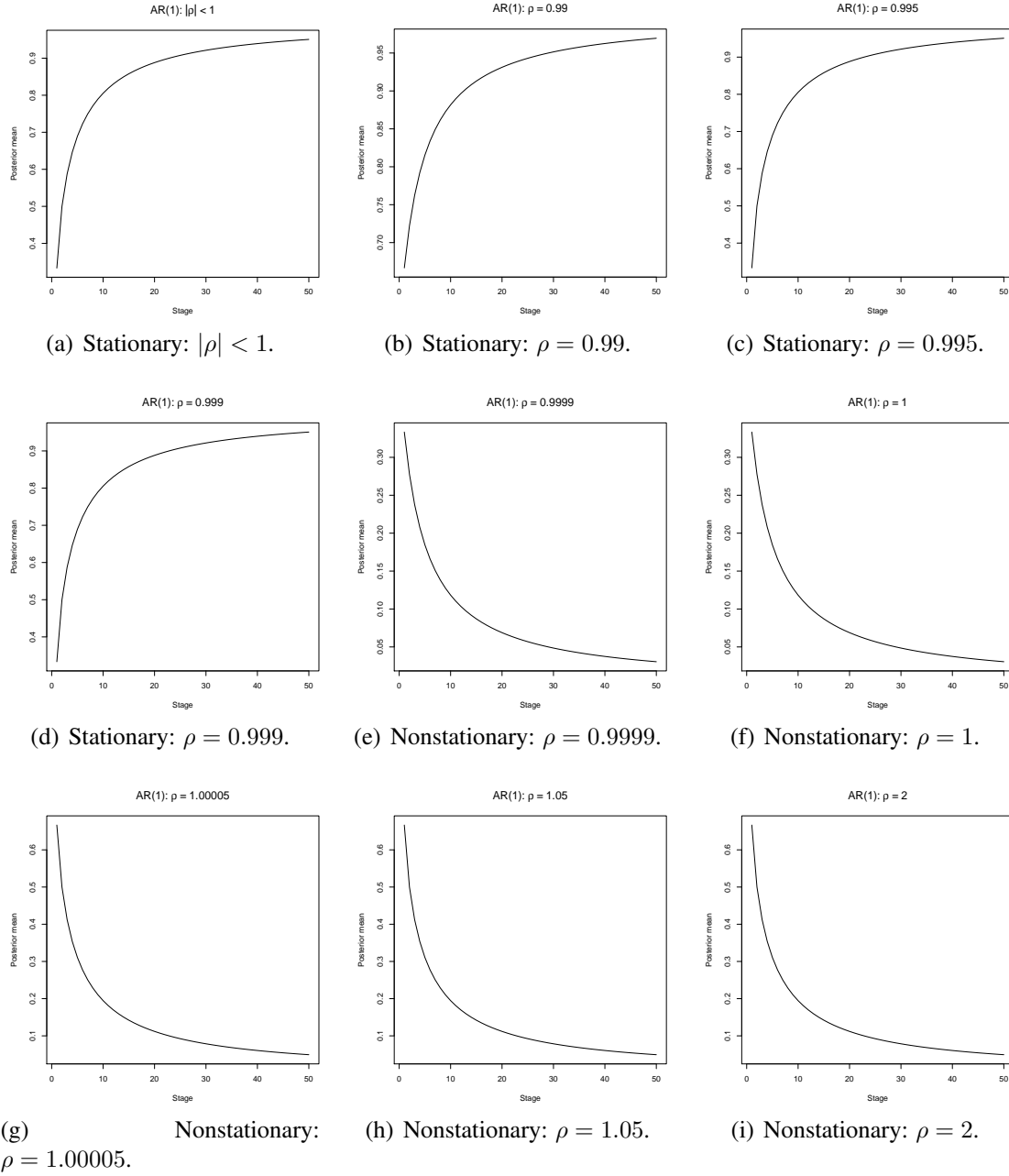


Figure 10.2: Parametric AR(1) example with $K = 50$ and $n = 50$.

Thus, as before, we favour stationarity at the next stage if at the current stage stationarity is favoured ($y_j = 1$) and nonstationarity otherwise. Note that unlike the previous cases, we have considered $\log(j+1)$ instead of $\log(\log(j+1))$. This faster rate turned out to be more appropriate in this situation of very less information about the true model.

10.3.3 Implementation

The implementation remains the same as before, only that here it is much simpler because of the simple structure of the bound. Again, for this small sample, even with 2 cores, the results are delivered almost instantaneously.

10.3.4 Results

As before, we implement our method when the data is generated from the AR(1) model with ρ randomly selected from $U(-1, 1)$, and with ρ taking the values 0.99, 0.995, 0.999, 0.9999, 1, 1.00005, 1.05 and 2. Figure 10.3 shows that, again except in the case where the true value of ρ is 0.9999, our method correctly detects stationarity and nonstationarity, albeit in a less precise manner as in Figure 10.2. That even with such small sample, with no assumption about the true model, and with such subtle differences among the true values of ρ , our method performs well, is quite encouraging, again, despite its fallibility at $\rho = 0.9999$, which is perhaps not expected to be detected correctly in this situation of so less information.

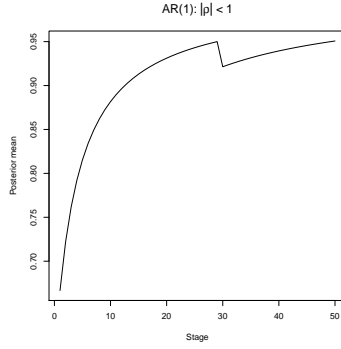
10.3.5 Comparison with classical tests of nonstationarity

To test stationarity of AR(1) model, there are well-known classical hypotheses tests, namely, the augmented Dickey-Fuller (ADF) test (Dickey and Fuller (1979)), the Philips-Perron (PP) test (Philips and Perron (1988)), and the Kwiatkowski, Phillips, Schmidt, Shin (KPSS) test (Kwiatkowski *et al.* (1992)).

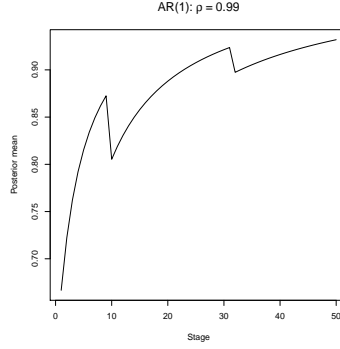
Researchers have noticed that the first two tests, PP and ADF, are not very efficient in distinguishing between stationarity and nonstationarity when the process is stationary, but at the verge of stationarity and nonstationarity. Indeed, when we apply these tests on our datasets with sample size 2500, we find that these two tests correctly determines stationarity/nonstationarity of the process when ρ is randomly chosen between $(-1, 1)$, $\rho = 0.99$ and $\rho = 0.995$, at the 5% level of significance, but fails when $\rho = 0.999$, 0.9999 and 1.05. However, both these tests correct conclude nonstationarity when $\rho = 1$ and 1.00005. For $\rho = 2$, both the tests turn out to be inapplicable.

On the other hand, at the 5% level of significance, the KPSS test provides correct answers whenever $|\rho| < 1$, but fails when $\rho \geq 1$.

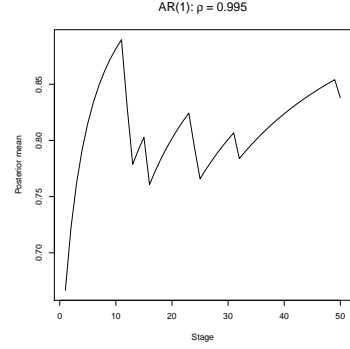
Thus, our proposed method outperforms all the three existing popular methods of testing stationarity in AR(1) models. Here we emphasize that the testing methods ADF, PP and KPSS are particularly designed to detect stationarity in autoregressive models, while ours is a completely general method. That our method still managed to outperform the existing specialized testing methods, is very encouraging.



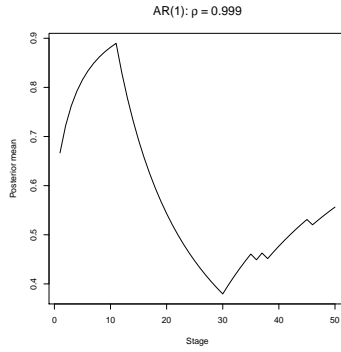
(a) Stationary: $|\rho| < 1$.



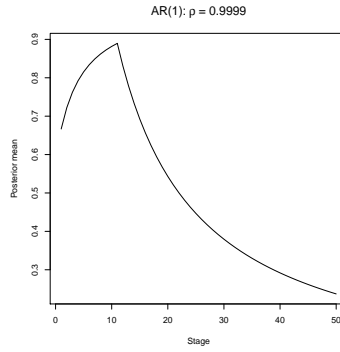
(b) Stationary: $\rho = 0.99$.



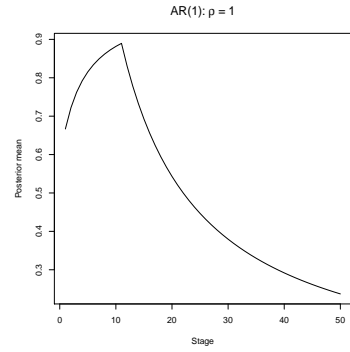
(c) Stationary: $\rho = 0.995$.



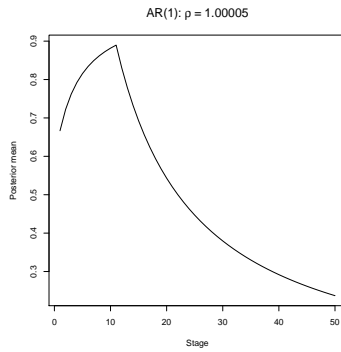
(d) Stationary: $\rho = 0.999$.



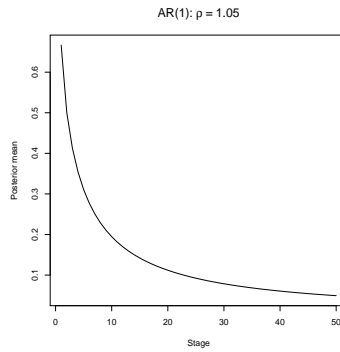
(e) Stationary: $\rho = 0.9999$.



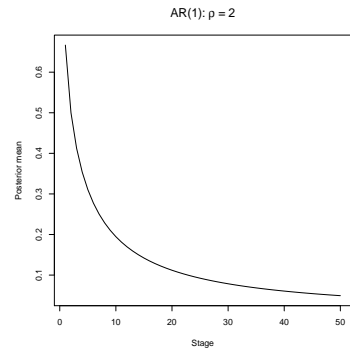
(f) Nonstationary: $\rho = 1$.



(g) Nonstationary: $\rho = 1.00005$.



(h) Nonstationary: $\rho = 1.05$.



(i) Nonstationary: $\rho = 2$.

Figure 10.3: Nonparametric AR(1) example with $K = 50$ and $n = 50$.

11 Second illustration: AR(2), ARCH(1) and GARCH(1,1) models

We now test our ideas on relatively more complex time series models. In particular, we consider autoregressive models of order 2 (AR(2)), first order autoregressive conditional heteroscedastic model (ARCH(1)) and generalized ARCH of order one (GARCH(1,1)). We consider samples of size 2500 for our investigation, since the relatively small sample size, as we observed in the context of AR(1), can pose beneficial challenge to our Bayesian method.

11.1 Application to AR(2)

The AR(2) model is given by

$$x_t = \alpha x_{t-1} + \beta x_{t-2} + \epsilon_t; \quad t = 1, 2, \dots, \quad (11.1)$$

where we set $x_1 = x_2 = 0$ and $\epsilon_t \stackrel{iid}{\sim} N(0, 1)$, for $t = 1, 2, \dots$. The necessary and sufficient conditions for stationarity of the AR(2) model (11.1) are given by (see, for example, Shumway and Stoffer (2006))

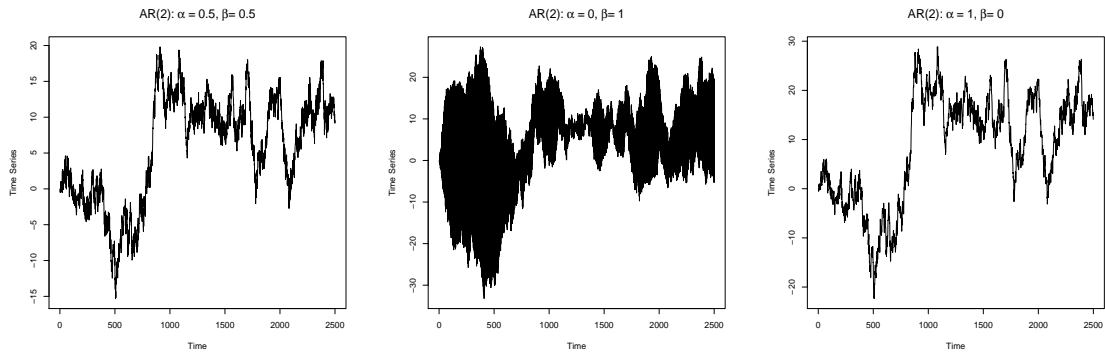
$$\begin{aligned} \alpha + \beta &< 1; \\ \beta - \alpha &< 1; \\ \beta &> -1. \end{aligned} \quad (11.2)$$

We simulate samples of size 2500 from (11.1) with various fixed values of α and β that satisfy and do not satisfy (11.2), and apply our Bayesian procedure to ascertain stationarity and nonstationarity, with the bound of the form (10.3), starting with $\hat{C}_1 = 1$. We initially consider ($n = 50, K = 50$) but in a few nonstationary cases ($(\alpha = 1, \beta = 0)$, $(\alpha = 0, \beta = 1)$ and $(\alpha = 0.5, \beta = 0.5)$) this failed to work satisfactorily, since a relatively large value of n in the context of relatively small sample size has the tendency to create overlaps among neighboring regions of local stationarity, in effect, destroying local stationarity which is at the heart of our Bayesian procedure. This happens when the underlying time series diverges slowly, as in the aforementioned values of (α, β) . Figure 11.1 captures such behaviours of such slowly diverging nonstationary processes in comparison to fast diverging nonstationary processes.

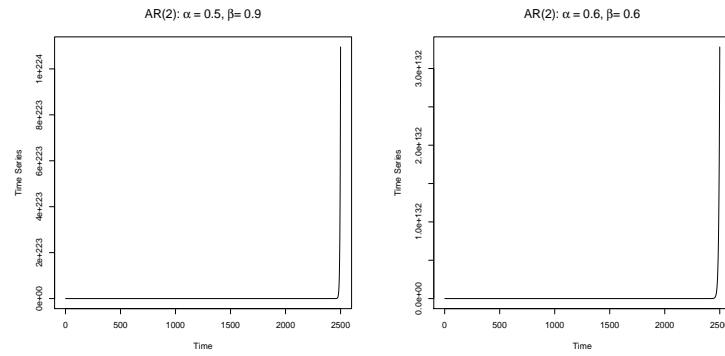
On the other hand, the choice ($n = 5, K = 500$) turned out to work very well in all the cases that we considered. Figure 11.2, depicting the results of our Bayesian method for various values of α and β for ($n = 5, K = 500$), shows that all the stationarity and nonstationarity situations are correctly identified.

11.2 Application to ARCH(1)

The ARCH models introduced by Engle (1982) attempts to take into account the heteroscedasticity of financial time series, which is often ignored by other popular financial models such as Black-Scholes (Black and Scholes (1973)) and the Ornstein-Uhlenbeck process (Ornstein and Uhlenbeck (1930)). In the ARCH(p) model, the conditional variance is modeled as an autoregressive process



(a) Slow divergence: $\alpha = 0.5$, $\beta = 0.5$. (b) Slow divergence: $\alpha = 0$, $\beta = 1$. (c) Slow divergence: $\alpha = 1$, $\beta = 0$.



(d) Fast divergence: $\alpha = 0.5$, $\beta = 0.9$. (e) Fast divergence: $\alpha = 0.6$, $\beta = 0.6$.

Figure 11.1: Slow and fast divergence tendencies of AR(2) model for several values of α and β .

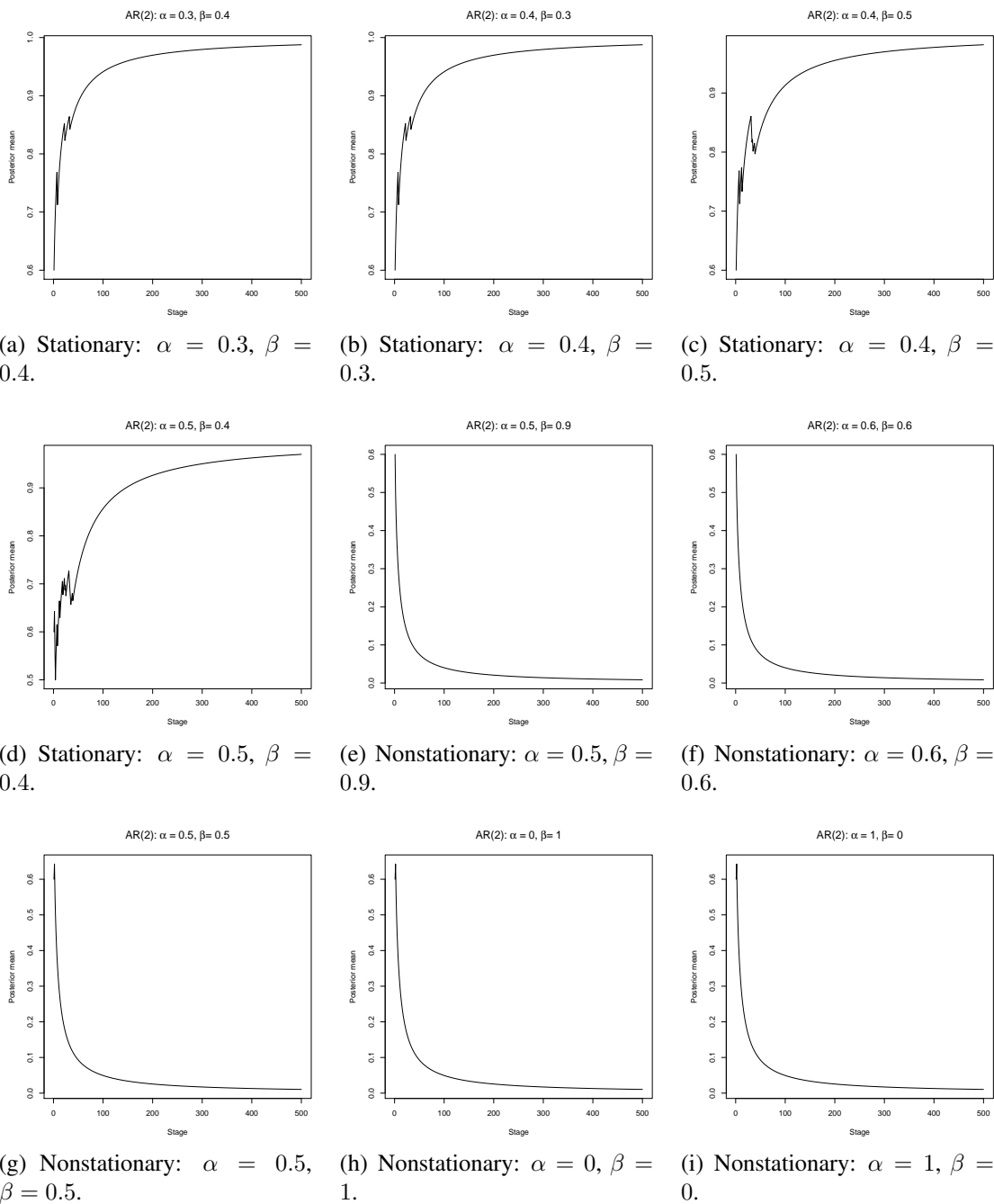


Figure 11.2: Nonparametric AR(2) example with $K = 500$ and $n = 5$.

of order p . For details on ARCH models, see Bera and Higgins (1993), Giraitis *et al.* (2005), Straumann (2005).

The ARCH(1) model is of the following form: for $t = 1, 2, \dots$,

$$\begin{aligned} x_t &= \epsilon_t \sigma_t \\ \sigma_t^2 &= \omega + \alpha x_{t-1}^2, \end{aligned} \quad (11.3)$$

where $\omega > 0$, $\alpha \geq 0$ and $\epsilon_t \stackrel{iid}{\sim} N(0, 1)$, for $t = 1, 2, \dots$. The necessary and sufficient condition for stationarity of (11.3) is $0 < \alpha < 1$. We set $\omega = 1$ and $x_1 = 0$ for our purpose.

As in the AR(2) situations, here we considered $n = 5$, $K = 500$, and the bound (10.3) with $\hat{C}_1 = 1$. With these, Figure 11.3 provides the results of our Bayesian analyses of the realizations of (11.3) for $\omega = 1$ and various values of α . Although for $0 < \alpha < 1$, our method correctly identifies stationarity in all the cases, for $\alpha = 1, 1.5, 2$, our procedure falsely declares nonstationarity as stationarity.

To understand the reason for this, it is necessary to recall some of the properties of the ARCH(1) model. Note that $E(x_t) = 0$ for $t \geq 1$ and for any $t \geq 1$, $Var(x_t) = \frac{\omega}{1-\alpha}$, provided $0 < \alpha < 1$. For $\alpha \geq 1$, $Var(x_t)$ increases with t . Moreover, $Cov(x_t, x_{t+j}) = 0$ for $j \geq 1$. The last fact shows that the ARCH(1) model is serially uncorrelated. Thus, even though for $\alpha \geq 1$, $Var(x_t)$ increases with t , the realizations will be centered around zero and will be serially uncorrelated, and these are instrumental in rendering the pattern of the realizations seem like stationary time series. Although the variances are increasing in such cases, the realizations need not have an increasing range pattern due to absence of serial correlation. Figure 11.4 shows ARCH(1) realizations for $\alpha = 0.9, 1, 1.5$ and 2 . Note that none of the realizations exhibit any trend of increasing range, even though only $\alpha = 0.9$ corresponds to stationarity. Moreover, the pattern of the nonstationary realization for $\alpha = 1$ is quite similar to that of the stationary realization $\alpha = 0.9$. Indeed, all the four realizations shown in Figure 11.4 have similar patterns; they essentially differ only at a few time points, where the realizations have different ranges.

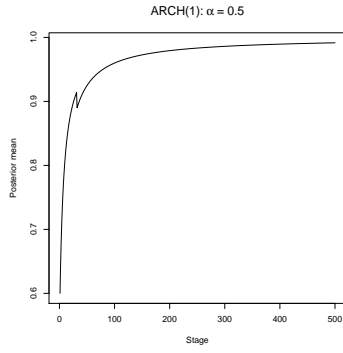
In other words, the realizations for $\alpha = 1, 1.5$ and 2 shown in Figure 11.4 do not seem to have enough information to distinguish them from stationarity. Hence, it is not surprising that our Bayesian method declared these realizations as stationary.

11.3 Application to GARCH(1,1)

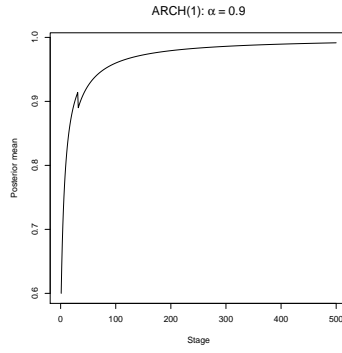
The ARCH model has been generalized by Bollerslev (1986) and Taylor (1986) independently to let σ_t^2 to have an autoregressive structure as well. This generalized ARCH, or GARCH model, is arguably the most widely used model in financial time series, particularly, for modeling stochastic volatility. For details on GARCH, see Bougerol and Picard (1992), Giraitis *et al.* (2005), Berkes *et al.* (2003) and Straumann (2005).

The GARCH(1,1) model, which generalizes ARCH(1), is of the following form: for $t = 1, 2, \dots$,

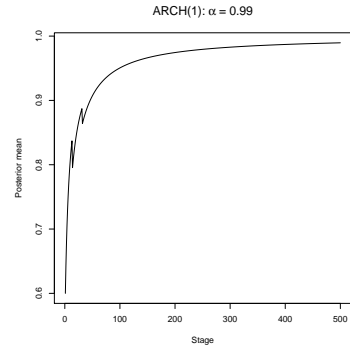
$$\begin{aligned} x_t &= \epsilon_t \sigma_t \\ \sigma_t^2 &= \omega + \alpha x_{t-1}^2 + \beta \sigma_{t-1}^2, \end{aligned} \quad (11.4)$$



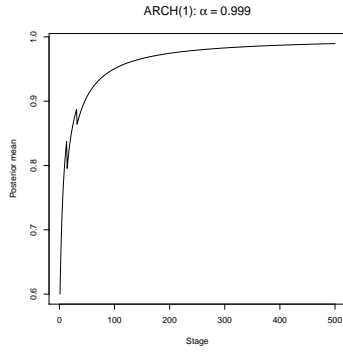
(a) Stationary: $\alpha = 0.5$.



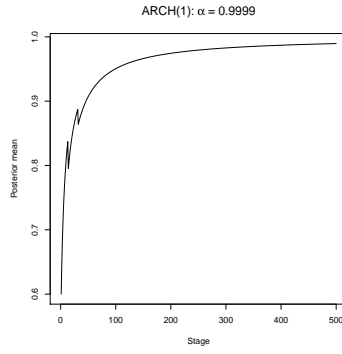
(b) Stationary: $\alpha = 0.9$.



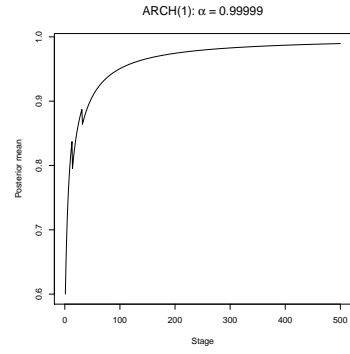
(c) Stationary: $\alpha = 0.99$.



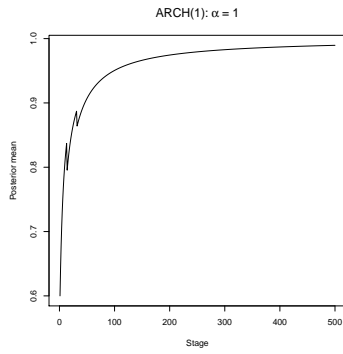
(d) Stationary: $\alpha = 0.999$.



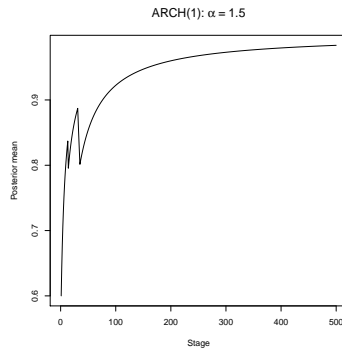
(e) Stationary: $\alpha = 0.9999$.



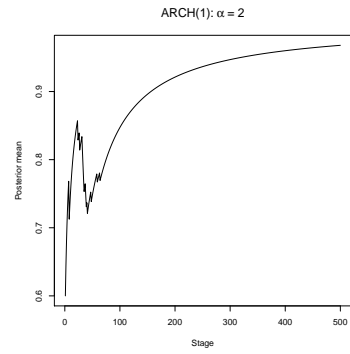
(f) Stationary: $\alpha = 0.99999$.



(g) Nonstationary: $\alpha = 1$.



(h) Nonstationary: $\alpha = 1.5$.



(i) Nonstationary: $\alpha = 2$.

Figure 11.3: Nonparametric ARCH(1) example with $K = 500$ and $n = 5$.

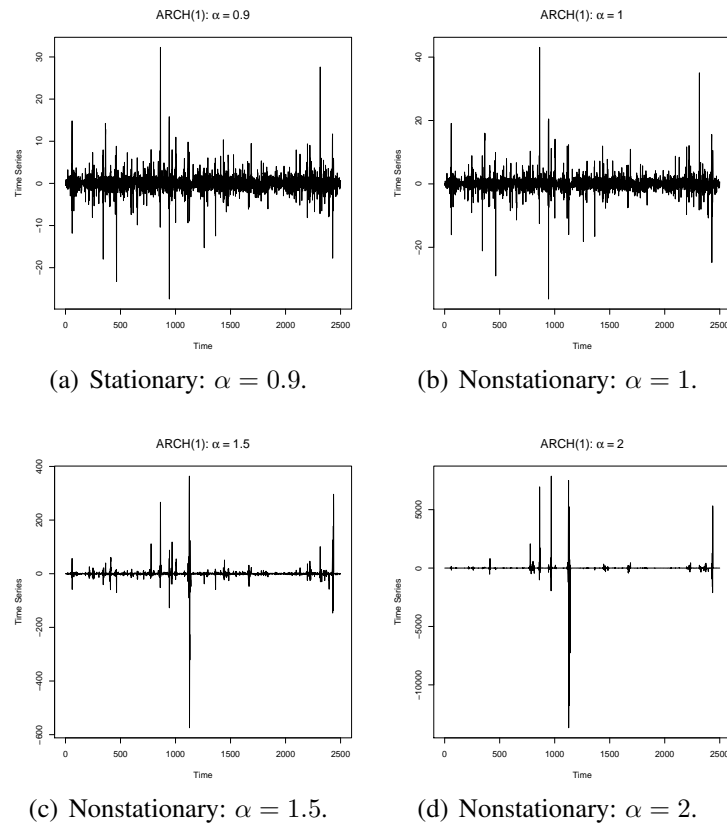


Figure 11.4: Comparison of ARCH(1) samples for several values of α where our Bayesian method failed.

where $\omega > 0$, $\alpha \geq 0$, $\beta \geq 0$ and $\epsilon_t \stackrel{iid}{\sim} N(0, 1)$, for $t = 1, 2, \dots$. The necessary and sufficient condition for stationarity of (11.4) is $0 < \alpha + \beta < 1$. We set $\omega = 1$ and $x_1 = 0$ and $\sigma_1 = 0$ for our purpose.

Again we set $n = 5$ and $K = 500$ and consider the nonparametric bound (10.3) for applying our Bayesian idea to model (11.4) for different values of α and β leading to stationarity and non-stationarity. Figure 11.5, summarizing the results of our Bayesian experiments, show that all the cases have been correctly identified, except the cases of $(\alpha = 1, \beta = 0)$ and $(\alpha = 0.5, \beta = 0.5)$. Note that the first case is the same as ARCH(1) with $\alpha = 1$, and the reason for failure of our Bayesian method for this case has already been explained in Section 11.2.

The diagram for the case of $(\alpha = 0.5, \beta = 0.5)$ is provided in Figure 11.6. Note that this realization is essentially of the same pattern as panels (a) and (b) of Figure 11.6 associated with ARCH(1) models with $\alpha = 0.9$ and 1, respectively, which do not seem to show any evidence of nonstationarity. Hence, again, quite unsurprisingly, our Bayesian method declared this case as stationary.

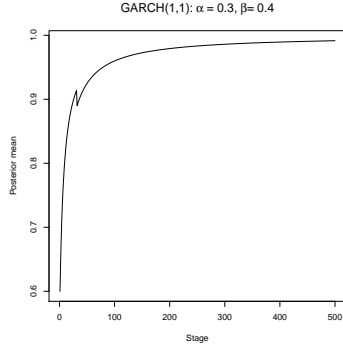
12 Third illustration: MCMC convergence diagnostics

We now test our Bayesian method on the very relevant problem of MCMC convergence diagnosis. For our purpose, we focus attention on transformation based Markov chain Monte Carlo (TMCMC) introduced by Dutta and Bhattacharya (2014). We consider three examples: in the first example, we assume that the target distribution is a product of 100 standard normal densities, and consider seven instances of additive TMCMC. Here we make use of the optimal scaling theory for additive TMCMC. In the next two examples, we consider mixtures of two normal densities. In all the cases, we evaluate convergence of TMCMC using our proposed Bayesian method.

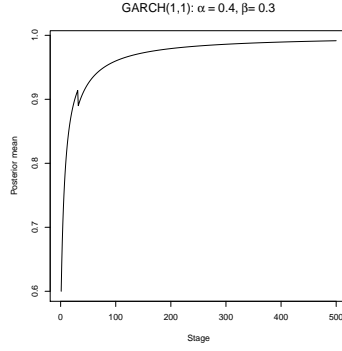
12.1 A brief overview of TMCMC

TMCMC enables updating an entire block of parameters using deterministic bijective transformations of some arbitrary low-dimensional random variable. Thus very high-dimensional parameter spaces can be explored using simple transformations of very low-dimensional random variables. In fact, transformations of some one-dimensional random variable always suffices, which we shall adopt in our examples. The underlying idea also greatly improves computational speed and acceptance rate compared to block Metropolis-Hastings methods. Interestingly, the TMCMC acceptance ratio is independent of the proposal distribution chosen for the arbitrary low-dimensional random variable. For implementation in our cases, we shall consider the additive transformation, since it is shown in Dutta and Bhattacharya (2014) that many fewer number of “move types” are required by this transformation compared to non-additive transformations. To elaborate the additive TMCMC mechanism, assume that a block of parameters $\mathbf{x} = (x_1, \dots, x_r)$ is to be updated simultaneously using additive TMCMC, where $r (\geq 2)$ is some positive integer. At the t -th iteration ($t \geq 1$) we shall then simulate $\theta \sim g(x)I_{\{x>0\}}$, where $g(\cdot)$ is some arbitrary distribution and $I_{\{x>0\}}$ is the indicator function of the set $\{x > 0\}$.

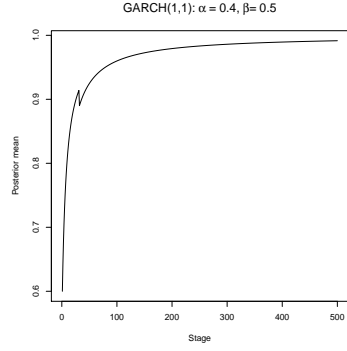
We then propose, for $j = 1, \dots, r$, $x_j^{(t)} = x_j^{(t-1)} \pm a_j \eta$, with equal probability (although equal probability is a convenience, not a necessity), where (a_1, \dots, a_r) are appropriate scaling constants.



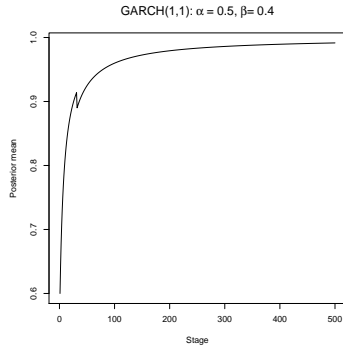
(a) Stationary: $\alpha = 0.3, \beta = 0.4$.



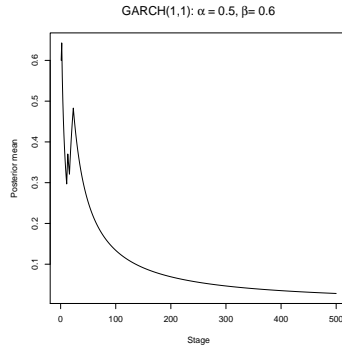
(b) Stationary: $\alpha = 0.4, \beta = 0.3$.



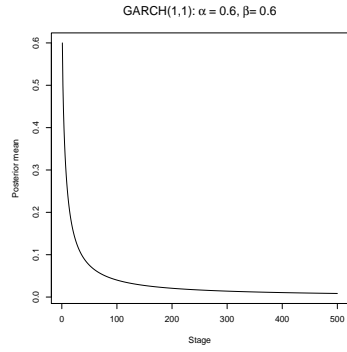
(c) Stationary: $\alpha = 0.4, \beta = 0.5$.



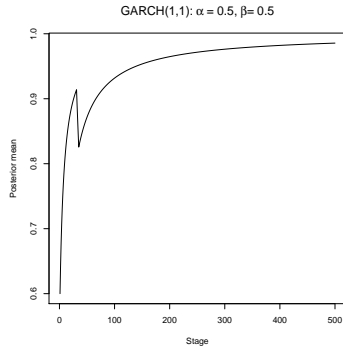
(d) Stationary: $\alpha = 0.5, \beta = 0.4$.



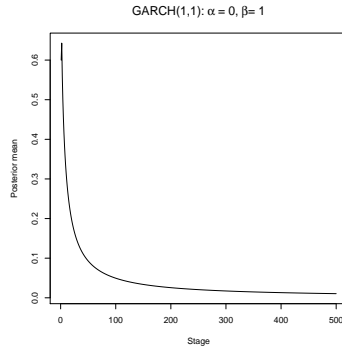
(e) Nonstationary: $\alpha = 0.5, \beta = 0.6$.



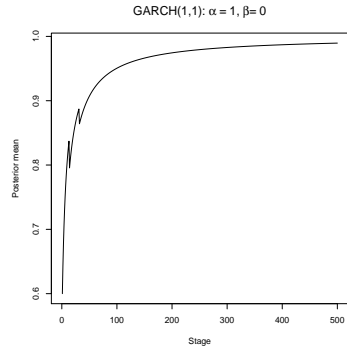
(f) Nonstationary: $\alpha = 0.6, \beta = 0.6$.



(g) Nonstationary: $\alpha = 0.5, \beta = 0.5$.

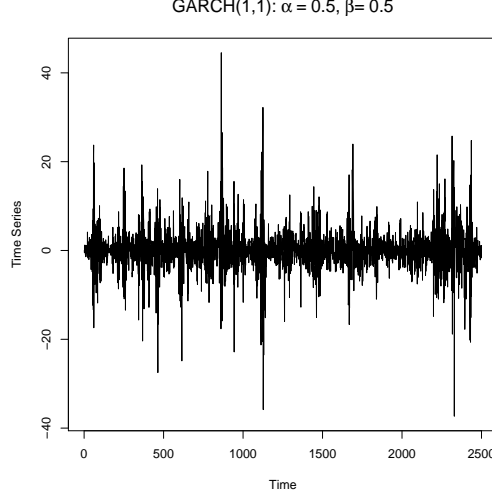


(h) Nonstationary: $\alpha = 0, \beta = 1$.



(i) Nonstationary: $\alpha = 1, \beta = 0$.

Figure 11.5: Nonparametric GARCH(1,1) example with $K = 500$ and $n = 5$.



(a) Nonstationary: $\alpha = 0.5, \beta = 0.5$.

Figure 11.6: GARCH(1,1) sample for $\alpha = 0.5$ and $\beta = 0.5$ where our Bayesian method failed.

Thus, using additive transformations of a single, one-dimensional x , we update the entire block \mathbf{x} at once.

12.2 Optimal scaling of TMCMC

In our examples we shall choose $r = d$, where d is the total number of parameters to be updated. In other words, we shall update all the parameters simultaneously, in a single block. We shall consider $a_i = 1$, for $i = 1, \dots, d$ and $g(\cdot)$ to be the $N(0, \frac{\ell^2}{d})$ density, so that η is simulated from a truncated normal distribution, with mean zero and variance ℓ^2/d . The optimum choice of ℓ is directly related to the optimal scaling problem (see Dey and Bhattacharya (2017) and Dey and Bhattacharya (2019)). Under appropriate regularity conditions it turns out that the optimal value of ℓ corresponds to the optimal additive TMCMC acceptance rate 0.439. When the target distribution $\pi(x_1, \dots, x_d)$ is a product of d iid standard normal densities, as we consider, then it turns out that the optimum choice of ℓ is 2.4.

12.3 TMCMC example 1: product of 100 standard normal densities

We apply additive TMCMC to generate 10^6 realizations from $\pi(x_1, \dots, x_d)$ being a product of d standard normal densities with $d = 100$. We consider seven values of ℓ , and hence seven different TMCMC chains, each corresponding to a value of ℓ . In particular, we set $\ell = 0.001, 0.01, 0.1, 2.4, 10, 100$ and 1000 . Of these, $\ell = 2.4$ is the optimum value that maximizes the “diffusion speed” associated with the TMCMC chain. The values relatively closer to 2.4, although not optimal, can still generate TMCMC chains with reasonable convergence properties. Significantly small values of ℓ generates TMCMC chains with very high acceptance rates but with very slow convergence rates, as at each iteration, the chain is allowed to take only small steps for movement. On the other hand, for significantly large values of ℓ , large steps are generally proposed, which are often rejected. Thus, the chain again has slow convergence, with poor acceptance rate.

It transpires from the above discussion that for values of ℓ equal to, or relatively close to 2.4, good convergence properties of the TMCMC chains can be expected, and it is desirable that our Bayesian method indicates convergence to stationarity for such cases. For other values of ℓ , since the convergence properties of the chains are expected to be poor, our Bayesian method must reflect so.

Generation of 10^6 TMCMC realizations from $\pi(x_1, \dots, x_d)$ with $d = 100$ takes less than 0.05 seconds on an ordinary 64 bit laptop. For implementation of our Bayesian idea, we need the bounds c_j . The general-purpose nonparametric bound (10.3) turned out to be quite appropriate in all the TMCMC examples that we consider. Indeed, in general there is no provision for parametric bounds in MCMC situations, as such bounds would require direct generation from π or some distribution close to π , but if such direct generation were at all possible, MCMC would not be needed in the first place.

For $K = 1000$ and $n = 1000$, Figures 12.1 and 12.2 display the trace plots (presented after thinning the original chain of length 10^6 by 100, to reduce the file sizes) and the corresponding Bayesian posterior means associated with our Bayesian stationarity detection idea, for different values of ℓ , for the first co-ordinate x_1 of (x_1, \dots, x_{100}) . It takes a few seconds even on a 64-bit dual core laptop for parallel implementation of our Bayesian idea in these cases.

The results are very much in keeping with our prior expectation that for significantly small and large values of ℓ convergence to stationarity for the given sample size is not expected, while for $\ell = 2.4$ and values relatively close to 2.4, stationarity is expected. Specifically, the figures for Bayesian stationarity detection strongly indicate convergence for $\ell = 0.1, 2.4$ and 10, but strongly indicate that the chains corresponding to $\ell = 0.001, 0.01, 100$ and 1000, are yet to achieve stationarity. Note that these results are also in accordance with the visual information obtained from the corresponding trace plots.

12.4 TMCMC example 2: mixture normal densities

We now consider two mixtures of normal densities. The first mixture is of the form

$$\pi(x) = \frac{1}{2}N(x : 0, 1) + \frac{1}{2}N(x, 10, 1), \quad (12.1)$$

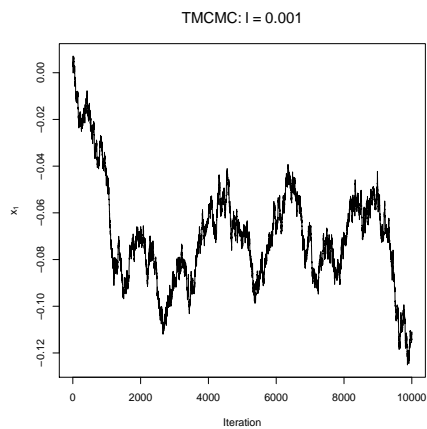
where $N(x, \mu, \sigma^2)$ denotes the normal density with mean μ and variance σ^2 , evaluated at x . The second mixture is of the form

$$\pi(x) = \frac{1}{2}N(x : 0, 1) + \frac{1}{2}N(x, 15, 1), \quad (12.2)$$

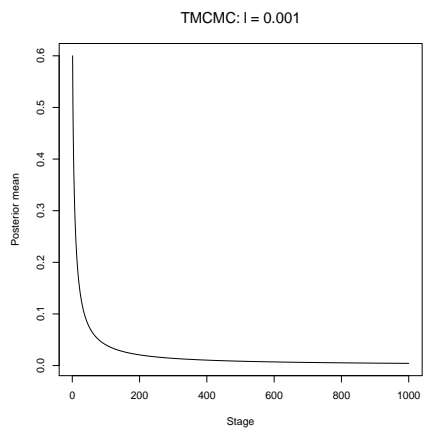
The mixtures differ slightly only in the means of the second mixture, but with TMCMC implementation, they reveal significant difference.

With the same implementation as before, with $\ell = 2.4$, and with the same bound c_j , we obtain Figure 12.3. The TMCMC trace plot and the Bayesian idea of stationarity detection reveals that for (12.1) stationarity is clearly reached. That this is achieved even though the chain concentrates around two values 0 and 10, is quite encouraging.

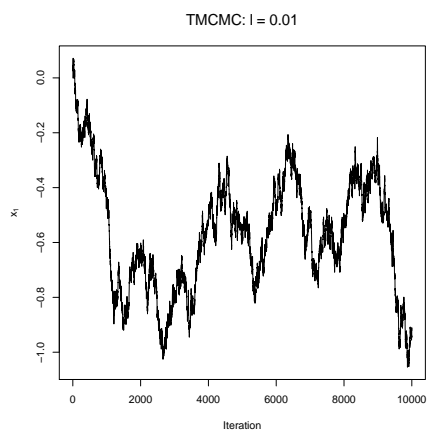
The trace plot for (12.2), with the same implementation as before displays two instances of very distinct and significant local stationarity. Consequently, for stationarity detection for this



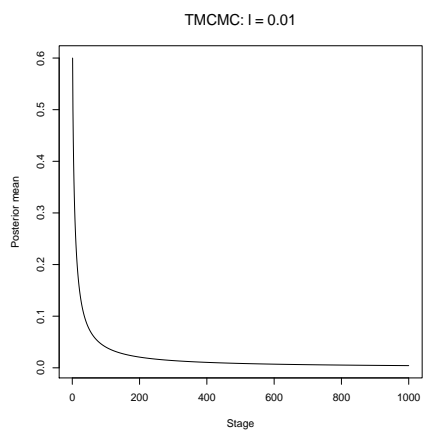
(a) TMCMC trace plot ($\ell = 0.001$).



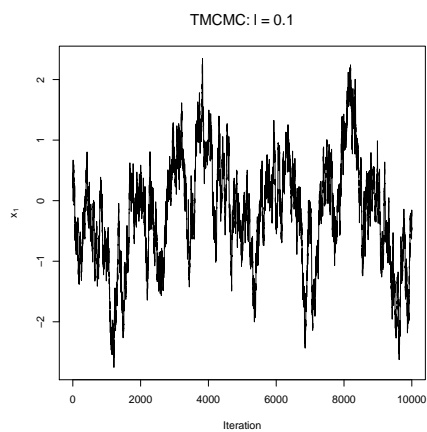
(b) Convergence ($\ell = 0.001$): Nonstationary.



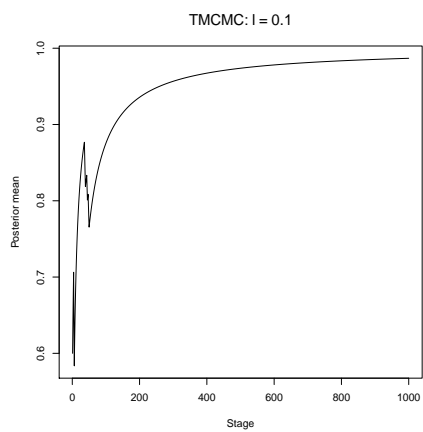
(c) TMCMC trace plot ($\ell = 0.01$).



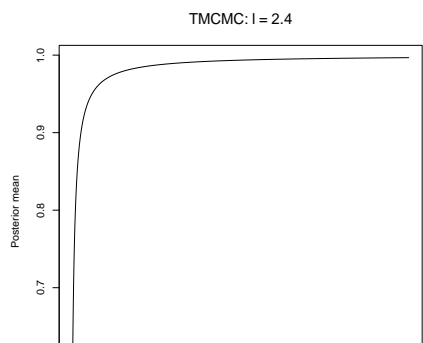
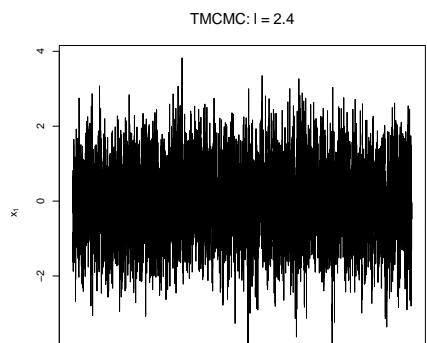
(d) Convergence ($\ell = 0.01$): Nonstationary.

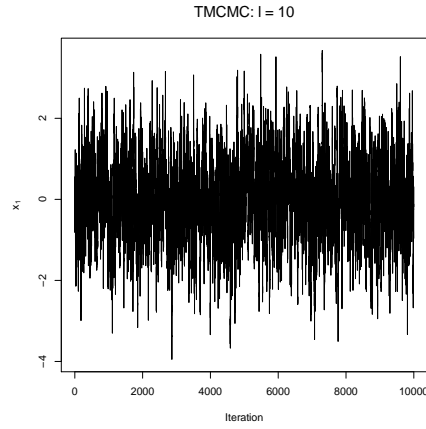


(e) TMCMC trace plot ($\ell = 0.1$).

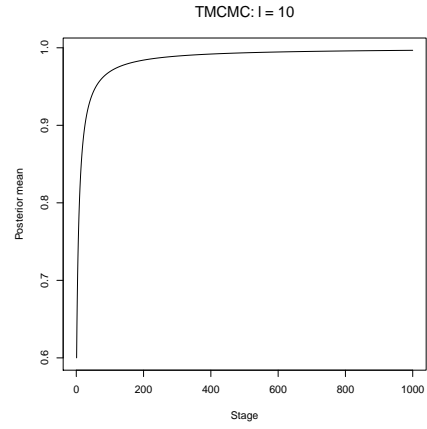


(f) Convergence ($\ell = 0.1$): Stationary.

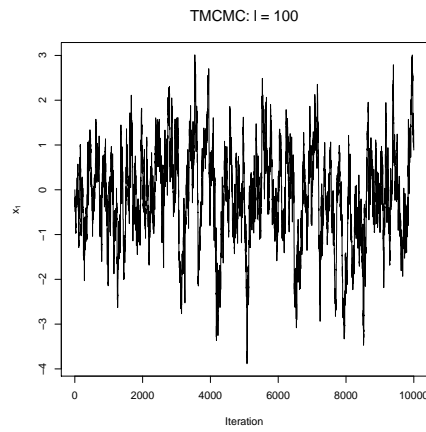




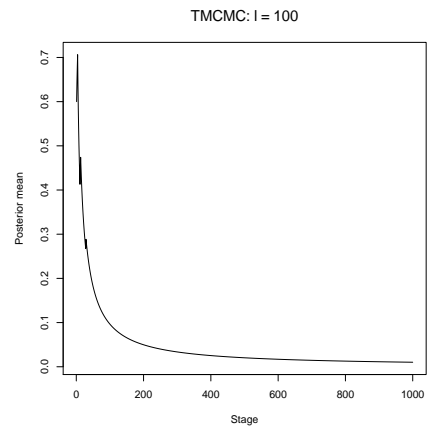
(a) TMCMC trace plot ($\ell = 10$).



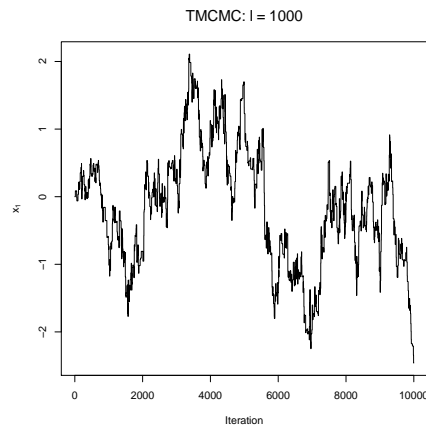
(b) Convergence ($\ell = 10$): Stationary.



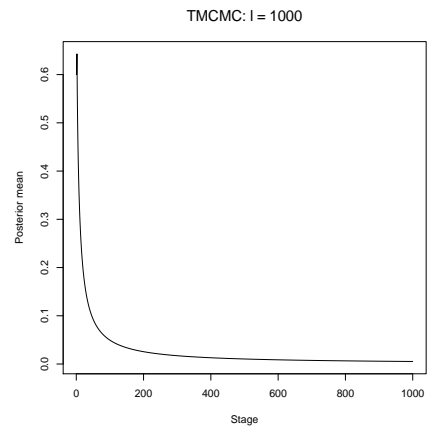
(c) TMCMC trace plot ($\ell = 100$).



(d) Convergence ($\ell = 100$): Nonstationary.

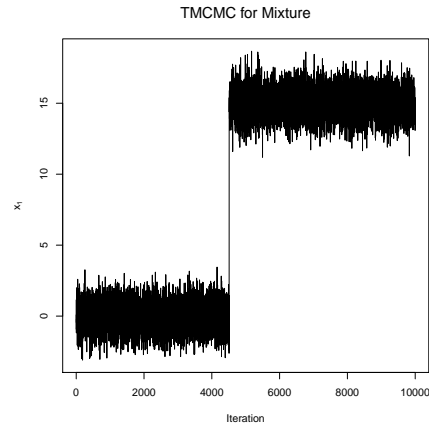
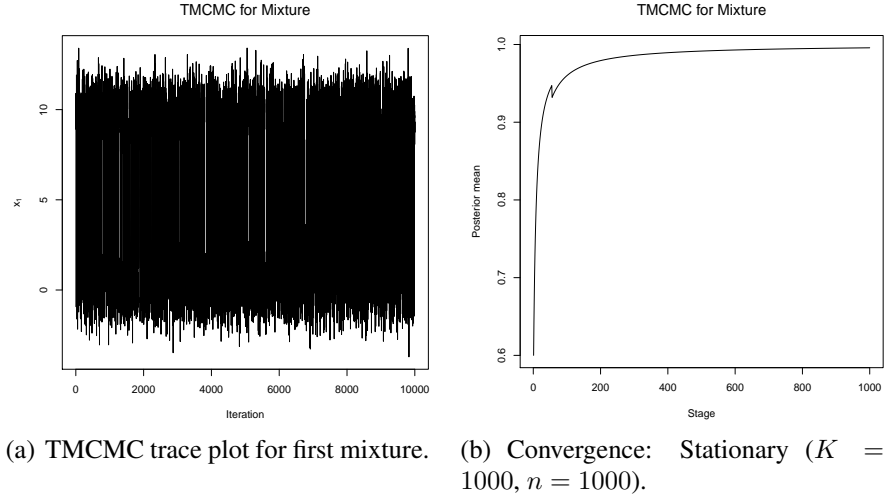


(e) TMCMC trace plot ($\ell = 1000$).



(f) Convergence ($\ell = 1000$): Nonstationary.

Figure 12.2: Additive TMCMC convergence example, with $K = 1000$ and $n = 1000$.



(c) TCMC trace plot for second mixture. Convergence: Nonstationary ($K = 2, n = 500000$)

Figure 12.3: Additive TCMC convergence example for mixture densities.

case, $K = 1000$ and $n = 1000$ is no longer appropriate. Rather, $K = 2$ and $n = 500000$, seems to be natural and appropriate. With this we obtain the posterior means for the two iterations (corresponding to $K = 2$) to be 0.6 and 0.5, respectively, with the associated posterior variances 0.04 and 0.03125. This is an indication that the chain did not yet reach stationarity, which is also evident from the trace plot. Indeed, for just two instances of significant local stationarities, global stationarity can not be ensured.

13 Fourth illustration: detection of stationarity and nonstationarity in spatial data

In this illustration, we shall consider detecting both strict and weak stationarity of the spatial processes that gave rise to the observed data.

13.1 Data generation

We now conduct simulation experiments with our theory for detecting stationarity and nonstationarity in spatial data. To conduct the experiment, we simulate two datasets from stationary and nonstationary zero-mean Gaussian processes (GPs) with covariance functions

$$Cov(X_{s_1}, X_{s_2}) = \exp(-5\|s_1 - s_2\|^2) \quad (13.1)$$

and

$$Cov(X_{s_1}, X_{s_2}) = C_1(\|s_1 - s_2\|) = \exp(-5\|\sqrt{s_1} - \sqrt{s_2}\|^2), \quad (13.2)$$

for all spatial locations $s_1, s_2 \in \mathbb{R}^2$. For our simulation studies, we restrict the spatial locations to $[0, 1]^2$. We simulate partial realizations of length 10000 from the two GPs. We begin by simulating first, for $i = 1, \dots, 10000$, $\tilde{s}_i \sim U([0, 1]^2)$, and then setting $s_i = \sqrt{\tilde{s}_i}$. Here for any $s = (u, v)^T \in [0, 1]^2$, $\sqrt{s} = (\sqrt{u}, \sqrt{v})^T$. The strategy of taking square roots of the components of \tilde{s}_i ensured numerical stability of the corresponding covariance matrices. We then simulate from 10000 zero-mean multivariate normals with covariance matrices defined by the above stationary and nonstationary covariance functions. Generating from the multivariate normal distributions by parallelising the required Cholesky decomposition of the covariance matrix and subsequent multiplication of the Cholesky factor with the vector of standard normal random variables using ScaLAPACK (Scalable Linear Algebra Package) takes less than 40 seconds in our C code implementation on our 64 bit laptop (8 GB RAM and 2.3 GHz CPU speed), with just 4 cores.

13.2 Implementation of our method to detect strict stationarity

For our purpose, we first need to form \mathcal{N}_i ; $i = 1, \dots, K$. In the spatial setting, the K -means clustering of the locations s_i ; $i = 1, \dots, 10000$, seems to be very appropriate. The nearby locations based on the distances from the centroid, will be classified within the same cluster, which is desirable from the spatial perspective. Thus, once we select K , the K -means clustering yields the K clusters, which are \mathcal{N}_i ; $i = 1, \dots, K$ in our notation. In our example, we select $K = 250$, so that there are about 40 observations per cluster on the average. We choose the clusterings such that there are at least 15 observations per cluster. As before, we consider the general purpose nonparametric bound c_j given by (10.3) for implementation of our method.

13.2.1 Choice of \hat{C}_1

For the choice of \hat{C}_1 , we first generate a sample of size 10000 from a zero mean GP with the Whittle covariance function of the form

$$Cov(X_{s_1}, X_{s_2}) = (\|s_1 - s_2\|/\psi)\mathcal{K}_1(\|s_1 - s_2\|/\psi), \quad (13.3)$$

where \mathcal{K}_1 is the second kind modified Bessel function of order 1. For the same value of ψ , this covariance function has thicker tails than exponential correlation functions of the forms $\exp(-\|s_1 - s_2\|^2/\psi)$ and $\exp(-\|s_1 - s_2\|/\psi)$. We set $\psi = 0.8$ to achieve reasonable thickness of the tail of (13.3). With this covariance function, we then use the bound (10.3) and set \hat{C}_1 to be the minimum positive value such that convergence to 1 is achieved. This \hat{C}_1 can be interpreted as providing a

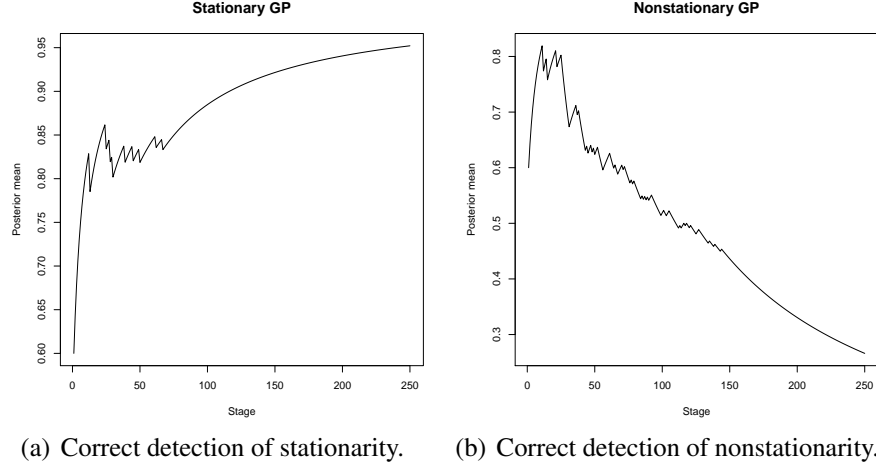


Figure 13.1: Detection of strong stationarity and nonstationarity in spatial data drawn from GPs.

reasonable bound for spatial processes with covariance functions with reasonably thick tails, but thinner than that of (13.3) with $\psi = 0.8$. With this method, we obtain $\hat{C}_1 = 0.89$. This value, being close to 1, suggests that the default choice $\hat{C}_1 = 1$ still makes sense. Indeed, both the choices yielded the same results regarding the decision on stationarity or nonstationarity of the underlying process.

13.3 Results

Figure 13.1 shows the results of implementation of our theory to detect strong stationarity and nonstationarity of the data obtained from the two GPs. The bounds (10.3) correspond to $\hat{C}_1 = 0.89$ obtained using the strategic procedure using (13.3). Panel (a) correctly asserts strict stationarity when the covariance is of the form (13.1) and correctly detects strict nonstationarity when the covariance is of the form (13.2). The entire methodology takes less than a second for parallel implementation on our 64 bit laptop using 4 cores.

13.4 Implementation of our method to detect covariance stationarity

As we demonstrated, our proposed method does an excellent job in capturing strict stationarity and nonstationarity of the underlying spatial stochastic process. In routine spatial modeling, however, strict stationarity and nonstationarity plays little role compared to covariance stationarity and covariance nonstationarity. Thus, it is more important to detect if the covariance in question is stationary or not. Although in our example it directly follows from our tests of strict stationarity that the covariances for the two GPs must be stationary and nonstationary, we directly check covariance stationarity using our Bayesian method formalized in Theorems 13 and 14.

For practical implementation, we convert the covariances \widehat{Cov}_{ih} given by (8.1) into correlations by dividing them by the relevant standard errors and initially set $\mathcal{N}_{i,h_j,h_{j+1}} = \{(s_1, s_2) \in \mathcal{N}_i : h_j \leq \|s_1 - s_2\| < h_{j+1}\}$, $j = 1, \dots, 10$, where $h_1 = 0$ and $h_j = h_{j-1} + 0.1$, for $j = 2, \dots, 10$. We consider the nonparametric bound c_j given by (10.3) for all $j = 1, \dots, 10$, for both the GPs. But we found that these $\mathcal{N}_{i,h_j,h_{j+1}}$ are too large to be useful, as $0 < \|s_1 - s_2\| < 0.04$, for all (s_1, s_2) in most of the K -

means clusters that we obtained. Indeed, only three neighborhoods defined by $h_1 = 0$, $h_2 = 0.02$, $h_3 = 0.03$ and $h_4 = 0.04$, turned out to be appropriate.

We again fix $K = 250$ clusters such that each cluster contains at least 15 observations.

13.4.1 Choice of \hat{C}_1

To obtain appropriate choice of \hat{C}_1 for detecting covariance stationarity, we consider three strategies. Our first method in this regard corresponds to using \hat{C}_1 for strict stationarity. Thus, the first strategy yields $\hat{C}_1 = 0.89$.

For the second strategy, we utilize the GP realization with covariance function (13.3). Here we choose the minimum value of \hat{C}_1 such that (10.3) yielded convergence to 1 for all $\mathcal{N}_{i,h_j,h_{j+1}}$; $j = 1, 2, 3$. This gave $\hat{C}_1 = 0.412$.

In the third strategy, we chose the minimum value of \hat{C}_1 that yielded convergence to 1 for all $\mathcal{N}_{i,h_j,h_{j+1}}$; $j = 1, 2, 3$ for one dataset and convergence to 0 for the other dataset. In our case, this strategy again gave $\hat{C}_1 = 0.412$.

The strategic choice $\hat{C}_1 = 0.412$ successfully detected covariance stationarity and nonstationarity. However, the choice $\hat{C}_1 = 0.89$ turned out to be too large to detect covariance nonstationarity. This is in keeping with the issue that detection of strict stationarity requires a bound that must also ensure covariance stationarity, and hence such a bound must be larger than that for covariance stationarity.

Again, our parallel implementation takes less than a second on our laptop, for each $\mathcal{N}_{i,h_j,h_{j+1}}$. This quick computation ensures that choice of \hat{C}_1 is not a computationally demanding exercise.

Figure 13.2 shows the results associated with \mathcal{N}_{i,h_1,h_2} , \mathcal{N}_{i,h_2,h_3} and \mathcal{N}_{i,h_3,h_4} , for $i = 1, \dots, K$, where $K = 250$ as before, and $\hat{C}_1 = 0.89$. The figure shows that whenever the data arises from the GP with covariance of the form (13.1), our Bayesian method correctly identifies covariance stationarity for every j . Indeed, for all $j = 1, 2, 3$, covariance stationarity is clearly indicated. On the other hand, when the data arises from the GP with the nonstationary covariance (13.2), convergence to 0 is indicated with \mathcal{N}_{i,h_3,h_4} . As per Theorem 14, this shows nonstationarity of the covariance structure.

13.5 Detection of strict nonstationarity in mixtures of stationary and nonstationary covariances

We now consider realizations from zero-mean GPs with covariances of the form

$$Cov(X_{s_1}, X_{s_2}) = p \exp(-5\|s_1 - s_2\|^2) + (1 - p) \exp(-5\|\sqrt{s_1} - \sqrt{s_2}\|^2), \quad (13.4)$$

where $0 < p < 1$. In particular, using our Bayesian theory, we attempt to detect strict and weak nonstationarity of the process when $p = 0.9, 0.99, 0.999, 0.9999, 0.99999$. Note that in these cases, although most of the weight concentrates on the stationary part of (13.4), the little mass on the nonstationary part makes the covariance nonstationary, and it is important to detect such subtle difference between stationarity and nonstationarity. As before, we set $K = 250$ clusters with each cluster containing at least 15 observations.

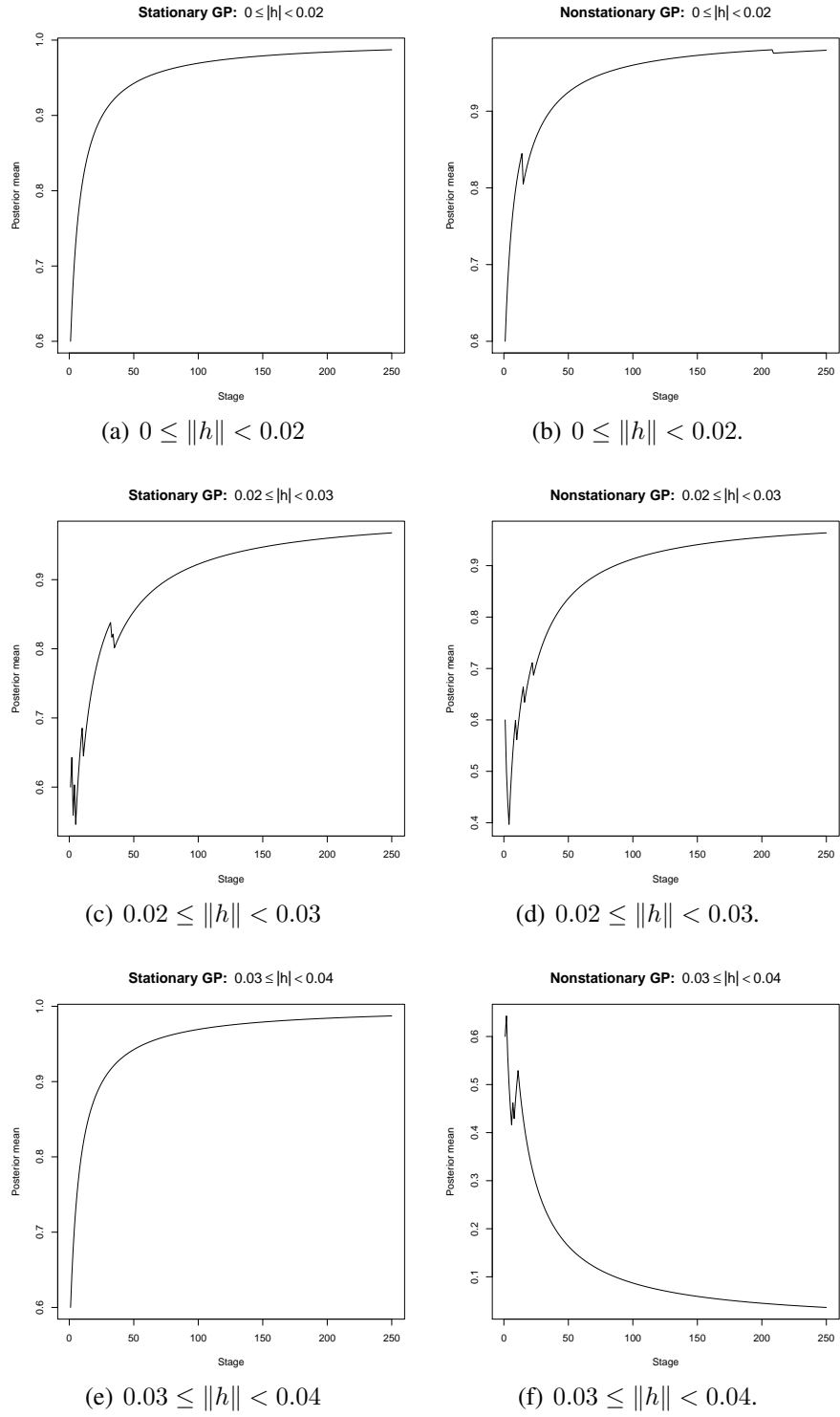


Figure 13.2: Detection of covariance stationarity and nonstationarity in spatial data drawn from GPs.

We consider the same way of data generation from GP as before, and the same way of implementation. We again use the same form of the bound c_j as (10.3), with $\hat{C}_1 = 0.89$ and $\hat{C}_1 = 1$ for detection of strict nonstationarity, as before. These choices put up excellent performances and are in agreement with each other, in spite of the subtlety involved in this exercise. Figure 13.3, corresponding to $\hat{C}_1 = 0.89$, shows that our Bayesian method correctly identifies nonstationarity in all the cases.

13.6 Detection of covariance nonstationarity in mixtures of stationary and nonstationary covariances

The same strategies discussed in Section 13.4, adapted in this situation, yielded effective bounds of the form (10.3) with $\hat{C}_1 = 0.412$, as before. We briefly discuss the second procedure of adapting the strategy to the current scenario. Note that the first procedure does not need any change at all.

To implement our second strategy in this case, we need a benchmark dataset for which covariance stationarity has been established. We thus consider the GP data with covariance of the form (13.1), whose covariance stationarity is established. For any new dataset for which covariance stationarity needs to be checked, in this case, any dataset with covariance structure of the form (13.4), we consider the same bound starting with $\hat{C}_1 = 0.89$. We then gradually decrease \hat{C}_1 for both the datasets until we arrive at a point that discriminates covariance stationarity and nonstationarity, in the same way as discussed in Section 13.4. With this method, we obtain $\hat{C}_1 = 0.412$, which shows covariance stationarity for (13.1) but covariance nonstationarity for (13.4). Recall that $\hat{C}_1 = 0.412$ also resulted with respect to the GP realization for the Whittle covariance function (13.3).

Again we set $K = 250$, with each cluster consisting of a minimum of 15 observations. Figure 13.4, corresponding to $\hat{C}_1 = 0.412$ and $p = 0.99999$ in the covariance structure (13.4), shows that this procedure does an excellent job in detecting covariance nonstationarity even in such a subtle situation. Indeed, the same $\hat{C}_1 = 0.412$ very successfully captured covariance nonstationarity for all other values of p , namely, $p = 0.9, 0.99, 0.999, 0.9999$ (figures omitted for brevity).

13.7 Spatial experiments with smaller data sets

We now repeat all the above experiments with datasets of sizes 1000. We consider $K = 100$ clusters with average cluster size 10. For checking strict stationarity, our first strategy of fixing \hat{C}_1 , using the Whittle covariance function (13.3) yielded $\hat{C}_1 = 0.02$, which produced too small bounds to be useful. On the other hand, the second procedure gave $\hat{C}_1 = 1.24$, which yielded reliable results, even for these small data sets. Figures 13.5 and 13.6 depict the results for $\hat{C}_1 = 1.24$. For covariance stationarity, these small data sets were able to produce a single valid region \mathcal{N}_{i,h_1,h_2} , defined by $h_1 = 0$ and $h_2 = 0.1$, and hence, with only this region, verification of covariance stationarity or nonstationarity is not possible. But since the underlying model is GP, covariance stationarity is equivalent to strict stationarity, and even for non-Gaussian processes, strict stationarity would imply covariance stationarity (although strict nonstationarity need not imply covariance nonstationarity).

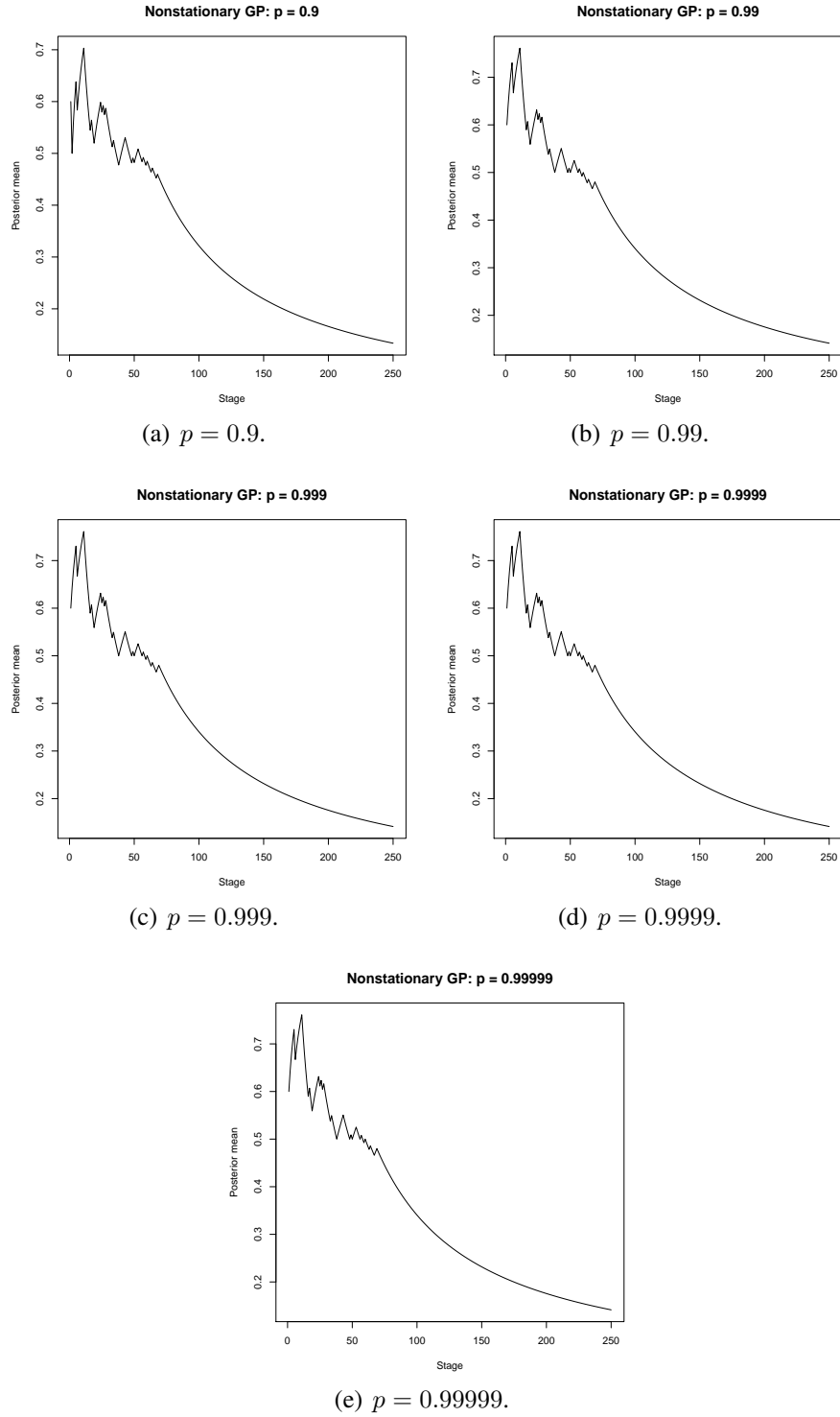


Figure 13.3: Detection of strong nonstationarity in spatial data drawn from GP with covariance structure (13.4) with $p = 0.99999$.

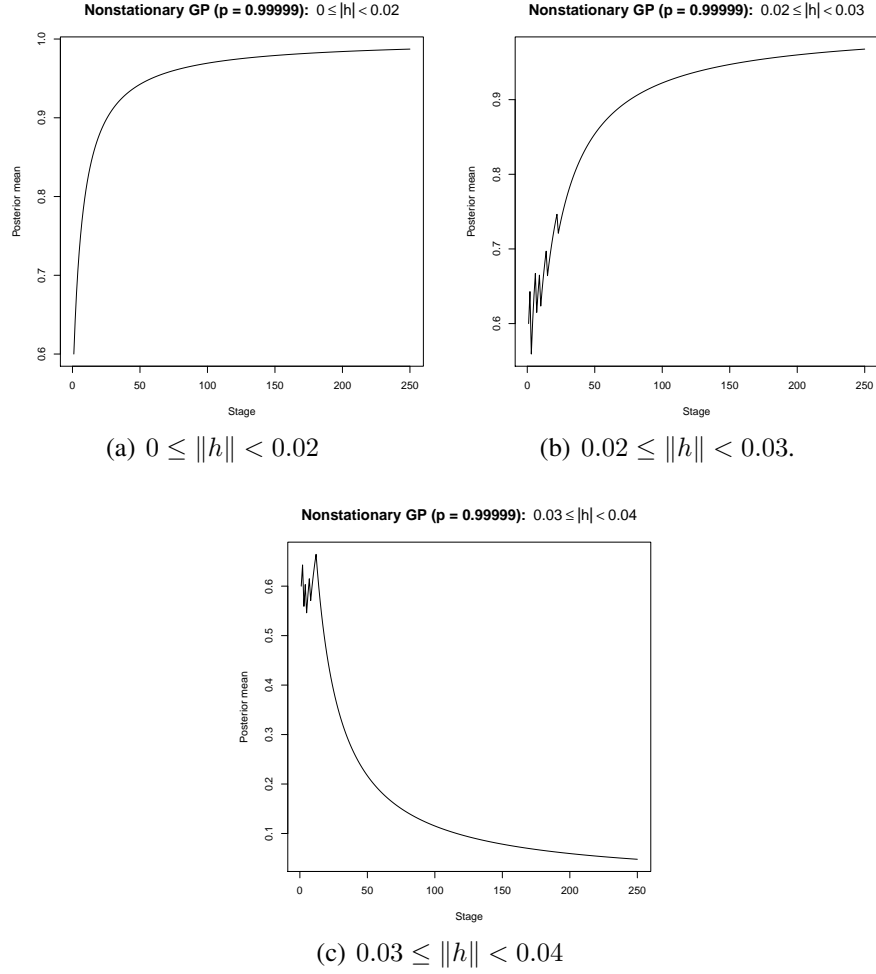


Figure 13.4: Detection of covariance nonstationarity in spatial data drawn from GP with covariance structure (13.4) with $p = 0.99999$.

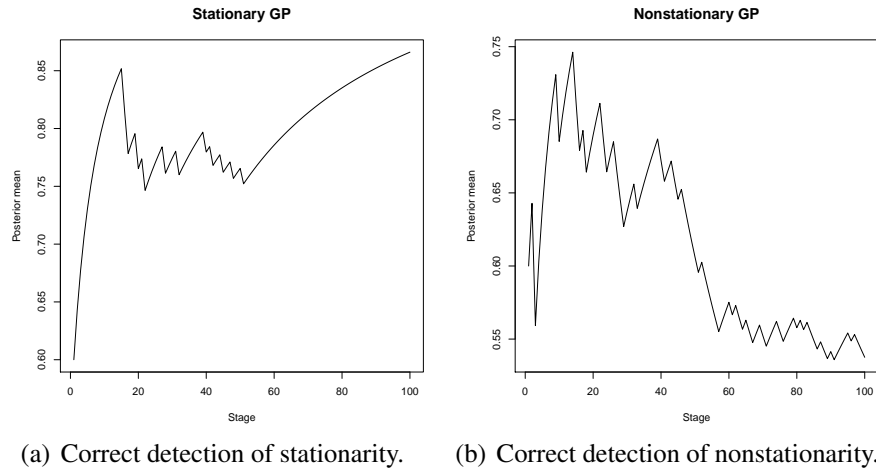


Figure 13.5: Detection of strong stationarity and nonstationarity in spatial data of size 1000 drawn from GPs.

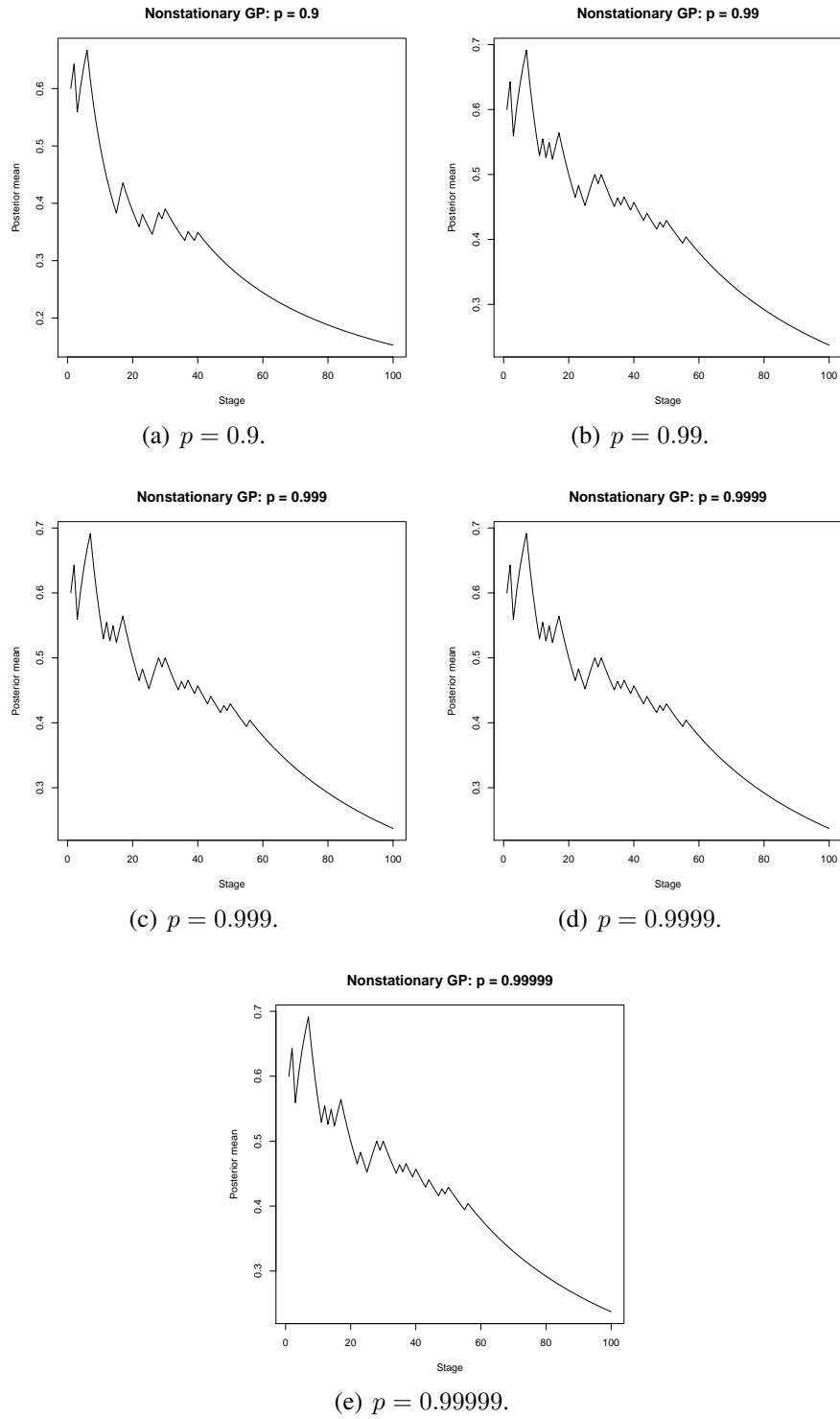


Figure 13.6: Detection of strong nonstationarity in spatial data of size 1000 drawn from GP with covariance structure (13.4) with $p = 0.99999$.

13.8 Comparison with existing methods

In spatial statistics, formal methods of testing stationarity or nonstationarity are rare, and mostly exploratory data analysis is used to informally check stationarity. However, Bandopadhyay and Rao (2017) have introduced some tests for checking covariance stationarity, under a variety of assumptions. These methods seem to be more general compared to the existing ones. An R -code for implementing their method is available at the webpage of the first author. Given a dataset, the code calculates two test statistics, denoted by T and V , along with the corresponding P -values under the null hypothesis of stationarity. The statistic V has been proposed in Bandopadhyay *et al.* (2017).

We apply their methods to our simulated spatial datasets in order to compare with our results. However, with data size 10000, it turned out that obtaining a result within reasonable time limits with the aforementioned R code is almost infeasible. Instead, we applied their methods to data sets of sizes 1000, 3000 and 5000. The run times for the R code for these data sizes are about 28 seconds, 5 minutes and 12 minutes, respectively.

Table 13.1 presents the results of the tests applied to our simulated datasets. In all the cases, the T statistic failed to reject the null hypothesis of stationarity, even though there is only one case of true null stationarity. On the other hand, the V -statistic performs much better, with its performance consistently improving with increasing sample size, as vindicated by the corresponding P -values. But observe that for sample size 1000, even the V -statistic fails to reject the null hypothesis of stationarity at the 5% level for most cases where the actual model is nonstationary. Moreover, at the 5% level, this statistic rejects the true null stationary model for sample sizes 3000 and 5000.

Thus, compared to our Bayesian idea, the overall performance of both the statistics T and V does not seem to be satisfactory for the models that we considered.

Moreover, from the methodological perspective, the tests of Bandopadhyay and Rao (2017) check covariance stationarity only, not strict stationarity. Various assumptions, which may be difficult to verify in practice, are also required. In contrast, our Bayesian method requires the only assumption of local stationarity that is expected to hold in practice, and allows for identification of both weak and strict stationarity.

14 Fifth illustration: detection of stationarity and nonstationarity in spatio-temporal data

We now apply our techniques in ascertaining stationarity and nonstationarity in spatio-temporal data, where both spatial and temporal components play important roles. For our simulation studies, we consider covariance functions of the following forms:

$$Cov(X_{(s_1, t_1)}, X_{(s_2, t_2)}) = \exp(-5\|s_1 - s_2\|^2) \times \frac{\rho^{|t_1 - t_2|}}{1 - \rho^2}, \quad (14.1)$$

$$Cov(X_{(s_1, t_1)}, X_{(s_2, t_2)}) = \exp(-5\|\sqrt{s_1} - \sqrt{s_2}\|^2) \times \frac{\rho^{|t_1 - t_2|}}{1 - \rho^2}, \quad (14.2)$$

and

$$\text{Cov}(X_{(s_1, t_1)}, X_{(s_2, t_2)}) = (p \exp(-5\|s_1 - s_2\|^2) + (1 - p) \exp(-5\|\sqrt{s_1} - \sqrt{s_2}\|^2)) \times \frac{\rho^{|t_1 - t_2|}}{1 - \rho^2}, \quad (14.3)$$

for all $s_1, s_2 \in \mathbb{R}^2$, $t_1, t_2 \in \mathbb{R}^+$ and $\rho \in \mathbb{R}$. Note that $\frac{\rho^{|t_1 - t_2|}}{1 - \rho^2}$ is the covariance function associated with an $AR(1)$ model with parameter ρ . The forms of the covariance functions (14.1), (14.2) and (14.3) show that the covariance parts associated with spatial and temporal components are separated from each other, thanks to the product forms. Covariance functions with such a property are known as separable covariance functions. In (14.3), $p \in [0, 1]$, as before. If $p = 0$, then (14.3) reduces to (14.3) and to (14.1) if $p = 1$.

Note that if $|\rho| < 1$, then (14.1) is a stationary covariance function, and nonstationary otherwise. On the other hand, (14.2) and (14.3) are both nonstationary covariance functions, irrespective of the value of ρ .

For our simulation experiments, we consider zero-mean GPs $X_{(s, t)}$ with the above covariance functions, restricting the spatial locations on $[0, 1]^2$ and setting the time points $t_i = i$, for $i \geq 1$. We simulate, for $i = 1, \dots, 100$, $\tilde{s}_i \sim U([0, 1]^2)$ and set $s_i = \sqrt{\tilde{s}_i}$. We set $t_i = i$, for $i = 1, \dots, 100$. This defines covariance matrices for 10000-dimensional multivariate normal associated with the underlying GPs. Note that such covariance matrices are Kronecker products of the spatial and temporal covariance matrices, thanks to separability.

Observe that the above separable covariance matrices correspond to separable spatio-temporal processes of the form

$$X_{(s, t)} = X_{(s, t-1)} + \epsilon_{(s, t)}, \quad (14.4)$$

for $t = 1, 2, \dots$, where $X_{(s, 0)} = \mathbf{0}$ (null vector), and $\epsilon_{(s, t)}$ are zero-mean GPs independent in time, but with spatial covariance with forms same as the spatial parts in (14.1), (14.2) and (14.3). With the above representation, generation of 10000 realization takes about a second, even in R .

To construct \mathcal{N}_i , $i = 1, \dots, K$, we consider K -means clustering of the points

$$\{(s_i, t_j); i = 1, \dots, 100; j = 1, \dots, 100\},$$

into $K = 250$ clusters.

14.1 Choice of the bound c_j in the spatio-temporal case

We consider the bound of the form (10.3) as before. As regards, \hat{C}_1 , we found that $\hat{C}_1 = 0.5$ performed adequately for the entire suite of our simulation experiments in the spatio-temporal scenario. However, we also consider a strategy for obtaining \hat{C}_1 using ideas similar to the spatial setup, detailed below.

We first generate a sample of size 10000 from a zero mean GP with the covariance function of the following form:

$$\text{Cov}(X_{(s_1, t_1)}, X_{(s_2, t_2)}) = (\|s_1 - s_2\|/\psi) \mathcal{K}_1(\|s_1 - s_2\|/\psi) \times \frac{\xi^{|t_1 - t_2|}}{1 - \xi^2}, \quad (14.5)$$

with $\psi = 0.8$ and $\xi = 0.999999$. Note that this covariance function corresponds to a model of the

form (14.4) with $X_{(s,0)} = \mathbf{0}$ and zero-mean GPs $\epsilon_{(s,t)}$ independent in time, with spatial covariance given by the spatial form in (14.5). The parameter values $\psi = 0.8$ and $\xi = 0.999999$ are chosen to make the underlying spatio-temporal process reasonably close to nonstationarity with respect to space and time.

We then choose that minimum value of \hat{C}_1 such that the spatio-temporal process remains stationary. This minimum value, for checking strict stationarity, is given by $\hat{C}_1 = 0.37$, which is reasonably close to $\hat{C}_1 = 0.5$ that worked well for our experiments. Again, we obtained same results for both the values of \hat{C}_1 , and we report results for $\hat{C}_1 = 0.37$.

However, for weak stationarity, we again failed to obtain multiple valid intervals for realizations of size 10000 from the zero-mean GP with covariance (14.5). Indeed, we could obtain only a single interval $[0, 0.15]$. Hence, in that case we consider $\hat{C}_1 = 0.5$.

Below we discuss the experimental designs for our various simulation experiments.

14.2 Spatial and temporal stationarity

We generate partial realizations of length 10000 from the zero mean GP with covariance function (14.1) using the formulation (14.4), with $\rho = 0.8$ and also with $\rho = 0.99999$. Thus, the spatio-temporal GPs are strictly stationary, and our Bayesian method is expected to reflect this. The latter situation is quite subtle, as the difference with temporal nonstationarity is negligible.

Apart from strict stationarity, we also investigate weak stationarity, focussing on the subtle situation where $\rho = 0.99999$.

14.3 Spatio-temporal nonstationarity

Recall that spatio-temporal nonstationarity occurs in our cases when $|\rho| \geq 1$ in (14.1) and when covariances (14.2) or (14.3) are chosen. We experiment with (14.1) with $\rho = 1$, (14.2) with $\rho = 0.8$ and $\rho = 1$, (14.3) with $p = 0.99999$ and $\rho = 0.8$. The latter is a subtle situation where nonstationarity is quite difficult to ascertain. Note that if nonstationarity can be captured by our Bayesian method in this situation, then so is possible for larger values of ρ taking the temporal part closer to nonstationarity. With the last, subtle situation, we also investigate covariance nonstationarity.

14.4 Results

Figure 14.1, diagrammatically representing our Bayesian procedure, vindicates that the stochastic processes associated with covariance function (14.1) with $\rho = 0.8$ and $\rho = 0.99999$, are indeed strictly stationary. On the other hand, the processes corresponding to (14.1) with $\rho = 1$, (14.2) with $\rho = 0.8$ and $\rho = 1$, (14.3) with $p = 0.99999$ and $\rho = 0.99999$, are all correctly detected by our Bayesian method as strictly nonstationary.

Figure 14.2 depicts the results of investigation of weak stationarity for the covariance (14.1) with $\rho = 0.99999$. For the covariance (14.3) with $p = 0.99999$ and $\rho = 0.8$, Figure 14.3 presents the results of our Bayesian technique. In both the cases, success of our Bayesian proposal is clearly borne out.

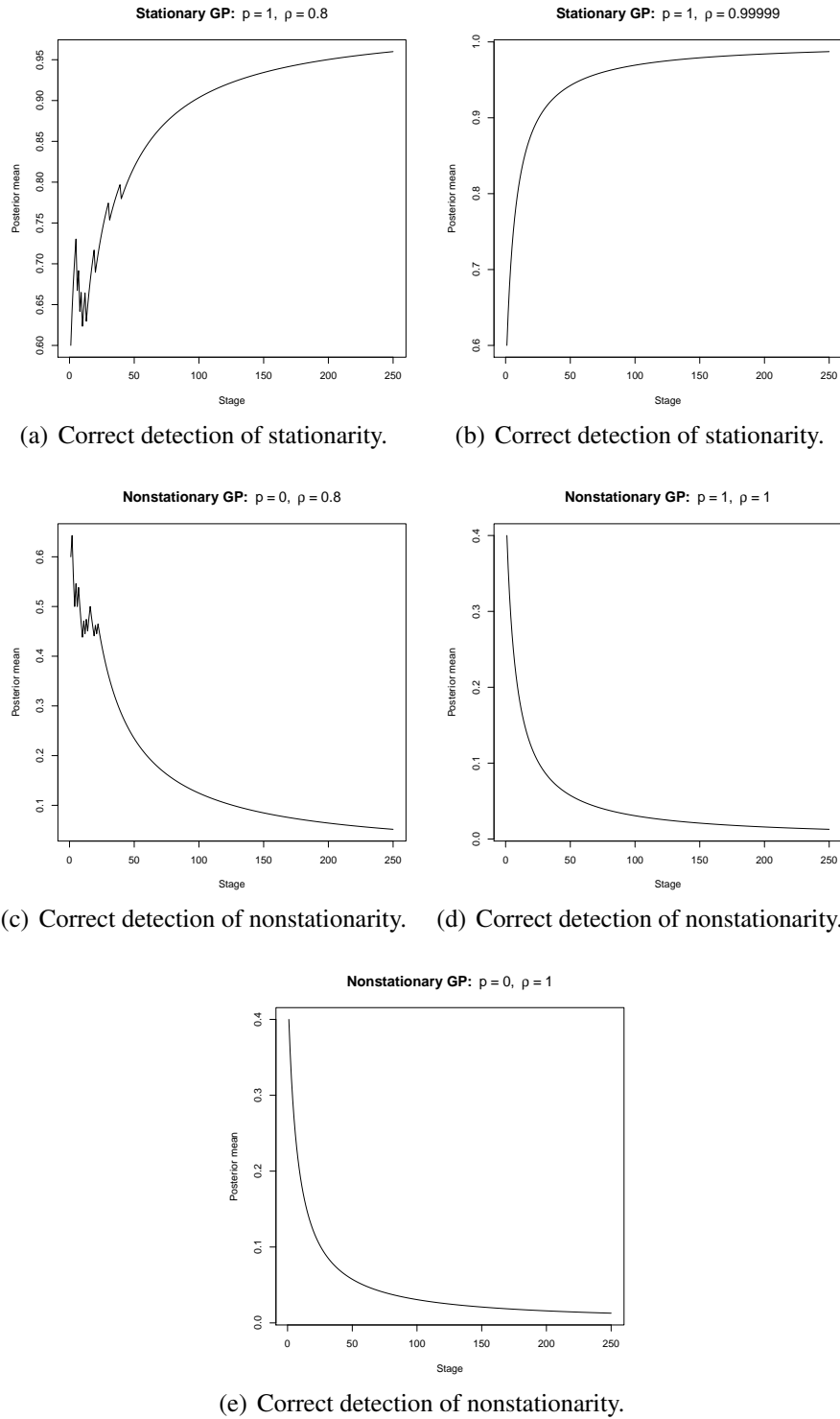


Figure 14.1: Detection of strong stationarity and nonstationarity in spatio-temporal data drawn from GPs.

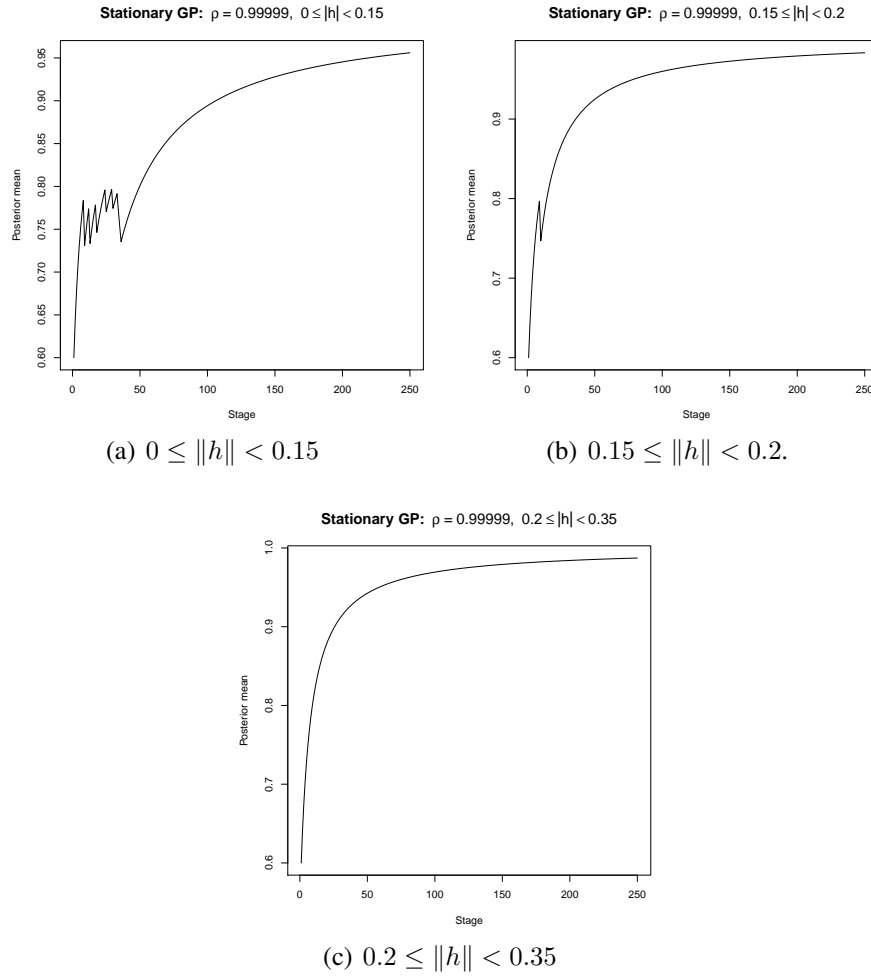


Figure 14.2: Detection of covariance stationarity in spatio-temporal data drawn from GP with covariance structure (14.1) with $\rho = 0.99999$.

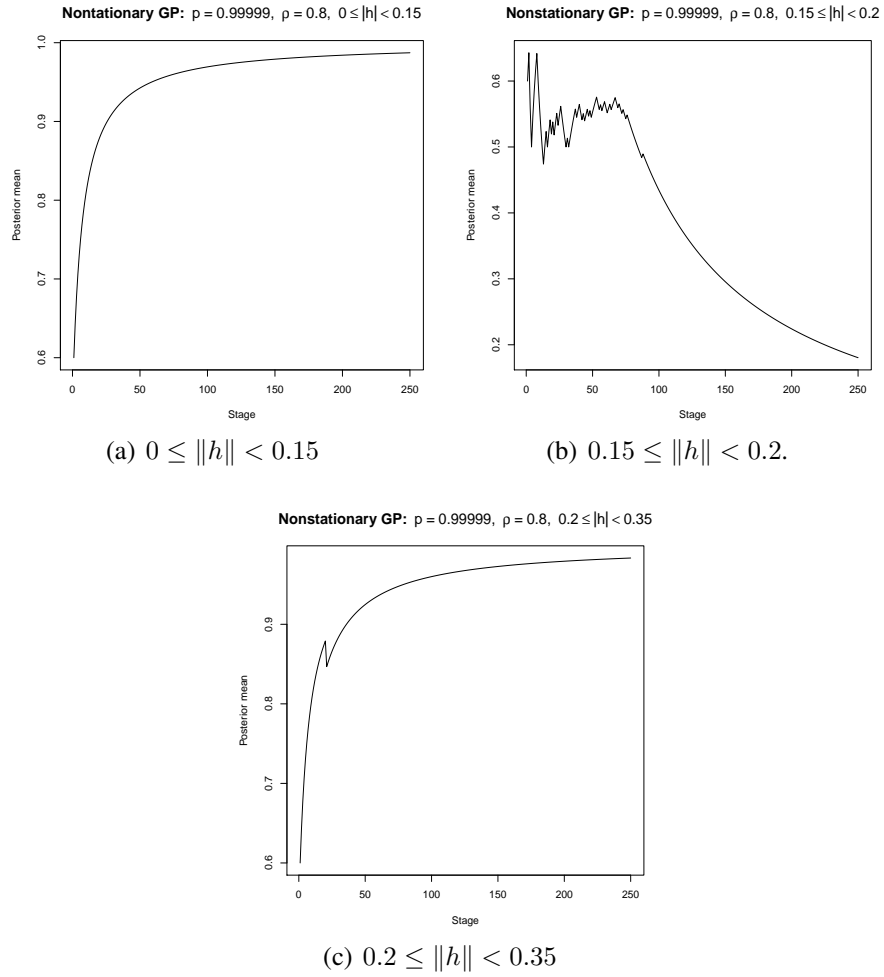


Figure 14.3: Detection of covariance nonstationarity in spatio-temporal data drawn from GP with covariance structure (14.3) with $p = 0.99999$ and $\rho = 0.8$.

14.5 Investigation of spatio-temporal stationarity with smaller sample size

We now investigate stationarity of the above spatio-temporal models using much smaller sample sizes. In particular, we consider 50 locations and 20 time points only, and $K = 100$ clusters. We ensured at least 3 data points in each cluster. Our strategy for choosing \hat{C}_1 , detailed in Section 14.1, gave $\hat{C}_1 = 0.87$ for investigating strict stationarity. Again, $\hat{C}_1 = 0.5$ yielded the same conclusions. Figure 14.4, depicting the results of our analysis for $\hat{C}_1 = 0.87$, indicates correct decisions on strict stationarity and nonstationarity in all the cases, even for such small data size.

However, validating covariance stationarity could not be achieved for such small samples, as we again ended up with the single interval \mathcal{N}_{i,h_1,h_2} with $h_1 = 0$ and $h_2 = 0.2$.

14.6 Comparison with existing methods

As in the spatial case, for the spatio-temporal setup, formal methods of testing stationarity are very rare in the literature. Recently, some methods in this direction are proposed in Bandopadhyay *et al.* (2017). Indeed, the authors propose as many as 10 test statistics to detect covariance stationarity, under a variety of assumptions. The main ideas are similar to the testing ideas in the spatial setup proposed in Bandopadhyay and Rao (2017). A relevant R code is provided in the webpage of the first author, but it failed to work for our simulated spatio-temporal datasets, possibly because the methods are heavily dependent on choices of the underlying parameters involved in their methods. Instead, we apply our Bayesian methodology on the spatio-temporal models and simulation designs to which Bandopadhyay *et al.* (2017) applied their testing methods.

Following Bandopadhyay *et al.* (2017), we consider zero mean spatio-temporal processes, with $T = 200$ time points and $m = 100$ or 500 locations drawn uniformly from $[-\frac{\lambda}{2}, \frac{\lambda}{2}]$. We then apply our Bayesian procedure to the 5 spatio-temporal models considered by Bandopadhyay *et al.* (2017), under the same setups, described below.

14.6.1 Simulations under stationarity with exponential spatial covariance function

We generate data from the following stationary models:

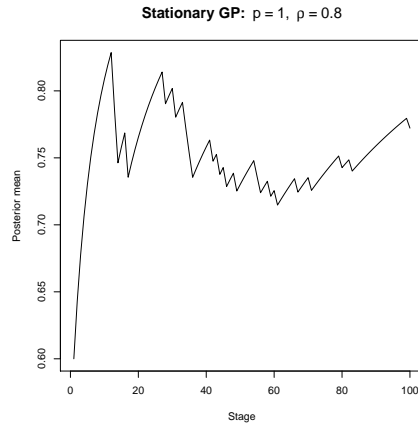
- (S1) $X_{(s,t)} = 0.5X_{(s,t-1)} + \epsilon_{(s,t)}$, where $X_{s,0} = \mathbf{0}$ and $\epsilon_{(s,t)}$ are zero mean GPs independent over time with spatial covariance structure

$$Cov(\epsilon_{(s_1,t)}, \epsilon_{(s_2,t)}) = \exp(-\|s_1 - s_2\|/\psi). \quad (14.6)$$

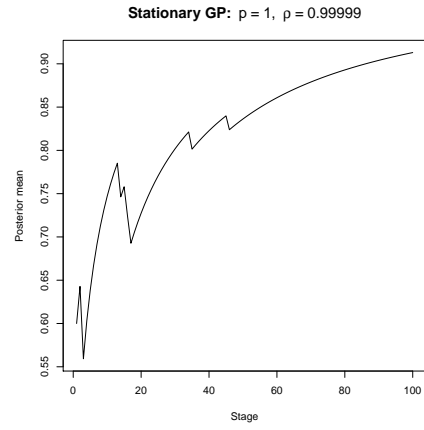
The above model defines a spatially and temporally stationary Gaussian random field.

- (S2) $X_{(s,t)} = 0.5X_{(s,t-1)} + 0.4X_{(s,t-1)}\epsilon_{(s,t-1)} + \epsilon_{(s,t)}$, where $X_{s,0} = \mathbf{0}$ and $\epsilon_{(s,t)}$ are zero mean GPs independent over time with spatial covariance (14.6). This model is a spatially and temporally non-Gaussian random field.

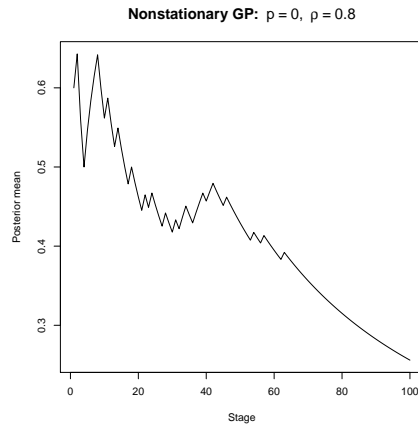
For both the above models, we set $\lambda = 5$ for simulating the locations, and fix $\psi = 0.5$ and 1 for two sets of data simulations for each of $(m = 100, T = 200)$ and $(m = 500, T = 200)$ sample sizes.



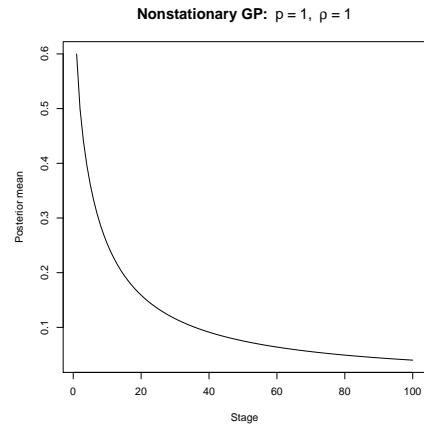
(a) Correct detection of stationarity.



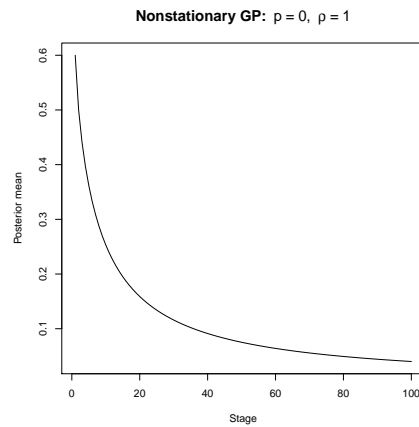
(b) Correct detection of stationarity.



(c) Correct detection of nonstationarity.



(d) Correct detection of nonstationarity.



(e) Correct detection of nonstationarity.

Figure 14.4: Detection of strong stationarity and nonstationarity in spatio-temporal data drawn from GPs with 50 locations and 20 time points.

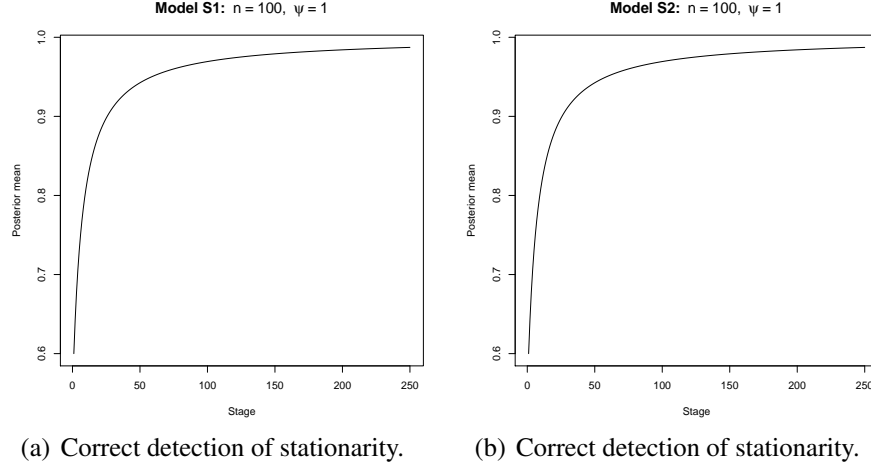


Figure 14.5: Detection of strong stationarity in spatio-temporal data drawn from models $S1$ and $S2$ with sample size 100 locations and 200 time points, with $\psi = 1$ and $\lambda = 5$.

For checking strict stationarity, for sample size $(m = 100, T = 200)$, our strategy for choosing \hat{C}_1 , detailed in Section 14.1, gave $\hat{C}_1 = 0.042$, and for $(m = 500, T = 200)$, we obtained $\hat{C}_1 = 0.045$. As before, we consider $K = 250$ clusters in both the cases.

For covariance stationarity, we obtained $\hat{C}_1 = 0.4$ for both $(m = 100, T = 200)$ and $(m = 500, T = 200)$. For the first sample size, we obtained $\mathcal{N}_{i, h_j, h_{j+1}}$ defined by $h_1 = 0, h_2 = 0.4, h_3 = 0.7, h_4 = 0.9, h_5 = 2, h_6 = 3$. For the second sample size, we also obtained $h_7 = 4$ for model $S1$ when $\psi = 5$ and for model $S2$ when $\psi = 1$ and $\psi = 5$.

For brevity we show the strict and weak stationarity convergence results only for $(m = 100, T = 200)$, with $\psi = 1$, depicted as Figures 14.5, 14.6 and 14.7.

14.6.2 Simulations under stationarity with Whittle spatial covariance function

Following Bandopadhyay *et al.* (2017) we now repeat the above experiments with the same models $S1$ and $S2$ but with the exponential covariance functions replaced with the Whittle covariance function (13.3), with $\psi = 0.37$ and 0.72 . Note that the values of \hat{C}_1 remain the same as before; however, the minimum values of \hat{C}_1 for which covariance stationarities were achieved, varied between 0.15, 0.2 and 0.3.

As expected, we obtained excellent results in all the cases, but present the results corresponding to $(m = 100, T = 200)$ and $\psi = 0.72$ for brevity. Figures 14.8, 14.9 and 14.10 depict our Bayesian results regarding strict and weak stationarities of the models $S1$ and $S2$.

14.6.3 Simulations under nonstationarity

We now apply our Bayesian methodology to the three nonstationary models and setups considered by Bandopadhyay *et al.* (2017).

(NS1) $X_{(s,t)} = 0.5X_{(s,t-1)} + \left(1.3 + \sin\left(\frac{2\pi t}{400}\right)\right) \epsilon_{(s,t)}$, where $X_{s,0} = \mathbf{0}$ and $\epsilon_{(s,t)}$ are zero mean GPs independent over time with spatial covariance structure (14.6). Note that this is a temporally

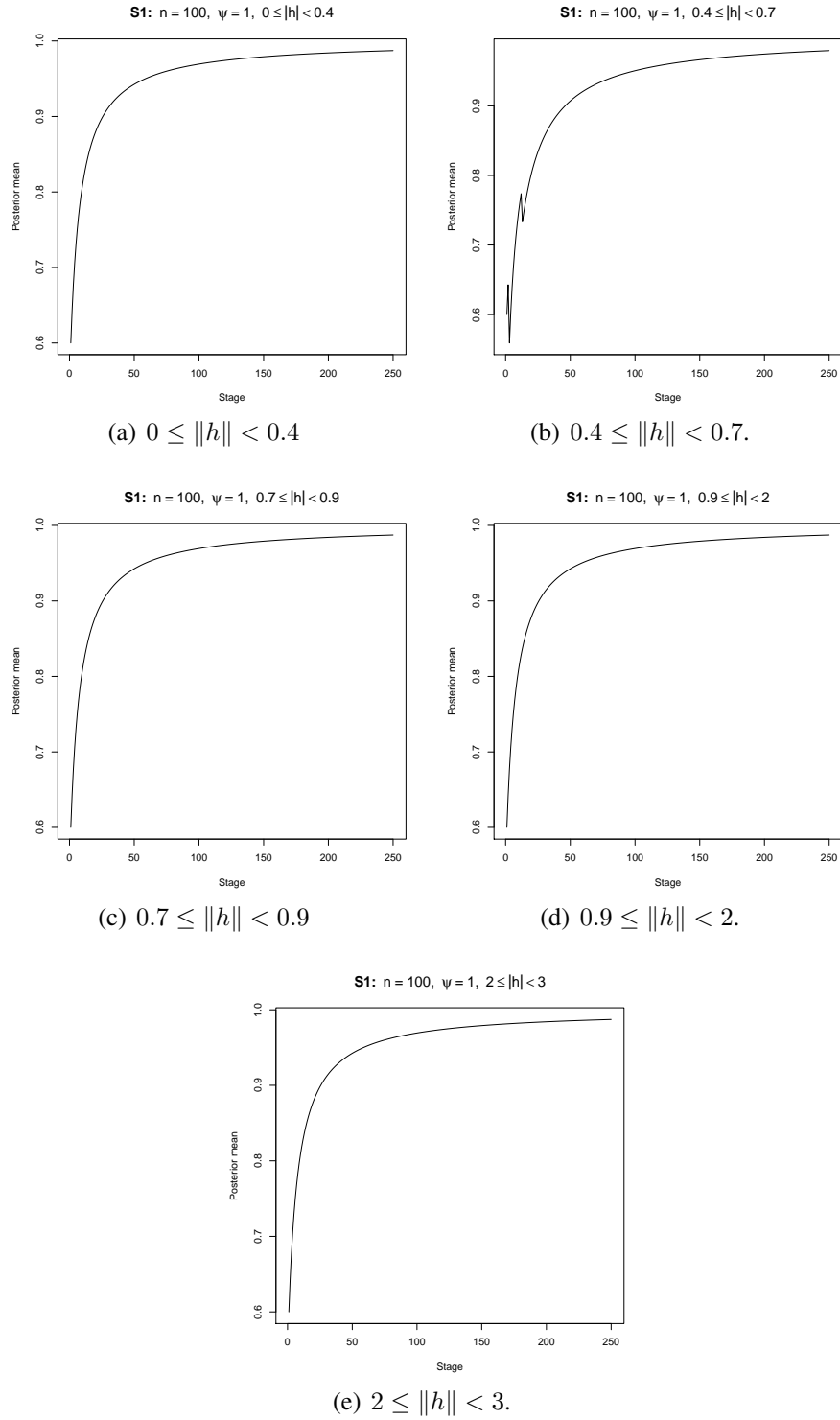


Figure 14.6: Detection of covariance stationarity in spatio-temporal data drawn from model $S1$ with sample size 100 locations and 200 time points, with $\psi = 1$ and $\lambda = 5$.

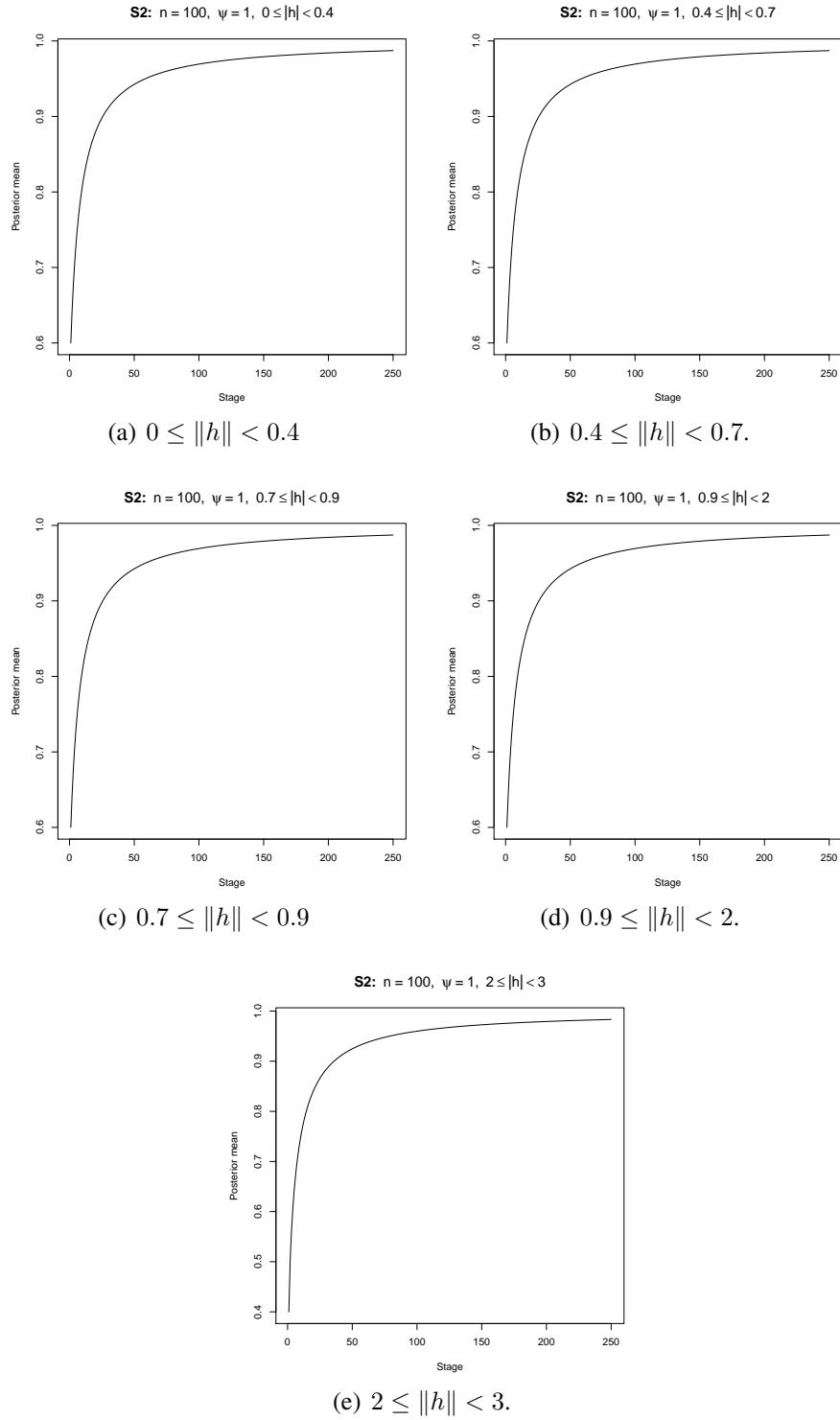


Figure 14.7: Detection of covariance stationarity in spatio-temporal data drawn from model $S2$ with sample size 100 locations and 200 time points, with $\psi = 1$ and $\lambda = 5$.

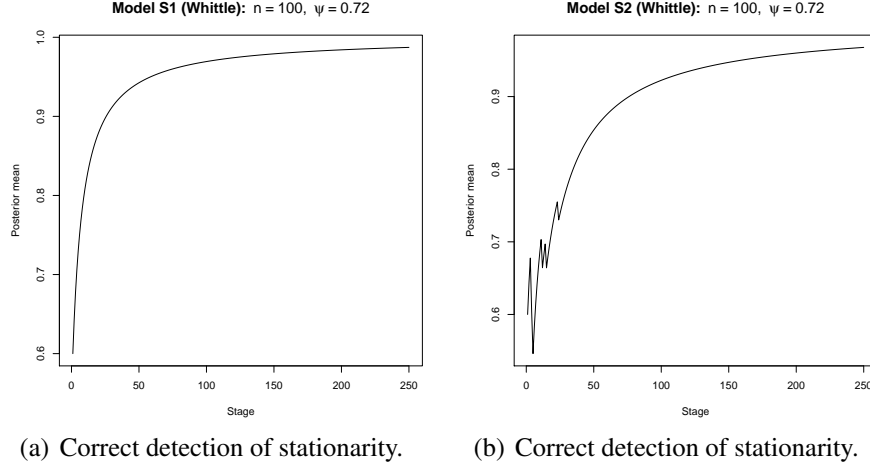


Figure 14.8: Detection of strong stationarity in spatio-temporal data drawn from models $S1$ and $S2$ with sample size 100 locations and 200 time points, corresponding to Whittle spatial covariance with $\psi = 0.72$ and $\lambda = 5$.

nonstationary but spatially stationary Gaussian random field. We consider $\psi = 0.5$ and 1, and $\lambda = 5$ for the simulations.

(NS2) $X_{(s,t)} = 0.5X_{(s,t-1)} + 0.4X_{(s,t-1)}\epsilon_{(s,t-1)} + \eta_{(s,t)}$, where $X_{s,0} = \mathbf{0}$ and $\eta_{(s,t)}$ are zero mean GPs independent over time with nonstationary spatial covariance given as follows.

$$Cov(\eta_{(s_1,t)}, \eta_{(s_2,t)}) = \left| \Sigma\left(\frac{s_1}{\lambda}\right) \right|^{\frac{1}{4}} \left| \Sigma\left(\frac{s_2}{\lambda}\right) \right|^{\frac{1}{4}} \left| \frac{\Sigma\left(\frac{s_1}{\lambda}\right) + \Sigma\left(\frac{s_2}{\lambda}\right)}{2} \right|^{-\frac{1}{2}} \exp\left[-\sqrt{Q_\lambda(s_1, s_2)}\right], \quad (14.7)$$

where $Q_\lambda(s_1, s_2) = 2(s_1 - s_2)^T [\Sigma(\frac{s_1}{\lambda}) + \Sigma(\frac{s_2}{\lambda})]^{-1} (s_1 - s_2)$ and $\Sigma(\frac{s}{\lambda}) = \Gamma(\frac{s}{\lambda}) \Lambda \Gamma(\frac{s}{\lambda})^T$. In the above,

$$\Gamma\left(\frac{s}{\lambda}\right) = \begin{pmatrix} \gamma_1\left(\frac{s}{\lambda}\right) & -\gamma_2\left(\frac{s}{\lambda}\right) \\ \gamma_2\left(\frac{s}{\lambda}\right) & \gamma_1\left(\frac{s}{\lambda}\right) \end{pmatrix}; \quad \Lambda = \begin{pmatrix} 1 & 0 \\ 0 & \frac{1}{2} \end{pmatrix},$$

where $\gamma_1\left(\frac{s}{\lambda}\right) = \log(u/\lambda + 0.75)$, $\gamma_2\left(\frac{s}{\lambda}\right) = (u/\lambda)^2 + (v/\lambda)^2$, and $s = (u, v)^T$.

With this, the model is a temporally stationary and spatially nonstationary Gaussian random field. For simulations, we consider $\lambda = 20$, following Bandopadhyay *et al.* (2017).

(NS3) $X_{(s,t)} = 0.5X_{(s,t-1)} + (1.3 + \sin(\frac{2\pi t}{400}))\eta_{(s,t)}$, where $X_{s,0} = \mathbf{0}$ and $\eta_{(s,t)}$ are zero mean GPs independent over time with nonstationary spatial covariance given by (14.7). This defines a temporally and spatially nonstationary Gaussian random field. Again, we set $\lambda = 20$ for simulations, following Bandopadhyay *et al.* (2017).

We obtained the right results in all the cases of nonstationarity, but present the results corresponding to $(m = 100, T = 200)$ and $\psi = 1$ for brevity. Figure 14.11 provides the results on strong stationarity and the result on covariance stationarity of $NS1$ is depicted in Figure 14.12. For detection of strict nonstationarity, \hat{C}_1 varied between 0.04 and 0.05. The same values also

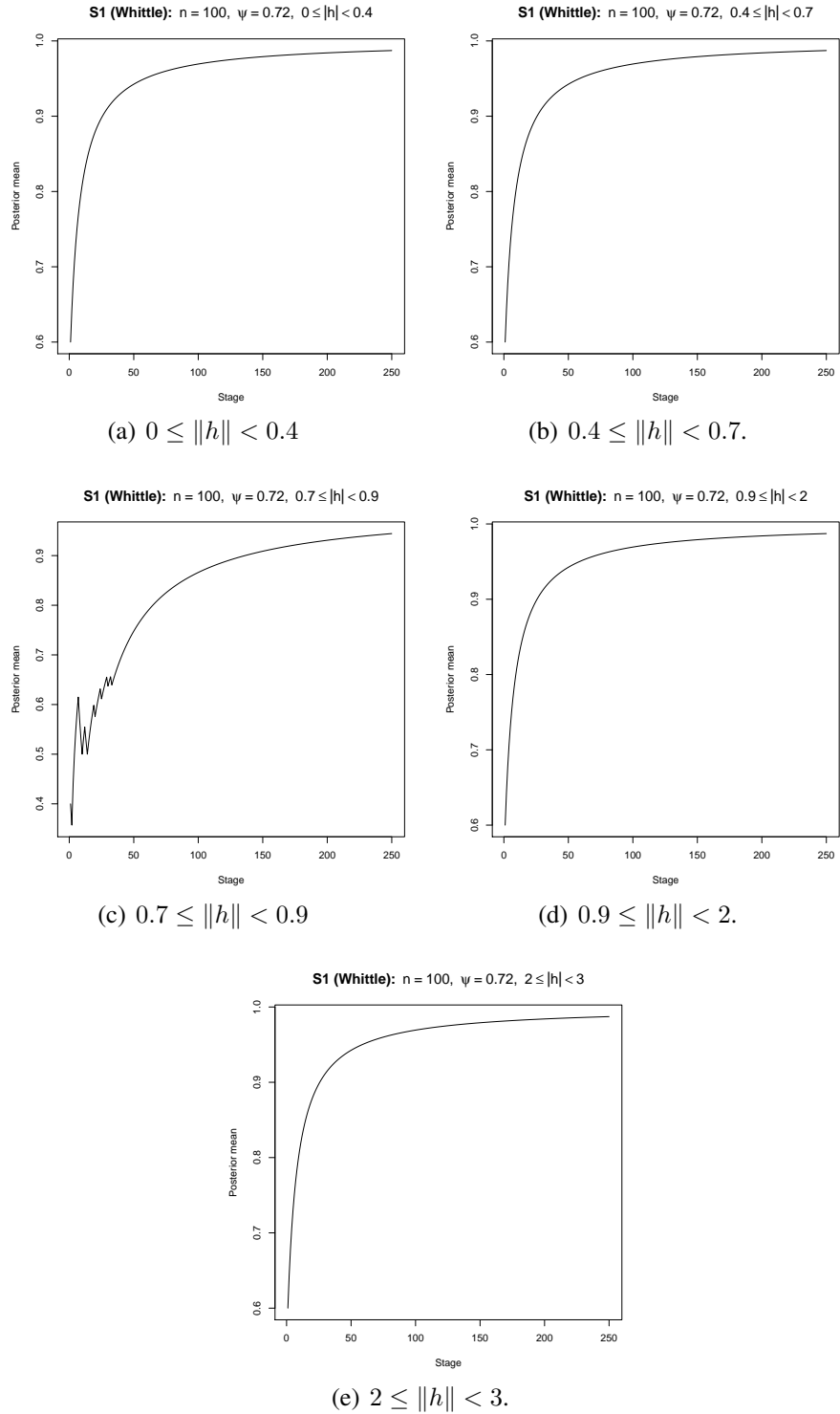


Figure 14.9: Detection of covariance stationarity in spatio-temporal data drawn from model $S1$ with sample size 100 locations and 200 time points, corresponding to Whittle spatial covariance with $\psi = 0.72$ and $\lambda = 5$.

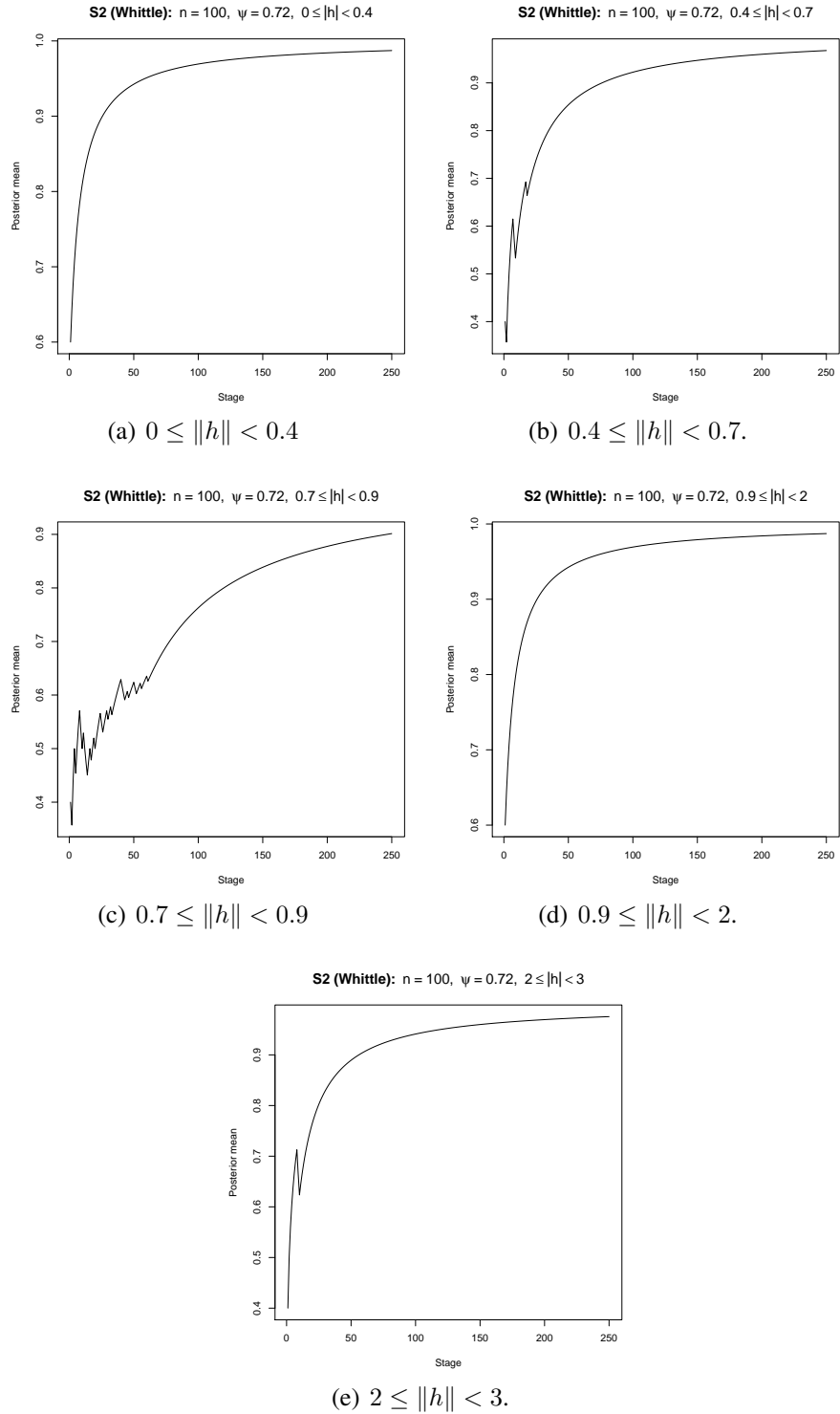


Figure 14.10: Detection of covariance stationarity in spatio-temporal data drawn from model $S2$ with sample size 100 locations and 200 time points, corresponding to Whittle spatial covariance with $\psi = 0.72$ and $\lambda = 5$.

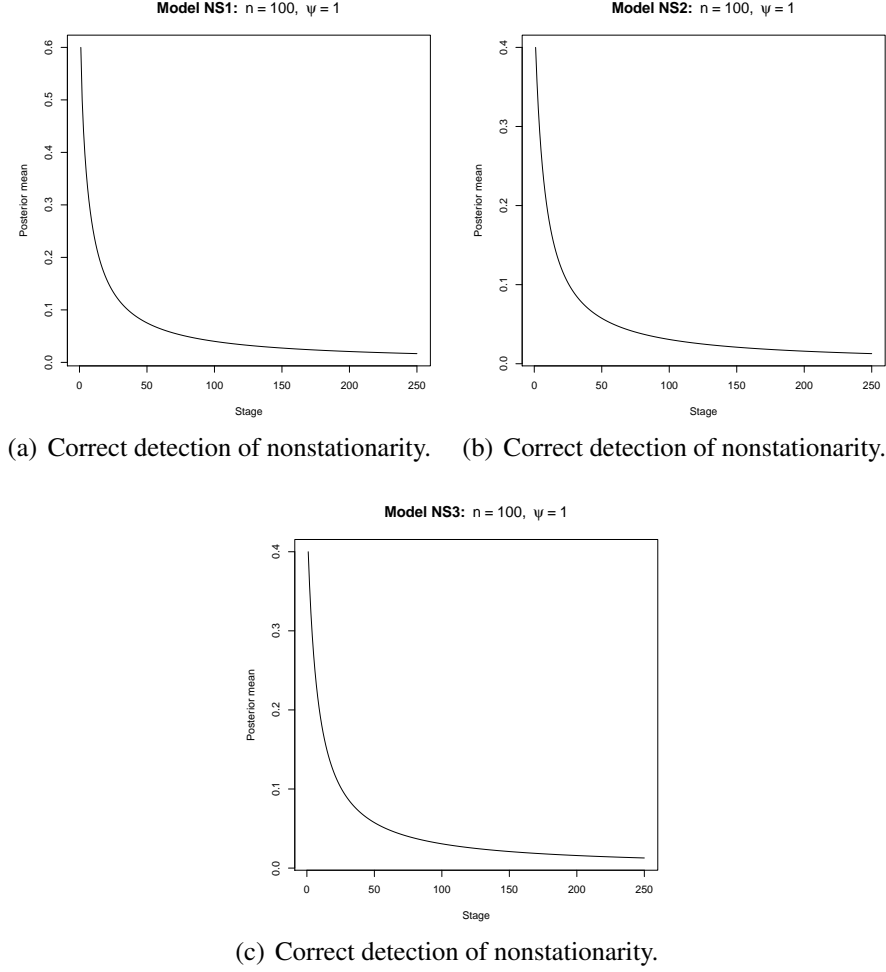


Figure 14.11: Detection of strong nonstationarity in spatio-temporal data drawn from models $NS1$, $NS2$ and $NS3$ with sample size 100 locations and 200 time points.

yielded respective covariance nonstationarities in these examples. However, the maximum values of \hat{C}_1 for detecting covariance nonstationarities varied between 0.05, 0.15, 0.2 and 0.3.

14.6.4 Overall comparison of our results with those of Bandopadhyay *et al.* (2017)

First, our Bayesian procedure is designed to identify both weak and strict stationarity of the underlying spatio-temporal process, while the methods of Bandopadhyay *et al.* (2017) are meant for detection of weak stationarity only, and not for strict stationarity.

Second, our method requires the only assumption of local stationarity, which is expected to hold in general. In contrast, the methods of Bandopadhyay *et al.* (2017) require a variety of assumptions, which may be difficult to verify in practice.

Overall, our Bayesian procedure worked adequately for all the strict stationarity and nonstationarity cases that we considered. The method also performed satisfactorily whenever there existed well-defined regions $\mathcal{N}_{i,h_j,h_{j+1}}$ in the data set. On the other hand, the methods of Bandopadhyay *et al.* (2017) did not yield satisfactory results particularly when the underlying process is non-

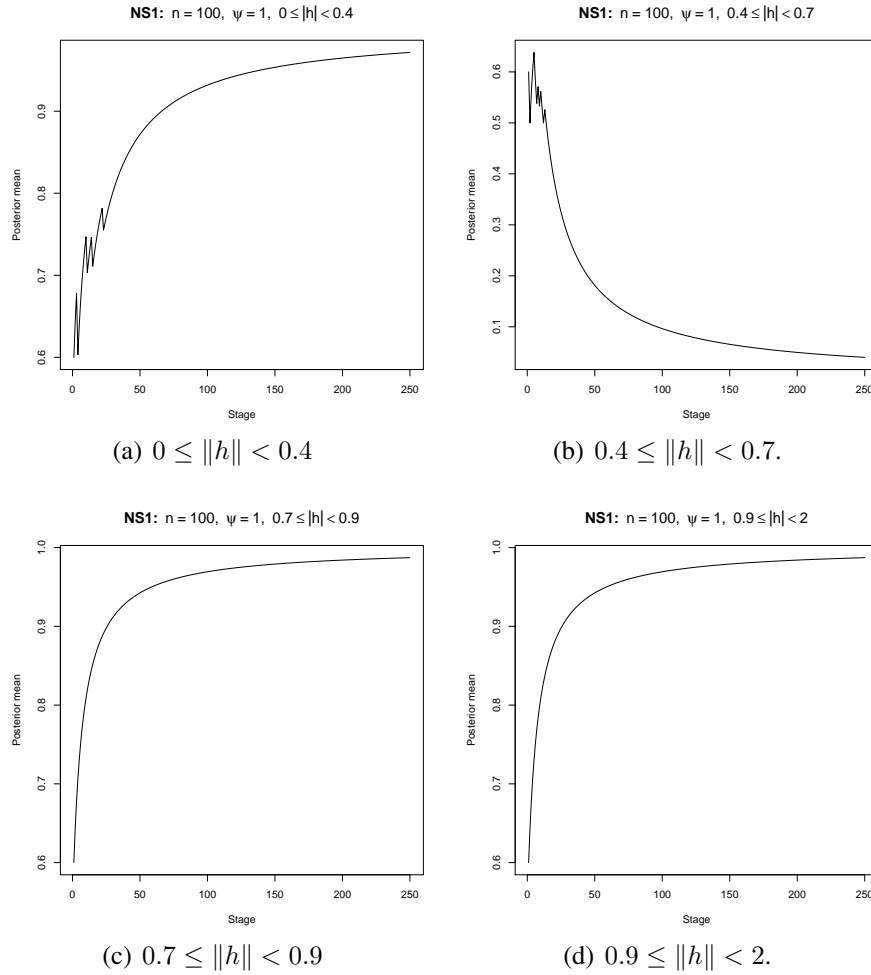


Figure 14.12: Detection of covariance nonstationarity in spatio-temporal data drawn from model *NS1* with sample size 100 locations and 200 time points.

Gaussian.

15 Real data analyses for spatial and spatio-temporal data

Das and Bhattacharya (2020) considered three real spatial and spatio-temporal data sets on pollutants for illustration of their new general nonparametric spatial and spatio-temporal model and methods. One is an ozone data set, which is a spatial data. Initially, Das and Bhattacharya (2020) fitted a stationary model, a special case of their general model, to the ozone data, but obtained unsatisfactory fit. This prompted them to fit the nonstationary instance of their model, which yielded adequate results. Thus, nonstationarity of the ozone data seems to be more plausible than stationarity. Here we establish with our Bayesian method that this is indeed the case.

The other two data sets are spatio-temporal data sets on particulate matters (PM), which are mixtures of solid particles and liquid droplets found in the air. The data sets correspond to measurements of air concentrations of two different size ranges – PM 10 and PM 2.5. The first one, PM 10, is suspected to be nonstationary, while PM 2.5 is suspected to be stationary in the literature (see, for example, Paciorek *et al.* (2009)). With our Bayesian method for characterizing stationarity and nonstationarity, we establish that such intuitions are correct.

For details regarding the three data sets, see Das and Bhattacharya (2020). There are also covariates associated with the three data sets, which have been utilized by Das and Bhattacharya (2020) for their modeling purpose. However, for checking stationarity and nonstationarity, only the responses are necessary. Hence, for our current purpose, the covariates are unnecessary. We evaluate all the final responses in their log scales.

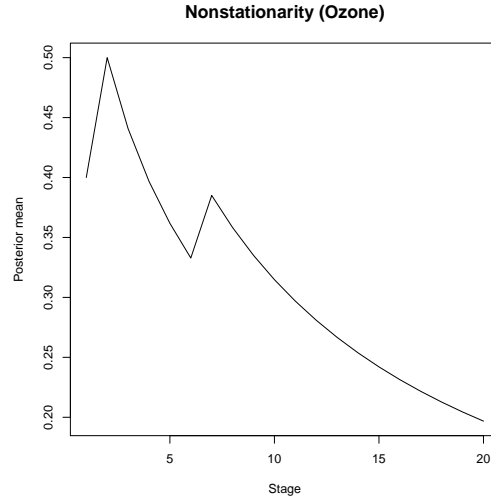
15.1 Spatial ozone data

After appropriate data transformations (see Das and Bhattacharya (2020)), we obtain 76 observations, evaluated in the log scale. To obtain \hat{C}_1 , we first generate 76 observations from a GP with the Whittle covariance function given by (13.3), with $\psi = 0.8$, and with the same set of locations as the ozone data. We set $K = 20$ for this small data set, and obtain the minimum value of \hat{C}_1 that ensured stationarity for this GP data with our Bayesian method, to be 0.38. With this value of \hat{C}_1 and larger (even with $\hat{C}_1 = 0.43$), we obtained clear evidence of nonstationarity for the ozone data, as depicted in Figure 15.1.

To check covariance stationarity, we obtain four neighborhoods $\mathcal{N}_{i,h_j,h_{j+1}}$, for $j = 1, 2, 3, 4$, where $h_1 = 0.0$, $h_2 = 0.2$, $h_3 = 0.4$, $h_4 = 0.6$ and $h_5 = 0.8$. With $K = 20$ and the same Whittle covariance based GP data for strict stationarity, the same value $\hat{C}_1 = 0.38$ turned out to be the minimum value ensuring covariance stationarity for the GP data. Figure 15.2 shows covariance nonstationarity for the ozone data with $\hat{C}_1 = 0.38$. Indeed, convergence to zero is indicated with \mathcal{N}_{i,h_2,h_3} .

15.2 Spatio-temporal PM 10 data

This data set consists of 70572 observations, a part of which has been used by Das and Bhattacharya (2020) for model fitting. However, here we use all 70572 log-response values to check strict and covariance stationarity. To obtain \hat{C}_1 , we need to generate GP samples of size 70572 with



(a) Nonstationarity (ozone data).

Figure 15.1: Detection of nonstationarity of the ozone data with our Bayesian method.

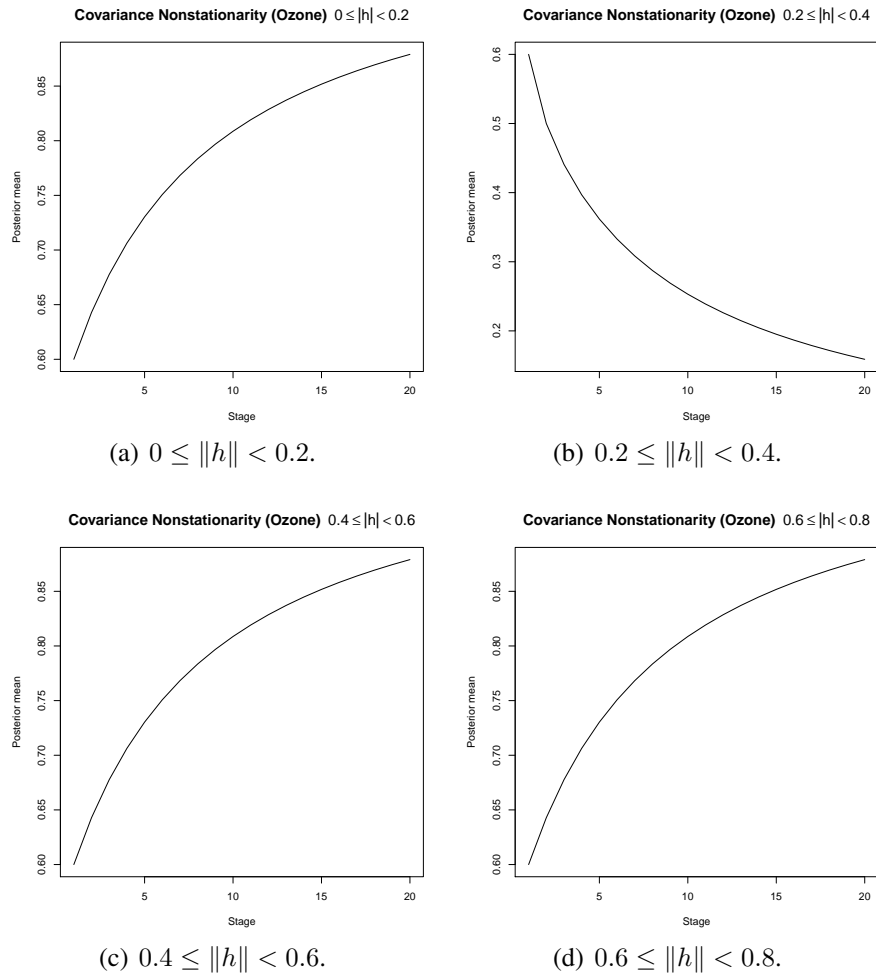
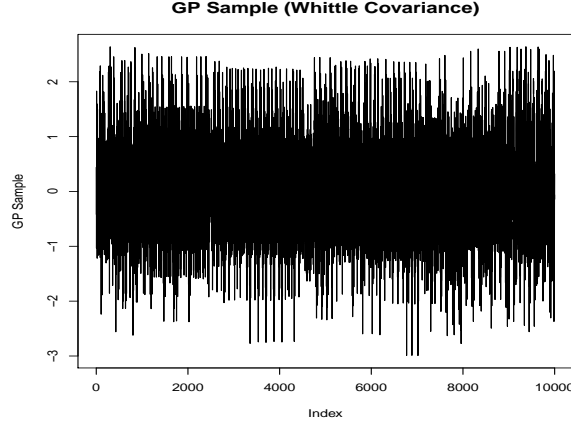
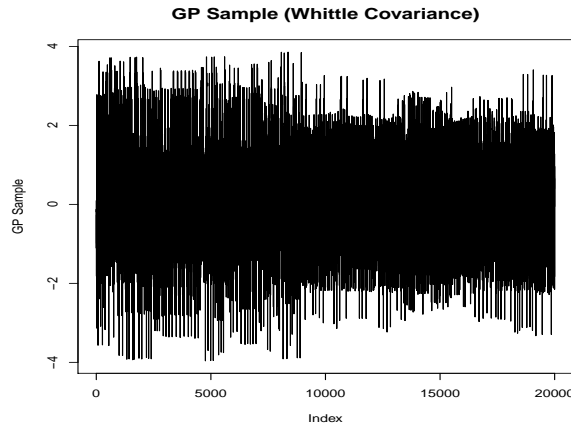


Figure 15.2: Detection of covariance nonstationarity of the ozone data.



(a) GP sample size 10000.

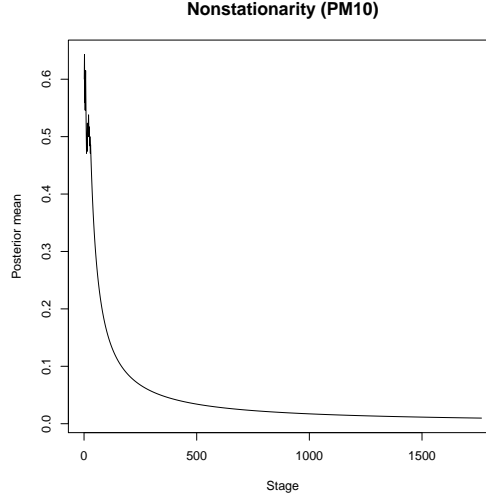


(b) GP sample size 20000.

Figure 15.3: GP samples of sizes 10000 and 20000 for Whittle covariance with $\psi = 0.8$ for PM 10 data.

the Whittle covariance function and the locations, time points corresponding to the real PM 10 data set. However, generation of such a large GP sample turned out to be prohibitive with our current infrastructure. But more of concern is the issue that the stability of the covariance matrix turned out to steadily deteriorate for dimensions larger than 100000. Figure 15.3 shows two GP samples of sizes 10000 and 20000 generated using the *R*-package “mvnfast”, using 80 parallel cores. Although the sample of size 10000 is stable, the other shows increasing variability from index 10000 onwards. Hence, to obtain \hat{C}_1 we consider the GP sample of size 10000. Setting $K = 250$ as in the simulation studies, we obtain $\hat{C}_1 = 0.16$ for checking strict stationarity. For the real PM 10 data of size 70572, we then set $\hat{C}_1 = 0.16$ and $K = 1764$. The latter is chosen such that the number of observations per cluster is on the average 40, to match the average number of observations per cluster in the simulated GP data. Figure 15.4 clearly indicates strict nonstationarity of the PM 10 data.

For checking covariance stationarity, our method with Whittle covariance failed to yield a valid \hat{C}_1 since we could obtain only a single neighborhood \mathcal{N}_{i,h_1,h_2} , with $h_1 = 0.0$ and $h_2 = 0.15$. Hence, we set $\hat{C}_1 = 0.16$, the same value obtained for checking strict stationarity. Again, for



(a) Nonstationarity (PM 10 data).

Figure 15.4: Detection of nonstationarity of the PM 10 data with our Bayesian method.

obtaining valid intervals, we needed to decrease the number of clusters and increase the number of observations per cluster. In this regard, setting $K = 500$ let us obtain four valid neighborhoods $\mathcal{N}_{i,h_j,h_{j+1}}$; $j = 1, 2, 3, 4$, with $h_1 = 0.0$, $h_2 = 0.1$, $h_3 = 0.2$, $h_4 = 0.3$ and $h_5 = 0.4$. Figure 15.5 shows covariance nonstationarity for the PM 10 data, as convergence to zero is indicated with \mathcal{N}_{i,h_1,h_2} and \mathcal{N}_{i,h_2,h_3} .

15.3 Spatio-temporal PM 2.5 data

The PM 2.5 data set consists of 17496 observations. For checking strict stationarity, we generated a GP sample of size 17496 with the Whittle covariance function with $\psi = 0.8$, with the same locations and time points as the real PM 2.5 data. Unlike the PM 10 case, here the GP sample turned out to be stable, as shown in Figure 15.6. Setting $K = 437$, so that there are 40 observations on the average in each cluster, we obtained $\hat{C}_1 = 0.02$ with the Whittle based GP sample. Figure 15.7 shows that the PM 2.5 data is strongly stationary. Hence, it is not necessary to check covariance stationarity of this data.

16 Bayesian characterization of point processes

Point pattern analysis is the study involving analysis of the spatial distribution of the observed events and to infer about the underlying data-generating process. In this regard, an important question to ask is whether or not interactions exist between the events. Hence, a pertinent test that is often used in point pattern analysis is the test of complete spatial randomness (CSR), that is, if the points are independently and uniformly distributed over the study area. Theoretically, homogeneous Poisson point process (HPP) corresponds to CSR, and thus tests for CSR can be devised on such basis, assuming the Poisson process framework for independent disjoint sets of events. However, rejecting CSR only rejects the HPP assumption and does not facilitate conclusion of stationarity or nonstationarity, Poisson or non-Poisson process. Bayesian characterization of

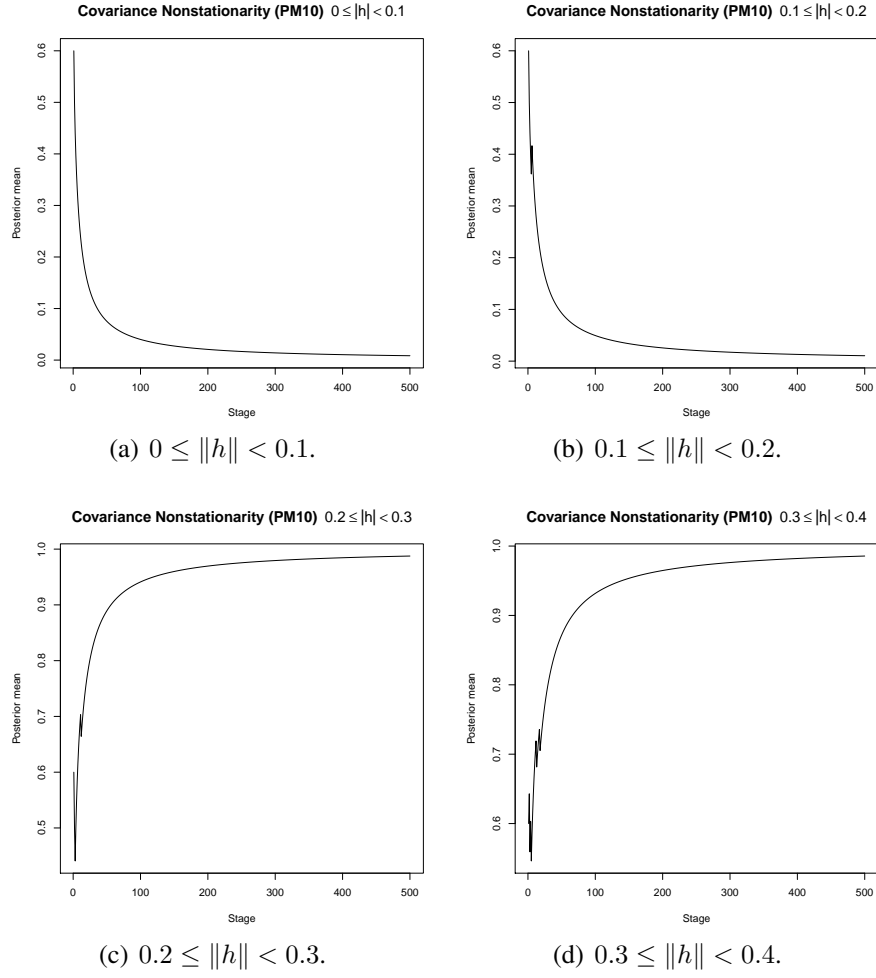


Figure 15.5: Detection of covariance nonstationarity of the PM 10 data.

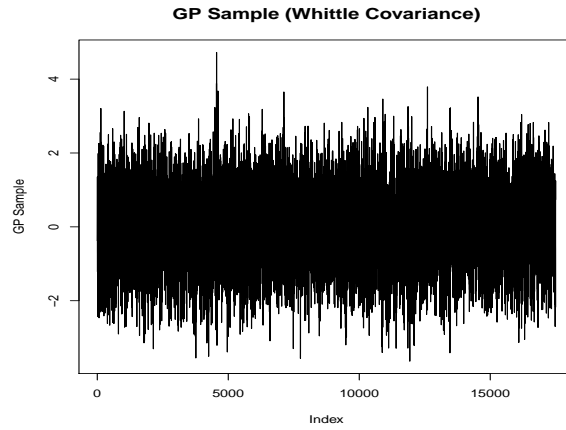
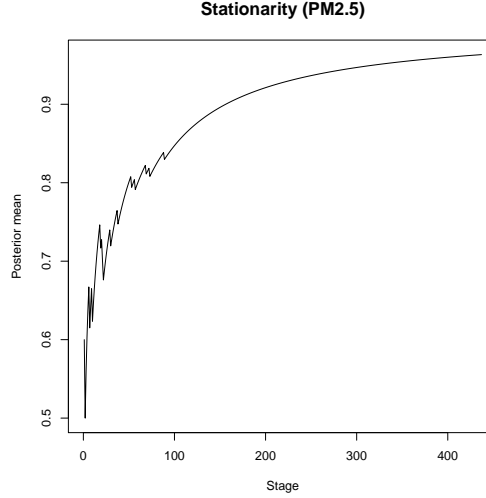


Figure 15.6: GP sample of size 17496 for Whittle covariance with $\psi = 0.8$ for PM 2.5 data.



(a) Stationarity (PM 2.5 data).

Figure 15.7: Detection of stationarity of the PM 2.5 data with our Bayesian method.

stationarity and nonstationarity can be achieved as before, while Bayesian characterization of CSR and Poisson assumption require further work. To characterize the Poisson assumption we exploit mutual independence of disjoint sets of events, under the assumption of orderliness and almost sure boundedly finite property of the process without fixed atoms.

Testing for CSR can be found in O’Sullivan and Unwin (2003), Waller and Gotway (2004) and Schabenberger and Gotway (2005). The key ingredient in such tests is the so-called G function that provides the distribution of the distance from any arbitrary event to its nearest event. Specifically, let d_{ij} denote the distance between the i -th and j -th events in a set of n events, and for $s = 1, \dots, n$, let $d_s = \min \{d_{st} : t \neq s\}$. Consider the empirical distribution function

$$\hat{G}(x) = \frac{\sum_{s=1}^n I(d_s \leq x)}{n}. \quad (16.1)$$

Under CSR, that is, under the assumption of homogeneous Poisson point process, $\hat{G}(x)$ has expectation

$$G(x) = 1 - \exp(-\lambda \pi x^2), \quad (16.2)$$

the G -function. Here λ is the intensity, or the number of events per unit area, the maximum likelihood estimator of which is given by $\tilde{\lambda} = n/|W|$, where W is the bounded region where the points are observed, and $|W|$ denotes the volume of W . Indeed, the entire point process \mathbf{X} defined on some region $\mathcal{S} \subset \mathbb{R}^d$, for some $d \geq 1$ can not be observed, and hence a bounded region $W \subset \mathcal{S}$ is considered where points are observed. Let

$$\tilde{G}(x) = 1 - \exp(-\tilde{\lambda} \pi x^2), \quad (16.3)$$

Let us assume that $\mathbf{X}_K = \{X_s : s \in \cup_{i=1}^K \mathcal{N}_i\}$ has been observed, for $K > 1$. Here $\cup_{i=1}^K \mathcal{N}_i$ corresponds to the observation window W . For the purpose of asymptotics, we assume that $|\mathcal{S}|$, the volume of \mathcal{S} tends to infinity, so that even though $|W|$ remains finite, n , the number of points

in W tends to infinity, almost surely.

For any $x > 0$, consider

$$\hat{G}_i(x) = n_i^{-1} \sum_{s \in \mathcal{N}_i} I(d_s \leq x), \quad (16.4)$$

where $n_i = |\mathcal{N}_i|$, as before. Note that $n = \sum_{i=1}^K n_i$.

Now let

$$\begin{aligned} \hat{G}_K(x) &= \frac{\sum_{s \in \cup_{i=1}^K \mathcal{N}_i} I(d_s \leq x)}{\sum_{i=1}^K n_i} \\ &= \frac{\sum_{i=1}^K n_i \hat{G}_i(x)}{\sum_{i=1}^K n_i} = \sum_{i=1}^K \hat{p}_{iK} \hat{G}_i(x), \end{aligned} \quad (16.5)$$

where $\hat{p}_{iK} = n_i / \sum_{j=1}^K n_j$, as before. Let us now assume (2.4), which we recall as

$$\hat{p}_{iK} = \frac{n_i}{\sum_{j=1}^K n_j} \rightarrow p_{iK} = \frac{p_i}{\sum_{j=1}^K p_j},$$

as $n_j \rightarrow \infty$, for $j = 1, \dots, K$. Here $0 \leq p_i \leq 1$, such that $\sum_{i=1}^K p_i = 1$.

Let W_d denote the space where the distances d_i , $i = 1, \dots, n$, associated with the observation window W , lie upon. However, for the asymptotic theory, we must let the window W and corresponding W_d to grow, otherwise the number of points n can not tend to infinity. Indeed, for fixed W , even the MLE $\tilde{\lambda} = n/|W|$ is not a consistent estimator for λ in the HPP case. Thus, in this regard, we consider the sequences W_r , W_{dr} , $K = K_r$, n_{ir} , n_r , K_r , \hat{p}_{iK_r} and $\tilde{\lambda}_r$, for $r = 1, 2, \dots$, where the suffix r is incorporated to our previous notation to signify sequences. Let $|W_r| \rightarrow \infty$ as $r \rightarrow \infty$. Note that K_r may remain finite even as $r \rightarrow \infty$. Let us also denote by G_{true} the true point process generating the data. Note that for HPP, $G_{true} = G$. In reality, the true point process, and hence G_{true} , is unknown.

A problem associated with HPP is that it is hard to establish $\sup_{x \in W_{dr}} |\hat{G}_K - \tilde{G}(x)| \rightarrow 0$, in either weak or strong sense. To see this, note that

$$\begin{aligned} \sup_{x \in W_{dr}} |\tilde{G}(x) - G(x)| &= \sup_{x \in W_{dr}} \left| \exp(-\lambda \pi x^2) \left(1 - \exp\left(-\pi x^2 (\tilde{\lambda}_r - \lambda)\right) \right) \right| \\ &\leq 1 - \inf_{x \in W_{dr}} \exp\left(-\pi x^2 |\tilde{\lambda}_r - \lambda|\right). \end{aligned}$$

Since $\exp\left(-\pi x^2 |\tilde{\lambda}_r - \lambda|\right)$ is decreasing in x^2 and W_{dr} is bounded, the infimum over W_{dr} is given by $\exp\left(-\pi \xi_r^2 |\tilde{\lambda}_r - \lambda|\right)$, where ξ_r is the maximum interpoint distance in W_{dr} . In other words,

$$\sup_{x \in W_d} |\tilde{G}(x) - G(x)| \leq 1 - \exp\left(-\pi \xi_r^2 |\tilde{\lambda}_r - \lambda|\right). \quad (16.6)$$

By Markov's inequality, for any $\epsilon > 0$,

$$P\left(\xi_r^2 \left|\tilde{\lambda}_r - \lambda\right| > \epsilon\right) < \epsilon^{-2} \xi_r^4 E\left(\frac{n_r}{|W_r|} - \lambda\right)^2 = \epsilon^{-2} \lambda \frac{\xi_r^4}{|W_r|},$$

which tends to zero if $\frac{\xi_r^4}{|W_r|} \rightarrow 0$ as $r \rightarrow \infty$. But as can be easily verified, this does not hold for regular window shapes such as squares, rectangles, circles, triangles, etc. Indeed, for these shapes, $\frac{\xi_r^4}{|W_r|} \rightarrow \infty$ as $r \rightarrow \infty$.

Instead of $\sup_{x \in W_{dr}} \left|\hat{G}_K(x) - \tilde{G}(x)\right|$ we shall thus deal with $\int_{W_{dr}} \left|\hat{G}_K(x) - \tilde{G}(x)\right| dG_{true}(x)$ in the following theorem.

Theorem 15 *Assume that \mathbf{X} follows homogeneous Poisson point process, and that the points are observed in the window W_r , where $|W_r| \rightarrow \infty$ as $r \rightarrow \infty$. Let W_{dr} denote the space of the distances associated with W_r . Then, for all values of $K_\infty = \lim_{r \rightarrow \infty} K_r$,*

$$\lim_{r \rightarrow \infty, n_{ir} \rightarrow \infty, i=1, \dots, K_r} \int_{W_{dr}} \left|\hat{G}_{K_r}(x) - \tilde{G}(x)\right| dG_{true}(x) = 0, \quad (16.7)$$

almost surely if $\sum_{r=1}^{\infty} |W_r|^{-1} < \infty$.

Proof. Observe that

$$\begin{aligned} & \int_{W_{dr}} \left|\hat{G}_{K_r}(x) - \tilde{G}(x)\right| dG_{true}(x) \\ & \leq \sup_{x \in W_{dr}} \left|\hat{G}_{K_r}(x) - G(x)\right| G_{true}(W_{dr}) + \int_{W_{dr}} \left|\tilde{G}(x) - G(x)\right| dG_{true}(x) \\ & \leq \sup_{x \in W_{dr}} \left|\hat{G}_{K_r}(x) - G(x)\right| + \int_{W_{dr}} \left|\tilde{G}(x) - G(x)\right| dG_{true}(x). \end{aligned} \quad (16.8)$$

Since

$$\sup_{x \in W_{dr}} \left|\hat{G}_{K_r}(x) - G(x)\right| = \sup_{x \in W_{dr}} \left|\sum_{i=1}^{K_r} \left(\hat{G}_i(x) - G(x)\right)\right| \leq \sum_{i=1}^{K_r} \hat{p}_{iK_r} \sup_{x \in W_{dr}} \left|\hat{G}_i(x) - G(x)\right|. \quad (16.9)$$

Now, as $r \rightarrow \infty$, the right hand side of (16.9) converges almost surely to

$$\sum_{i=1}^{K_\infty} p_{iK_\infty} \lim_{r \rightarrow \infty} \sup_{x \in W_{dr}} \left|\hat{G}_i(x) - G(x)\right|, \quad (16.10)$$

since $\hat{p}_{iK_r} \rightarrow p_{iK_\infty}$ in the same way as (2.4). Also, $\sup_{x \in W_{dr}} \left|\hat{G}_i(x) - G(x)\right| \xrightarrow{a.s.} 0$, as $r \rightarrow \infty$ and $n_{ir} \rightarrow \infty$ by Glivenko-Cantelli theorem for stationary random variables (Stute and Schumann (1980)). That is, given any K_∞ , (16.10) converges to zero almost surely. Thus, (16.10) converges to zero almost surely, even as $K_\infty \rightarrow \infty$. Hence, it follows from these arguments and (16.9) that

for all values of K_∞ ,

$$\sup_{x \in W_{dr}} \left| \hat{G}_K(x) - G(x) \right| \xrightarrow{a.s.} 0, \text{ as } n_{ir} \rightarrow \infty, i = 1, \dots, K_r, r \rightarrow \infty,$$

and hence

$$\int_{W_{dr}} \left| \hat{G}_K(x) - G(x) \right| dG_{true}(x) \xrightarrow{a.s.} 0, \text{ as } n_{ir} \rightarrow \infty, i = 1, \dots, K_r, r \rightarrow \infty. \quad (16.11)$$

Now note that, for $\tilde{\lambda}_r = n_r/|W_r|$,

$$\begin{aligned} \int_{W_{dr}} \left| \tilde{G}(x) - G(x) \right| dG_{true}(x) &= \int_{W_{dr}} \left| \exp(-\lambda \pi x^2) \left(1 - \exp(-\pi x^2 (\tilde{\lambda} - \lambda)) \right) \right| dG_{true}(x) \\ &\leq G_{true}(W_{dr}) - \int_{W_{dr}} \exp(-\pi x^2 |\tilde{\lambda} - \lambda|) dG_{true}(x). \end{aligned} \quad (16.12)$$

In (16.12),

$$G_{true}(W_{dr}) \rightarrow 1, \text{ as } r \rightarrow \infty. \quad (16.13)$$

Now, by Markov's inequality, for any $\epsilon > 0$,

$$\begin{aligned} \sum_{r=1}^{\infty} P \left(|\tilde{\lambda}_r - \lambda| > \epsilon \right) &= \sum_{r=1}^{\infty} P \left(\left| \frac{n_r}{|W_r|} - \lambda \right| > \epsilon \right) \\ &< \epsilon^{-2} \sum_{r=1}^{\infty} E \left(\frac{n_r}{|W_r|} - \lambda \right)^2 = \epsilon^{-2} \lambda \sum_{r=1}^{\infty} \frac{1}{|W_r|} < \infty, \end{aligned}$$

where the last step is due to our assumption. Hence, by Borel-Cantelli lemma, $|\tilde{\lambda}_r - \lambda| \xrightarrow{a.s.} 0$, as $r \rightarrow \infty$. By dominated convergence theorem, it follows that

$$\int_{W_{dr}} \exp(-\pi x^2 |\tilde{\lambda} - \lambda|) dG_{true}(x) \xrightarrow{a.s.} 1, \text{ as } r \rightarrow \infty. \quad (16.14)$$

It follows from (16.12), (16.13) and (16.14) that

$$\int_{W_{dr}} \left| \tilde{G}(x) - G(x) \right| dG_{true}(x) \xrightarrow{a.s.} 0, \text{ as } r \rightarrow \infty. \quad (16.15)$$

The result follows by combining (16.8), (16.11) and (16.15). ■

Remark 16 Note that unlike in the previous cases where we required $K \rightarrow \infty$, here we did not require the assumption $K_\infty \rightarrow \infty$. Theorem 15 explicitly mentions that the result holds for all values of K_∞ . This difference is due to the fact that in the asymptotics of point process we assumed that the observation window W_r is growing with r , and with such growing observation window, the entire point process can be ultimately captured. Hence increasing the number of clusters is not required. From a more mathematical perspective, note that \hat{G}_K uses all the observations in the observation window, and so the value of K is irrelevant mathematically.

Remark 17 Note that by direct application of Glivenko-Cantelli theorem for stationary random variables we can obtain,

$$\sup_{x \in W_{dr}} \left| \hat{G}_{K_r}(x) - G(x) \right| \xrightarrow{a.s.} 0, \text{ as } r \rightarrow \infty. \quad (16.16)$$

This does not require breaking up the observation window W_r into sub-regions $\mathcal{N}_1, \dots, \mathcal{N}_{K_r}$, and the assumption $n_{ir} \rightarrow \infty$ for $i = 1, \dots, K_r$. However, it is important to detect which sub-regions of W_r are not representatives of CSR. From this perspective, it is important to consider the sub-regions $\mathcal{N}_1, \dots, \mathcal{N}_{K_r}$, and consideration of the form (16.5), which we formalize in our Bayesian characterization.

Let $\{c_j\}_{j=1}^\infty$ be a non-negative decreasing sequence and

$$Y_{j,n_{jr}} = \mathbb{I} \left\{ \int_{W_{dr}} \left| \hat{G}_j(x) - \tilde{G}(x) \right| dG(x) \leq c_j \right\}. \quad (16.17)$$

In practice, we shall approximate $\int_{W_{dr}} \left| \hat{G}_j(x) - \tilde{G}(x) \right| dG(x)$ by $\frac{1}{n_{jr}} \sum_{i=1}^{n_{jr}} \left| \hat{G}_j(d_i) - \tilde{G}(d_i) \right|$, where the distances d_i are assumed to correspond to the true data-generating point process G_{true} .

As before, let, for $j \geq 1$,

$$P(Y_{j,n_{jr}} = 1) = p_{j,n_{jr}}. \quad (16.18)$$

Hence, the likelihood of $p_{j,n_{jr}}$, given $y_{j,n_{jr}}$, is given by the form (4.3).

As before, we construct a recursive Bayesian methodology that formally characterizes homogeneous Poisson process and otherwise in terms of formal posterior convergence. The relevant theorems in this regard, the proofs of which are similar to stationarity and nonstationarity characterizations, are presented below as Theorems 18 and 19.

Theorem 18 For all $\omega \in \mathfrak{S} \cap \mathfrak{N}^c$, where \mathfrak{N} is some null set having probability measure zero, $\mathbf{X} \cap W$ follows homogeneous Poisson process if and only if for any monotonically decreasing sequence $\{c_j(\omega)\}_{j=1}^\infty$,

$$\pi(\mathcal{N}_1 | y_{k,n_{kr}}(\omega)) \rightarrow 1, \quad (16.19)$$

as $k \rightarrow \infty$ and $n_{jr} \rightarrow \infty$ for $j = 1, \dots, K_r$ satisfying (2.4) and $K_r \rightarrow \infty$ as $r \rightarrow \infty$, where \mathcal{N}_1 is any neighborhood of 1 (one).

Theorem 19 $\mathbf{X} \cap W$ does not follow homogeneous Poisson process if and only if for any $\omega \in \mathfrak{S} \cap \mathfrak{N}^c$ where \mathfrak{N} is some null set having probability measure zero, for any choice of the non-negative, monotonically decreasing sequence $\{c_j(\omega)\}_{j=1}^\infty$,

$$\pi(\mathcal{N}_0 | y_{k,n_{kr}}(\omega)) \rightarrow 1, \quad (16.20)$$

as $k \rightarrow \infty$ and $n_{jr} \rightarrow \infty$, $j = 1, \dots, K_r$ satisfying (2.4), and $K_r \rightarrow \infty$ as $r \rightarrow \infty$, where \mathcal{N}_0 is any neighborhood of 0 (zero).

Remark 20 Note that Theorems 18 and 19 require $K_r \rightarrow \infty$ as $r \rightarrow \infty$, even though Theorem 15 does not have this requirement. But this arises entirely for convergence of the recursive Bayesian algorithm as the stage number $k \rightarrow \infty$.

16.1 Discussion on edge correction

Since the data are observed in the bounded window W , the minimum distance d_i in the window may be larger than the true minimum distance had the complete point process \mathbf{X} been observed. In classical point process analysis, this may induce a bias in estimating the true distribution function, which is known as edge effect. Needless to mention, various corrections for such edge effect is available in the literature.

However, in the way we proceed with our Bayesian method, the edge effects do not influence our final results. The reason for this is the following. We partition the point pattern in the observation window W into K clusters using the K-means clustering algorithm. Thus, within each cluster in the interior of W , the edge effect is minimized. This is because the K-means clustering algorithm guarantees that within cluster variation is minimized and the between cluster variation is maximized, which entails that the minimum distance d_i of any point i within each cluster is often indeed the minimum when all the points are considered. Note that this is actually the case for ‘empty distances’, if the distances are measured from the centroid of each cluster. Our experiments demonstrate the validity of our aforementioned arguments in this regard.

16.2 Characterization of stationarity and nonstationarity of point processes

The characterization of stationarity and nonstationarity in the point process setup remains essentially the same as in the general situation, with the conceptual difference being consideration of W_r in the point process setup, with $|W_r| \rightarrow \infty$. We present the main results regarding stationarity and nonstationarity in the point process setup, which are slight modifications of Theorems 3, 4, 5, 6 and 7.

Theorem 21 *Let $K_r \rightarrow \infty$ as $r \rightarrow \infty$. Then*

$$\lim_{r \rightarrow \infty} \lim_{n_{jr} \rightarrow \infty, j=1, \dots, K_r} \sup_C \left| \tilde{P}_{K_r}(C) - P_\infty(C) \right| = 0, \text{ almost surely.}$$

Theorem 22 *The point process \mathbf{X} is stationary if and only if $\sup_C \left| \hat{P}_j(C) - \tilde{P}_{K_r}(C) \right| \rightarrow 0$ almost surely, as $n_{jr} \rightarrow \infty$ satisfying (2.4), $j = 1, \dots, K_r$, $K_r \rightarrow \infty$, as $r \rightarrow \infty$.*

Theorem 23 *\mathbf{X} is nonstationary if and only if $\sup_C \left| \hat{P}_j(C) - \tilde{P}_{K_r}(C) \right| > 0$ almost surely, as $n_{jr} \rightarrow \infty$ satisfying (2.4), $j = 1, \dots, K_r$, $K_r \rightarrow \infty$, as $r \rightarrow \infty$.*

Let $\{c_j\}_{j=1}^\infty$ be a non-negative decreasing sequence and

$$Y_{j,n_{jr}} = \mathbb{I} \left\{ \sup_C \left| \hat{P}_j(C) - \tilde{P}_{K_r}(C) \right| \leq c_j \right\}.$$

Let, for $j \geq 1$,

$$P(Y_{j,n_{jr}} = 1) = p_{j,n_{jr}}.$$

Theorem 24 For all $\omega \in \mathfrak{S} \cap \mathfrak{N}^c$, where \mathfrak{N} is some null set having probability measure zero, X is stationary if and only if for any monotonically decreasing sequence $\{c_j(\omega)\}_{j=1}^\infty$,

$$\pi(\mathcal{N}_1 | y_{k, n_{kr}}(\omega)) \rightarrow 1,$$

as $k \rightarrow \infty$ and $n_{jr} \rightarrow \infty$ for $j = 1, \dots, K_r$ satisfying (2.4) and $K_r \rightarrow \infty$ as $r \rightarrow \infty$, where \mathcal{N}_1 is any neighborhood of 1 (one).

Theorem 25 X is nonstationary if and only if for any $\omega \in \mathfrak{S} \cap \mathfrak{N}^c$ where \mathfrak{N} is some null set having probability measure zero, for any choice of the non-negative, monotonically decreasing sequence $\{c_j(\omega)\}_{j=1}^\infty$,

$$\pi(\mathcal{N}_0 | y_{k, n_{kr}}(\omega)) \rightarrow 1,$$

as $k \rightarrow \infty$ and $n_{jr} \rightarrow \infty$, $j = 1, \dots, K_r$ satisfying (2.4), and $K_r \rightarrow \infty$ as $r \rightarrow \infty$, where \mathcal{N}_0 is any neighborhood of 0 (zero).

16.3 Characterization of mutual independence among random variables

In this section we first characterize mutual independence among a general set of random variables $\mathbf{X}_K = (X_1, \dots, X_K)$, as $K \rightarrow \infty$, and then specialize the characterization in the point process setup. Indeed, although characterizations and tests for mutual independence among a set of random variables is available in the literature (see, for example, Puri and Sen (1971), Gieser and Randles (1997), Um and Randles (2001), Cl  roux *et al.* (1995), Bilodeau and L de Micheaux (2005), Hoffding (1948), Blum *et al.* (1961), Ghoudi *et al.* (2001), Beran *et al.* (2007), Bilodeau and Nangue (2017)), they are meant for a finite set of random variables. Moreover, such characterizations are often not computationally manageable. Here we attempt to provide a characterization for number of random variables tending to infinity, with manageable computation. Also, unlike the previous approaches, we need only asymptotic stationarity of the realizations of the random variables, not even independence.

The key idea is to consider the differences

$$\zeta_i = \sup_{t_1, \dots, t_i \in \mathbb{R}} |P(X_i \leq t_i | X_1 \leq t_1, \dots, X_{i-1} \leq t_{i-1}) - P(X_i \leq t_i)|, \quad (16.21)$$

for $i = 2, \dots, K$, with $\zeta_1 = 0$. If all ζ_i ; $i = 2, \dots, K$, are sufficiently small, then the random variables (X_1, \dots, X_K) are mutually independent. For practical purposes, we must replace

$$P(X_i \leq t_i | X_1 \leq t_1, \dots, X_{i-1} \leq t_{i-1})$$

and $P(X_i \leq t_i)$ with their corresponding empirical probabilities. In other words, we write

$$P(X_i \leq t_i | X_1 \leq t_1, \dots, X_{i-1} \leq t_{i-1}) = \frac{P(X_1 \leq t_1, \dots, X_{i-1} \leq t_{i-1}, X_i \leq t_i)}{P(X_1 \leq t_1, \dots, X_{i-1} \leq t_{i-1})}, \quad (16.22)$$

and replace $P(X_1 \leq t_1, \dots, X_{i-1} \leq t_{i-1}, X_i \leq t_i)$ and $P(X_1 \leq t_1, \dots, X_{i-1} \leq t_{i-1})$ with their corresponding empirical distribution functions

$$F_{n,1:i}(X_1 \leq t_1, \dots, X_{i-1} \leq t_{i-1}, X_i \leq t_i)$$

and

$$F_{n,1:(i-1)}(X_1 \leq t_1, \dots, X_{i-1} \leq t_{i-1}),$$

respectively. We also replace $P(X_i \leq t_i)$ with its empirical distribution function $F_{n,i}(X_i \leq t_i)$. We denote the differences of the empirical distribution functions corresponding to (16.21) by $\hat{\zeta}_i$; $i = 2, \dots, k$, with $\hat{\zeta}_1 = 0$.

However, computation of the joint empirical distribution functions $F_{n,1:i}$ often turn out to be zero numerically, even if i is not too large. To address this, we resort to Bayesian nonparametrics, with Dirichlet process prior for the joint distribution of \mathbf{X}_K . In fact, more generally, we consider a stochastic process prior for the sequence of random variables $\mathbf{X} = (X_1, X_2, X_3, \dots)$. Let G_0 denote the expected parametric stochastic process for \mathbf{X} . Specifically, we assume that $\mathbf{X} \sim G$ and $G \sim DP(\alpha G_0)$, where $DP(\alpha G_0)$ stands for Dirichlet process with base measure G_0 and strength parameter $\alpha > 0$. More transparently, let $\mathbf{X}_{i_1, i_2, \dots, i_K} = (X_{i_1}, X_{i_2}, \dots, X_{i_K})$, for any set of indices i_1, \dots, i_K . Then $\mathbf{X}_{i_1, i_2, \dots, i_K} \sim G_{i_1, i_2, \dots, i_K}$ and $G_{i_1, i_2, \dots, i_K} \sim DP(\alpha G_{0, i_1, i_2, \dots, i_K})$, where G_{i_1, i_2, \dots, i_K} and $G_{0, i_1, i_2, \dots, i_K}$ are k -dimensional distributions associated with $\mathbf{X}_{i_1, i_2, \dots, i_K}$.

Now, if data $\mathbf{X}_{i_1, i_2, \dots, i_K}^j$; $j = 1, 2, \dots$, are available which are not necessarily *iid* or not even independent, we consider the following recursive strategy for sequentially updating the posterior distribution of the Dirichlet process. We assume that

$$\mathbf{X}_{i_1, i_2, \dots, i_K}^1 \sim G_1; G_1 \sim DP(\alpha G_{0, i_1, i_2, \dots, i_K}). \quad (16.23)$$

so that the posterior distribution of the random distribution given $\mathbf{X}_{i_1, i_2, \dots, i_K}^1$ is given by

$$[G_1 | \mathbf{X}_{i_1, i_2, \dots, i_K}^1] \sim DP\left(\alpha G_{0, i_1, i_2, \dots, i_K} + \delta_{\mathbf{X}_{i_1, i_2, \dots, i_K}^1}\right). \quad (16.24)$$

Now, assuming $[G_1 | \mathbf{X}_{i_1, i_2, \dots, i_K}^1]$ to be the prior for the distribution of $\mathbf{X}_{i_1, i_2, \dots, i_K}^2$, we have

$$[G_2 | \mathbf{X}_{i_1, i_2, \dots, i_K}^2] \sim DP\left(\alpha G_{0, i_1, i_2, \dots, i_K} + \delta_{\mathbf{X}_{i_1, i_2, \dots, i_K}^1} + \delta_{\mathbf{X}_{i_1, i_2, \dots, i_K}^2}\right). \quad (16.25)$$

Continuing as (16.23), (16.24) and (16.25), we obtain in general, for $j \geq 1$,

$$[G_j | \mathbf{X}_{i_1, i_2, \dots, i_K}^j] \sim DP\left(\alpha G_{0, i_1, i_2, \dots, i_K} + \sum_{r=1}^j \delta_{\mathbf{X}_{i_1, i_2, \dots, i_K}^r}\right). \quad (16.26)$$

Note that the posterior in this case is of the same form as that of $[G_j | \mathbf{X}_{i_1, i_2, \dots, i_K}^r; r = 1, \dots, j]$, had $\mathbf{X}_{i_1, i_2, \dots, i_K}^r; r = 1, \dots, j$ been *iid* with distribution G_{i_1, i_2, \dots, i_K} and $G_{i_1, i_2, \dots, i_K} \sim DP(\alpha G_{0, i_1, i_2, \dots, i_K})$.

In particular, for n data points $\{\mathbf{X}_K^j; j = 1, 2, \dots, n\}$, following (16.26) we obtain the posterior mean as

$$E[G_n | \mathbf{X}_K^n] = \frac{\alpha G_{0, 1:K} + \sum_{r=1}^n \delta_{\mathbf{X}_K^r}}{\alpha + n}, \quad (16.27)$$

which involves all the available data points $\{\mathbf{X}_K^j; j = 1, 2, \dots, n\}$. With (16.27), we deal with the following form of the conditional distribution function of $[X_j | X_1, \dots, X_{j-1}]$ for $j \geq 1$:

$$\tilde{\zeta}_{jn}(t_1, \dots, t_j) = \frac{E[G_n(X_1 \leq t_1, \dots, X_j \leq t_j) | \mathbf{X}_j^n]}{E[G_n(X_1 \leq t_1, \dots, X_{j-1} \leq t_{j-1}) | \mathbf{X}_{j-1}^n]}. \quad (16.28)$$

The marginal distribution of X_j in this case that we shall consider is

$$\tilde{\zeta}_{jn}(t_j) = \frac{\alpha G_{0,j}(X_j \leq t_j) + \sum_{r=1}^n \delta_{X_j^r}(X_j^r \leq t_j)}{\alpha + n} \quad (16.29)$$

With these, we have the following result.

Theorem 26 *For any $K \geq 2$, let \mathbf{X}_K^j ; $j \geq 1$, be stationary. Then (X_1, \dots, X_K) are mutually independent if and only if, for $j = 1, \dots, K$,*

$$\sup_{t_1, \dots, t_j \in \mathbb{R}} \left| \tilde{\zeta}_{jn}(t_1, \dots, t_j) - \tilde{\zeta}_{jn}(t_j) \right| \xrightarrow{a.s.} 0, \quad n \rightarrow \infty. \quad (16.30)$$

Proof. Let (X_1, \dots, X_K) be mutually independent. Then $[X_j | X_1, \dots, X_{j-1}] = [X_j]$, for $j \geq 2$. In other words, it holds that $P(X_j \leq t_j | X_1 \leq t_1, \dots, X_{j-1} \leq t_{j-1}) = P(X_j \leq t_j)$, for all $t_1, \dots, t_j \in \mathbb{R}$, and $j \geq 2$. Now,

$$\sup_{t_j \in \mathbb{R}} \left| \tilde{\zeta}_{jn}(t_1, \dots, t_j) - \tilde{\zeta}_{jn}(t_j) \right| \leq \sup_{t_j \in \mathbb{R}} \left| \tilde{\zeta}_{jn}(t_1, \dots, t_j) - P(X_j \leq t_j) \right| + \sup_{t_j \in \mathbb{R}} \left| P(X_j \leq t_j) - \tilde{\zeta}_{jn}(t_j) \right|. \quad (16.31)$$

Let us first focus on the first term of (16.31). For fixed α , as $n \rightarrow \infty$, due to Glivenko-Cantelli theorem for stationarity, it is easily seen that

$$E[G_n(X_1 \leq t_1, \dots, X_{j-1} \leq t_{j-1}) | \mathbf{X}_{j-1}^n] \xrightarrow{a.s.} P(X_1 \leq t_1, \dots, X_{j-1} \leq t_{j-1}), \quad (16.32)$$

for any $t_1, \dots, t_{j-1} \in \mathbb{R}$. Also, for any $t_1, \dots, t_{j-1} \in \mathbb{R}$, again due to Glivenko-Cantelli theorem for stationarity,

$$\sup_{t_j \in \mathbb{R}} \left| E[G_n(X_1 \leq t_1, \dots, X_j \leq t_j) | \mathbf{X}_j^n] - P(X_1 \leq t_1, \dots, X_j \leq t_j) \right| \xrightarrow{a.s.} 0, \quad \text{as } n \rightarrow \infty. \quad (16.33)$$

Combining (16.32) and (16.33) yields

$$\sup_{t_j \in \mathbb{R}} \left| \frac{E[G_n(X_1 \leq t_1, \dots, X_j \leq t_j) | \mathbf{X}_j^n]}{E[G_n(X_1 \leq t_1, \dots, X_{j-1} \leq t_{j-1}) | \mathbf{X}_{j-1}^n]} - \frac{P(X_1 \leq t_1, \dots, X_j \leq t_j)}{P(X_1 \leq t_1, \dots, X_{j-1} \leq t_{j-1})} \right| \xrightarrow{a.s.} 0, \quad \text{as } n \rightarrow \infty,$$

for all $t_1, \dots, t_{j-1} \in \mathbb{R}$. That is, for all $t_1, \dots, t_{j-1} \in \mathbb{R}$,

$$\sup_{t_j \in \mathbb{R}} \left| \tilde{\zeta}_{jn}(t_1, \dots, t_j) - P(X_j \leq t_j | X_1 \leq t_1, \dots, X_{j-1} \leq t_{j-1}) \right| \xrightarrow{a.s.} 0,$$

and since under mutual independence, $P(X_j \leq t_j | X_1 \leq t_1, \dots, X_{j-1} \leq t_{j-1}) = P(X_j \leq t_j)$,

$$\sup_{t_j \in \mathbb{R}} \left| \tilde{\zeta}_{jn}(t_1, \dots, t_j) - P(X_j \leq t_j) \right| \xrightarrow{a.s.} 0, \quad \text{as } n \rightarrow \infty,$$

for all $t_1, \dots, t_{j-1} \in \mathbb{R}$, under mutual independence. More transparently, since $\tilde{\zeta}_{jn}(t_1, \dots, t_j)$ is asymptotically independent of t_1, \dots, t_{j-1} , for any $\epsilon > 0$ under mutual independence, there exists

$n_0(\epsilon) \geq 1$ such that for $n > n_0(\epsilon)$,

$$\sup_{t_j \in \mathbb{R}} \left| \tilde{\zeta}_{jn}(t_1, \dots, t_j) - P(X_j \leq t_j) \right| < \epsilon,$$

for all $t_1, \dots, t_{j-1} \in \mathbb{R}$. That is, (16.30)

$$\sup_{t_1, \dots, t_j \in \mathbb{R}} \left| \tilde{\zeta}_{jn}(t_1, \dots, t_j) - P(X_j \leq t_j) \right| \xrightarrow{a.s.} 0, \text{ as } n \rightarrow \infty. \quad (16.34)$$

For the second term of (16.31), note that

$$\sup_{t_j \in \mathbb{R}} \left| P(X_j \leq t_j) - \tilde{\zeta}_{jn}(t_j) \right| \xrightarrow{a.s.} 0, \quad (16.35)$$

as $n \rightarrow \infty$, due to Glivenko-Cantelli theorem for stationarity,

Combining (16.31), (16.34) and (16.35) yields (16.30) under mutual independence.

Now if (16.30) holds for $j \geq 2$, then this clearly implies mutual independence of the random variables. ■

Remark 27 *Apart from being much more stable numerically compared to the approach of comparison between classical empirical conditional and marginal distributions, our DP-based approach also allows incorporation of the dependence structure, if any, through the base measure G_0 . This can be achieved by empirically estimating the dependence structure from the data, and incorporating it in G_0 . For example, if G_0 corresponds to Gaussian process, then its mean and the covariance structure can be estimated from the data. This is expected to improve efficiency of inference regarding mutual independence. Note that such dependence structure can not be exploited in the approach of comparison between classical empirical conditional and marginal distributions.*

For our Bayesian characterization of mutual independence, let n_j denote the minimum number of observations associated with (X_1, \dots, X_j) , for $j \geq 2$. Now let $\{c_j\}_{j=1}^\infty$ be a non-negative decreasing sequence and

$$Y_{j,n_j} = \mathbb{I} \left\{ \sup_{t_1, \dots, t_j \in \mathbb{R}} \left| \tilde{\zeta}_{jn_j}(t_1, \dots, t_j) - \tilde{\zeta}_{jn_j}(t_j) \right| \leq c_j \right\}.$$

Let, for $j \geq 1$,

$$P(Y_{j,n_j} = 1) = p_{j,n_j}.$$

Let the rest of the recursive Bayesian procedure be the same as in Section 4. Then, using Theorem 26, the following theorem can be proved in almost the same way as Theorem 6.

Theorem 28 *Let $X^i; i = 1, 2, \dots$, be stationary. Then (X_1, X_2, \dots) are mutually independent if and only if for all $\omega \in \mathfrak{S} \cap \mathfrak{N}^c$, where \mathfrak{N} is some null set having probability measure zero, for any monotonically decreasing sequence $\{c_j(\omega)\}_{j=1}^\infty$,*

$$\pi(\mathcal{N}_1 | y_{k,n_k}(\omega)) \rightarrow 1,$$

as $k \rightarrow \infty$ and $n_j \rightarrow \infty$ for $k = 2, 3, \dots, K$ and $K \rightarrow \infty$, where \mathcal{N}_1 is any neighborhood of 1 (one).

16.4 Mutual independence in the point process setup

Recall that for a Poisson point process, if for any set of disjoint regions C_i ; $i = 1, \dots, K$, where $C_i \subset S$, \mathbf{X}_{C_i} , denoting the set of points in C_i , are independent, for any $K > 1$. This is referred to as the complete independence property in Daley and Vere-Jones (2003). However, complete independence alone is not sufficient to characterize Poisson point process. In this regard, let us consider the following assumptions.

- (A1) Let $N(A)$, the number of points in the set A , be defined and finite for every bounded set A in the Borel sigma-field generated by the open spheres of S . This can be simply expressed by saying that the trajectories of $N(\cdot)$ are almost surely boundedly finite (Daley and Vere-Jones (2003)).
- (A2) $P_r \{N(S_\epsilon(x)) > 1\} = o(P_r \{N(S_\epsilon(x)) > 1\})$, as $\epsilon \rightarrow 0$. Here $S_\epsilon(x)$ denotes the open sphere with radius ϵ and center x . This property is called orderliness.

With these, the Poisson process can be characterized as follows.

Theorem 29 (Daley and Vere-Jones (2003)) *Let $N(\cdot)$ be almost surely boundedly finite and without fixed atoms. Then $N(\cdot)$ is a Poisson process if and only if it is orderly and has the complete independence property.*

We also note the following lemma.

Lemma 30 (Daley and Vere-Jones (2003)) *A point x_0 is an atom of the parameter measure Λ if and only if it is a fixed atom of the process.*

Corollary 31 *Theorem 29 and Lemma 30 together imply that if Λ corresponds to a continuous distribution, then (A1)–(A2) along with complete independence characterize Poisson process.*

We now characterize Poisson process in a recursive Bayesian framework using our Bayesian characterization of mutual independence assuming (A1)–(A2) and non-atomicity of the process. In all our examples, we consider Λ to be associated with continuous distributions, hence non-atomic; (A1)–(A2) also hold in all our simulation studies.

Assume that \mathbf{X}_{C_i} are locally stationary and let D_{C_i} denote the set of minimum inter-point distances associated with \mathbf{X}_{C_i} . As before, for $r = 1, 2, \dots$, let W_r and W_{dr} be the observation window and the space of inter-point distances corresponding to W_r at the r -th stage, where $|W_r| \rightarrow \infty$ as $r \rightarrow \infty$. Let us also replace n_j and K with n_{jr} and K_r , respectively, as before.

Now let $\{c_j\}_{j=1}^\infty$ be a non-negative decreasing sequence and

$$Y_{j,n_{jr}} = \mathbb{I} \left\{ \sup_{t_1, \dots, t_j \in \mathbb{R}} \left| \tilde{\zeta}_{jn_{jr}}(t_1, \dots, t_j) - \tilde{\zeta}_{jn_{jr}}(t_j) \right| \leq c_j \right\},$$

and, for $j \geq 1$,

$$P(Y_{j,n_{jr}} = 1) = p_{j,n_{jr}}.$$

Then we have the following result for point processes corresponding to Theorem 28.

Theorem 32 Let \mathbf{X} be a point process in \mathcal{S} . Assume that for the disjoint regions $C_i \subset \mathcal{S}$; $i = 1, \dots, K_r$, \mathbf{X}_{C_i} are locally stationary. Then $(D_{C_1}, \dots, D_{C_{K_r}})$ are mutually independent if and only if for all $\omega \in \mathfrak{S} \cap \mathfrak{N}^c$, where \mathfrak{N} is some null set having probability measure zero, for any monotonically decreasing sequence $\{c_j(\omega)\}_{j=1}^\infty$, and any set of disjoint regions C_i ; $i = 1, \dots, K_r$, where $C_i \subset \mathcal{S}$,

$$\pi(\mathcal{N}_1 | y_{k, n_{kr}}(\omega)) \rightarrow 1, \quad (16.36)$$

as $k \rightarrow \infty$ and $n_{kr} \rightarrow \infty$ for $k = 2, 3, \dots, K_r$ and $K_r \rightarrow \infty$ as $r \rightarrow \infty$, where \mathcal{N}_1 is any neighborhood of 1 (one).

Proof. Using Theorem 26, the proof follows in almost the same way as that of Theorem 6. ■

Theorem 33 Consider any point process $\mathbf{X} \in \mathcal{S}$. Assume that the σ -algebra for \mathcal{S} is separable and generated by the mutually disjoint sets $\{C_i; i \geq 1\}$, and that \mathbf{X}_{C_i} are locally stationary. Then, provided that (A1)–(A2) hold and the process is non-atomic, \mathbf{X} is a Poisson point process if and only if (16.36) holds.

Proof. By Theorem 32, $(D_{C_1}, \dots, D_{C_{K_r}})$ are mutually independent if and only if (16.36) holds. Since the mutually disjoint sets $\{C_i; i \geq 1\}$ generates the σ -field for \mathcal{S} , it follows that any set of mutually disjoint sets $\{B_1, \dots, B_\ell\}$ in the σ -field for \mathcal{S} , for any $\ell > 1$, $(D_{B_1}, \dots, D_{B_\ell})$, are mutually independent.

Also, it is easy to see that $(D_{B_1}, \dots, D_{B_\ell})$ are mutually independent if and only if $(\mathbf{X}_{B_1}, \dots, \mathbf{X}_{B_\ell})$ are mutually independent.

Hence, by the hypothesis of the theorem it follows that \mathbf{X} is a Poisson point process if and only if (16.36) holds. ■

16.5 Computational strategy for mutual independence assessment

Note that for relatively large j , it may not be feasible to directly compute $\sup_{t_1, \dots, t_j \in \mathbb{R}} |\tilde{\zeta}_{jn_j}(t_1, \dots, t_j) - \tilde{\zeta}_{jn_j}(t_j)|$.

Hence we consider the following strategy. For $j = 2$, let \tilde{t}_1, \tilde{t}_2 be the maximizers of $|\tilde{\zeta}_{jn_j}(t_1, \dots, t_j) - \tilde{\zeta}_{jn_j}(t_j)|$, and for $j \geq 3$, let

$$\begin{aligned} & \sup_{t_1, \dots, t_j \in \mathbb{R}} |\tilde{\zeta}_{jn_j}(t_1, \dots, t_j) - \tilde{\zeta}_{jn_j}(t_j)| \\ &= \sup_{t_j \in \mathbb{R}} \left| \frac{E[G_n(X_1 \leq \tilde{t}_1, \dots, X_{j-1} \leq \tilde{t}_{j-1}, X_j \leq t_j) | \mathbf{X}_j^n]}{E[G_n(X_1 \leq \tilde{t}_1, \dots, X_{j-1} \leq \tilde{t}_{j-1}) | \mathbf{X}_{j-1}^n]} - \frac{\alpha G_{0,j}(X_j \leq t_j) + \sum_{r=1}^n \delta_{X_j^r}(X_j^r \leq t_j)}{\alpha + n} \right|, \end{aligned} \quad (16.37)$$

where $\tilde{t}_3, \dots, \tilde{t}_{j-1}$ are the maximizers of $|\tilde{\zeta}_{j-1n_{j-1}}(t_1, \dots, t_{j-1}) - \tilde{\zeta}_{j-1n_{j-1}}(t_{j-1})|$, for $j \geq 3$.

16.6 Example 1: Detection of HPP and IHPP and their properties

We generate a HPP with intensity $\lambda = 1$ on a window of the form $[0, 100] \times [0, 100]$, using the R package “spatstat” (Baddeley and Turner (2005)), and obtain 9949 points in this exercise. We

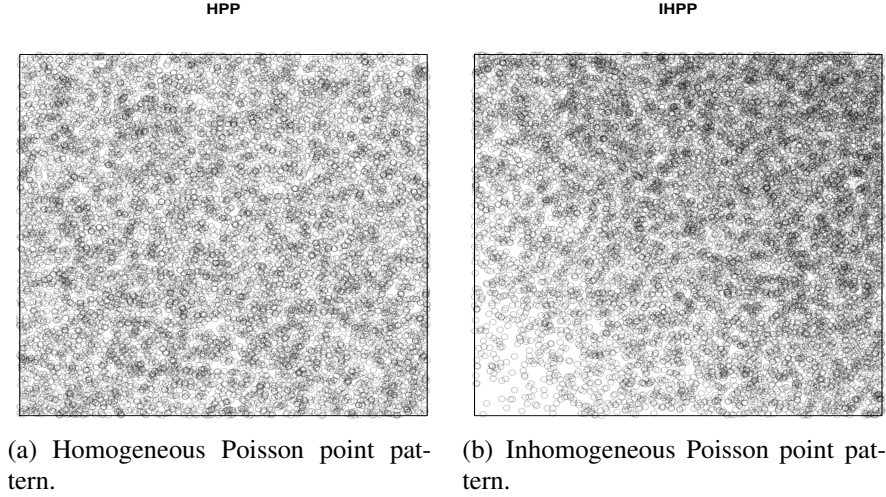


Figure 16.1: Homogeneous and inhomogeneous Poisson point processes.

also simulate an IHPP using the spatstat package with $\lambda(x, y) = 100(x + y)$ on $[0, 5] \times [0, 5]$, generating 12447 observations. The plots of the point patterns are provided in Figure 16.1. Observe that while the HPP pattern in panel (a) is reasonably uniform on the observed window, the IHPP pattern in panel (b) shows sparsity in the bottom left corner and density in the top right corner of the observation window. Our goal is to identify the true point processes that generated the data, pretending that they are unknown and that only the data are observed.

16.6.1 Homogeneity detection

Let us first concentrate on the HPP data. With $K = 1000$ clusters, we use bound (10.3) and obtain $\hat{C}_1 = 0.25$ as the minimum value of \hat{C}_1 that led to convergence of our recursive Bayesian algorithm to 1. The result is depicted in panel (a) of Figure 16.2. Panel (b) of Figure 16.2 is the simultaneous critical envelope associated with classical test of HPP, prepared using spatstat with 1000 simulations of CSR. Here r stands for the distance argument, and $\hat{G}_{obs}(r)$, $\hat{G}_{theo}(r)$, $\hat{G}_{lo}(r)$ and $\hat{G}_{hi}(r)$ stand for the observed empirical distribution function for the distances with Kaplan-Meier edge correction, the theoretical distribution function under CSR, the lower critical boundary and the upper critical boundary for the distribution functions under CSR, respectively. Here the significance level of simultaneous Monte Carlo test is given by 0.000999. Since the observed distribution function fall well within the lower and upper critical boundaries, the result is in agreement with our Bayesian result and indeed, the truth.

We now analyse the point pattern obtained from the IHPP. Panel (c) of Figure 16.2 shows the result of our Bayesian analysis with $K = 1000$ clusters and $\hat{C}_1 = 0.25$. Divergence to zero, that is, inhomogeneity is clearly indicated. However, this does not validate or invalidate Poisson process. To validate Poisson process, we need to create a characterization of mutual independence between the points contained in the K clusters. Panel (d) of Figure 16.2 is similar to panel (b) except that the observed distribution function in this case now corresponds to IHPP. Note that the observed distribution function $\hat{G}_{obs}(r)$ falls almost entirely within the limits $\hat{G}_{lo}(r)$ and $\hat{G}_{hi}(r)$, which makes it considerably difficult to distinguish this IHPP from HPP. The advantage of our Bayesian method depicted in panel (c) is clearly pronounced over this classical method in this

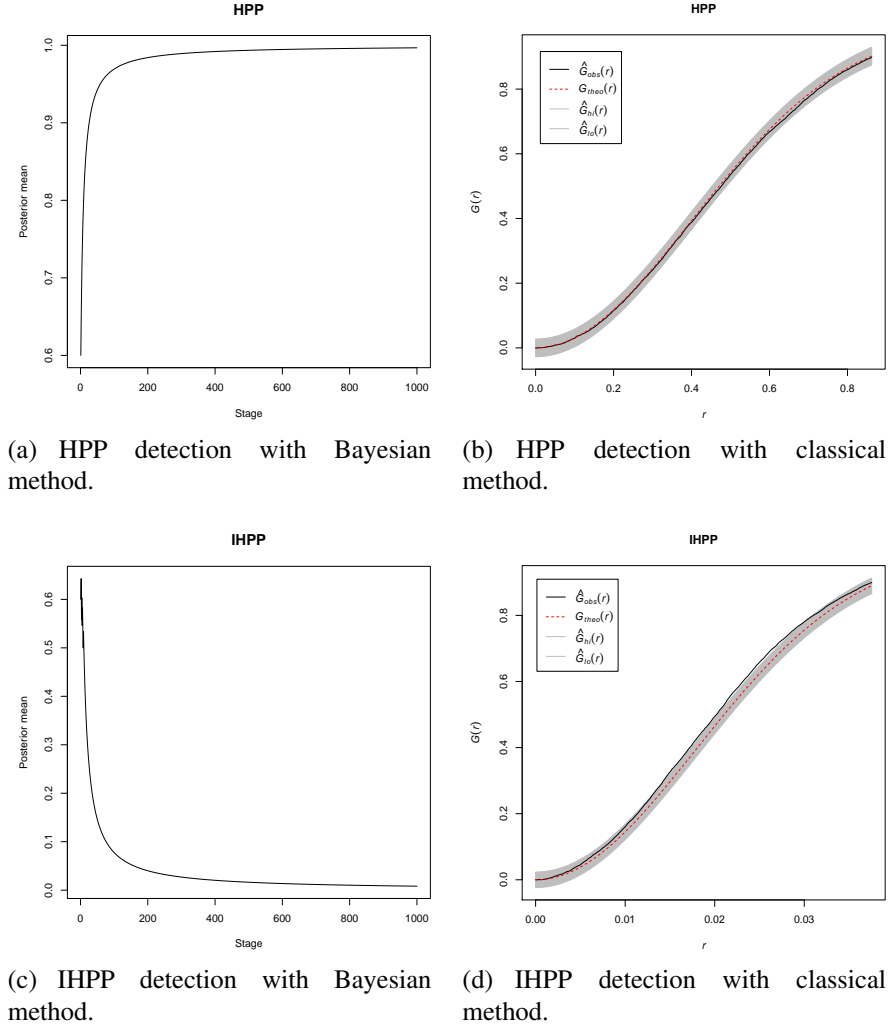


Figure 16.2: Detection of CSR with our Bayesian method and traditional classical method.

regard.

16.6.2 Stationarity detection

The traditional tests of CSR tests for HPP only. But inhomogeneity neither rejects the Poisson assumption, nor either of stationarity and nonstationarity. In this regard, we first address the question of stationarity and nonstationarity with our Bayesian method in our current examples of HPP and IHPP. Recall that for point processes, we regard the minimum distances $d_i; i = 1, \dots, n$, as the spatial data, along with their corresponding locations. Indeed, with this, we obtain the correct results with $K = 1000$ clusters, bound (10.3) with $\hat{C}_1 = 0.06$, the minimum value for which convergence to 1 is obtained under the HPP example. The results presented in Figure 16.3, correctly identifies HPP and IHPP as stationary and nonstationary, respectively. Larger values of \hat{C}_1 , such as $\hat{C}_1 = 0.1$ led to the same result.

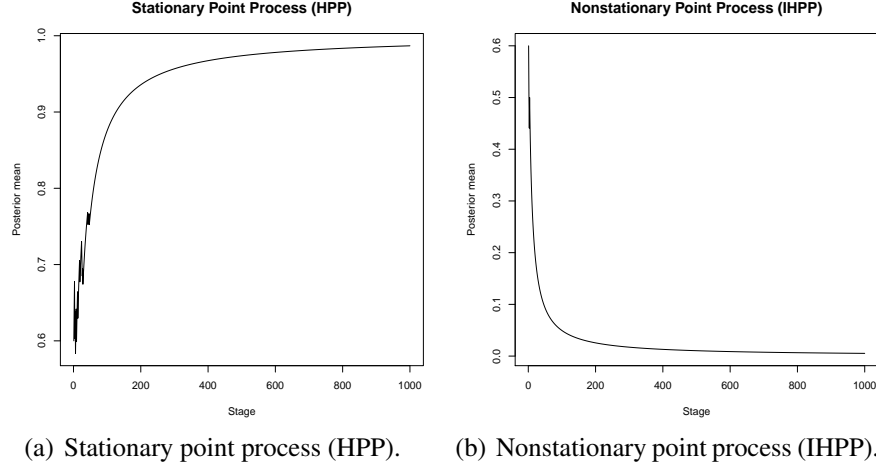


Figure 16.3: Detection of stationarity and nonstationarity of point processes (here HPP and IHPP) with our Bayesian method.

16.6.3 Validation of Poisson assumption

We finally examine, with our recursive Bayesian method for characterizing mutual independence, if the two point patterns that we generated can be safely assumed to be Poisson point patterns. Note that Poisson point process is equivalent to mutual independence of the points in disjoint subsets of W . In this regard, for $i = 1, \dots, K$, let \mathbf{X}_{C_i} denote the points in cluster C_i . If \mathbf{X}_{C_i} are mutually independent for all possible clusters C_i and K , then \mathbf{X} can be regarded as Poisson point process. For practical purposes, we restrict attention to a single set of clusters C_1, \dots, C_K . For numerical stability of the computations, we set $K = 50$, so that in most cases we investigate mutual independence among $K = 50$ variables, where each variable is considered to take values in one and only one of the clusters. We set the strength parameter α of the Dirichlet process to 1, which is quite standard, and use the ‘emcdf’ function of the ‘Emcdf’ package in R to parallelise the computations of the joint empirical distribution functions required for our Bayesian method. Here the joint distribution functions are those of the log-distances associated with the clusters. For the base distribution G_0 of the Dirichlet process, we considered the multivariate normal distribution with mean vector and covariance matrices obtained empirically from the log-distances associated with \mathbf{X}_{C_i} ’s. Specifically, for K dimensions, G_0 is a K -variate normal distribution with mean vector being the K -component vector obtained by taking the means of the log-distances in \mathbf{X}_{C_i} ; $i = 1, \dots, K$ and the covariance matrix being the empirical covariance obtained from the log-distances in the K clusters. The lower-dimensional distributions are then simply the marginalized versions of the higher-dimensional cases.

The entire exercise beginning from clustering the observed point pattern to yielding the maximum absolute differences between the conditional distribution functions and the marginal distribution functions, takes about 20 minutes in a 4-core laptop. The results of our Bayesian analyses with the bound (10.3) and $\hat{C}_1 = 0.5$, the minimum value for convergence in the HPP case, are provided in Figure 16.4. Indeed, both the panels indicate convergence, and hence independence. Hence, both the point processes can be safely assumed to be Poisson point processes.

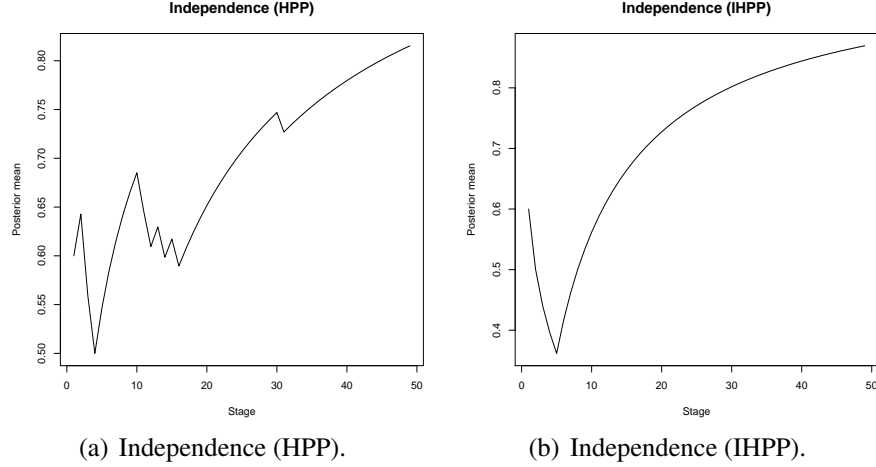


Figure 16.4: Detection of independence in point patterns (here HPP and IHPP) with our Bayesian method, suggesting that both the point processes are Poisson point processes.

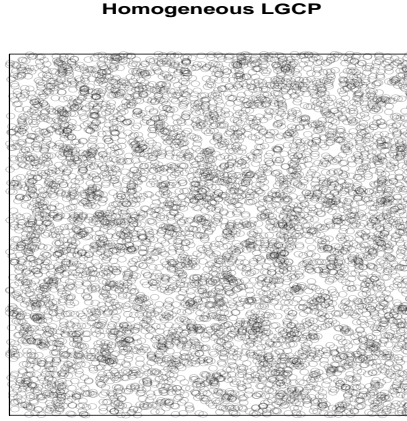


Figure 16.5: Homogeneous LGCP.

16.7 Example 2: Homogeneous log-Gaussian Cox process

We now consider analyses of simulated data obtained from log-Gaussian Cox process. \mathbf{X} is a Cox process if conditional on a non-negative process $\{\Lambda(u) : u \in S\}$, \mathbf{X} is a Poisson process with intensity function Λ (see, for example, Daley and Vere-Jones (2003)), and \mathbf{X} is a log-Gaussian Cox process if $\log \Lambda$ is a Gaussian process. In this example, let us consider a log-Gaussian Cox process with mean function $E[\log \Lambda(u)] = \mu(u) = 3$ for all u , and exponential covariance function given by $Cov(\log \Lambda(u), \log \Lambda(v)) = \sigma^2 \times \exp(a \|u - v\|)$, where $\|\cdot\|$ denotes Euclidean distance, $\sigma^2 = 0.2$ and $a = 10$. This is a stationary non-Poisson point process, and homogeneous in the sense that the marginalized intensity $E[\log \Lambda(u)]$, integrating out the random function Λ , is constant.

We choose $W = [0, 15] \times [0, 20]$ and obtain 6553 observations from this point process using spatstat, which are displayed in Figure 16.5.

We consider $K = 800$ and algorithm (10.3) with $\hat{C}_1 = 0.24$ for our Bayesian method. Figure 16.6 compares our Bayesian method with the classical method regarding CSR detection. Observe that the Bayesian method correctly identifies that the point process is not CSR, while the classical

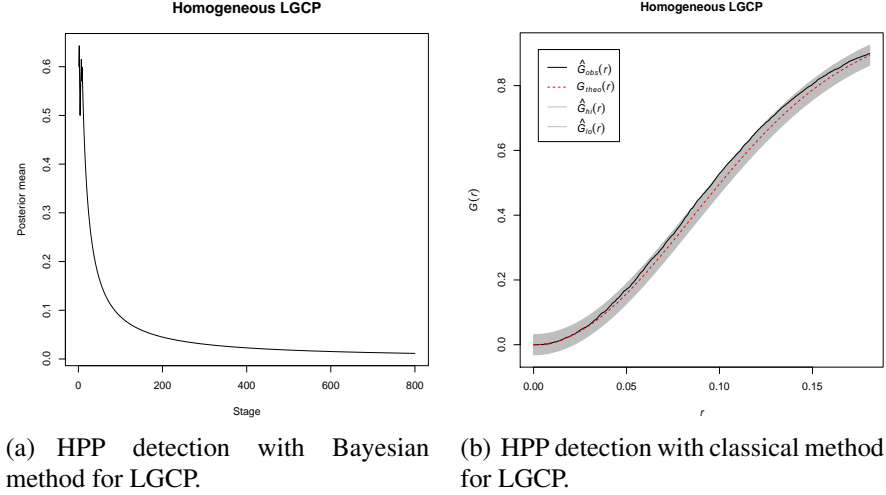


Figure 16.6: Detection of CSR with our Bayesian method and traditional classical method for LGCP. The Bayesian method correctly identifies that the underlying point process is not CSR, but the classical method falsely indicates CSR.

method fails to correctly recognize the process.

For addressing stationarity, we set $K = 800$ and $\hat{C}_1 = 0.15$. Panel (a) of Figure 16.7 shows that stationarity is clearly indicated by our Bayesian approach.

For testing if the underlying point process is Poisson process, we test independence as before, among $K = 70$ random variables $X_{C_i}; i = 1, \dots, K$. With $\hat{C}_1 = 0.5$, panel (b) of Figure 16.7 indicates independence, validating the Poisson assumption, given Λ , as mentioned above.

16.8 Example 3: Inhomogeneous log-Gaussian Cox process

We now consider a log-Gaussian Cox process where the covariance is now of the Matérn form

$$Cov(\log \Lambda(u), \log \Lambda(v)) = \sigma^2 \frac{2^{1-\nu}}{\Gamma(\nu)} \left(\sqrt{2\nu} \frac{\|u - v\|}{\rho} \right)^\nu \mathcal{K}_\nu \left(\sqrt{2\nu} \frac{\|u - v\|}{\rho} \right), \quad (16.38)$$

where Γ is the gamma function, \mathcal{K}_ν is the modified Bessel function of the second kind of the order ν , and ρ^{-1} is the scale parameter. We chose $\sigma^2 = 2$, $\rho^{-1} = 0.7$ and $\nu = 0.5$. For the mean function, we chose $\mu(u_1, u_2) = 5 - 1.5(u_1 - 0.5)^2 + 2(u_2 - 0.5)^2$. Thus, the underlying LGCP is nonstationary. Since the expected intensity is not constant, the point process is inhomogeneous from this perspective.

Using spatstat, we obtained 8814 observations on $W = [0, 3] \times [0, 2.2]$, displayed in Figure 16.8.

Panel (a) of Figure 16.9 shows the result of our Bayesian approach to CSR detection With $K = 800$ and $\hat{C}_1 = 0.24$, while panel (b) shows the result of the classical method. Both the methods successfully identify that the underlying point process is not CSR.

As shown in panel (a) of Figure 16.10, our Bayesian approach captures nonstationarity of the point process. As before, for detection of nonstationarity, we set $K = 800$ and $\hat{C}_1 = 0.15$.

To test mutual independence among X_{C_i} , for $i = 1, \dots, K$, we set $K = 45$ (due to reasons

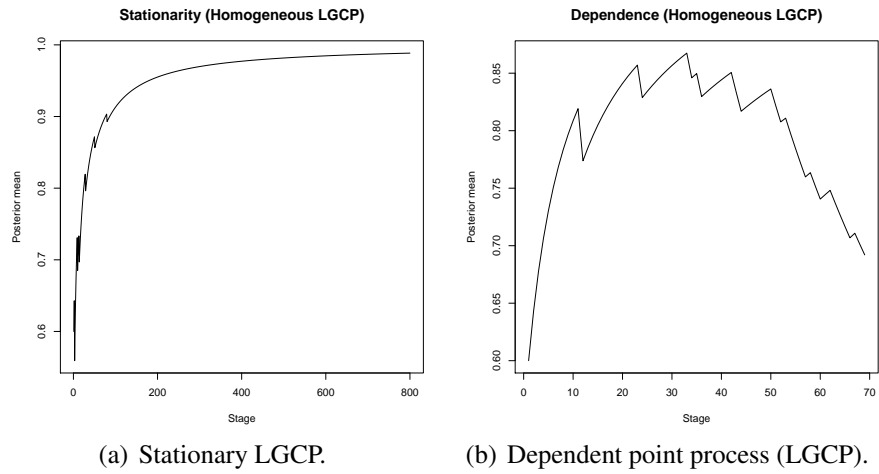


Figure 16.7: Detection of stationarity and dependence of homogeneous LGCP with our Bayesian method.

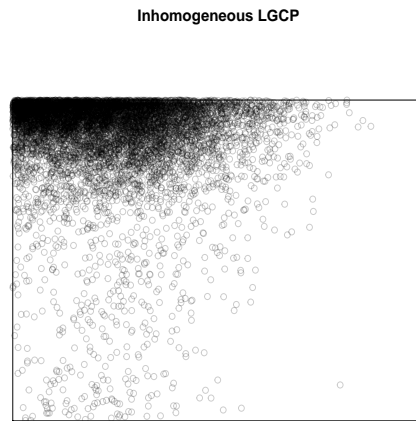


Figure 16.8: Inhomogeneous LGCP.

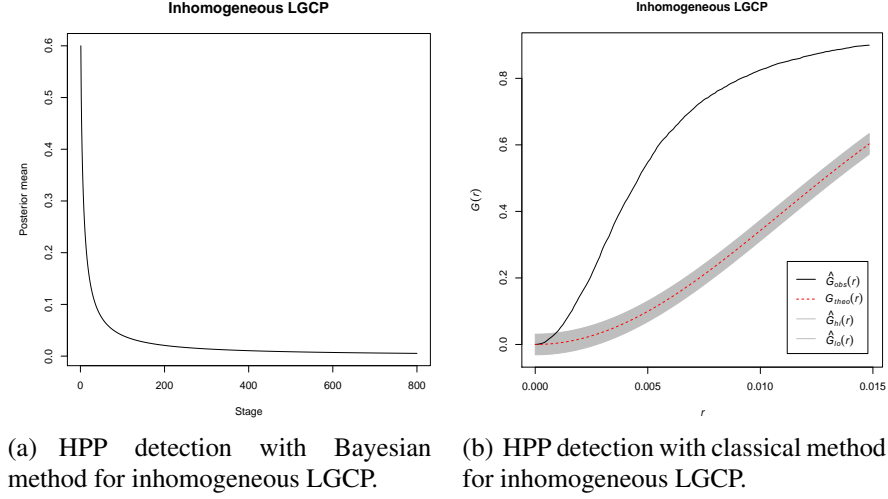


Figure 16.9: Detection of CSR with our Bayesian method and traditional classical method for LGCP. Both the methods correctly identify that the underlying point process is not CSR.

of numerical stability) and $\hat{C}_1 = 0.5$, as before. Panel (b) of Figure 16.10 shows approximately stable behaviour around 0.6 till the last few points, where steady decrease is noticed. The stability around the relatively large value 0.6 for most part of the series indicates mutual independence among most of the random variables \mathbf{X}_{C_i} , but the last few values of the series suggest that the entire set of random variables $\mathbf{X}_{C_i}; i = 1, \dots, 45$, are perhaps not mutually independent. Hence, the entire set of random variables can not be regarded as mutually independent, leading to non-Poisson conclusion.

16.9 Example 4: Inhomogeneous log-Gaussian Cox process

In this example, we choose the same Matérn covariance function (16.38), with the same values of σ^2 , ρ and ν as before, but now we set $\mu(u_1, u_2) = 1 - 0.4u_1$. The resulting inhomogeneous LGCP obtained using spatstat, consisting of 7245 points, is depicted in Figure 16.11.

With $K = 800$ and $\hat{C}_1 = 0.24$, our Bayesian method successfully identifies the process as not CSR. The classical method is also successful in this regard. The results are shown in Figure 16.12.

Again with $K = 800$ and $\hat{C}_1 = 0.15$, our Bayesian method detects nonstationarity of the underlying point process. Also, with $K = 40$ and $\hat{C}_1 = 0.5$ as before, our method correctly detects dependence among $\mathbf{X}_{C_i}; i = 1, \dots, K$.

16.10 Example 5: Homogeneous Matérn cluster process

The Matérn cluster process is a special case of shot-noise Cox process where the offspring points are distributed uniformly inside a disc around the cluster center. To clarify, first consider a Poisson point process with intensity κ . Then each ‘parent’ point of this Poisson point process is replaced with a random cluster of ‘offspring’ points, where the number of points per cluster is distributed as Poisson with intensity μ on a disc with center being the parent point. This point process is

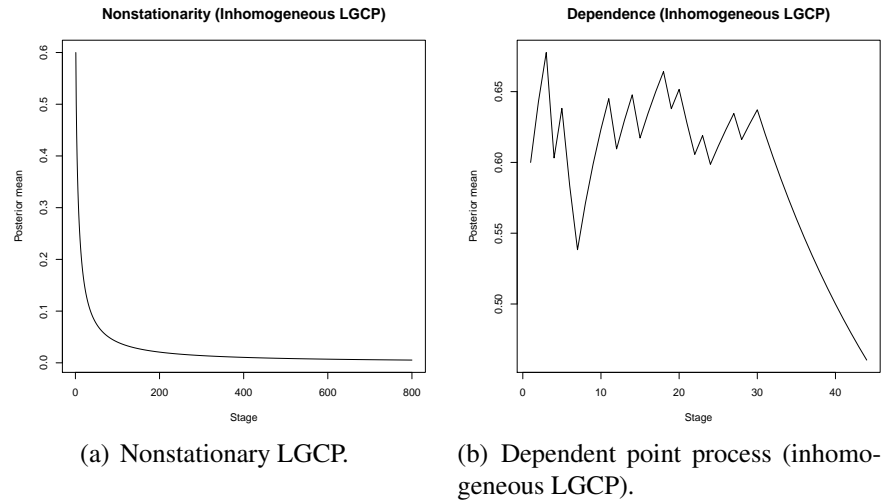


Figure 16.10: Detection of nonstationarity and dependence of inhomogeneous LGCP with our Bayesian method.

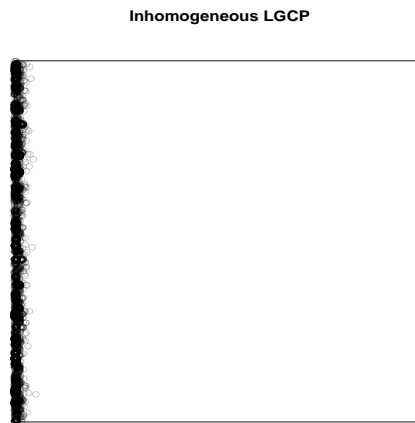


Figure 16.11: Inhomogeneous LGCP.

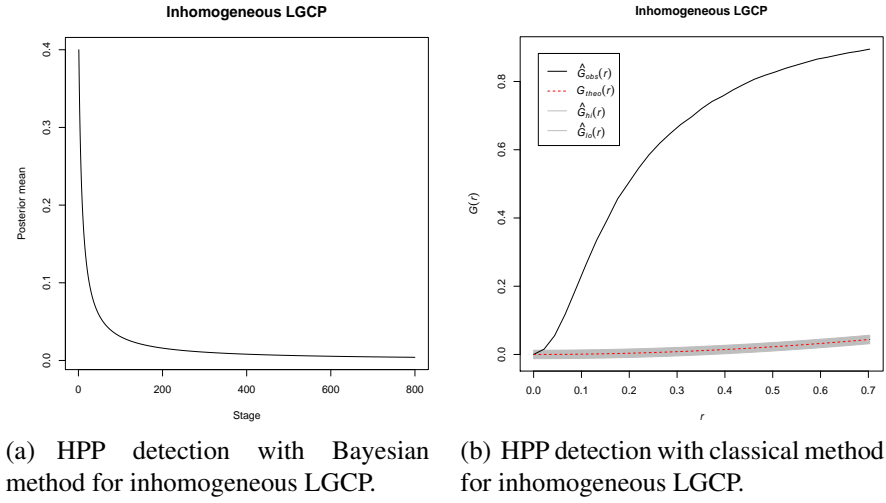


Figure 16.12: Detection of CSR with our Bayesian method and traditional classical method for LGCP. Both the methods correctly identify that the underlying point process is not CSR.

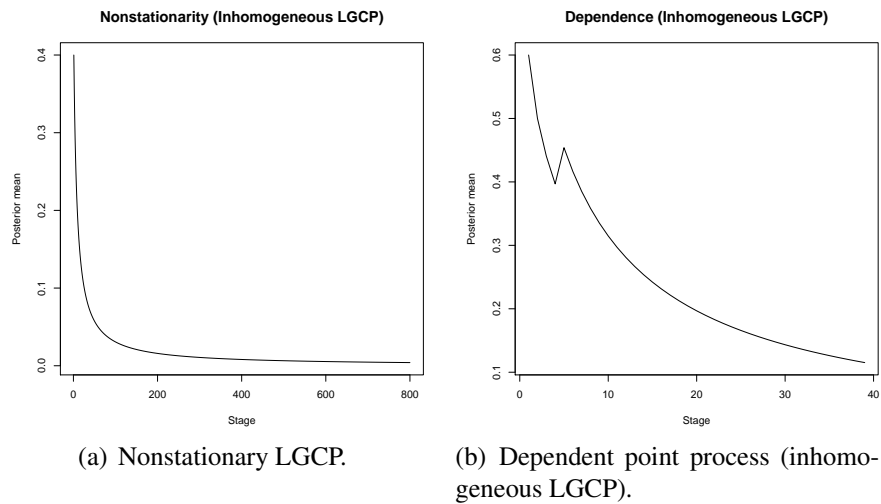


Figure 16.13: Detection of nonstationarity and dependence of inhomogeneous LGCP with our Bayesian method.

Matern Cluster Process

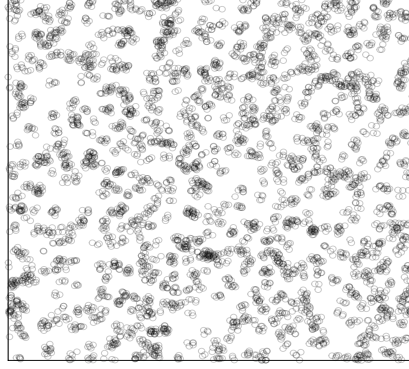


Figure 16.14: Matérn cluster point process pattern.

non-Poisson. Mathematically, consider

$$\Lambda(u) = \sum_{(c,\gamma) \in \Phi} \gamma k(c, u), \quad (16.39)$$

where $c \in \mathbb{R}^2$, $\gamma > 0$, Φ is a Poisson process on $\mathbb{R}^2 \times (0, \infty)$, and $k(c, \cdot)$ is a density for a two-dimensional continuous random variable. Then \mathbf{X} is a shot noise Cox process if given Λ defined by (16.39), \mathbf{X} is a Poisson process with intensity function Λ . It follows that \mathbf{X} is the superposition (union) of independent Poisson processes $\mathbf{X}_{(c,\gamma)}$ with intensity functions $\gamma k(c, \cdot)$, where $(c, \gamma) \in \Phi$. If γ is a variable (either random or non-random), then $\mathbf{X}_{(c,\gamma)}$ can be thought of as a cluster with center c and mean number of points γ . In this sense, \mathbf{X} is a Poisson cluster process.

The Matérn cluster process is a special case of the above process, where the centre points c arise from a Poisson process with intensity function κ and $\gamma \equiv \mu$, a positive non-random function, and $k(c, \cdot)$ is the density of the uniform distribution on a disc of radius r , with center c .

In this example, we simulate a Matérn cluster process on a window $W = [0, 10] \times [0, 10]$, $\kappa = 10$, $\mu = 5$, and disc radius $r = 0.1$, and obtain 4882 points, shown in Figure 16.14. As can be easily verified from (16.39) and the following expositions, the random intensity function Λ in this case is stationary, and hence, \mathbf{X} is stationary.

Figure 16.15 shows the results of our Bayesian method and the classical method for detecting CSR. Both the methods correctly point out that the underlying point process is not CSR. Here, for the Bayesian method, we set $K = 500$ and $\hat{C}_1 = 0.25$, the maximum value leading to the conclusion of not CSR.

Panel (a) of Figure 16.16 shows that stationarity of the point process has been correctly captured by our Bayesian procedure, with $K = 500$ and $\hat{C}_1 = 0.06$, the minimum value of \hat{C}_1 leading to stationarity.

The result of our test for independence is depicted by panel (b) of Figure 16.16, for $K = 50$ and $\hat{C}_1 = 0.5$ as usual. Dependence is indicated, correctly leading to the non-Poisson conclusion.

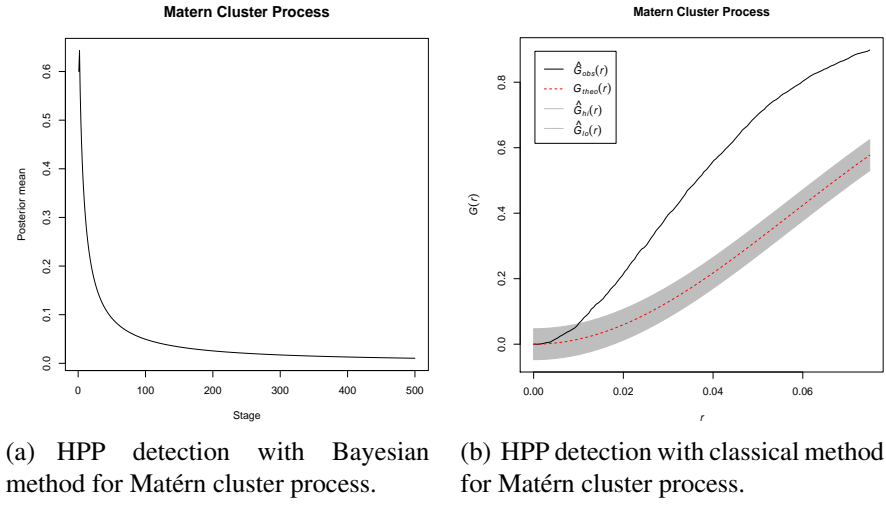


Figure 16.15: Detection of CSR with our Bayesian method and traditional classical method for Matérn cluster process. Both the methods correctly identify that the underlying point process is not CSR.

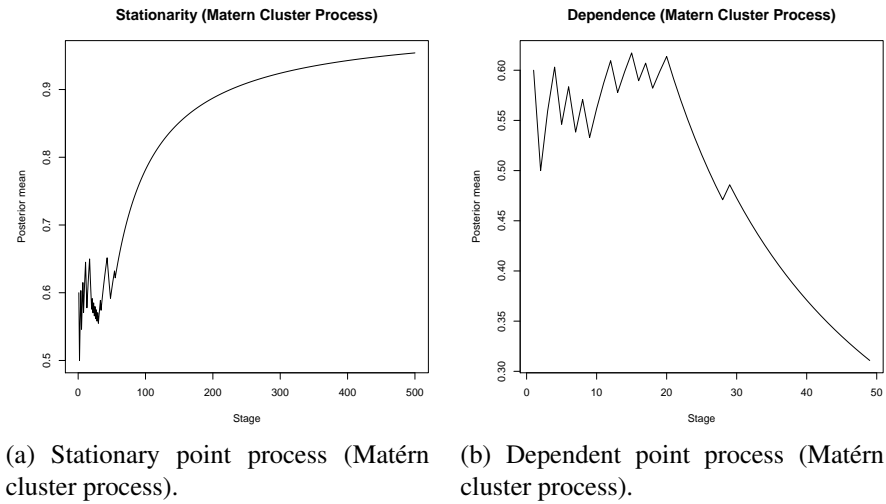


Figure 16.16: Detection of stationarity and dependence of Matérn cluster process with our Bayesian method.

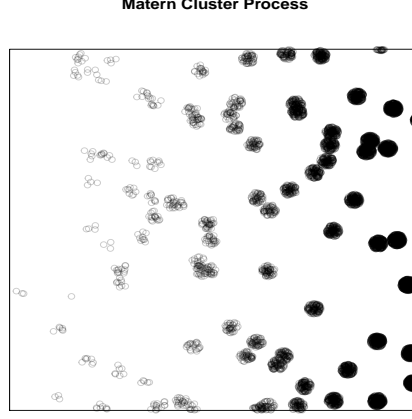


Figure 16.17: Inhomogeneous Matérn cluster point process pattern.

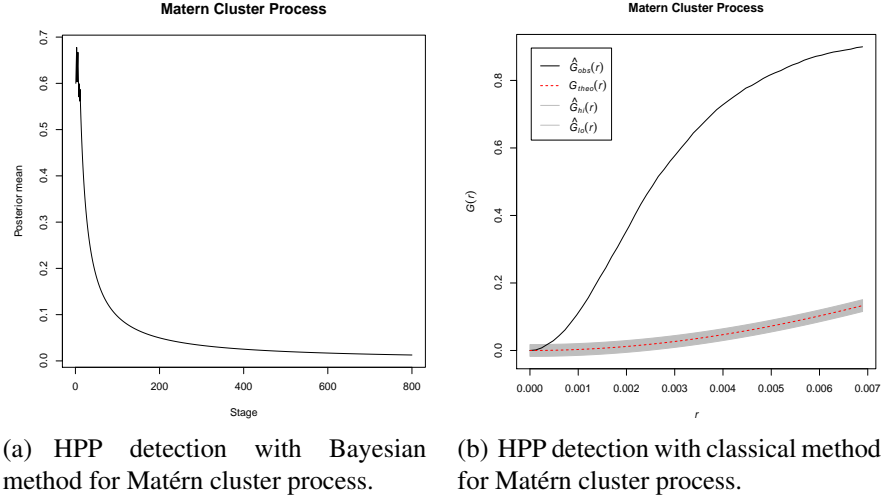


Figure 16.18: Detection of CSR with our Bayesian method and traditional classical method for inhomogeneous Matérn cluster process. Both the methods correctly identify that the underlying point process is not CSR.

16.11 Example 6: Inhomogeneous Matérn cluster process with μ inhomogeneous

We now consider an inhomogeneous Matérn cluster process with $\kappa = 10$, disc radius $r = 0.05$, and $\mu(u_1, u_2) = 2 \exp(2|u_1| - 1)$, an obtain 8606 points in $W = [0, 3] \times [0, 3]$. The points are plotted in Figure 16.17.

Figure 16.18 shows that both the methods for detecting CSR correctly detect non-CSR. For the Bayesian method, we set $K = 800$ and $\hat{C}_1 = 0.6$, the maximum value leading to the conclusion of not CSR.

With $K = 800$ and $\hat{C}_1 = 0.27$, our Bayesian method correct points out nonstationarity. This value of \hat{C}_1 is the maximum value leading to nonstationarity. As before, the Bayesian method correctly detects dependence with $K = 50$ and $\hat{C}_1 = 0.5$. The results are depicted in Figure 16.19.

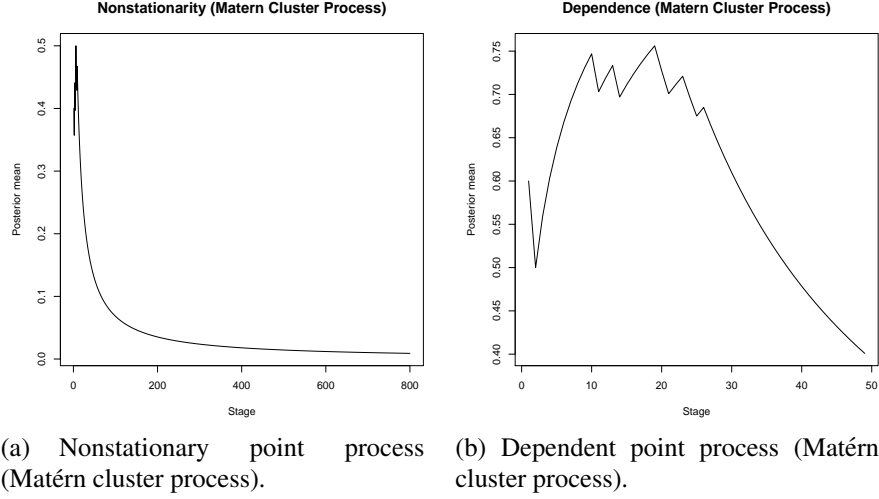


Figure 16.19: Detection of nonstationarity and dependence of Matérn cluster process with our Bayesian method.

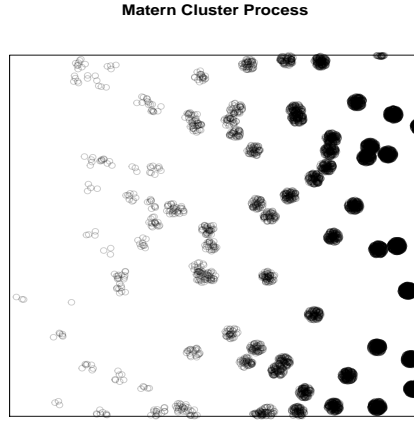


Figure 16.20: Inhomogeneous Matérn cluster point process pattern.

16.12 Example 7: Matérn cluster process with κ Inhomogeneous

We consider another inhomogeneous Matérn cluster process with $\kappa(u_1, u_2) = 2 \exp(2|u_1| - 1)$, disc radius $r = 0.05$, and $\mu = 3$. The 2625 points that we obtained in $W = [0, 3] \times [0, 3]$ are displayed in Figure 16.20.

With $K = 300$ and $\hat{C}_1 = 0.4$, the Bayesian algorithm correctly detects non-CSR. The classical method also performs adequately. Figure 16.21 shows that both the methods for detecting CSR correctly detect non-CSR.

Nonstationarity is also correctly detected by the Bayesian method with $K = 300$ and $\hat{C}_1 = 0.26$, the maximum value leading to nonstationarity. Correct detection of dependence among \mathbf{X}_{C_i} ; $i = 1, \dots, 50$, has also been possible with the Bayesian algorithm with $\hat{C}_1 = 0.5$. Figure 16.22 presents the relevant results.

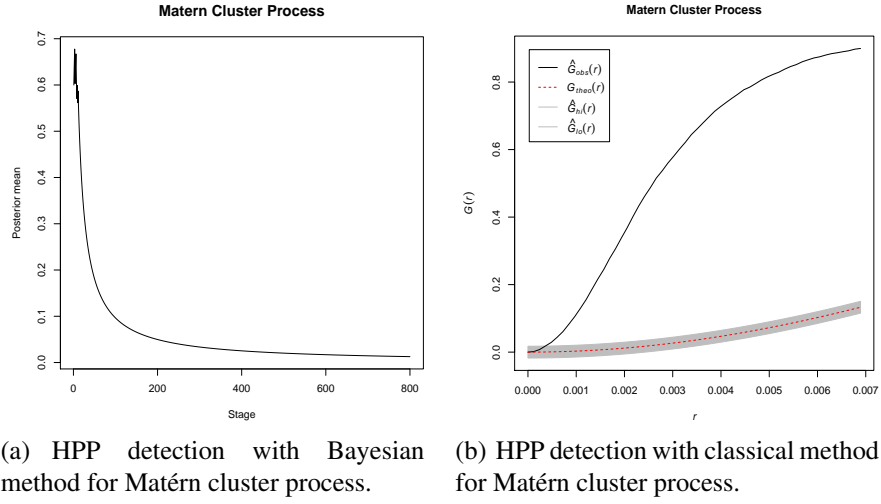


Figure 16.21: Detection of CSR with our Bayesian method and traditional classical method for inhomogeneous Matérn cluster process. Both the methods correctly identify that the underlying point process is not CSR.

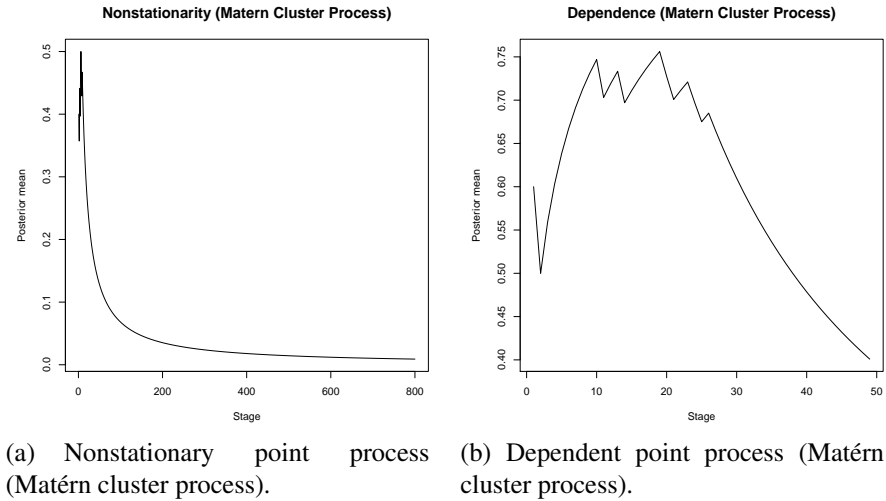


Figure 16.22: Detection of nonstationarity and dependence of Matérn cluster process with our Bayesian method.

Homogeneous Thomas Process

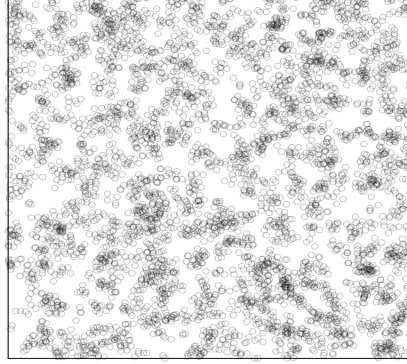


Figure 16.23: Homogeneous Thomas point process pattern.

16.13 Example 8: Homogeneous Thomas process

The (modified) Thomas process is a special case of the general shot-noise Cox process in the same way as Matérn cluster process, but where $k(c, \cdot)$ is the bivariate normal density with mean c and covariance $\sigma^2 I$. From (16.39) it is seen that a stationary process \mathbf{X} results provided κ and μ are constants. The intensity after integrating out Λ is constant in this case, leading to homogeneous Thomas process.

In this example, we first simulate a Thomas process with $\kappa = 10$, $\mu = 5$, $\sigma^2 = 10$, on the window $W = [0, 10] \times [0, 10]$, and obtained 4858 points. The point pattern for this homogeneous Thomas process is displayed in Figure 16.23.

To test CSR, here we set $K = 500$ and $\hat{C}_1 = 0.23$ for the Bayesian method. The Bayesian method, as well as the classical method, correctly indicate that the underlying point process is not CSR. The results are displayed in Figure 16.24.

With $K = 500$ and $\hat{C}_1 = 0.18$, we are able to identify stationarity of the underlying homogeneous Thomas point process using our Bayesian method. Also, with $K = 500$ and $\hat{C}_1 = 0.5$, our Bayesian procedure suggests dependence among \mathbf{X}_{C_i} ; $i = 1, \dots, 50$, leading us to correctly conclude that the point process is not Poisson.

16.14 Example 9: Inhomogeneous Thomas process with μ inhomogeneous

We now test our methods on an inhomogeneous Thomas process in $W = [0, 3] \times [0, 3]$ with $\kappa = 10$, $\sigma^2 = 10$, but $\mu(u_1, u_2) = 5 \exp(2u_1 - 1)$. That this process is also nonstationary follows from (16.39), since Λ is nonstationary in this case. The 10735 points we obtained using spatstat are shown in Figure 16.26.

With $K = 1000$ and $\hat{C}_1 = 0.23$, our Bayesian method correctly identifies non-CSR. The classical method also does as well. The results of both these methods are shown in Figure 16.27.

Our Bayesian algorithm correctly captures nonstationarity with $K = 1000$ and $\hat{C}_1 = 0.18$, the maximum value of \hat{C}_1 leading to nonstationarity. Dependence among \mathbf{X}_{C_i} ; $i = 1, \dots, 50$ is borne out by our Bayesian strategy with $\hat{C}_1 = 0.5$. The results are presented in Figure 16.28.

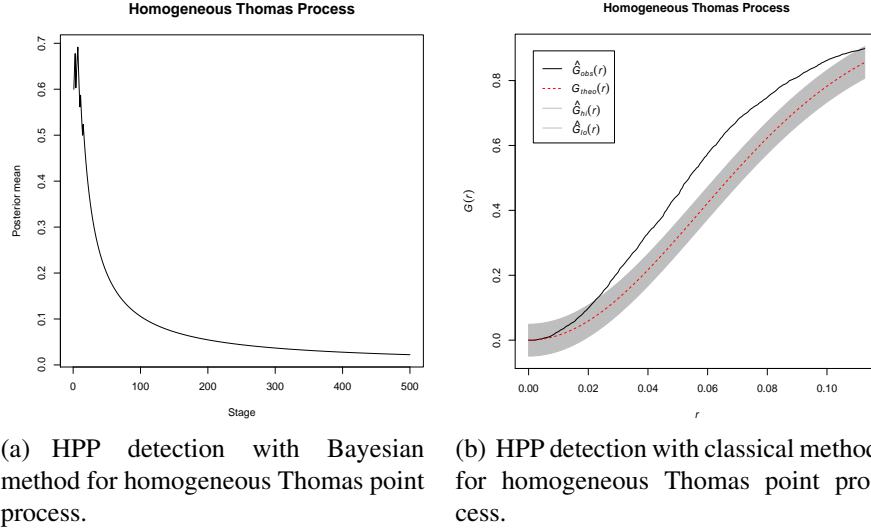


Figure 16.24: Detection of CSR with our Bayesian method and traditional classical method for homogeneous Thomas point process. Both the methods correctly identify that the underlying point process is not CSR.

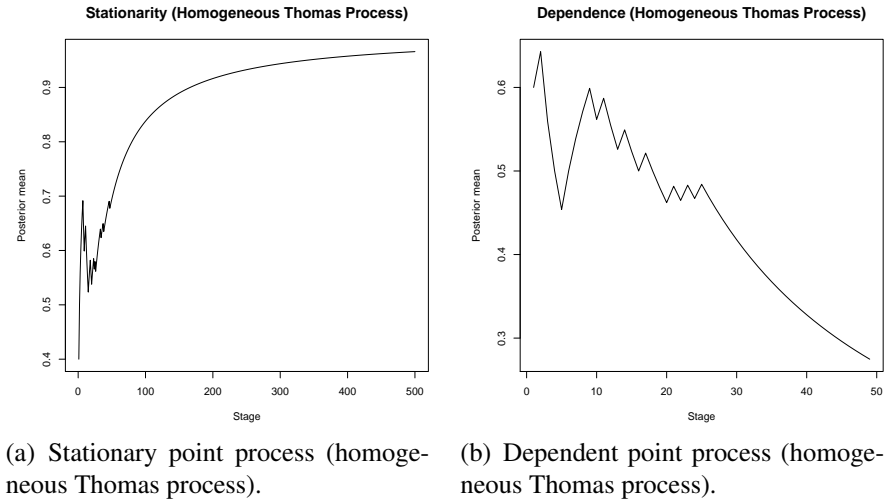


Figure 16.25: Detection of stationarity and dependence of homogeneous Thomas process with our Bayesian method.

Inhomogeneous Thomas Process

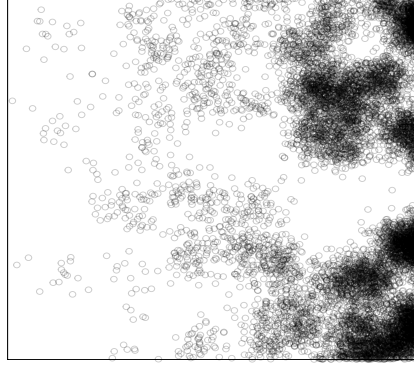
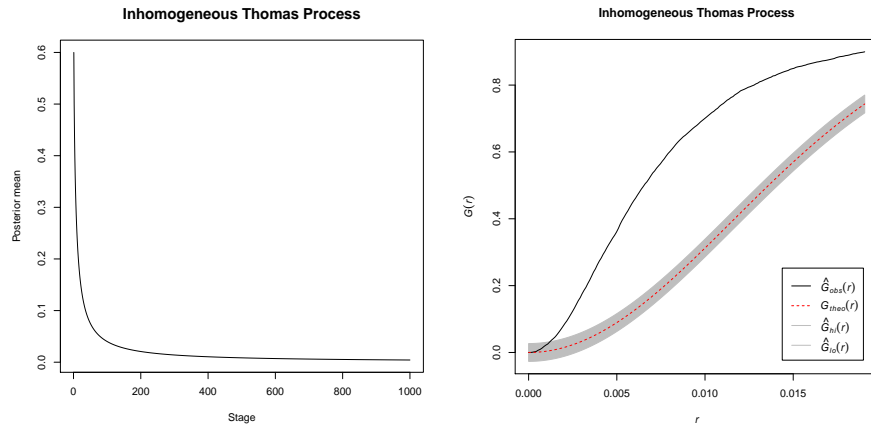


Figure 16.26: Inhomogeneous Thomas point process pattern.



(a) HPP detection with Bayesian method for inhomogeneous Thomas point process.

(b) HPP detection with classical method for inhomogeneous Thomas point process.

Figure 16.27: Detection of CSR with our Bayesian method and traditional classical method for Inhomogeneous Thomas point process. Both the methods correctly identify that the underlying point process is not CSR.

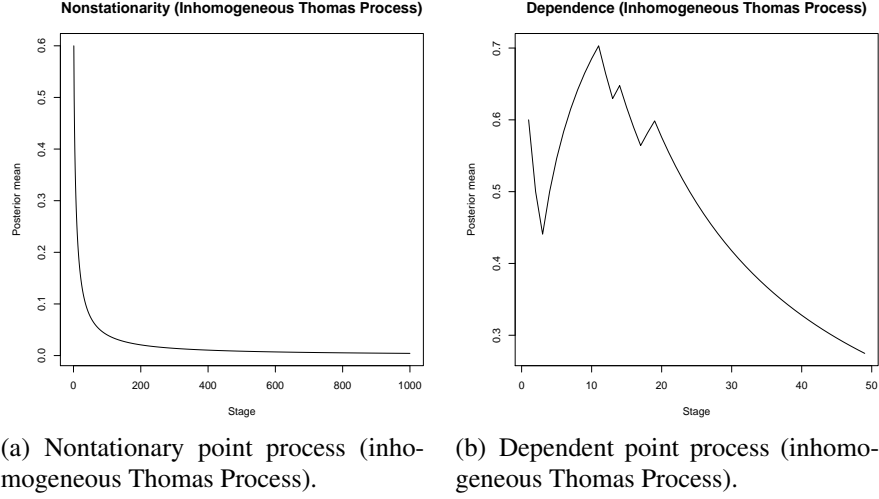


Figure 16.28: Detection of nonstationarity and dependence of inhomogeneous Thomas process with our Bayesian method.

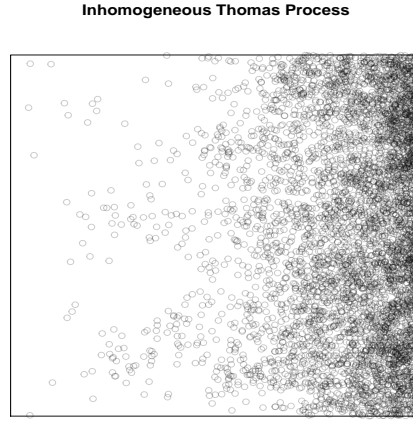


Figure 16.29: Inhomogeneous Thomas point process pattern.

16.15 Example 10: Inhomogeneous Thomas process with κ inhomogeneous

We now consider another inhomogeneous Thomas process on $W = [0, 3] \times [0, 3]$ with $\mu = 5$, $\sigma^2 = 10$ but $\kappa(u_1, u_2) = 5 \exp(2x - 1)$. This is also a nonstationary, non-Poisson, non-homogeneous point process. Figure 16.29 displays the 5608 points that we obtained from this process.

With $K = 500$ and $\hat{C}_1 = 0.23$, our Bayesian correctly detected non-CSR. The classical method also performed adequately in this case. The results are shown in Figure 16.30.

As before, our Bayesian method correctly detected nonstationarity with $K = 500$ and $\hat{C}_1 = 0.18$. Also, as before, dependence among \mathbf{X}_{C_i} ; $i = 1, \dots, 50$, is correctly indicated by our Bayesian method, with $\hat{C}_1 = 0.5$.

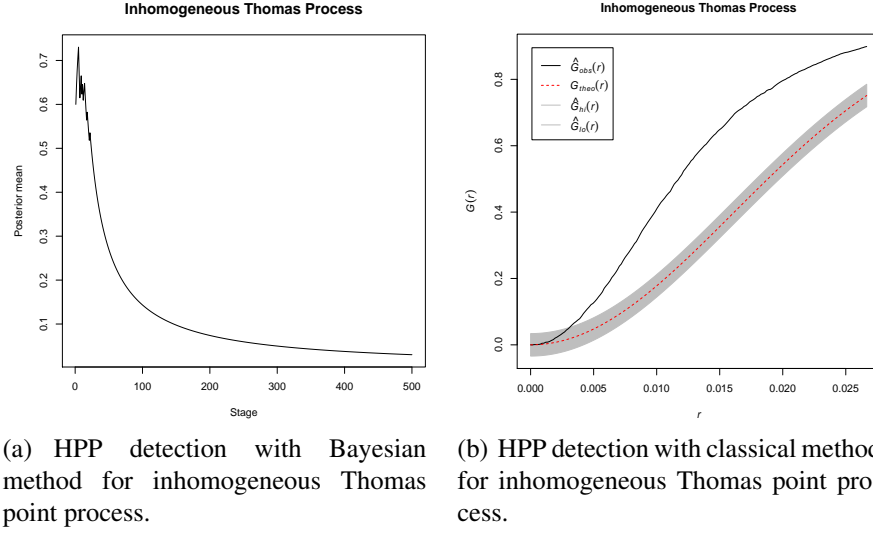


Figure 16.30: Detection of CSR with our Bayesian method and traditional classical method for inhomogeneous Thomas point process. Both the methods correctly identify that the underlying point process is not CSR.

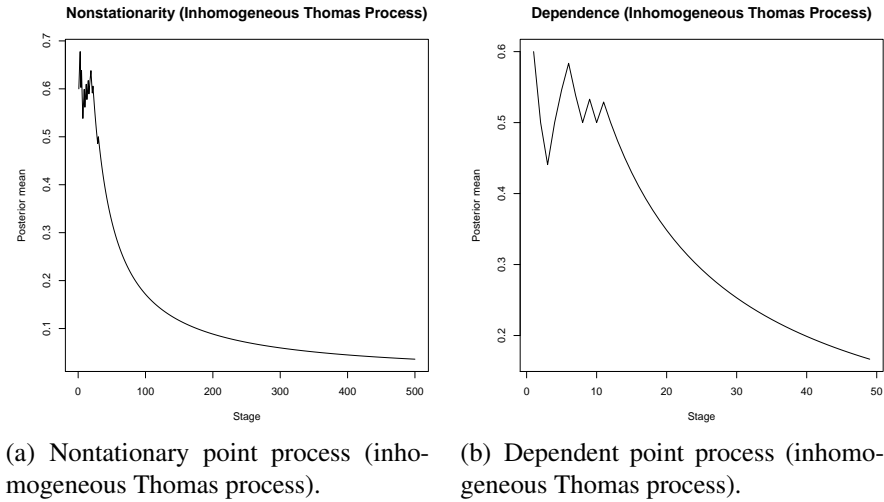


Figure 16.31: Detection of nonstationarity and dependence of inhomogeneous Thomas process with our Bayesian method.

Inhomogeneous Thomas Process

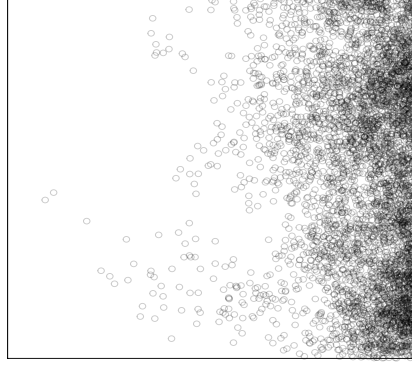


Figure 16.32: Inhomogeneous Thomas point process pattern.

16.16 Example 11: Inhomogeneous Thomas process with κ and μ the same inhomogeneous function

Let us consider simulation from another inhomogeneous Thomas process where $\kappa(u_1, u_2) = \mu(u_1, u_2) = 5 \exp(2u_1 - 1)$. With $\sigma^2 = 10$, we obtained 5302 points on the window $W = [0, 2] \times [0, 2]$, displayed in Figure 16.32.

Figure 16.33 shows the results of Bayesian and classical CSR detection methods; both the methods performed adequately, correctly identifying non-CSR. For the Bayesian method we set $K = 500$ and $\hat{C}_1 = 0.23$.

Nonstationarity of this point process has been correctly detected by our Bayesian method with $K = 810$ and $\hat{C}_1 = 0.18$. As regards our Bayesian test for mutual independence, we correctly obtained dependence with $K = 50$ and $\hat{C}_1 = 0.5$. The results are presented in Figure 16.34.

16.17 Example 12: Inhomogeneous Thomas process with κ and μ different inhomogeneous functions

Let us now consider another inhomogeneous Thomas process, where $\mu(u_1, u_2) = 5 \exp(2u_1 - 1)$ and $\kappa(u_1, u_2) = 10(u_1^2 + u_2^2)$. We obtained 3573 observations with $\sigma^2 = 10$ on the window $W = [0, 2] \times [0, 2]$. The data are displayed in Figure 16.35.

With $K = 500$ and $\hat{C}_1 = 0.23$, we correctly obtained non-CSR with our Bayesian method. The classical method also correctly detected non-CSR. The results are presented in Figure 16.36.

Our Bayesian algorithm correctly detected nonstationarity with $K = 500$ and $\hat{C}_1 = 0.18$. The Bayesian test for independence also correctly detected dependence with $K = 50$ and $\hat{C}_1 = 0.5$. Both these results are presented in Figure 16.37.

16.18 Example 13: Inhomogeneous Thomas Process with interchanged inhomogeneous κ and μ

We consider a final inhomogeneous Thomas process with $\mu(u_1, u_2) = 10(u_1^2 + u_2^2)$ and $\kappa(u_1, u_2) = 5 \exp(2u_1 - 1)$. In this case, we obtained 4008 observations on the window $W = [0, 2] \times [0, 2]$,

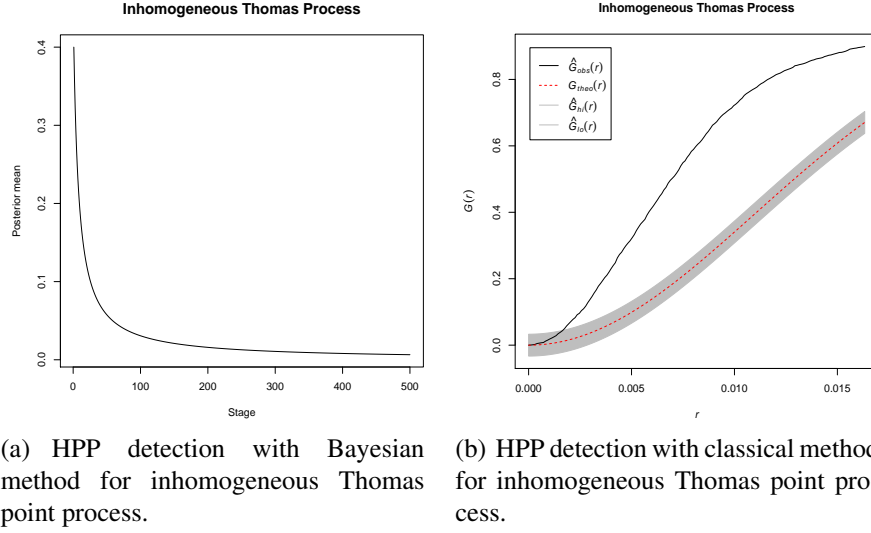


Figure 16.33: Detection of CSR with our Bayesian method and traditional classical method for inhomogeneous Thomas point process. Both the methods correctly identify that the underlying point process is not CSR.

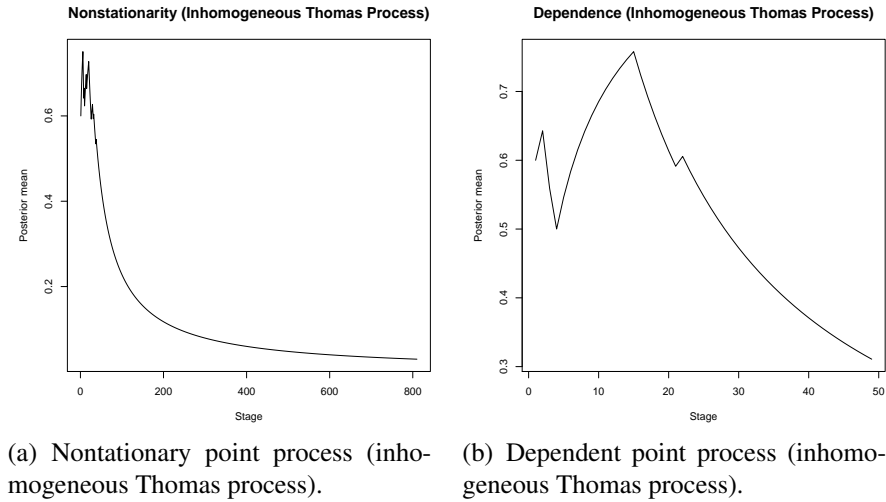


Figure 16.34: Detection of nonstationarity and dependence of inhomogeneous Thomas process with our Bayesian method.

Inhomogeneous Thomas Process

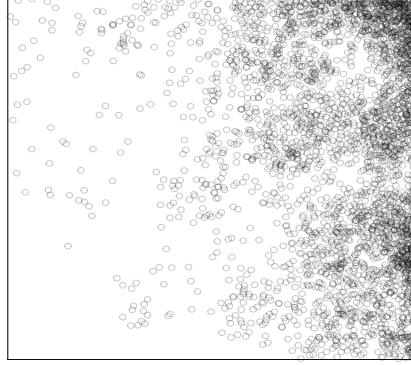
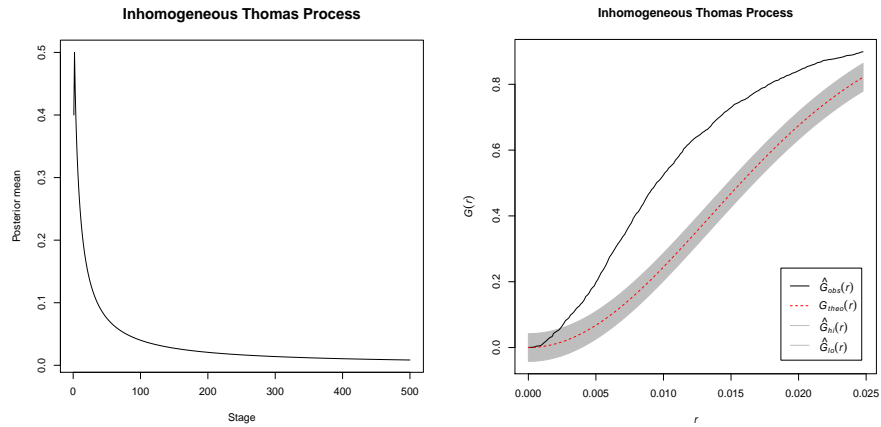


Figure 16.35: Inhomogeneous Thomas point process pattern.



(a) HPP detection with Bayesian method for inhomogeneous Thomas point process.

(b) HPP detection with classical method for inhomogeneous Thomas point process.

Figure 16.36: Detection of CSR with our Bayesian method and traditional classical method for inhomogeneous Thomas point process. Both the methods correctly identify that the underlying point process is not CSR.

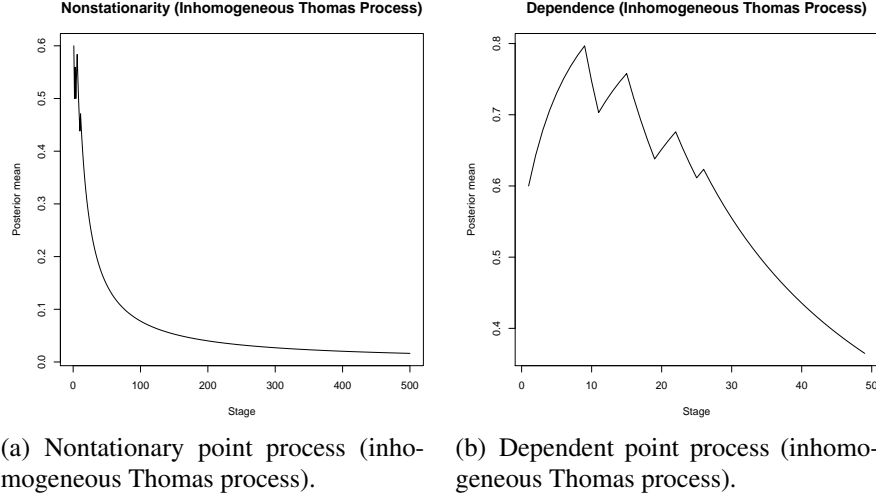


Figure 16.37: Detection of nonstationarity and dependence of inhomogeneous Thomas process with our Bayesian method.

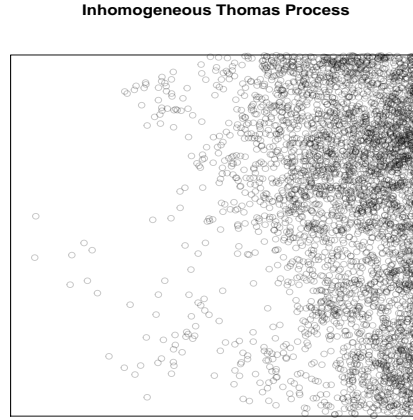


Figure 16.38: Inhomogeneous Thomas point process pattern.

which we display in Figure 16.38.

For CSR detection, we set $K = 500$ and $\hat{C}_1 = 0.23$ for the Bayesian method. As shown by Figure 16.39, both the Bayesian and the classical method successfully detect non-CSR.

Our Bayesian method also successfully detected nonstationarity with $K = 500$ and $\hat{C}_1 = 0.18$, and dependence, with $K = 27$ (smaller value chosen to ensure numerical stability) and $\hat{C}_1 = 0.5$. These results are depicted in Figure 16.40.

16.19 Example 14: Homogeneous Neyman-Scott process

A Neyman-Scott process is a Cox process where the centers c in (16.39) arising from a Poisson process with intensity function and κ and $\gamma \equiv \mu$, where μ is some deterministic function. Note that the Neyman-Scott process is more general than the Thomas process in the sense that the density function $k(c, \cdot)$ is left unspecified in the Neyman-Scott case, whereas for the Thomas process, this is a specific bivariate normal density.

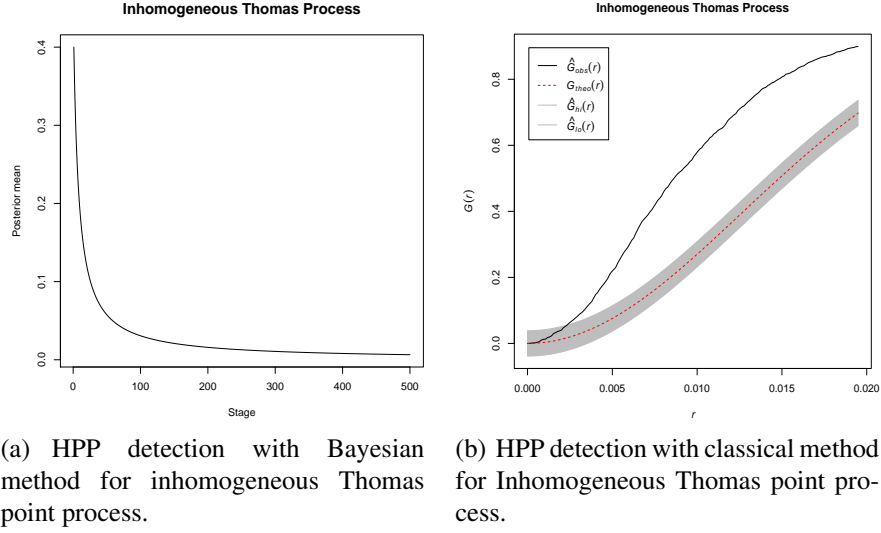


Figure 16.39: Detection of CSR with our Bayesian method and traditional classical method for inhomogeneous Thomas point process. Both the methods correctly identify that the underlying point process is not CSR.

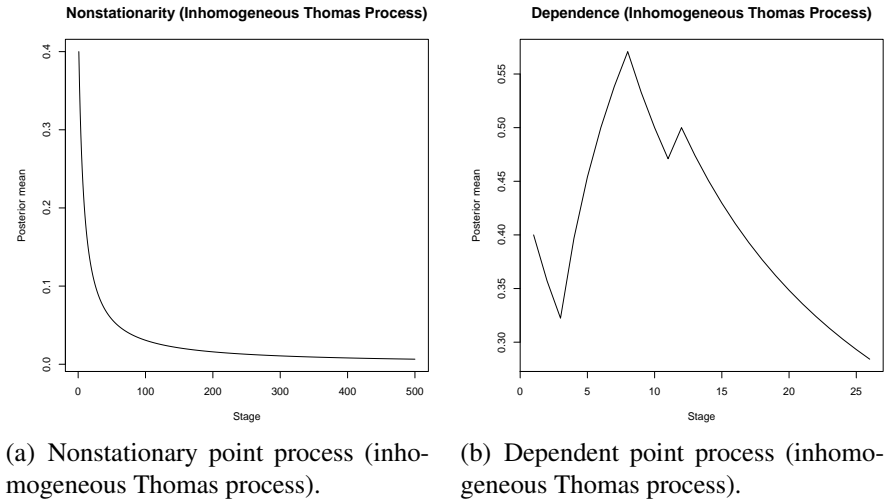


Figure 16.40: Detection of nonstationarity and dependence of Inhomogeneous Thomas process with our Bayesian method.

Homogeneous Neyman-Scott Process

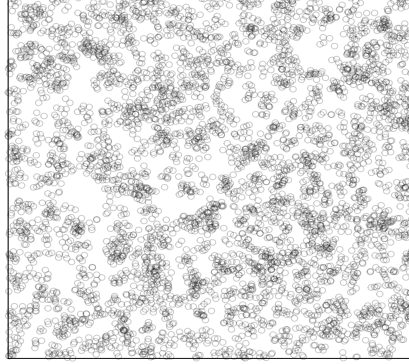


Figure 16.41: Homogeneous Neyman-Scott point process pattern.

More generally, the Neyman-Scott process allows a fixed number of offsprings on a disc with the parent point being the center of the disc. Here even though the centers arise from a Poisson process with intensity κ , the offsprings no longer follow the Poisson process, since given the parent points, the number of offsprings given each parent, is non-random. In such a case, the Neyman-Scott process is no longer a Cox process.

In order to test our methods on Neyman-Scott process, we first consider a homogeneous general Neyman-Scott process with $\kappa = 10$, with 5 points generated uniformly on each disc of radius 0.2 around the parent centers. The point pattern, simulated on $W = [0, 10] \times [0, 10]$, consisting of 4867 observations, is shown in Figure 16.41.

Both the Bayesian and the traditional method of checking CSR correctly indicate that the underlying process is not CSR. In the Bayesian case, we set $K = 500$ and $\hat{C}_1 = 0.20$. The results are displayed in Figure 16.42.

Stationarity is correctly detected by our Bayesian method with $K = 500$ and $\hat{C}_1 = 0.23$. Also, with $K = 50$ and $\hat{C}_1 = 0.5$, Poisson process is correctly ruled out. The results are depicted in Figure 16.43.

16.20 Example 15: Inhomogeneous Neyman-Scott process

In this case, we generate a sample of size 8358 on $W = [0, 4] \times [0, 4]$ from a Neyman-Scott process with the same setup as above, but with $\kappa(u_1, u_2) = 10(u_1^2 + u_2^2)$. The point pattern thus generated from this inhomogeneous Neyman-Scott process is shown in Figure 16.44.

With $K = 800$ and $\hat{C}_1 = 0.19$, we obtain the correct non-CSR conclusion with the Bayesian method. The correct result is also identified by the classical method. Both the results are depicted in Figure 16.45.

Nonstationarity of this process is correctly detected by the Bayesian method with $K = 1000$ and $\hat{C}_1 = 0.23$; this is shown in panel (a) of Figure 16.46. For $K = 50$ and $\hat{C}_1 = 0.5$, panel (b) of Figure 16.46 shows steady increase for about the first 35 stages, but sharply decreases thenceforward, indicating dependence.

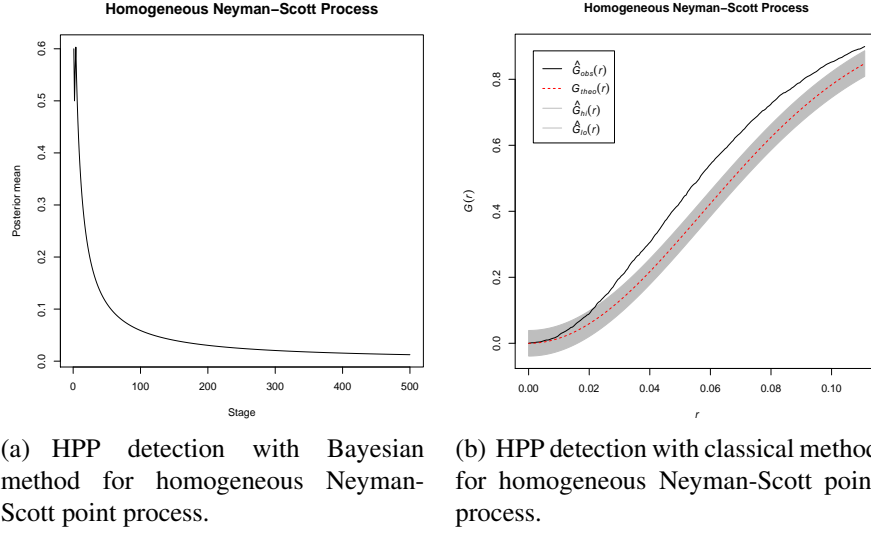


Figure 16.42: Detection of CSR with our Bayesian method and traditional classical method for homogeneous Neyman-Scott point process. Both the methods correctly identify that the underlying point process is not CSR.

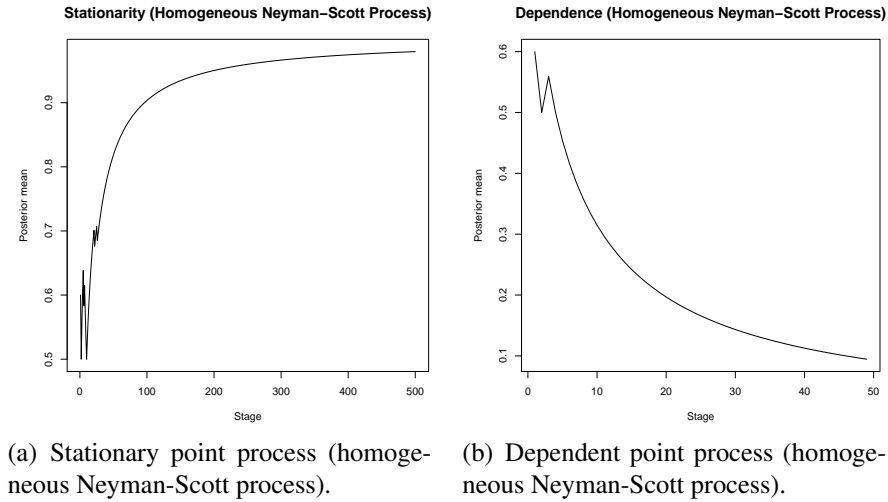


Figure 16.43: Detection of stationarity and dependence of homogeneous Neyman-Scott process with our Bayesian method.

Inhomogeneous Neyman-Scott Process

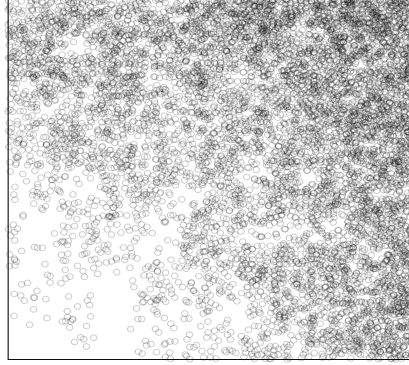
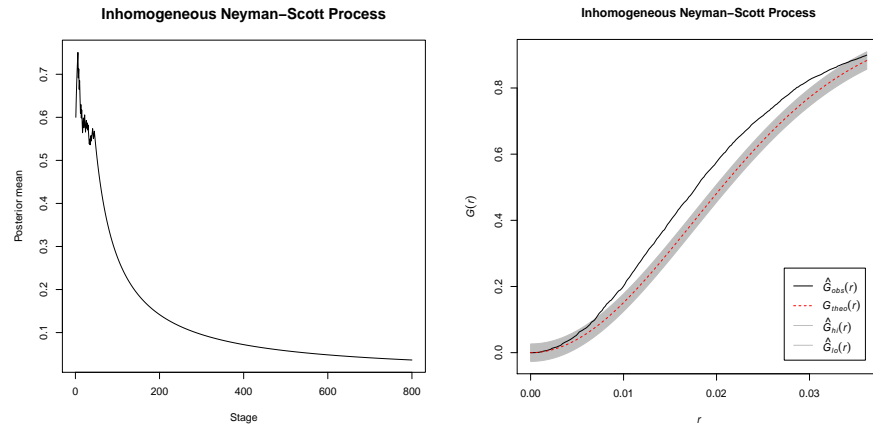


Figure 16.44: Inhomogeneous Neyman-Scott point process pattern.



(a) HPP detection with Bayesian method for inhomogeneous Neyman-Scott point process.

(b) HPP detection with classical method for homogeneous Neyman-Scott point process.

Figure 16.45: Detection of CSR with our Bayesian method and traditional classical method for homogeneous Neyman-Scott point process. Both the methods correctly identify that the underlying point process is not CSR.

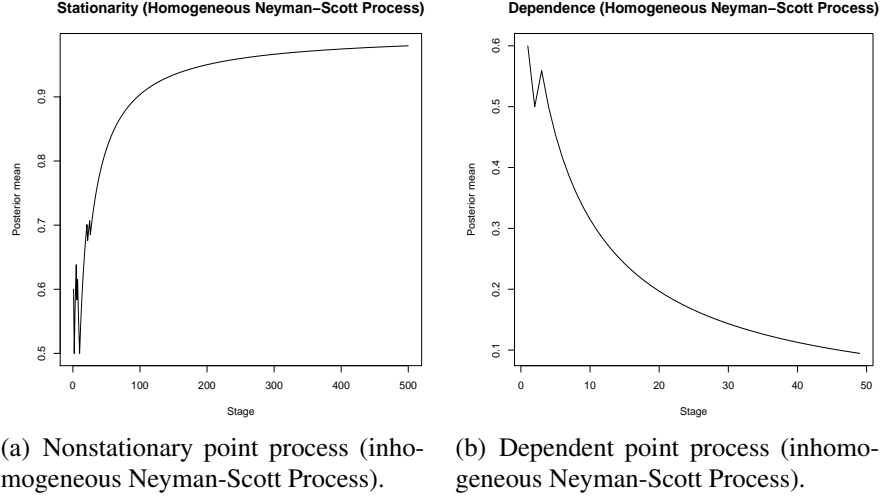


Figure 16.46: Detection of nonstationarity and dependence of homogeneous Neyman-Scott process with our Bayesian method.

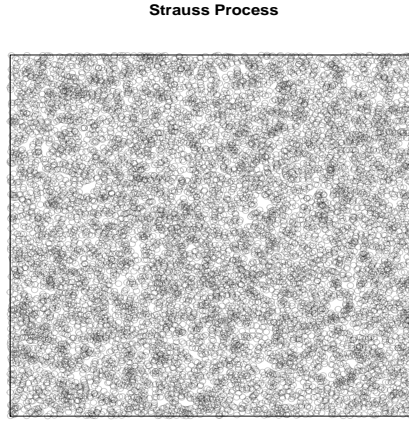


Figure 16.47: Strauss point process pattern.

16.21 Example 16: Strauss process

The Strauss process (Strauss (1975); see also Møller and Waagepetersen (2004)) is an instance of pairwise interaction point process with density (with respect to unit intensity Poisson process)

$$f(x) \propto \beta^{n(x)} \gamma^{s_R(x)}, \quad (16.40)$$

where $\beta > 0$, $n(x)$ is the number of points in x and $s_R(x) = \sum_{(\xi, \eta) \subseteq x} I\{\|\xi - \eta\| \leq R\}$ is the number of R -close pairs of points in x . Note that if $\gamma = 1$, we obtain Poisson process on \mathcal{S} with intensity β , and if $\gamma < 1$, there is repulsion between the R -close points pairs of points in \mathcal{X} .

Using spatstat, we generate 9790 points from a Strauss process with $\beta = 0.05$, $\gamma = 0.2$ and $R = 1.5$ on $W = [0, 500] \times [0, 500]$. The points are displayed in Figure 16.47.

To detect CSR, we set $K = 800$ and $\hat{C}_1 = 0.15$ for the Bayesian algorithm. As Figure 16.48 shows, both the classical and the Bayesian methods correctly identify that the underlying process

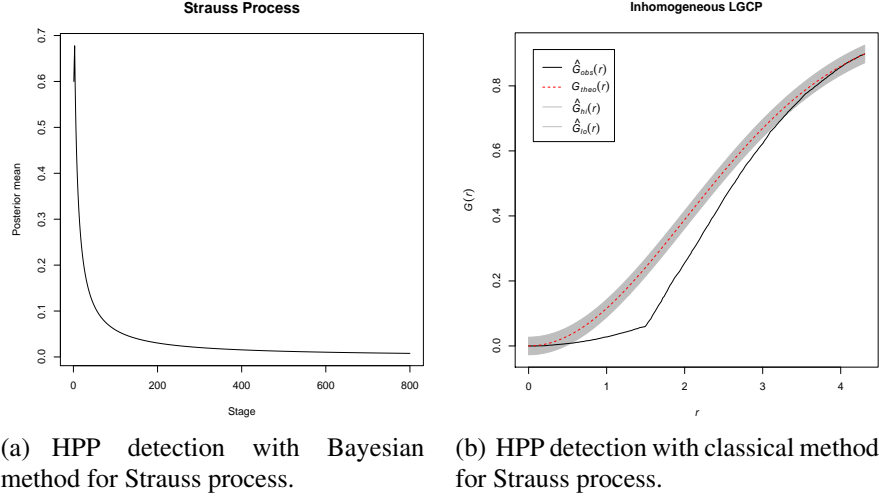


Figure 16.48: Detection of CSR with our Bayesian method and traditional classical method for Strauss process. Both the methods correctly identify that the underlying point process is not CSR.

is not CSR.

The left panel of Figure 16.49 captures the stationarity property of the Strauss process with $K = 800$ and $\hat{C}_1 = 0.15$. As before, larger values of \hat{C}_1 also lead to stationarity. The right panel of Figure 16.49 correctly indicates dependence among \mathbf{X}_{C_i} , for $i = 1, \dots, 100$, with $\hat{C}_1 = 0.5$.

16.22 Example 17: Another Strauss process

We now consider simulation from another homogeneous Strauss process with $\beta = 100$, $\gamma = 0.7$ and $R = 0.05$ on $W = [0, 8] \times [0, 8]$. The 5168 points that we obtained, are plotted in Figure 16.50.

Again, both the Bayesian and classical method correctly detects non-CSR, as shown by Figure 16.51. For the Bayesian method, we set $K = 500$ and $\hat{C}_1 = 0.15$.

Again, stationarity of the process is clearly indicated by panel (a) of Figure 16.52; here $K = 500$ and $\hat{C}_1 = 0.15$. Panel (b) shows dependence with $K = 50$ and $\hat{C}_1 = 0.5$.

17 Bayesian determination of frequencies of oscillatory stochastic processes

In this section we assume that the underlying stochastic process has multiple frequencies of oscillations almost surely, including the possibility that the number of such frequencies is countably infinite.

17.1 The key idea for Bayesian frequency determination

Let us assume that there are $N (\geq 1)$ frequencies of oscillations of the stochastic process $\mathbf{X} = \{X_1, X_2, \dots\}$. Here N may even be countably infinite. Consider the transformed process $\mathbf{Z} =$

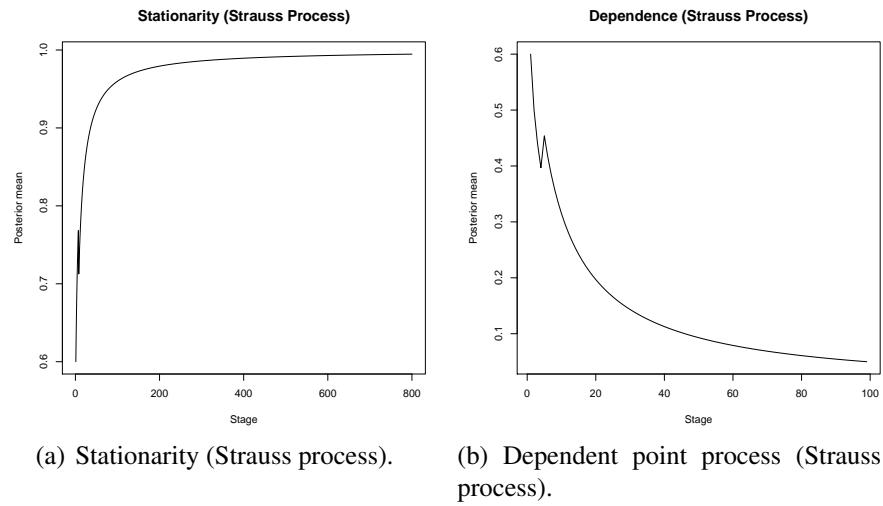


Figure 16.49: Detection of stationarity and dependence of Strauss process with our Bayesian method.

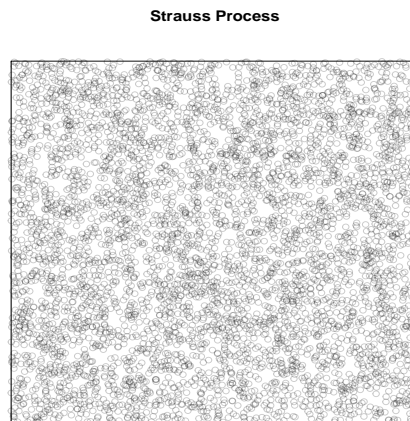


Figure 16.50: Strauss Process.

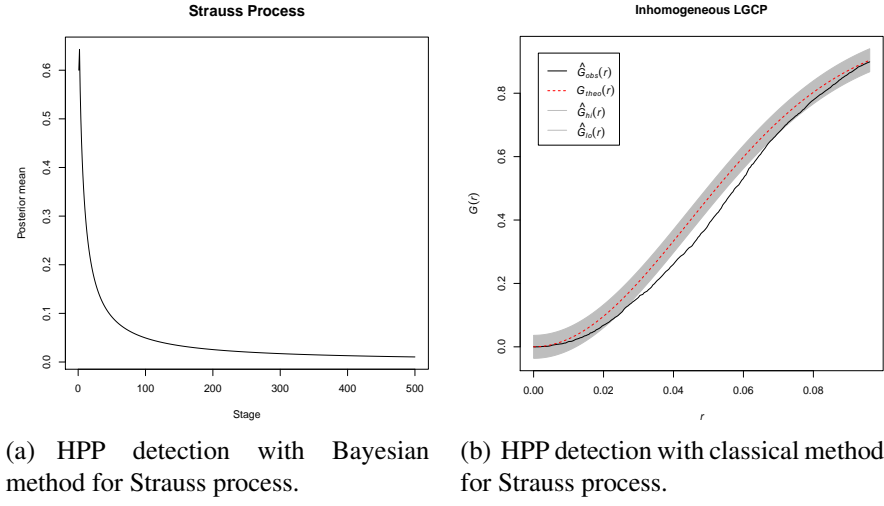


Figure 16.51: Detection of CSR with our Bayesian method and traditional classical method for Strauss process. Both the methods correctly identify that the underlying point process is not CSR.

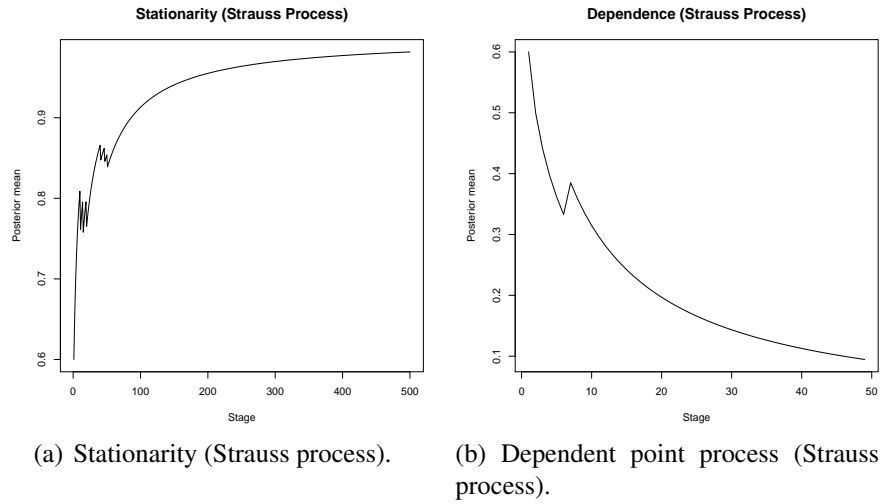


Figure 16.52: Detection of stationarity and dependence of Strauss process with our Bayesian method.

$\{Z_1, Z_2, \dots\}$, with $Z_j = \frac{\exp(X_j)}{1+\exp(X_j)}$; $j \geq 1$. Hence, $Z_j \in [0, 1]$. Now consider dividing up the interval $[0, 1]$ into $\cup_{m=1}^M [\tilde{p}_{m-1}, \tilde{p}_m]$, for $M > 1$, such that $\tilde{p}_0 = 0$, $\tilde{p}_m = \tilde{p}_{m-1} + q_m$, where $\{q_m : m = 1, \dots, M\}$ is some probability distribution satisfying $0 \leq q_m \leq 1$ for $m = 1, \dots, M$, and $\sum_{m=0}^M q_m = 1$. Here M can be even be infinite.

For oscillating stochastic process \mathbf{X} , for any $r > 0$, $\mathbf{Z}^r = \{Z_1^r, Z_2^r, \dots\}$ is also an oscillating stochastic process taking values in $[0, 1]$. Crucially, when raised to some sufficiently large positive power r , the originally smaller values of \mathbf{Z} tend to be much smaller compared to the originally larger values. These larger values of \mathbf{Z}^r will be contained in $[\tilde{p}_{m-1}, \tilde{p}_m]$, for large values of m . In particular, the largest values of \mathbf{Z}^r are expected to be contained in $(\tilde{p}_{M-1}, 1]$, or in $[\tilde{p}_{m_0-1}, \tilde{p}_{m_0}]$ for $1 \leq M_0 < m_0 < M$. Here M_0 is expected to be reasonably close to M . In the latter case, intervals of the form $[\tilde{p}_{m-1}, \tilde{p}_m]$ will remain empty for $m > m_0$. The next largest values of \mathbf{Z}^r will be concentrated in $[\tilde{p}_{m_1-1}, \tilde{p}_{m_1}]$ for some $1 \leq M_1 < m_1 < m_0$. In this case, $[\tilde{p}_{m-1}, \tilde{p}_m]$ will remain empty for $m_1 + 1 < m < m_0 - 1$, and so on.

Note that the proportions of the values contained in the intervals constitute the frequencies of oscillations of the original process \mathbf{X} . We formalize this key idea into a Bayesian theory, treating M as finite as well as infinite.

17.2 Bayesian theory for finite M

To fix ideas, let us define

$$Y_j = m \text{ if } \tilde{p}_{m-1} < Z_j^r \leq \tilde{p}_m; \quad m = 1, 2, \dots, M. \quad (17.1)$$

We assume that

$$(\mathbb{I}(Y_j = 1), \dots, \mathbb{I}(Y_j = M)) \sim \text{Multinomial}(1, p_{1,j}, \dots, p_{M,j}), \quad (17.2)$$

where $p_{m,j}$ can be interpreted as the probability that $Z_j^r \in (\tilde{p}_{m-1}, \tilde{p}_m]$.

Now note that for large M , the intervals $(\tilde{p}_{m-1}, \tilde{p}_m]$ correspond to small regions of the index set of the stochastic process \mathbf{X} , and hence, the part of the process \mathbf{Z}^r falling in $(\tilde{p}_{m-1}, \tilde{p}_m]$ can be safely regarded as stationary. Further, assuming ergodicity of the process falling in the interval, it is expected that $p_{m,j}$ will tend to the correct proportion of the process \mathbf{Z}^r falling in $(\tilde{p}_{m-1}, \tilde{p}_m]$, as $j \rightarrow \infty$. Notationally, we let $\{p_{m,0} : m = 1, \dots, M\}$ denote the actual proportions of the process \mathbf{Z}^r falling in $(\tilde{p}_{m-1}, \tilde{p}_m]$; $m = 1, \dots, M$.

Following the same principle discussed in Section 4, and extending the Beta prior to the Dirichlet prior, at the k -th stage we arrive at the following posterior of $\{p_{m,k} : m = 1, \dots, M\}$:

$$\pi(p_{1,k}, \dots, p_{M,k} | y_k) \equiv \text{Dirichlet} \left(\sum_{j=1}^k \frac{1}{j^2} + \sum_{j=1}^k \mathbb{I}(y_j = 1), \dots, \sum_{j=1}^k \frac{1}{j^2} + \sum_{j=1}^k \mathbb{I}(y_j = M) \right). \quad (17.3)$$

The posterior mean and posterior variance of $p_{m,k}$, for $m = 1, \dots, M$, are given by:

$$E(p_{m,k}|y_k) = \frac{\sum_{j=1}^k \frac{1}{j^2} + \sum_{j=1}^k \mathbb{I}(y_j = m)}{M \sum_{j=1}^k \frac{1}{j^2} + k}; \quad (17.4)$$

$$Var(p_{m,k}|y_k) = \frac{\left(\sum_{j=1}^k \frac{1}{j^2} + \sum_{j=1}^k \mathbb{I}(y_j = m)\right) \left((M-1) \sum_{j=1}^k \frac{1}{j^2} + k - \sum_{j=1}^k \mathbb{I}(y_j = m)\right)}{\left(M \sum_{j=1}^k \frac{1}{j^2} + k\right)^2 \left(M \sum_{j=1}^k \frac{1}{j^2} + k + 1\right)}. \quad (17.5)$$

Since the process \mathbf{Z}^r falling in $(\tilde{p}_{m-1}, \tilde{p}_m]$ is stationary and ergodic, it follows from (17.4) and (17.5) it is easily seen, using $\frac{\sum_{j=1}^k \mathbb{I}(y_j = m)}{k} \rightarrow p_{m,0}$, almost surely, as $k \rightarrow \infty$, that, almost surely,

$$E(p_{m,k}|y_k) \rightarrow p_{m,0}, \quad \text{and} \quad (17.6)$$

$$Var(p_{m,k}|y_k) = O\left(\frac{1}{k}\right) \rightarrow 0, \quad (17.7)$$

as $k \rightarrow \infty$.

Theorem 34 formalizes the above arguments in terms of the limits of the marginal posterior probabilities of $p_{m,k}$, denoted by $\pi_m(\cdot|y_k)$, as $k \rightarrow \infty$.

Theorem 34 Assume that M is so large that \mathbf{Z}^r falling in the intervals $(\tilde{p}_{m-1}, \tilde{p}_m]$; $m = 1, \dots, M$, constitute stationary processes, and that such stationary processes are also ergodic.

Let $\mathcal{N}_{p_{m,0}}$ be any neighborhood of $p_{m,0}$, with $p_{m,0}$ satisfying $0 < p_{m,0} < 1$ for $m = 1, \dots, M$ such that $\sum_{m=1}^M p_{m,0} = 1$. Then

$$\pi_m(\mathcal{N}_{p_{m,0}}|y_k) \rightarrow 1, \quad (17.8)$$

almost surely as $k \rightarrow \infty$.

Proof. For any neighborhood of $p_{m,0}$, denoted by $\mathcal{N}_{p_{m,0}}$, let $\epsilon > 0$ be sufficiently small so that $\mathcal{N}_{p_{m,0}} \supseteq \{|p_{m,k} - p_{m,0}| < \epsilon\}$. Then by Chebychev's inequality, using (17.6) and (17.7), it is seen that $\pi_m(\mathcal{N}_{p_{m,0}}|y_k) \rightarrow 1$, almost surely, as $k \rightarrow \infty$. ■

Corollary 35 For adequate choices of r and M , the non-zero distinct elements of $\{p_{m,0}; m = 2, \dots, M\}$ are the desired frequencies of the oscillating stochastic process \mathbf{X} . Note that for adequately large M , $p_{1,0}$ is associated with the small values of Z^r , and hence does not correspond to any frequency of the original stochastic process.

17.3 Choice of r , M and $\{q_1, \dots, q_M\}$

In principle, the probability distribution $\{q_1, \dots, q_M\}$ should be chosen based on prior information regarding which intervals contain the desired frequencies. Given sufficiently large M , the values of q_m can then be chosen to shorten or widen any given interval. Short intervals are preferable when there is strong prior information of some frequency falling in the vicinity of some point. On the other hand, larger intervals are appropriate in the case of weak prior information. Such prior knowledge may be obtained, say, by periodogram analysis of the underlying time series.

However, in our experiments, the uniform distribution $q_m = 1/M$, for $m = 1, \dots, M$, yielded excellent results. For the choice of r , we recommend that value for which the oscillations of \mathbf{Z}^r as distinctly visible as possible. The choice of M should be such that $\{(\tilde{p}_{m-1}, \tilde{p}_m]; m = 1, \dots, M\}$ covers the range of \mathbf{Z}^r with adequately fine intervals. We discuss these issues in details with simulation studies and real data examples.

17.4 Infinite number of frequencies

We now assume that the number of frequencies, m , is countably infinite, and that $\{p_{m,0}; m = 1, 2, 3, \dots\}$, where $0 \leq p_{m,0} \leq 1$ and $\sum_{m=1}^{\infty} p_{m,0} = 1$, are the true proportions of the process \mathbf{Z}^r falling in the intervals $(\tilde{p}_{m-1}, \tilde{p}_m]; m = 1, 2, \dots$

Now we define

$$Y_j = m \text{ if } \tilde{p}_{m-1} < Z_j^r \leq \tilde{p}_m; m = 1, 2, \dots, \infty. \quad (17.9)$$

Let $\mathcal{X} = \{1, 2, \dots\}$ and let $\mathcal{B}(\mathcal{X})$ denote the Borel σ -field on \mathcal{X} (assuming every singleton of \mathcal{X} is an open set). Let \mathcal{P} denote the set of probability measures on \mathcal{X} . Then, at the j -th stage,

$$[Y_j | P_j] \sim P_j, \quad (17.10)$$

where $P_j \in \mathcal{P}$. We assume that P_j is the following Dirichlet process (see Ferguson (1973)):

$$P_j \sim DP \left(\frac{1}{j^2} G \right), \quad (17.11)$$

where, the probability measure G is such that, for every $j \geq 1$,

$$G(Y_j = m) = \frac{1}{2^m}. \quad (17.12)$$

It then follows using the same previous principles that, at the k -th stage, the posterior of P_k is again a Dirichlet process, given by

$$[P_k | y_k] \sim DP \left(\sum_{j=1}^k \frac{1}{j^2} G + \sum_{j=1}^k \delta_{y_j} \right), \quad (17.13)$$

where δ_{y_j} denotes point mass at y_j . It follows from (17.13) that

$$E(p_{m,k} | y_k) = \frac{\frac{1}{2^m} \sum_{j=1}^k \frac{1}{j^2} + \sum_{j=1}^k \mathbb{I}(y_j = m)}{\sum_{j=1}^k \frac{1}{j^2} + k}; \quad (17.14)$$

$$Var(p_{m,k} | y_k) = \frac{\left(\sum_{j=1}^k \frac{1}{j^2} + \sum_{j=1}^k \mathbb{I}(y_j = m) \right) \left(\left(1 - \frac{1}{2^m} \right) \sum_{j=1}^k \frac{1}{j^2} + k - \sum_{j=1}^k \mathbb{I}(y_j = m) \right)}{\left(\sum_{j=1}^k \frac{1}{j^2} + k \right)^2 \left(\sum_{j=1}^k \frac{1}{j^2} + k + 1 \right)}. \quad (17.15)$$

As before, it easily follows from (17.14) and (17.15) that for $m = 1, 2, 3, \dots$,

$$E(p_{m,k}|y_k) \rightarrow p_{m,0}, \text{ and} \quad (17.16)$$

$$Var(p_{m,k}|y_k) = O\left(\frac{1}{k}\right) \rightarrow 0, \quad (17.17)$$

almost surely, as $k \rightarrow \infty$.

The theorem below formalizes the above arguments in the infinite number of frequency situation in terms of the limit of the marginal posterior probabilities of $p_{m,k}$, as $k \rightarrow \infty$.

Theorem 36 *Assume that Z^r falling in the intervals $(\tilde{p}_{m-1}, \tilde{p}_m]$; $m = 1, 2, \dots$, constitute stationary processes, and that such stationary processes are also ergodic.*

Let $\mathcal{N}_{p_{m,0}}$ be any neighborhood of $p_{m,0}$, with $p_{m,0}$ satisfying $0 \leq p_{m,0} \leq 1$ for $m = 1, 2, \dots$ such that $\sum_{m=1}^{\infty} p_{m,0} = 1$, with at most finite number of m such that $p_{m,0} = 0$. Then with Y_j defined as in (17.9),

$$\pi_m(\mathcal{N}_{p_{m,0}}|y_k) \rightarrow 1, \quad (17.18)$$

almost surely, as $k \rightarrow \infty$.

Proof. Follows using the same ideas as the proof of Theorem 34. ■

Corollary 37 *The non-zero distinct elements of $\{p_{m,0}; m = 1, 2, \dots\}$ are the desired frequencies of the oscillating stochastic process \mathbf{X} . Again, $p_{1,0}$ does not correspond to any frequency of the original stochastic process.*

Remark 38 *As regards the choice of the quantities q_m , we suggest setting $q_m = 2^{-m}$, for $m \geq 1$, which is the same as the base measure for the Dirichlet process prior. For countably infinite number of frequencies, the choice of r is difficult to decide. But we hope that selecting r such that most of the oscillations are visible as much as possible, will work even in this situation.*

Remark 39 *It is useful to remark that our theory with countably infinite number of frequencies is readily applicable to situations where the number of frequencies is finite but unknown. In such cases, only a finite number of the probabilities $\{p_{m,j}; m = 2, 3, \dots\}$ will have posterior probabilities around positive quantities, while the rest will concentrate around zero. For known finite number of limit points, it is only required to specify G such that it gives positive mass to only a specific finite set.*

We now illustrate our Bayesian theory for detecting frequencies using simulation studies.

17.5 Simulation study with a single frequency

Following Example 2.8 of Shumway and Stoffer (2006), we generate $T = 500$ observations from the model

$$x_t = A \cos(2\pi\omega t + \varphi) + \epsilon_t, \quad (17.19)$$

where $\omega = 1/50$, $A = 2$, $\varphi = 0.6\pi$, and $\epsilon_t \stackrel{iid}{\sim} N(0, \sigma^2)$, with $\sigma = 5$. Figure 17.1 displays the generated time series. Observe that due to the relatively large σ , the true frequency is blurred in the

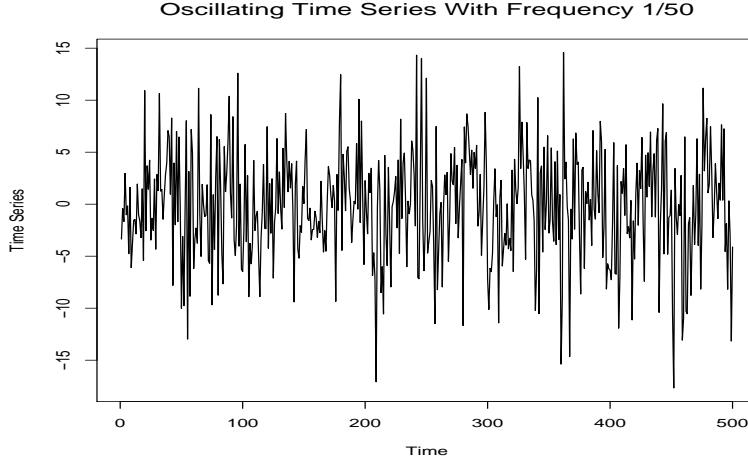


Figure 17.1: Simulated oscillating time series with true frequency 0.02.

observed time series. Our goal is to recover the frequency $\omega = 1/50$ using our Bayesian method, pretending that the true frequency is unknown.

We apply our Bayesian technique based on Dirichlet process, but with the base measure G_0 giving probability $1/M$ to each of the values $1, \dots, M$. Since our method depends crucially on the choices of r and M , it is important to carefully choose these quantities. As we had already prescribed, r should be so chosen that the oscillations of \mathbf{Z}^r are easy to visualize. Figure 17.2 shows the transformed time series \mathbf{Z}^r for different values of r . In this example we see that as r is increased, the oscillations tend to be more and more explicit. Thus, it seems that $r = 1000$ is the best choice among those experimented with.

For the choice of M we need to select a large enough value such that the range of \mathbf{Z}^r gets adequately partitioned within $\{(\tilde{p}_{m-1}, \tilde{p}_m]; m = 1, \dots, M\}$. In other words, relatively large values of r and M are expected to yield good Bayesian results. We investigate this by implementing our Bayesian method for different values of r and M and comparing the results.

Figures 17.3 and 17.4 depict the results of our Bayesian method for various choices of r and M . As shown by the figures, for increasing values of $r = 10, 50, 100, 500, 1000$, and $M = 10, 50, 100$, the posterior of $p_{M,j}$ associated with the interval $(\tilde{p}_{M-1}, \tilde{p}_M]$, increasingly converges to the true frequency 0.02. Note that for relatively small values of either r or M , the relevant posteriors fail to converge. Thus, the results are in keeping with our expectation of obtaining superior results for large values of r and M . Note that the rate of convergence of the posterior seems to be faster with respect to increasing values of r compared to increasing values of M . Thus, appropriate choice of r seems to be more important than M .

Following Shumway and Stoffer (2006) we have generated only 500 observations from (17.19) for inference, due to reasons of comparability with the results obtained by Shumway and Stoffer (2006). If large enough datasets are not available in reality, our Bayesian inference needs to be as accurate as possible based on the available data, and our analyses indeed provide glimpses of such reliable Bayesian inference. But in the current “big data” era large datasets are making their appearances, and it is important to weigh our inference with respect to large datasets, which also provide opportunities to properly validate our convergence theory, which is usually not viable for small datasets.

We thus generate a dataset from (17.19) with $T = 5 \times 10^5$, and apply our Bayesian procedure

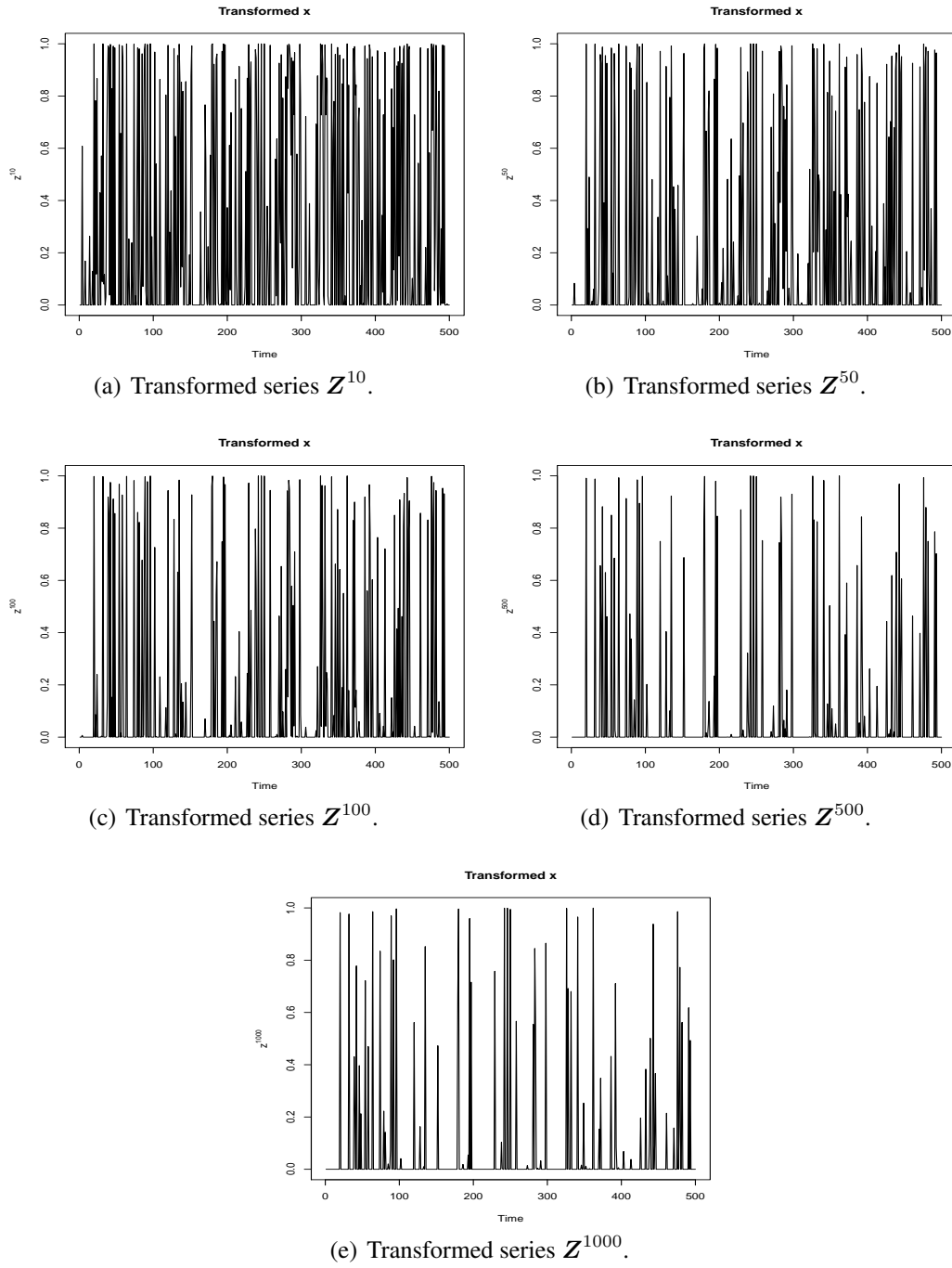


Figure 17.2: Illustration of effects of r in Z^r in determining single frequency in (17.19). Here the true frequency is 0.02.

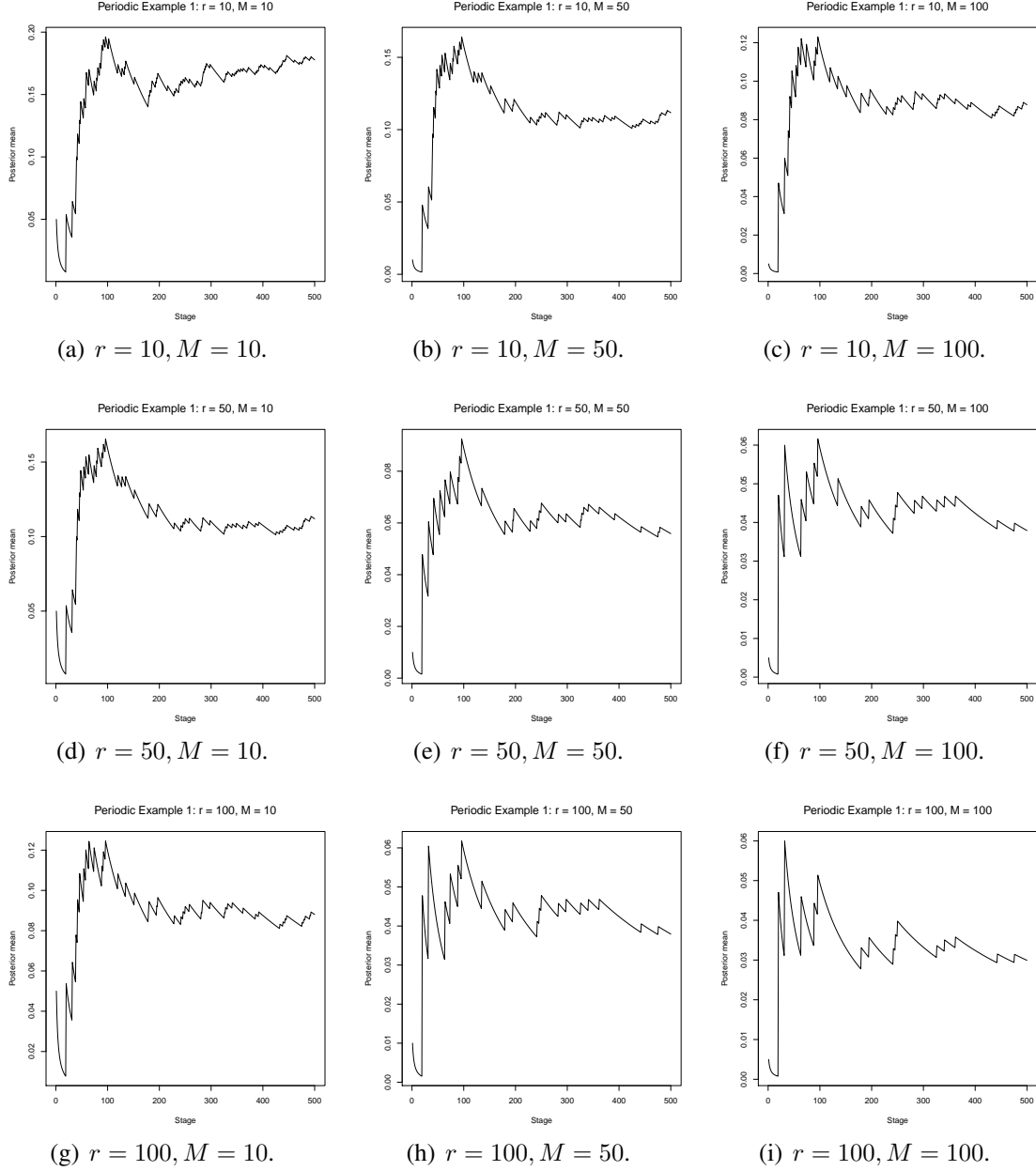


Figure 17.3: Illustration of our Bayesian method for determining single frequency. Here the true frequency is 0.02.

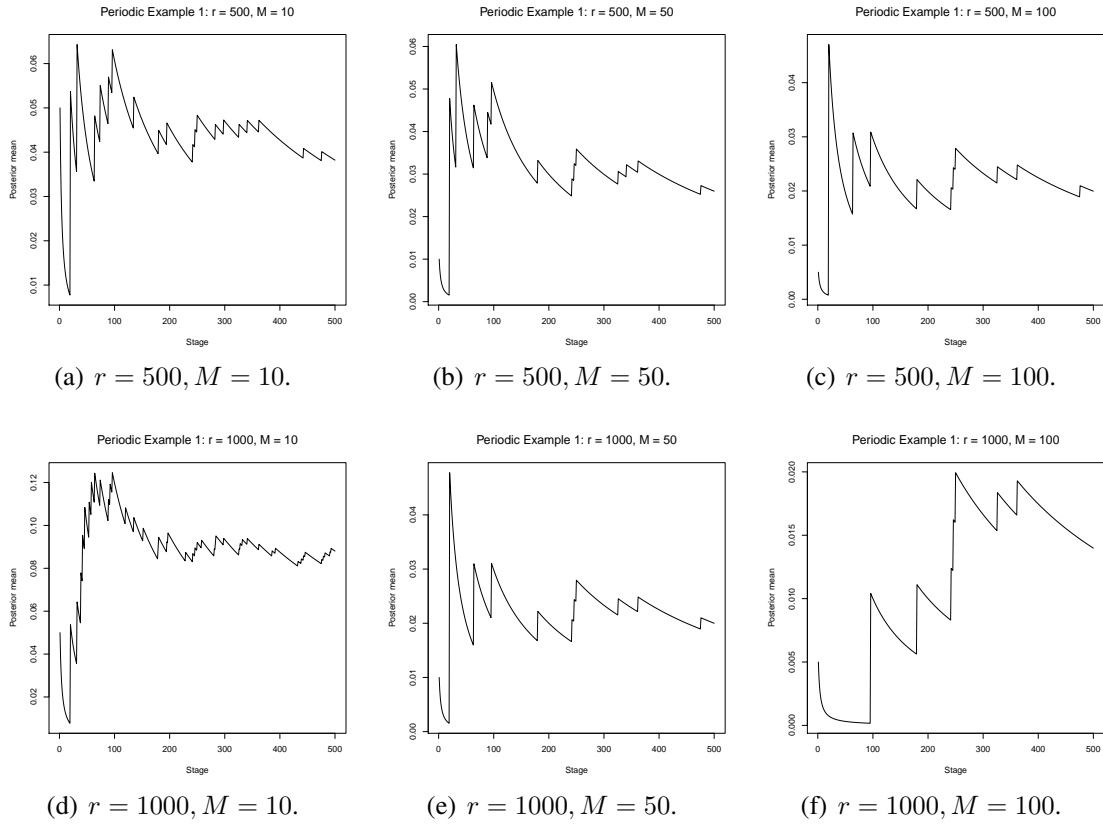


Figure 17.4: Illustration of our Bayesian method for determining single frequency. Here the true frequency is 0.02.

with $r = 1000$ and $M = 10, 50, 100$, in order to detect the true frequency 0.02. The results are displayed in Figure 17.5. Observe that for $M = 10$, the true frequency is overestimated, as shown in panel (a) associated with convergence of $p_{10,j}$ as $j \rightarrow \infty$, and for $M = 100$, underestimation occurs, as captured by panel (c) associated with convergence of $p_{100,j}$ as $j \rightarrow \infty$. Panel (b) shows convergence of $p_{50,j}$ as $j \rightarrow \infty$, where convergence occurs around 0.019, quite close to the truth. Panel (d) displays the result of convergence of $p_{100,j} + p_{99,j}$, as $j \rightarrow \infty$. This sum converges around 0.019. The reason for over and under estimation for $M = 10$ and 100 can be attributed to too coarse and too fine partitions of $[0, 1]$ via the choice of M , while for $M = 50$, the partitioning seems more reasonable in comparison. Adding up $p_{100,j}$ and $p_{99,j}$ compensates for the too fine partitioning of $[0, 1]$ in this case.

The effects of partitioning also points towards another issue – even $p_{50,j}$ and $p_{100,j} + p_{99,j}$ fail to capture the true frequency as $j \rightarrow \infty$, since the posterior variance becomes negligibly small as $j \rightarrow \infty$. In principle, it is possible to partition $[0, 1]$ appropriately (perhaps, using good choices of q_m), such that convergence to the exact true frequency is achieved. In this example, setting $M = 40$ is enough, as depicted in Figure 17.6. Note that such subtle issues can not be detected or analyzed for sample size as small as 500. Nevertheless, our final Bayesian results do convey very reliable analysis even for such small dataset.

17.6 Simulation study with multiple frequencies

As in Example 4.1 of Shumway and Stoffer (2006), for $t = 1, \dots, 100$, first we generate the following three series:

$$\begin{aligned}x_{t_1} &= 2 \cos(2\pi t_6/100) + 3 \sin(2\pi t_6/100); \\x_{t_2} &= 4 \cos(2\pi t_{10}/100) + 5 \sin(2\pi t_{10}/100); \\x_{t_3} &= 6 \cos(2\pi t_{40}/100) + 7 \sin(2\pi t_{40}/100),\end{aligned}$$

and set

$$x_t = x_{t_1} + x_{t_2} + x_{t_3}. \quad (17.20)$$

The series x_t , which consists of the three frequencies 0.4, 0.1 and 0.06, is shown in Figure 17.7.

Before applying our Bayesian method based on Dirichlet process to this example, we again need to choose r and M properly. Regarding the choice of r , Figure 17.8 depicts the process Z^r for $r = 1, 5, 10, 50, 100$. Here although it seems at first glance that increasing r leads to increasing isolation of the oscillations, actually, it is evident from closer look that increasing the power here has the effect of reducing the peaks of many relevant oscillations quite close to the highest peaks that are present in panel (a) of the figure, corresponding to $r = 1$. Thus, in this example, large values of r are inappropriate, unlike in the first example on single frequency. Here $r = 1$ seems more appropriate compared to the other values of r .

Regarding adequacy of the choice of r and M , a detailed analysis of our Bayesian results for this multiple frequency example is provided by Figures 17.9, 17.10, 17.11, 17.12 and 17.13. Most of these diagrams, for given r and M , are obtained by summing up the $p_{m,j}$ for nearby values of m . These yielded the three frequencies associated with our Bayesian technique. The values of m that are summed up, are provided on the top of each panel. Indeed, for relatively larger values of M , the frequencies are divided up into several nearby intervals $(\tilde{p}_{m-1}, \tilde{p}_m]$.

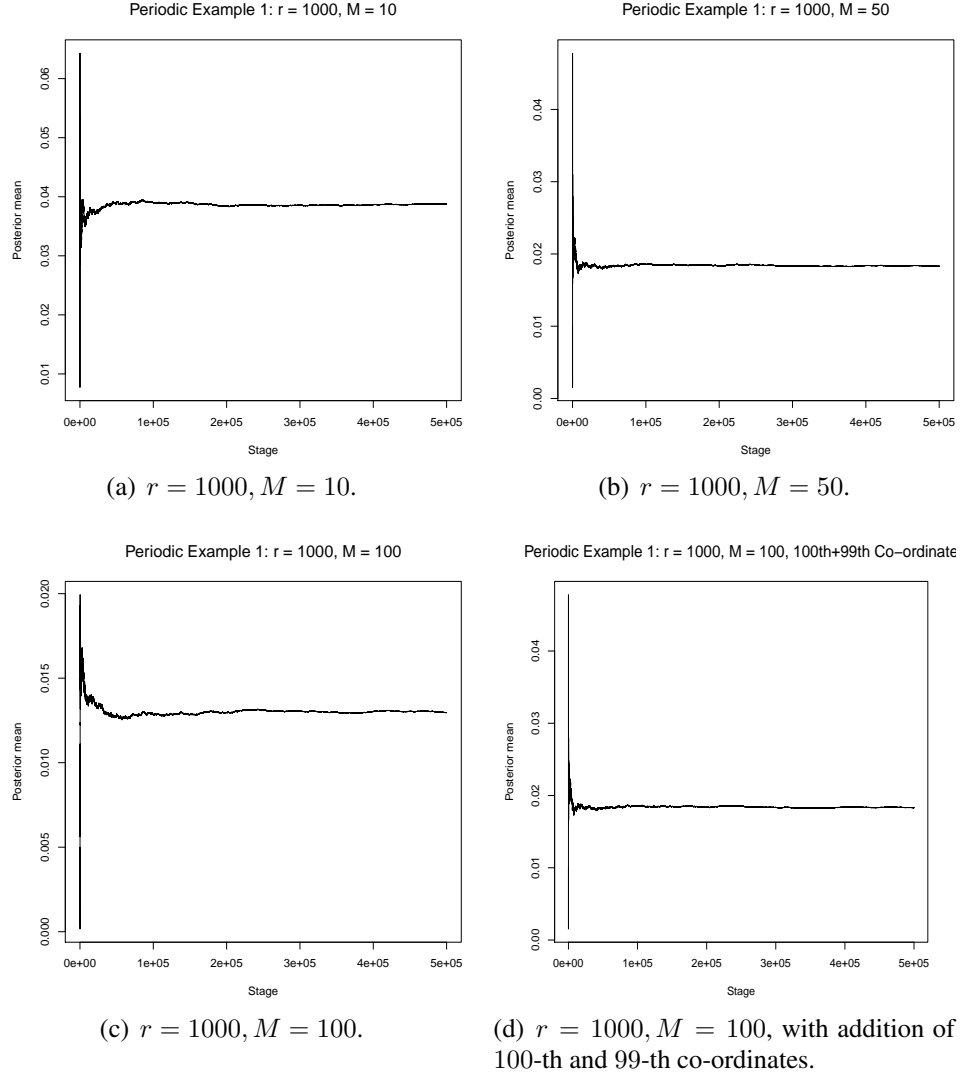


Figure 17.5: Illustration of our Bayesian method for determining single frequency for long enough time series. Here the true frequency is 0.02.

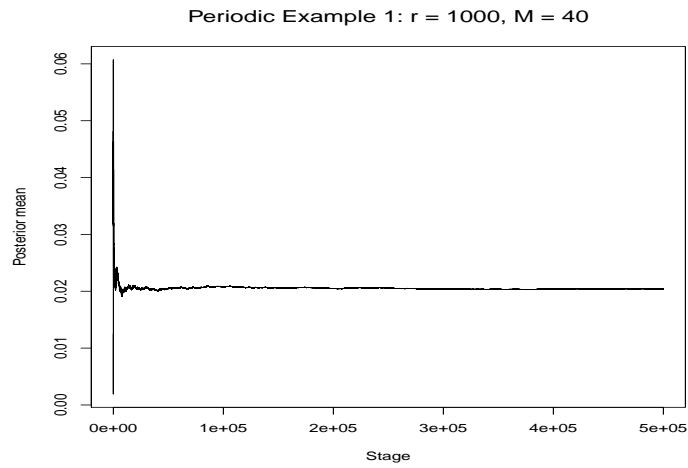


Figure 17.6: Convergence of our Bayesian method to the true frequency 0.02 for long enough time series with $r = 1000$ and $M = 40$.

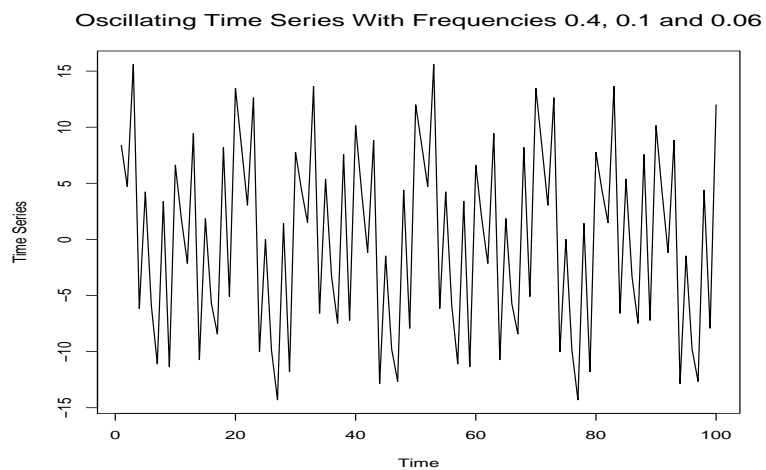
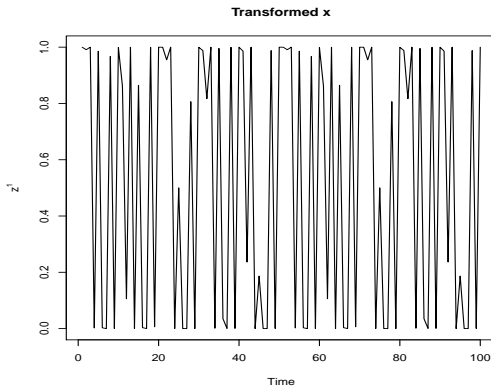
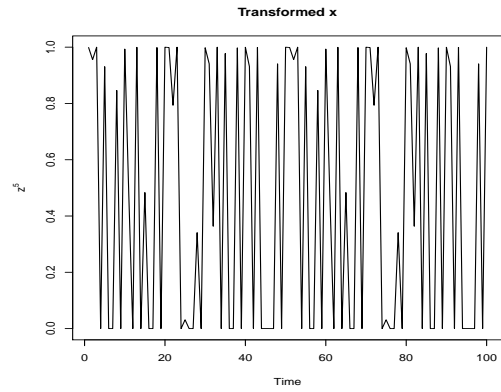


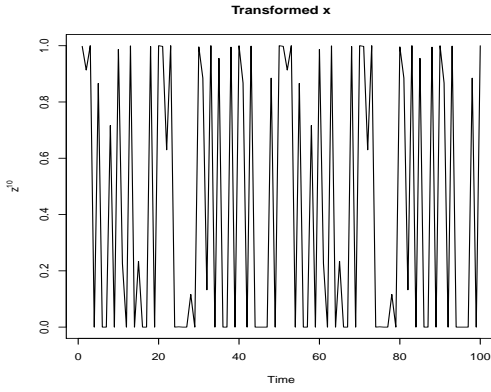
Figure 17.7: Simulated oscillating time series with true frequencies 0.4, 0.1 and 0.06.



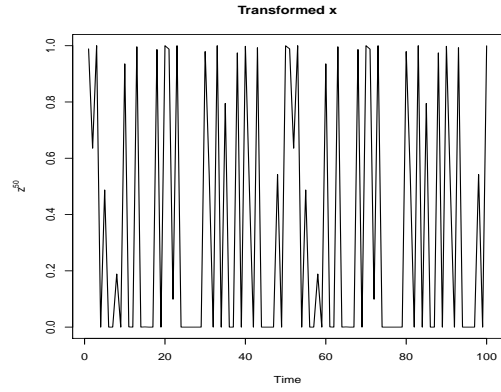
(a) Transformed series Z^1 .



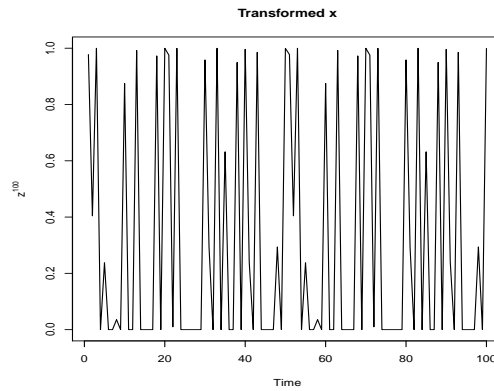
(b) Transformed series Z^5 .



(c) Transformed series Z^{10} .



(d) Transformed series Z^{50} .



(e) Transformed series Z^{100} .

Figure 17.8: Illustration of effects of r in Z^r in determining multiple frequencies in (17.20). Here the true frequencies are 0.4, 0.1 and 0.06.

Recall that we do not consider the first interval $(\tilde{p}_0, \tilde{p}_1]$ at all as it is a small interval around zero for relatively large M and hence not associated with any true frequency significantly different from zero. The proportions of the intervals that converged to zero, are not considered either.

Figures 17.9, 17.10 and 17.11 depict the details of our results for $r = 1, 5, 10$ and $M = 10, 50, 100$. Observe that $r = 1$ gives the best performance, while the performance deteriorates for $r = 5$ is also close. But observe that for $r = 5, M = 10$, the frequency 0.06 seems to be somewhat underestimated. However importantly, for $r = 10$, while the frequencies 0.4 and 0.1 are correctly converged to for these values of r , the frequency 0.06 seems to be significantly underestimated, for $M = 10, 50, 100$.

As seen in Figures 17.12 and 17.13, for $r = 50$ and 100 , although the frequency 0.06 is underestimated in some cases, the most conspicuous is the case of underestimation of the highest frequency 0.4. This is due to the fact that for relatively large values of r , about half of the peaks of the original process close to the highest peaks, die down. Since half of these peaks close to the highest peaks contribute half of the total frequency 0.4 (obvious from direct counting of the highest and second highest peaks in Figure 17.7, this results in significant underestimation of the highest frequency.

Hence, consistent from the insight gained from Figure 17.8, $r = 1$ yields the best performance. The choice of M seems to be less important compared to that of r , as in the previous example with single frequency.

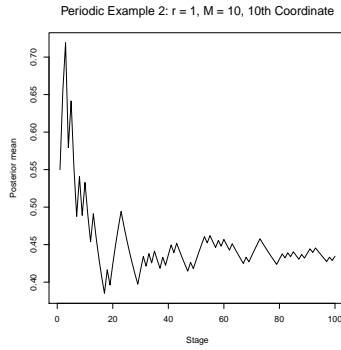
17.7 Real data example: El Niño and fish population

Based on data provided by Dr. Roy Mendelssohn of the Pacific Environmental Fisheries Group, Shumway and Stoffer (2006) analyse two oscillating time series on monthly values of an environmental series called the Southern Oscillation Index (SOI) and associated Recruitment (number of new fish), available for a period of 453 months, ranging over the years 1950–1987. The plots are provided in Shumway and Stoffer (2006); see also panel (a) of Figure 17.14 and panel (a) of Figure 17.18. The quantity SOI is a measurement of air pressure change associated with sea surface temperatures in the central Pacific Ocean. The El Niño effect is considered to cause warming of the central Pacific every three to seven years, which is turn, is presumed to be responsible for causing floods in the midwestern portions of the United States in the year 1997. It is thus important to identify the frequency of oscillation of the SOI series and the associated dependent Recruitment series, which seem to have slightly slower frequency of oscillation in comparison to the SOI series. At first glance, both the series seem to have two significant frequencies of oscillations. For instance, the Recruitment series seems to oscillate once in every 12 months and also once in every 50 months. Slightly faster frequencies can be expected of the SOI series. The periodogram analyses provided in Shumway and Stoffer (2006) indeed give weight to these frequencies.

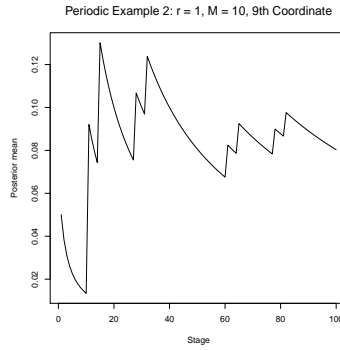
We now apply our Bayesian method to investigate the frequencies hidden in the two underlying time series. Although the two series seem to be dependent, we consider their analyses one by one. In the case of dependence, the frequencies in this situation are expected to be close.

17.7.1 SOI series

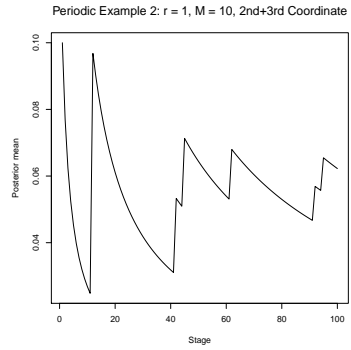
We first take up the case of the SOI series, centering it first to remove any possible trend. Denoting the centered series by X_t , for our purpose, we need to consider a transformation of the series to Z_t^r ,



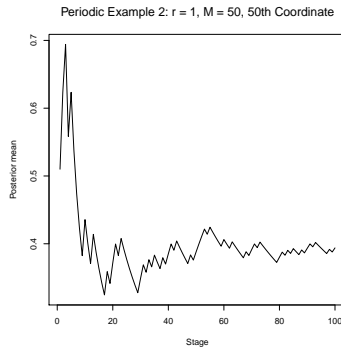
(a) $r = 1, M = 10$. True frequency = 0.4.



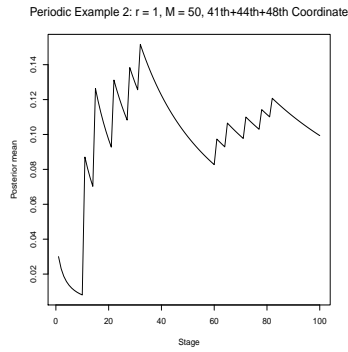
(b) $r = 1, M = 10$. True frequency = 0.1.



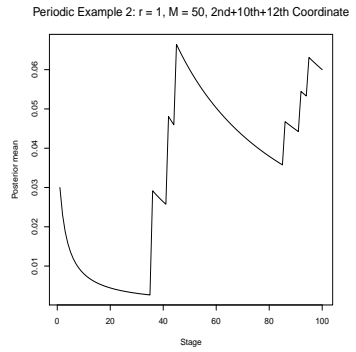
(c) $r = 1, M = 10$. True frequency = 0.06.



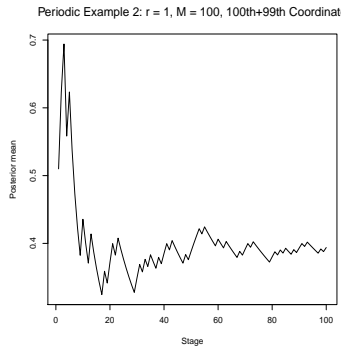
(d) $r = 1, M = 50$. True frequency = 0.4.



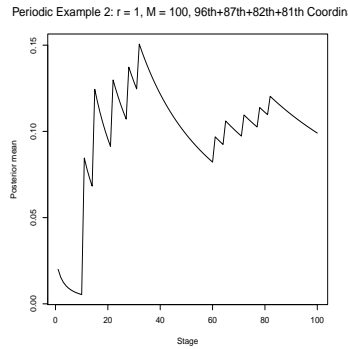
(e) $r = 1, M = 50$. True frequency = 0.1.



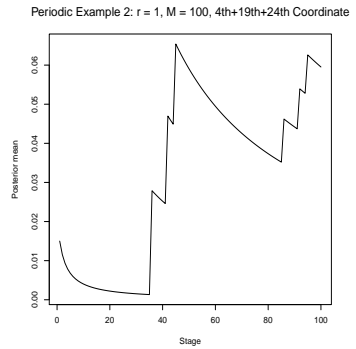
(f) $r = 1, M = 50$. True frequency = 0.06.



(g) $r = 1, M = 100$. True frequency = 0.4.

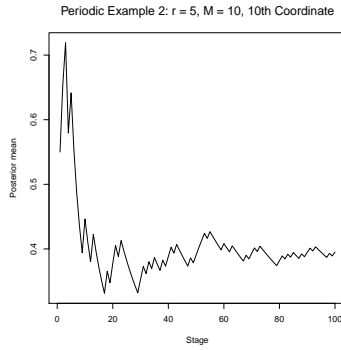


(h) $r = 1, M = 100$. True frequency = 0.1.

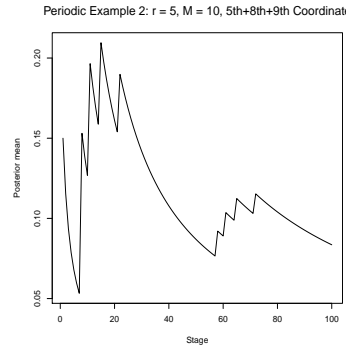


(i) $r = 1, M = 100$. True frequency = 0.06.

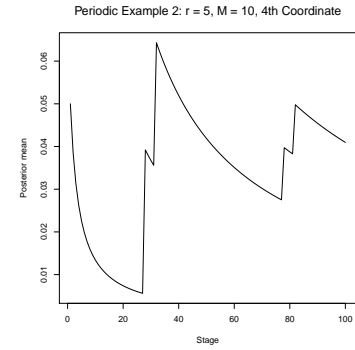
Figure 17.9: Illustration of our Bayesian method for determining multiple frequencies. Here the true frequencies are 0.4, 0.1 and 0.06.



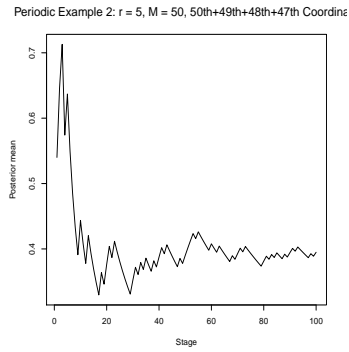
(a) $r = 5, M = 10$. True frequency = 0.4.



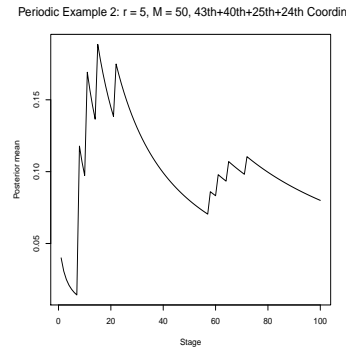
(b) $r = 5, M = 10$. True frequency = 0.1.



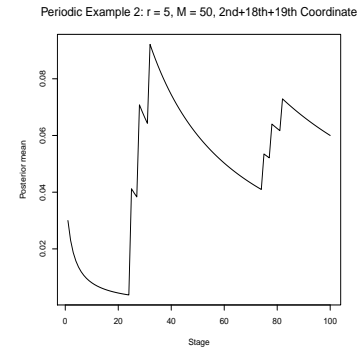
(c) $r = 5, M = 10$. True frequency = 0.06.



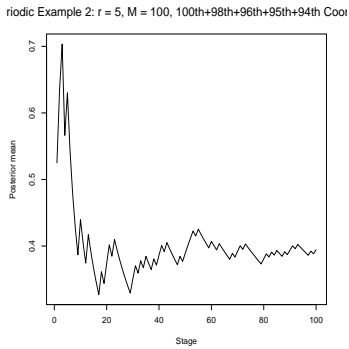
(d) $r = 5, M = 50$. True frequency = 0.4.



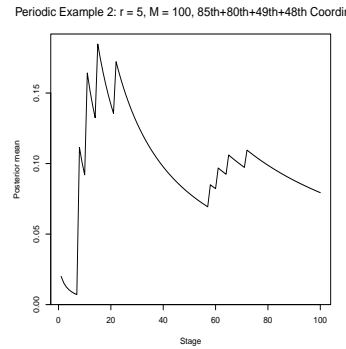
(e) $r = 5, M = 50$. True frequency = 0.1.



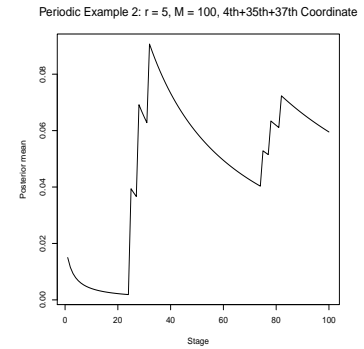
(f) $r = 5, M = 50$. True frequency = 0.06.



(g) $r = 5, M = 100$. True frequency = 0.4.

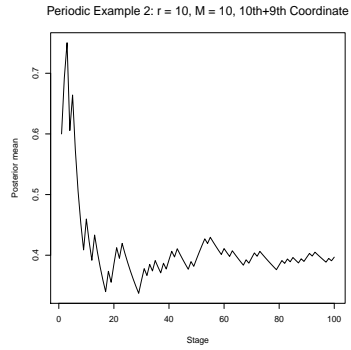


(h) $r = 5, M = 100$. True frequency = 0.1.

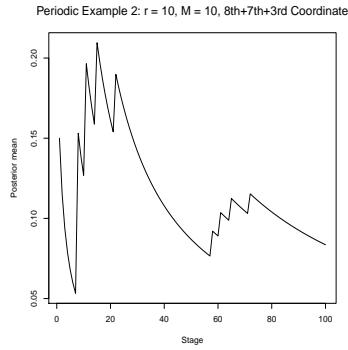


(i) $r = 5, M = 100$. True frequency = 0.06.

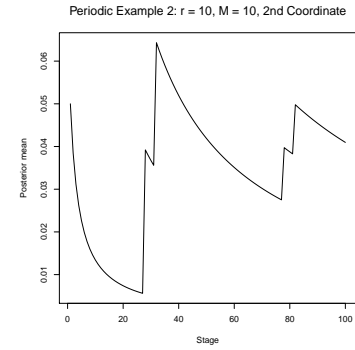
Figure 17.10: Illustration of our Bayesian method for determining multiple frequencies. Here the true frequencies are 0.4, 0.1 and 0.06.



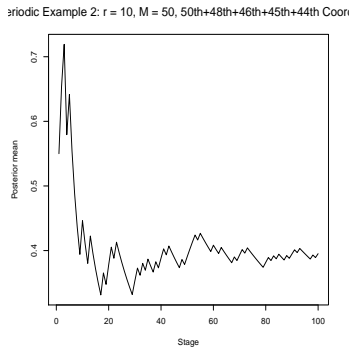
(a) $r = 10, M = 10$. True frequency = 0.4.



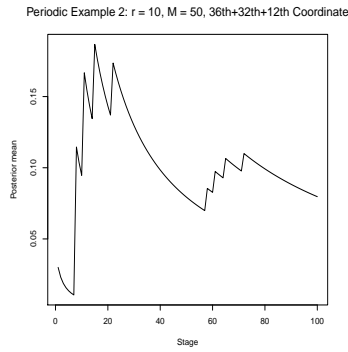
(b) $r = 10, M = 10$. True frequency = 0.1.



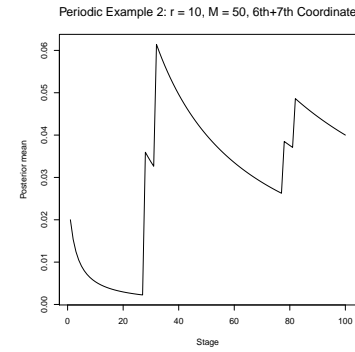
(c) $r = 10, M = 10$. True frequency = 0.06.



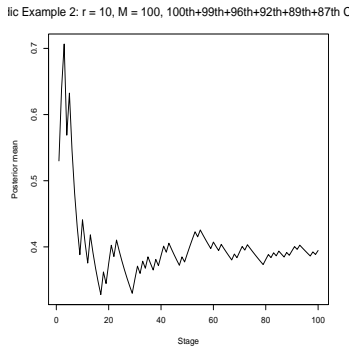
(d) $r = 10, M = 50$. True frequency = 0.4.



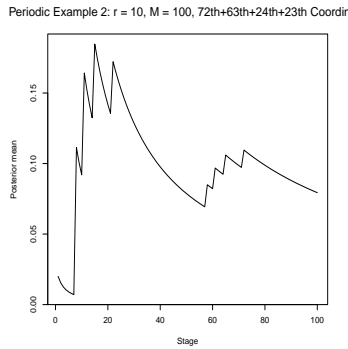
(e) $r = 10, M = 50$. True frequency = 0.1.



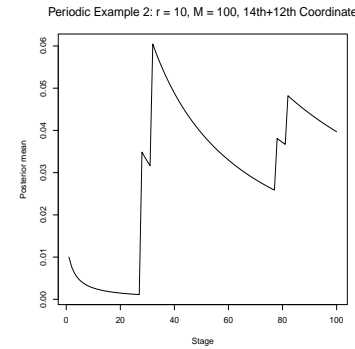
(f) $r = 10, M = 50$. True frequency = 0.06.



(g) $r = 10, M = 100$. True frequency = 0.4.

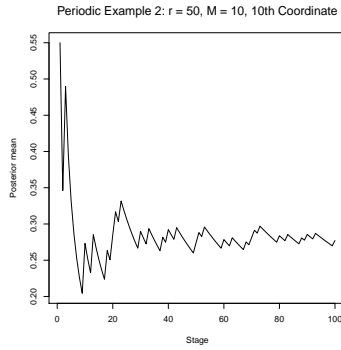


(h) $r = 10, M = 100$. True frequency = 0.1.

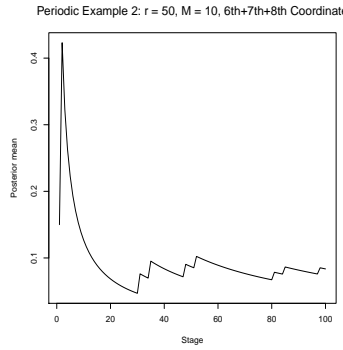


(i) $r = 10, M = 100$. True frequency = 0.06.

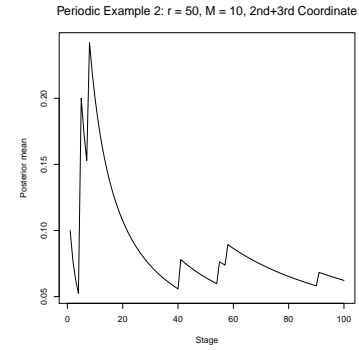
Figure 17.11: Illustration of our Bayesian method for determining multiple frequencies. Here the true frequencies are 0.4, 0.1 and 0.06.



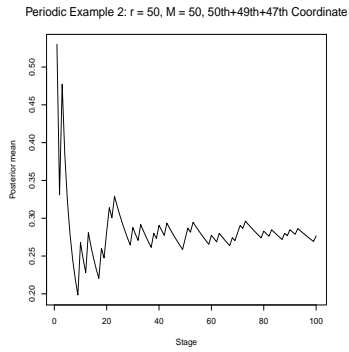
(a) $r = 50, M = 10$. True frequency = 0.4.



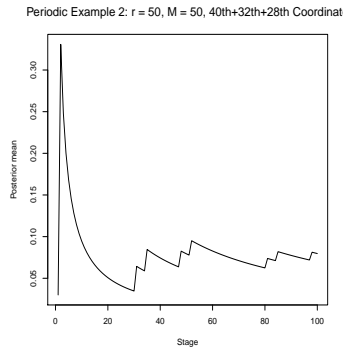
(b) $r = 50, M = 10$. True frequency = 0.1.



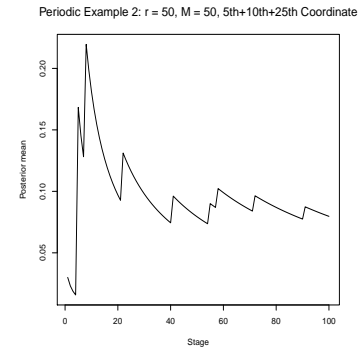
(c) $r = 50, M = 10$. True frequency = 0.06.



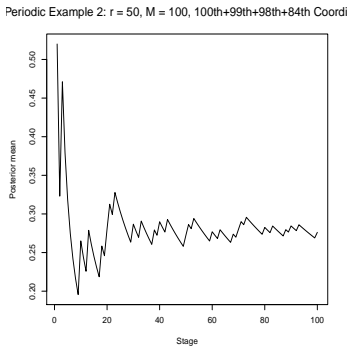
(d) $r = 50, M = 50$. True frequency = 0.4.



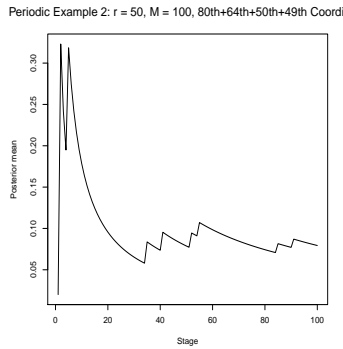
(e) $r = 50, M = 50$. True frequency = 0.1.



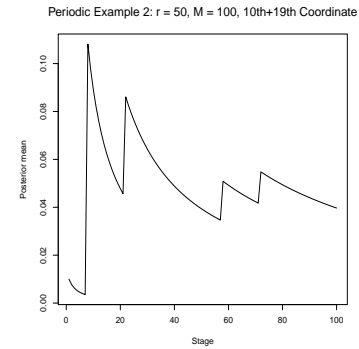
(f) $r = 50, M = 50$. True frequency = 0.06.



(g) $r = 50, M = 100$. True frequency = 0.4.

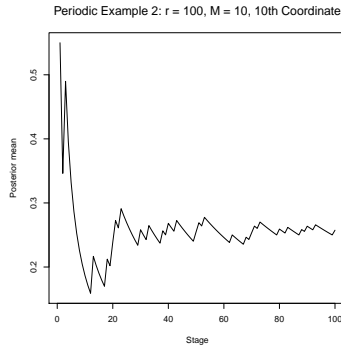


(h) $r = 50, M = 100$. True frequency = 0.1.

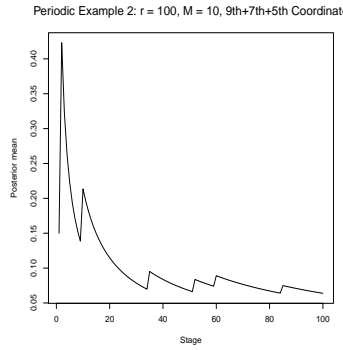


(i) $r = 50, M = 100$. True frequency = 0.06.

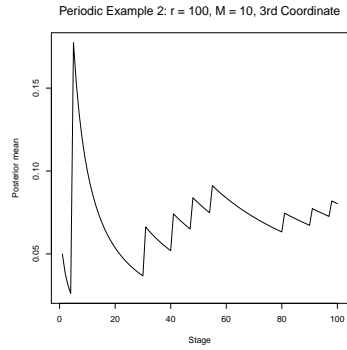
Figure 17.12: Illustration of our Bayesian method for determining multiple frequencies. Here the true frequencies are 0.4, 0.1 and 0.06.



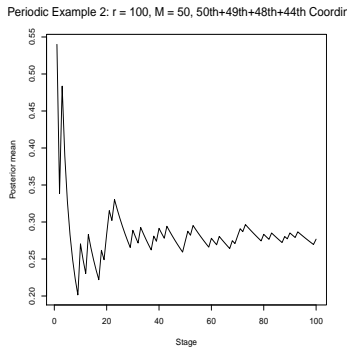
(a) $r = 100, M = 10$. True frequency = 0.4.



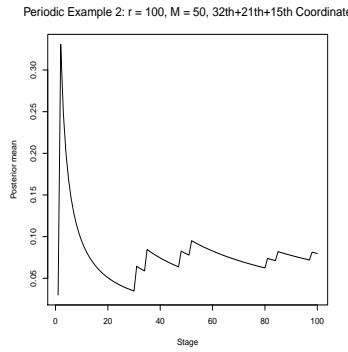
(b) $r = 100, M = 10$. True frequency = 0.1.



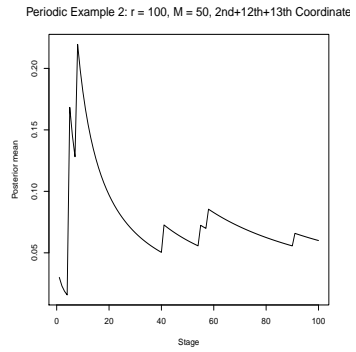
(c) $r = 100, M = 10$. True frequency = 0.06.



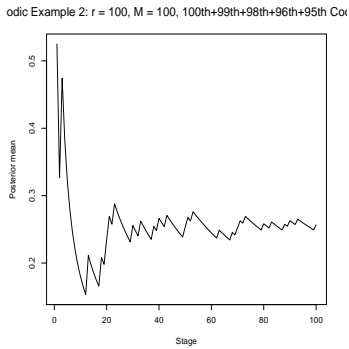
(d) $r = 100, M = 50$. True frequency = 0.4.



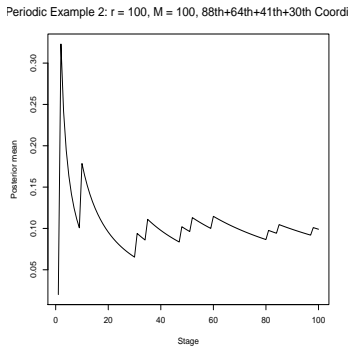
(e) $r = 100, M = 50$. True frequency = 0.1.



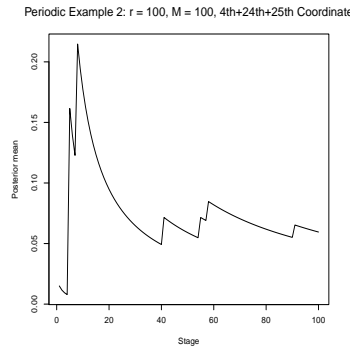
(f) $r = 100, M = 50$. True frequency = 0.06.



(g) $r = 100, M = 100$. True frequency = 0.4.

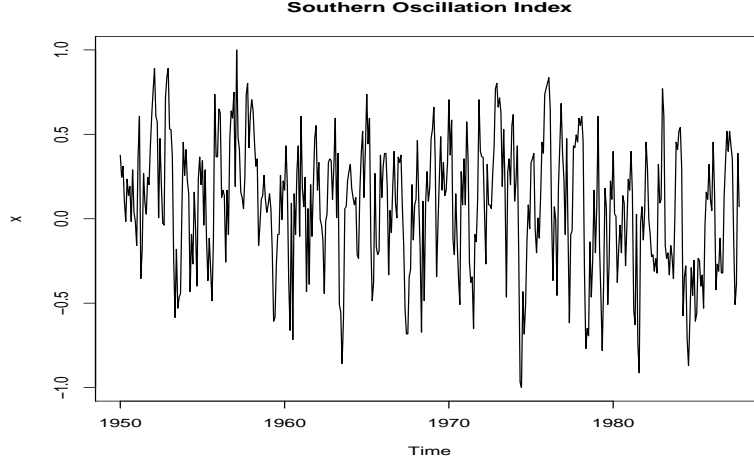


(h) $r = 100, M = 100$. True frequency = 0.1.

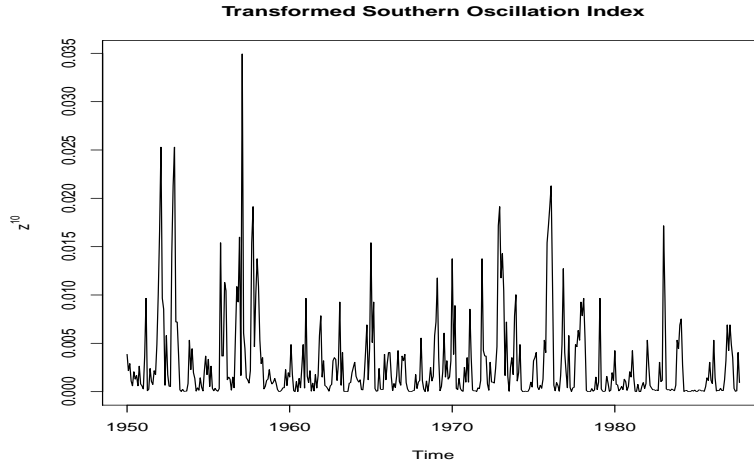


(i) $r = 100, M = 100$. True frequency = 0.06.

Figure 17.13: Illustration of our Bayesian method for determining multiple frequencies. Here the true frequencies are 0.4, 0.1 and 0.06.



(a) The original SOI time series.



(b) The transformed SOI time series.

Figure 17.14: The original and the transformed SOI time series.

with $Z^t = \exp(X_t) / (1 + \exp(X_t))$. We choose $r (> 0)$ such that the oscillations in the process $\mathbf{Z}^r = \{Z_t^r\}$ become as explicit as possible. With $r = 10$, this goal seems to be achieved. The original SOI time series and the transformed time series \mathbf{Z}^{10} are shown in Figure 17.14.

The range of Figure 14(b) reveals that a very fine partition of the interval $[0, 1]$ is necessary in order to capture the hidden frequencies. As such, we set $M = 5000$. We then implement our Dirichlet process based Bayesian method with $r = 10$ and $M = 5000$. Figure 17.15 shows the results of our implementation. Panel (a) of the figure shows convergence of the relevant posterior of $p_{25,j} + p_{27,j}$ approximately to the frequency 0.02, while panel (b) shows convergence of $p_{16,j} + p_{18,j} + p_{19,j} + p_{21,j} + p_{22,j}$ approximately to 0.08. The fine partition of $[0, 1]$ is the reason for dissipating of the proportions to many intervals $(\tilde{p}_{m-1,j}, \tilde{p}_{m,j}]$. Other than the aforementioned $p_{m,j}$'s contributing to the frequencies, the rest of the $p_{m,j}$'s, except $p_{1,j}$, converged to zero. Thus, our results are consistent with the periodogram analysis of Shumway and Stoffer (2006).

The above analysis requires very fine partition of $[0, 1]$, using large values of M . This considerably increases the number of $p_{m,j}$ s in the Bayesian model, most of which do not contribute

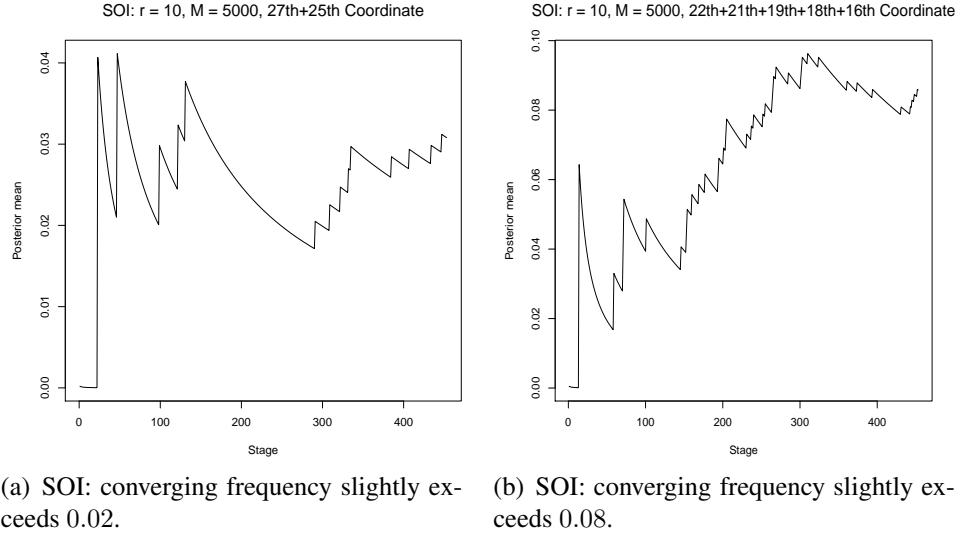


Figure 17.15: Bayesian results for frequency determination of the SOI time series.

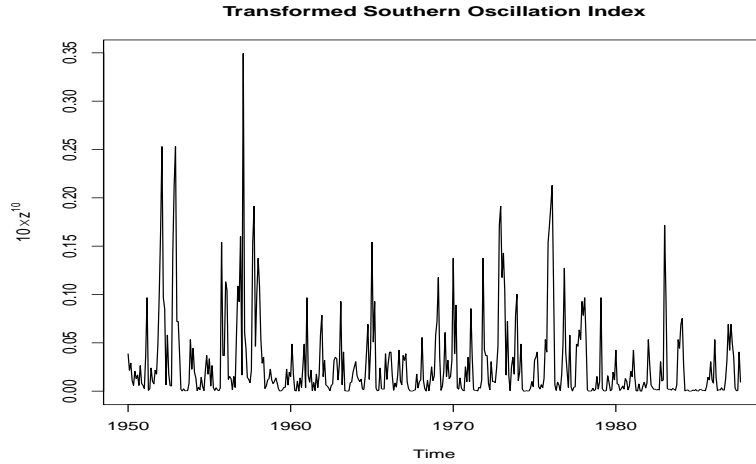


Figure 17.16: The transformed SOI time series $10 \times \mathbf{Z}^{10}$.

to frequency determination. Apart from being wasteful, this also slows down the implementation of the Bayesian code. Since the small range of the transformed time series \mathbf{Z}^{10} is responsible for these issues, it makes sense to consider a transformation that increases the range, while preserving easy visualization of the oscillations. In this particular example, simply multiplication of \mathbf{Z}^{10} by 10 seems to have the desired effect. Figure 17.16 shows the series $10 \times \mathbf{Z}^{10}$. Here, considering $M = 1000$ turned out to be sufficient. Indeed, Figure 17.17 shows that the relevant frequencies to which our Bayesian posteriors converged to, are consistent with those obtained for \mathbf{Z}^{10} and $M = 5000$, and hence again approximately in keeping with the periodogram analysis of Shumway and Stoffer (2006). Here we remark that the choice $M = 1000$ is still somewhat large, but smaller values such as 100 and 500 did not yield enough (almost) empty intervals $(\tilde{p}_{m-1}, \tilde{p}_m]$ between the strings of intervals contributing significantly to the frequencies. Hence, these smaller choices did not enable us to easily identify the different frequencies characterizing the SOI time series.

We now turn to the Recruitment time series; as in SOI, we first center the time series. The

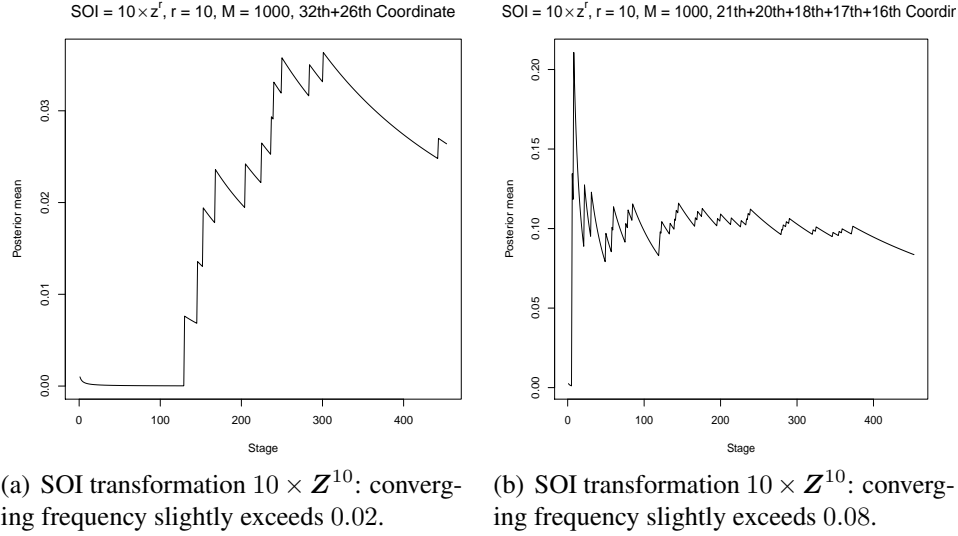


Figure 17.17: Bayesian results for frequency determination of the SOI time series with transformed time series $10 \times \mathbf{Z}^{10}$.

original Recruitment series and the transformation $\exp(25) \times \mathbf{Z}^{50}$ are displayed in Figure 17.18. This transformation enabled the most explicit visualization of the oscillations, among those that we experimented with. The multiplicative factor $\exp(25)$ raises the range to a reasonable limit. We consider $M = 1000$ for our Bayesian implementation based on Dirichlet process. Figure 17.19 depicts the posterior convergence path to the relevant frequencies. Note that the convergences in panel (a) occurs towards slightly larger than 0.02, while that in panel (b) occurs around 0.08. In contrast, for the SOI series, the convergences in panels (b) of Figure 17.15 and 15(b) seemed to take place at values somewhat larger than 0.08.

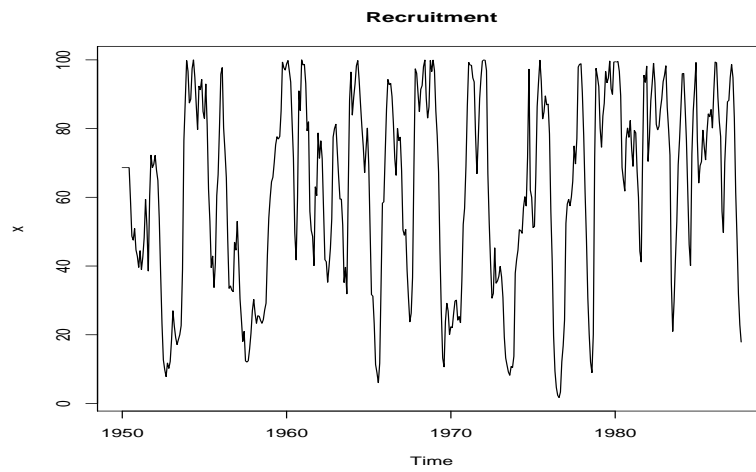
17.7.2 Harmonics

Since in reality most signals are not sinusoidal, it is preferable to use harmonics to model such signals. In this respect, we consider Example 4.12 of Shumway and Stoffer (2006) where a signal is constructed using a sinusoid oscillating at two cycles per unit time, and 5 harmonics obtained from the sinusoid oscillating at decreasing amplitudes. Specifically, their signal is given by

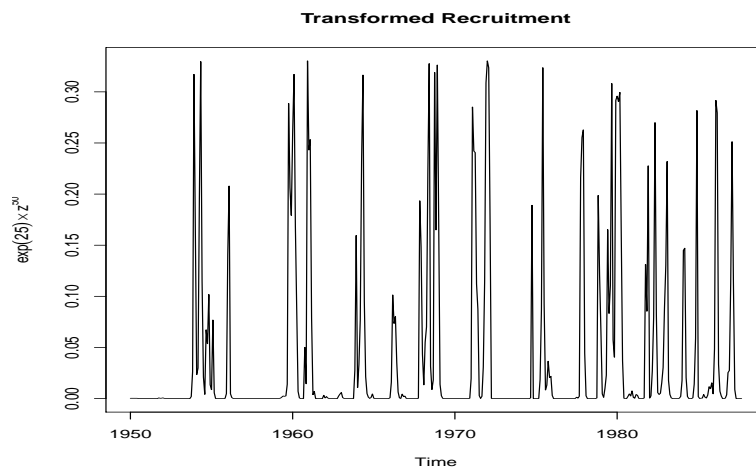
$$x_t = \sin(2\pi 2t) + 0.5 \sin(2\pi 4t) + 0.4 \sin(2\pi 6t) + 0.3 \sin(2\pi 8t) + 0.2 \sin(2\pi 10t) + 0.1 \sin(2\pi 12t), \quad (17.21)$$

for $0 \leq t \leq 1$. The original signal \mathbf{X} and the transformation \mathbf{Z}^2 are displayed in Figure 17.20, after considering 201 equidistant points in the time interval $[0, 1]$. Note that the original signal is not even close to sinusoidal. For the transformation \mathbf{Z}^r , we chose $r = 2$ such that the structure of \mathbf{X} is essentially retained, but the gaps between the oscillations are increased to facilitate detection of the frequencies.

Since \mathbf{Z}^2 suggests multiple frequencies that are likely to be close to each other, we chose $M = 150$ to divide $[0, 1]$ into larger number of finer sub-intervals compared to the previous examples to properly detect the oscillations. Application of our Bayesian procedure revealed 6 distinct values out of $M = 150$ at the end of the 201-th iteration, while the rest converged to zero. We take

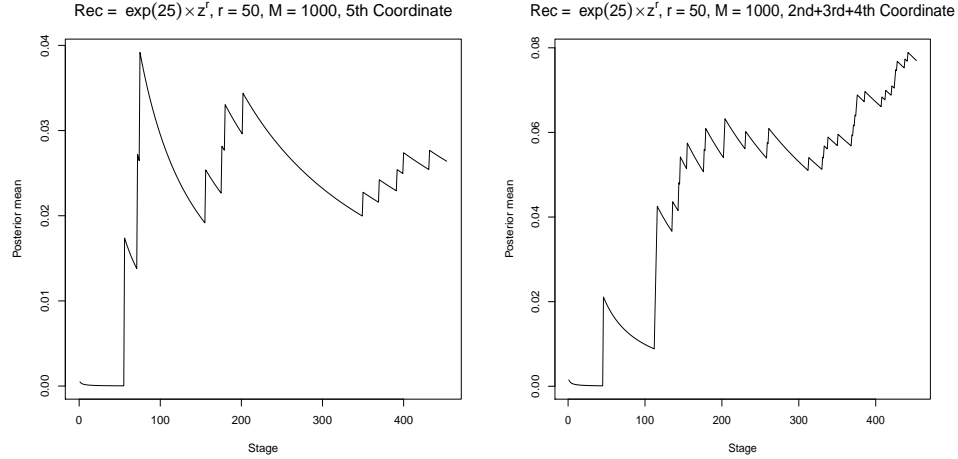


(a) The original Recruitment time series.



(b) The transformed Recruitment time series.

Figure 17.18: The original and the transformed Recruitment time series.



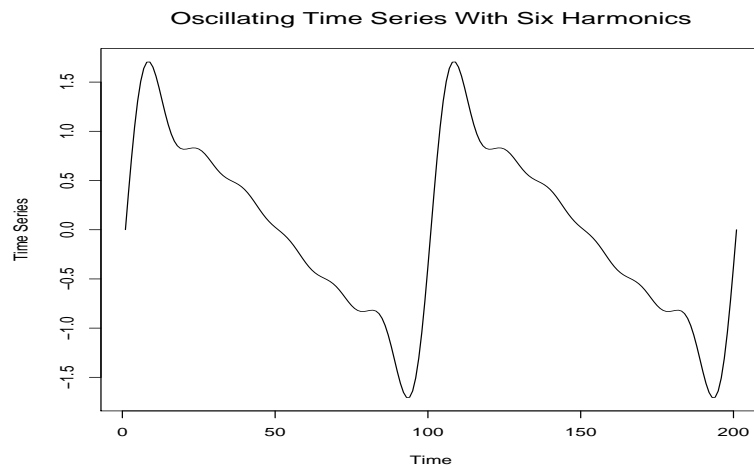
(a) Rec transformation $\exp(25) \times \mathbf{Z}^{50}$: converging frequency slightly larger than 0.02. (b) Rec transformation $\exp(25) \times \mathbf{Z}^{50}$: converging frequency around 0.08.

Figure 17.19: Bayesian results for frequency determination of the Recruitment time series with transformed time series $\exp(25) \times \mathbf{Z}^{50}$.

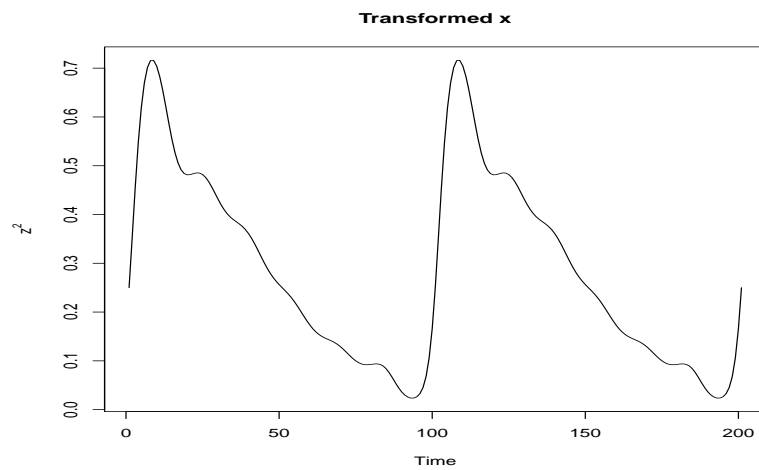
the averages of the co-ordinates yielding the same distinct value, and present the results in Figure 17.21, after multiplication by 201, to yield the Bayesian results on frequencies per unit time. As is evident from the diagrams, the final iterations produced the frequencies 2, 4, 6, 8, 10, 14, obtained after rounding off the values. Except the frequency 14, which somewhat overestimates the true frequency 12, the others are indeed the true frequencies. That so accurate results are obtained by our Bayesian method even for a challenging time series with small length, is really encouraging.

Acknowledgment

We are grateful to Dr. Satyaki Mazumder for helpful comments.



(a) The original signal with 6 harmonics.



(b) The transformed signal with 6 harmonics.

Figure 17.20: The original and the transformed signal with 6 harmonics.

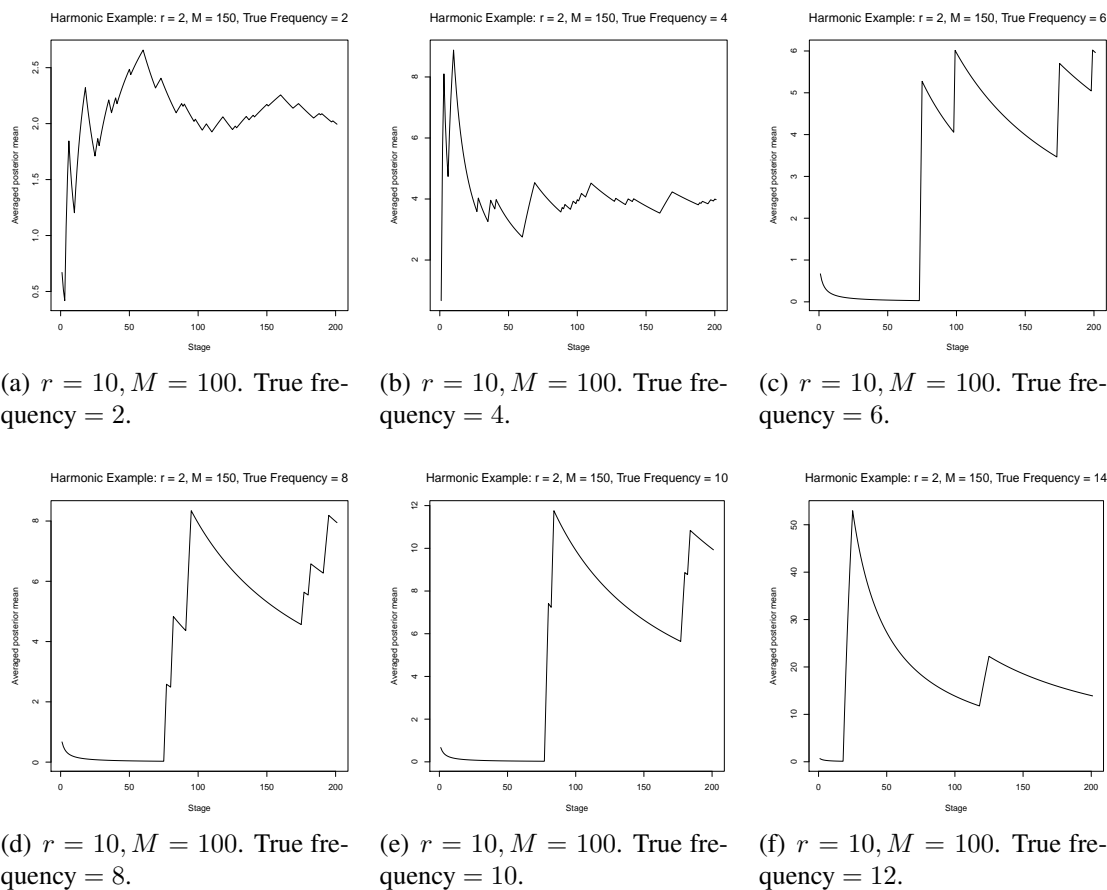


Figure 17.21: Illustration of our Bayesian method for determining multiple frequencies in non-sinusoidal signals. Here the true frequencies are 2, 4, 6, 8, 10 and 12 oscillations per unit time.

References

- Adler, R. J. (1981). *The Geometry of Random Fields*. John Wiley and Sons, New York.
- Adler, R. J. and Taylor, J. E. (2007). *Random Fields and Geometry*. Springer, New York.
- Baddeley, A. and Turner, R. (2005). Spatstat: an R Package for Analyzing Spatial Point Patterns. *Journal of Statistical Software*, **12**, 1–42. URL: www.jstatsoft.org, ISSN: 1548–7660.
- Bandopadhyay, S. and Rao, S. S. (2017). A Test for Stationarity for Irregularly Spaced Spatial Data. *Journal of the Royal Statistical Society. Series B*, **79**, 95–123.
- Bandopadhyay, S., Jentsch, C., and Rao, S. S. (2017). A Spectral Domain Test for Stationarity of Spatio-Temporal Data. *Journal of Time Series Analysis*, **38**, 326–351.
- Basu, P., Rudoy, D., and Wolfe, P. J. (2009). A Nonparametric Test for Stationarity Based on Local Fourier Analysis. In *2009 IEEE International Conference on Acoustics, Speech and Signal Processing*, pages 3005–3008.
- Bera, A. K. and Higgins, M. L. (1993). ARCH Models: Properties, Estimation and Testing. *Journal of Economic Surveys*, **7**, 305–366.
- Beran, R., Bilodeau, M., and L de Micheaux, P. (2007). Nonparametric Tests of Independence Between Random Vectors. *Journal of Multivariate Analysis*, **98**, 1805–1824.
- Berkes, I., Horváth, L., and Kokoszka, P. (2003). GARCH Processes: Structure and Estimation. *Bernoulli*, **9**, 201–227.
- Bilodeau, M. and L de Micheaux, P. (2005). A Multivariate Empirical Characteristic Function Test of Independence With Normal Marginals. *Journal of Multivariate Analysis*, **95**, 345–369.
- Bilodeau, M. and Nangue, A. G. (2017). Tests of Mutual or Serial Independence of Random Vectors with Applications. *Journal of Machine Learning Research*, **18**, 1–40.
- Black, F. and Scholes, M. (1973). The Pricing of Options and Corporate Liabilities. *Journal of Political Economy*, **81**, 637–654.
- Blum, J. R., Kiefer, J., and Rosenblatt, M. (1961). Distribution Free Tests of Independence Based on the Sample Distribution Function. *Annals of Mathematical Statistics*, **32**, 485–498.
- Bollerslev, T. (1986). Generalized Autoregressive Conditional Heteroskedasticity. *Journal of Econometrics*, **31**, 307–327.
- Bougerol, P. and Picard, N. (1992). Stationarity of GARCH Processes and of Some Nonnegative Time Series. *Journal of Econometrics*, **52**, 115–127.
- Breitung, J. (2002). Nonparametric Tests for Unit Roots and Cointegration. *Journal of Econometrics*, **10**, 343–363.

- Brooks, S., Gelman, A., Jones, G., and Meng, X.-L. (2011). *Handbook of Markov Chain Monte Carlo*. Chapman and Hall/CRC, Boca Raton. First Edition.
- Brooks, S. P. and Gelman, A. (1998). General Methods for Monitoring Convergence of Iterative Simulations. *Journal of Computational and Graphical Statistics*, **7**, 434–455.
- Brooks, S. P. and Roberts, G. O. (1998). Assessing Convergence of Markov Chain Monte Carlo Algorithms. *Statistics and Computing*, **8**, 319–335.
- Cardinali, A. and Nason, G. P. (2018). Practical Powerful Wavelet Packet Tests for Second-Order Stationarity. *Applied and Computational Harmonic Analysis*, **44**, 558–583.
- Cl  roux, R., Lazraq, A., and Lepage, Y. (1995). Vector Correlation Based on Ranks and a Non-parametric Test of No Association Between Vectors. *Communications in Statistics. Theory and Methods*, **24**, 713–733.
- Cowles, M. K. and Carlin, B. P. (1996). Markov Chain Monte Carlo Convergence Diagnostics: A Comparative Review. *Journal of the American Statistical Association*, **91**, 883–904.
- Daley, D. J. and Vere-Jones, D. (2003). *An Introduction to the Theory of Point Processes*. Springer-Verlag, New York. Second Edition.
- Das, M. and Bhattacharya, S. (2020). Nonstationary Nonparametric Bayesian Spatio-Temporal Modeling Using Kernel Convolution of Order Based Dependent Dirichlet Process. ArXiv preprint.
- Dey, K. K. and Bhattacharya, S. (2017). A Brief Tutorial on Transformation Based Markov Chain Monte Carlo and Optimal Scaling of the Additive Transformation. *Brazilian Journal of Probability and Statistics*, **31**, 509–617.
- Dey, K. K. and Bhattacharya, S. (2019). A Brief Review of Optimal Scaling of the Main MCMC Approaches and Optimal Scaling of Additive TMCMC Under Non-Regular Cases. *Brazilian Journal of Probability and Statistics*, **33**, 222–266.
- Dickey, D. and Fuller, W. (1979). Distribution of the Estimators for Autoregressive Time Series With a Unit Root. *Journal of the American Statistical Association*, **74**, 427–431.
- Dutta, S. and Bhattacharya, S. (2014). Markov Chain Monte Carlo Based on Deterministic Transformations. *Statistical Methodology*, **16**, 100–116. Also available at <http://arxiv.org/abs/1106.5850>. Supplement available at <http://arxiv.org/abs/1306.6684>.
- Engle, R. F. (1982). Autoregressive Conditional Heteroskedasticity With Estimates of the Variance of U.K. Inflation. *Econometrica*, **50**, 987–1008.
- Ephraty, A., Tabrikian, J., and Messer, H. (2001). Underwater Source Detection Using a Spatial Stationary Test. *The Journal of the Acoustical Society of America*, **109**, 1053–1063.
- Ferguson, T. S. (1973). A Bayesian Analysis of Some Nonparametric Problems. *The Annals of Statistics*, **1**, 209–230.

- Ferguson, T. S. (1974). Prior Distributions on Spaces of Probability Measures. *The Annals of Statistics*, **2**, 615–629.
- Fuentes, M. (2002). Spectral Methods for Nonstationary Spatial Processes. *Biometrika*, **89**, 197–210.
- Fuentes, M. (2005). A Formal Test for Non-Stationarity of Spatial Stochastic Processes. *Journal of Multivariate Analysis*, **96**, 30–54.
- Gelman, A. and Rubin, D. B. (1992). Inference From Iterative Simulation Using Multiple Sequences. *Statistical Science*, **7**, 457–472.
- Geweke, J. (1992). Evaluating the Accuracy of Sampling-Based Approaches to Calculating Posterior Moments. In J. M. Bernardo, J. O. Berger, A. P. Dawid, and A. F. M. Smith, editors, *Bayesian Statistics 4*, pages 169–193, Oxford. Clarendon Press.
- Ghoudi, K., Kulperger, R. J., and Rémillard, B. (2001). A Nonparametric Test of Serial Independence for Time Series and Residuals. *Journal of Multivariate Analysis*, **79**, 191–218.
- Gieser, P. W. and Randles, R. H. (1997). A Nonparametric Test of Independence Between Two Vectors. *Journal of the American Statistical Association*, **92**, 561–567.
- Gilks, W. R. and Roberts, G. O. (1996). Strategies for improving MCMC. In W. Gilks, S. Richardson, and D. Spiegelhalter, editors, *Markov Chain Monte Carlo in Practice*, Interdisciplinary Statistics, pages 89–114, London. Chapman and Hall.
- Giraitis, L., Leipus, R., and Surgailis, D. (2005). Recent Advances in ARCH Modelling. In *Long Memory in Economics*, pages 3–39, Berlin. Springer.
- Giraud, C. (2015). *Introduction to High-Dimensional Statistics*. CRC Press, New York.
- Guan, Y., Sherman, M., and Calvin, J. A. (2004). A Nonparametric Test For Spatial Isotropy Using Subsampling. *Journal of the American Statistical Association*, **99**, 810–821.
- Hoeffding, W. (1948). A Nonparametric Test of Independence. *Annals of Mathematical Statistics*, **19**, 546–557.
- Jun, M. and Genton, M. (2012). A Test For Stationarity of Spatio-Temporal Random Fields On Planar and Spherical Domains. *Statistica Sinica*, **22**, 1737–1764.
- Kwiatkowski, D., Schmidt, P., and Shin, Y. (1992). Testing the Null Hypothesis of Atationarity Against the Alternative of a Unit Root. *Journal of Econometrics*, **54**, 159–178.
- Li, B., Genton, M. G., and Sherman, M. (2008). Testing the Covariance Structure of Multivariate Random Fields. *Biometrika*, **95**, 813–829.
- Møller, J. and Waagepetersen, R. P. (2004). *Statistical Inference and Simulation for Spatial Point Processes*. Chapman & Hall/CRC, Boca Raton, Florida.

- Øksendal, B. (2000). *Stochastic Differential Equations*. Springer-Verlag, Hiedelberg, New York. 5th Edition.
- Ornstein, L. S. and Uhlenbeck, G. E. (1930). On the Theory of Brownian Motion. *Physical Review*, **36**, 823–841.
- O’Sullivan, D. and Unwin, D. J. (2003). *Geographical Information Analysis*. Wiley, Hoboken, NJ.
- Paciorek, C. J., Yanosky, J. D., and Puett, R. C. (2009). Practical Large-Scale Spatio-Temporal Modeling of Particulate Matter Concentrations. *The Annals of Applied Statistics*, **3**, 370–397.
- Philips, P. C. B. and Perron, P. (1988). Testing for a Unit Root in Time Series Regression. *Biometrika*, **75**, 335–346.
- Puri, M. L. and Sen, P. K. (1971). *Nonparametric Methods in Multivariate Analysis*. Wiley, New York.
- Raftery, A. E. and Lewis, S. M. (1992). How Many Iterations in the Gibbs Sampler? In J. M. Bernardo, J. O. Berger, A. P. Dawid, and A. F. M. Smith, editors, *Bayesian Statistics 4*, pages 763–773, Oxford. Clarendon Press.
- Robert, C. P. (1995). Convergence Control Methods for Markov Chain Monte Carlo Algorithms. *Statistical Science*, **10**, 231–253.
- Robert, C. P. and Casella, G. (2004). *Monte Carlo Statistical Methods*. Springer-Verlag, New York.
- Roy, S. and Bhattacharya, S. (2020). Bayes Meets Riemann – Bayesian Characterization of Infinite Series With Application to Riemann Hypothesis. *International Journal of Applied Mathematics and Statistics*. To appear. Available at “<https://arxiv.org/abs/1601.01452>”.
- Roy, V. (2019). Convergence Diagnostics for Markov Chain Monte Carlo. *Annual Review of Statistics and its Application*. To appear. Available at “<https://arxiv.org/pdf/1909.11827.pdf>”.
- Schabenberger, D. and Gotway, C. A. (2005). *Statistical Methods for Spatial Data Analysis*. Chapman and Hall, London.
- Schervish, M. J. (1995). *Theory of Statistics*. Springer-Verlag, New York.
- Shumway, R. H. and Stoffer, D. S. (2006). *Time Series Analysis and Its Applications With R Examples*. Springer, New York.
- Straumann, D. (2005). Estimation in Conditionally Heteroscedastic Time Series Models. In *Volume 181 of Lecture Notes in Statistics*, Berlin. Springer-Verlag.
- Strauss, D. J. (1975). A Model for Clustering. *Biometrika*, **63**, 467–475.
- Stute, W. and Schumann, G. (1980). A General Glivenko-Cantelli Theorem for Stationary Sequences of Random Observations. *Scandinavian Journal of Statistics*, **7**, 102–104.

- Taylor, S. J. (1986). *Modelling Financial Time Series*. Wiley, Chichester.
- Um, Y. and Randles, R. H. (2001). A Multivariate Nonparametric Test of Independence Among Many Vectors. *Journal of Nonparametric Statistics*, **13**, 699–708.
- van Delft, A., Characiejus, V., and Dette, H. (2018). A Nonparametric Test for Stationarity in Functional Time Series. arXiv preprint arXiv:1708.05248.
- Waller, L. A. and Gotway, C. A. (2004). *Applied Spatial Statistics for Public Health Data*. Wiley, Hoboken, NJ.

Table 13.1: The performance evaluation of the test statistics T and V of Bandopadhyay and Rao (2017) and Bandopadhyay *et al.* (2017) applied to our simulated spatial datasets.

	Test \ Model	Stationary	Nonstationary	$p = 0.9$	$p = 0.99$	$p = 0.999$	$p = 0.9999$	$p = 0.99999$
1000	T	7.692	2.444	2.290	4.717	9.151	8.105	9.254
	P -value (T)	0.158	0.751	0.776	0.387	0.103	0.141	0.099
	V	11.405	4.643	4.429	9.999	12.411	11.766	12.603
3000	P -value (V)	0.056	0.398	0.424	0.080	0.043	0.051	0.041
	T	4.921	11.466	6.743	5.286	5.162	4.964	5.106
	P -value (T)	0.361	0.055	0.206	0.322	0.335	0.356	0.341
5000	V	13.483	16.527	16.631	14.073	13.432	13.508	13.432
	P -value (V)	0.031	0.014	0.014	0.023	0.031	0.031	0.031
	T	3.307	4.234	3.196	3.313	3.385	3.342	3.385
	P -value (T)	0.595	0.451	0.615	0.595	0.583	0.589	0.583
	V	18.160	20.233	16.787	17.843	18.160	18.160	18.238
	P -value (V)	0.010	0.006	0.014	0.011	0.010	0.010	0.010